CHEMISTRY OF GOLD COMPLEXES
RELATED TO ANTI-ARTHRITIS DRUGS

By

MARY ALICE TURNER, B.Sc.

A Thesis

Submitted to the Faculty of Graduate Studies

in Partial Fulfilment of the Requirements

for the Degree

Doctor of Philosopy

McMaster University

October, 1988

DOCTOR OF PHILOSOPHY (1988)   McMASTER UNIVERSITY
Department of Chemistry   Hamilton, Ontario

TITLE: Chemistry of Gold Complexes Related
                to Anti-arthritis Drugs

AUTHOR: Mary Alice Turner, B.Sc. (McMaster University)

SUPERVISOR: Professor C.J.L.Lock

NUMBER OF PAGES: xl, 237

for

MOM AND DAD

ABSTRACT

The synthesis and characterization of complexes analogous to the novel anti-arthritis gold drug auranofin is presented. The general composition of these compounds is L-Au-X where L=triethylphosphine and X=tetraacetylthioglucose or chloride in the case of auranofin or its synthetic precursor. Incorporation of ligands (L) such as isocyanides and aromatic nitrogen donors fail to impart the same stability to gold(I) that phosphines or thiols are capable of. Complexes of aromatic nitrogen ligands are prone to decomposition and those of isocyanides, although thermodynamically stable, are labile and subject to relatively rapid isocyanide substitution as well as the expected substitution of the halide group.

Complexes have been investigated with regard to their _in vitro_ and _in vivo_ DNA-binding capabilities in light of the reported anti-cancer properties of auranofin itself. Isocyanide and phosphine gold(I) complexes as well as a series of gold(III) complexes have shown their ability to bind to DNA _in vitro_ but lose their viability _in vivo_. This is likely a result of reduction of the gold by thiol groups present in a living system and is associated with the observed cytotoxicity at increasing concentrations.

The tris-2-pyridylphosphine (TPP) ligand has also been utilized as a choice for L which has led to the synthesis of the auranofin analogue, (tris-2-pyridylphosphine)(tetraacetylthioglucose)gold(I). Metal ions such as Zn(II), Co(III), Cu(II), Fe(II), Fe(III) and Cr(III) have been incorporated at the pyridyl nitrogen sites and this series of

complexes has been studied crystallographically. N-bound and mixed N- and P-bound complexes have been studied by other techniques as well, depending on the nature of the metal ion involved. Copper(II) complexes have been investigated by E.S.R. and UV/Visible spectroscopies, Moessbauer data is presented for iron(II) and iron(III) complexes and infrared data has been collected and summarized for all complexes. In general, the TPP ligand is an accomodating chelate; N-bound complexes are octahedral and little ligand strain is observed upon coordination. The nitrogen and phosphorus sites are independent in that there appear to be no electronic effects exerted by one site on the other. An important effect of coordinating metal ions to the nitrogen sites is to alter the solubility of the hydrophobic ClAuTPP complex to one with hydrophilic properties.

Abbreviations

A	adenine
AlbSH	albumin
AlbSSCy	cysteinyl albumin disulphide
bipy	2,2'-bipyridine
C	cytosine
CD	circular dichroism
cisplatin	<u>cis</u>-diamminedichloroplatinum(II)
dien	diethylenetriamine
DIPHOS	1,2(diphenylphosphino)ethane
DMF	N,N-dimethylformamide
DMSO	dimethylsulphoxide
DNA	deoxyribonucleic acid
d-pen	d-penicillamine
DTE	dithioerythritol
EDS	Electron Diffraction Spectroscopy
en	ethylenediamine
ESR	electron spin resonance
Et_3P	triethylphosphine
Et_3PAuCl	chlorotriethylphosphinegold(I)
$(Et_3P)_2AuCl$	bis(triethylphosphine)gold(I) chloride
Et_3PO	triethylphosphine oxide
EXAFS	Extended X-ray Absorption Fine Structure
<u>fac</u>	<u>facial</u>
G	guanosine

Abbreviations continued

GST	gold sodium thiomalate
GtSH	glutathione
HB(pz)$_3$	hydro(tris-1-pyrazolyl)borate
HB(Mepz)$_3$	hydrotris(N-methylpyrazol-1-yl)borate
HCA	human carbonic anhydrase
HSAtg	thioglucose
IR	infrared
IS	isomer shift
iso	isotropic
MeOD	deuterated methanol
mer	meridional
N-MeIm	N-methylimidazole
NMR	nuclear magnetic resonance
Ph	phenyl
phen	1,10-phenanthrolene
py	pyridine
QS	quadrupole splitting
RA	rheumatoid arthritis
RBC	red blood cell
T	thymine
TACN	triazacyclononane
TATG	tetraacetylthioglucose
TPP	tris-2-pyridylphosphine
UV/VIS	ultraviolet/visible

Abbreviations continued

WAXS   Wide Angle X-ray Scattering

XANES   X-ray Absorption Near Edge Spectroscopy

Abbreviations for complexes of TPP

ClAuTPP   chloro(tris-2-pyridylphosphine)gold(I)

(ClAuTPP)CrCl$_3$ trichloro(chloro(tris-2-pyridylphosphine-P-)-

                                  gold(I)-N,N',N"-)chromium(III)

(ClAuTPP)CoCl$_3$ trichloro(chloro(tris-2-pyridylphosphine-P-

                                  gold(I)-N,N',N"-)cobalt(III)

(ClAuTPP)Co(NO$_2$)$_3$ trinitrito(chloro(tris-2-pyridylphosphine-P-

                                  gold(I)-N,N',N"-)cobalt(III)

(ClAuTPP)$_2$Cu   bis(chloro(tris-2-pyridylphosphine-P-gold(I))-

                                  N,N',N"-)copper(II) dinitrate

(ClAuTPP)$_2$Fe(ClO$_4$)2   bis(chloro(tris-2-pyridylphosphine-P-

                                  gold(I))-N,N',N"-)iron(II) diperchlorate

(ClAuTPP)FeSO$_4$ diaquochloro(tris-2-pyridylphosphine-P-

                                  gold(I)-N,N',N"-)sulphato iron(II)

[ClAuTPPZn(H$_2$O)$_3$](NO$_3$)$_2$ triaquo(chloro(tris-2-pyridylphosphine-P-

                                  gold(I))-N,N',N"-)zinc(II) dinitrate

[(ClAuTPP)$_2$Zn](NO$_3$)$_2$ bis(chloro(tris-2-pyridylphosphine-P-

                                  gold(I))-N,N',N"-)zinc(II) dinitrate

TPPCrCl$_3$ trichloro(tris-2-pyridylphosphine-N,N',N"-)

                                  chromium(III)

Abbreviations for complexes of TPP continued

$TPPCoCl_3$ — trichloro(tris-2-pyridylphosphine-N,N',N"-)cobalt(III)

$TPPCo(NO_2)_3$ — trinitrito(tris-2-pyridylphosphine-N,N',N"-)cobalt(III)

$TPPCu(NO_3)2$ — dinitrato(tris-2-pyridylphosphine-N,N',N"-)-copper(II)

$(TPP)_2Cu(NO_3)_2$ — bis(tris-2-pyridylphosphine-N,N',N"-)copper(II) dinitrate

$TPPFeCl_3$ — trichloro(tris-2-pyridylphosphine)iron(III)

$(TPP)_2Fe(ClO_4)$ — bis(tris-2-pyridylphosphine-N,N',N"-)iron(II) diperchlorate

$TPPFeSO_4(H2O)_2$ — diaquo(tris-2-pyridylphosphine-N,N',N"-)sulphatoiron(II) trihydrate

$(TPP)_2Zn(ClO_4)_2$ — bis(tris-2-pyridylphosphine-N,N',N"-)zinc(II) diperchlorate

$TPPZn(H_2O)_3(NO_3)_2$ — triaquo(tris-2-pyridylphosphine-N,N',N"-)-zinc(II) dinitrate trihydrate

ACKNOWLEDGEMENTS

I would like to extend my gratitude to Professor Colin Lock for years of patience, encouragement and friendship. There couldn't be a nicer guy to work for.

I would also like to thank the members of my committee, Drs. McGlinchey and McCarry for helpful discussions and Mr. Romolo Faggiani for help with the first crystal structures and advice during solution of the later ones.

A friendly atmosphere has made life here very enjoyable. For this I have to thank the rest of the lab group, past and present, Mike Abrams (mentor), Brian Allore, Brenda Brown, Jim Britten, Mary Duarte, Debbie Harvey, Kathy McKague, Chris Orvig and Pierre Pilon. As well, I am grateful to every friend associated with baseball, soccer, the Phoenix and the coffee lounge.

Special thanks go to Alan and my family who make any accomplishment worthwhile.

TABLE OF CONTENTS

TABLE OF CONTENTS

continued

page

LIST OF TABLES

LIST OF TABLES continued

LIST OF TABLES continued

LIST OF FIGURES

CHAPTER 1

INTRODUCTION

1.1 Rheumatoid Arthritis

Rheumatoid arthritis (RA) has been treated successfully with the use of gold salts for more than fifty years, but the action of gold compounds in the suppression of the disease remains unclear. Many medication schedules used act to suppress pain and acute inflammation but rarely affect the chronic disease process (1). Gold compounds have been shown to induce disease remission in about ten percent of cases (2).
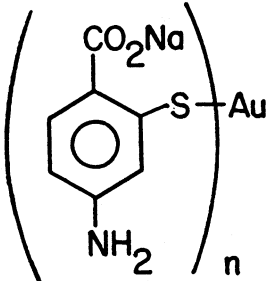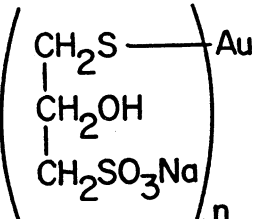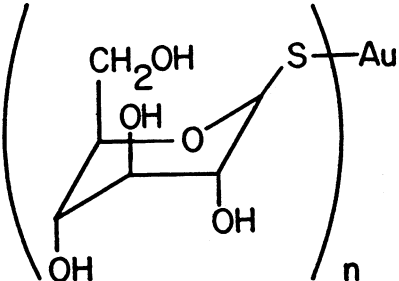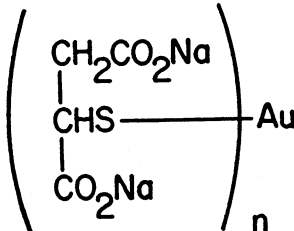
Gold has been shown to possess a variety of biological effects even though there is no evidence for its essential function in living organisms (3). Studies of the role of injectable gold in RA treatment (both in vivo and in vitro) are grouped into anti-microbial, anti-immunologic, anti-inflammatory and anti-enzymatic effects among others (4). Unfortunately, it is not known which of these effects are involved in the etiology of rheumatoid arthritic disease, but histocompatibility antigen studies suggest a genetic origin in that the HLA-DR4 gene occurs approximately four times more often in patients afflicted by RA than in healthy people (5). The HLA-D4 gene has been associated with immune response. Anti-inflammatory and anti-enzymatic effects are certainly implicated during disease progression as well (4).

1

Since RA is an exclusively human disease, preliminary testing
of gold drugs (and other anti-rheumatoid compounds) is performed on
induced adjuvant arthritis in experimental animals. Adjuvant arthritis
has been described as a manifestation of delayed hypersensitivity (6).
Its response to drug treatment, both gold-based and otherwise, may
differ depending on the strain of disease or irritant used to produce
adjuvant inflammation as well as the type of animal under investigation
(7). To date, the best models can only cause symptoms similar, but not
identical, to those observed in RA. Possibly some of the same
biochemical pathways are involved but, because the cause of RA has not
been determined, it cannot be mimicked.

1.2 Overview of gold drugs;

A list of injectable gold compounds currently in use for
treatment of RA is given in Table 1.2.1. Features common to each of
the compounds listed are the following; 1) gold is present in its +1
oxidation state, 2) a thiolate or other sulphur-containing ligand is
coordinated to the gold atom, 3) the gold thiolates are frequently
formulated as simple monomers. It is clear from general gold(I)
chemistry that the metal is likely to have linear two-coordinate
geometry (8) thus compounds in Table 1.2.1 which are certainly
polymeric are denoted as such. Compounds such as sodium thiosulphate-
S-aurate(I) (Sanochrysin[TM]), disodium thiomalato-S-aurate(I)
(Myochrysine[TM]) and thioglucosato-S-aurate(I) (Solganol[TM]) are the most
widely used throughout the world. Myochrysine is the drug of choice in
Canada (9). Analyses of Myochrysine and Solganol give one to one gold

Table 1.2.1 A description of some gold drugs

	Ligand	Trade Name
Au_2S_3	sulphide	Aurol sulphide
$Na_3Au(S_2O_3)_2$	thiosulphate	Sanochrysin
	4-amino-2-mercapto benzoic acid	Krysolgan
	thiopropanol sulphonate	Allochrysine
	β-D-thioglucose	Solganol
	disodiumthiomalate	Myochrysin

to ligand ratios, but complete characterization of the compounds is difficult because of their necessarily polymeric nature. In support of polymeric structures for most gold(I) thiol complexes is the structure of the analogous silver compound $AgSC_6H_{11}$ which is a cyclic dodecamer $[\{Ag(SC_6H_{11})\}_{12}]$ involving two-coordinate silver sites which may be stabilized by some inter-polymeric cross-linking giving three-coordination (10,11). The gold(I) thiolate drugs give rise to [197]Au Moessbauer spectra consistent with two-coordinate compounds and the occurrence of three-coordination is unlikely (12).

On the basis of ^{1}H NMR and ^{13}C NMR data, a cyclic hexameric structure featuring alternate Au and S bridges has been proposed for Myochrisine (13). Support for this suggestion and the possibility of an open chain pentamer has come from WAXS results (Wide Angle X-ray Scattering) which indicate an Au-S-Au angle of 94º based on Au···Au second neighbour distances (14). Information from other ^{1}H NMR studies fits a five-membered ring structure (15). This has also been suggested on the basis of EXAFS studies (14). The postulates assume the compound is homogeneous and not a mixture where the degree of association is dependent on the ionic strength of aqueous solution (16). In fact, Shaw states, "the exact structure of the gold(I) monothiolates is one of the most perplexing questions in their inorganic chemistry" (17). Recent developments suggest that the form of Myochrysine administered to patients is a mixture consisting of at least five components. It is a yellow solution the colour of which is achieved during the sterilization process (thirty minutes at 100ºC) of the originally colourless aqueous solution (18). As well, solutions of the well-

characterized (i.e. X-ray structure determined (19)) sodium

thiosulphato-S-aurate(I) soon become yellow on standing at room

temperature and NMR spectra of Solganol indicate the presence of an

impurity deduced by Shaw et al. to be the sulphinic or sulphonic acid

derivative of thioglucose (20). The majority of gold compounds

currently in use for RA treatment are so poorly characterized that,

were they presently undergoing trial, it is doubtful their use would be

sanctioned (15). Also to their detriment are statistics which show

that thirty to fifty percent of patients treated with gold drugs

develop adverse reactions ranging from skin rashes to proteinuria and

thrombocytopenia (9). It has thus far not been possible to prove which

component of the mixture is responsible for toxicity or for benefit.

In spite of their questionable makeup, the use of these compounds as

drugs is justified because they offer relief to seventy percent of the

patients who take them (9). It is often the case that because of

potential toxicity, these drugs are prescribed as a last resort to

patients for whom other drugs have failed. Information can be gathered

with regard to the disease itself and the expected alteration in

biochemistry upon receipt of gold treatment even though the exact

nature of the gold drugs is not known. For example, serum protein

thiol group depletion through oxidation is thought to be a contributing

factor to diseases such as RA (21). The suspected involvement of

thiol/disulphide equilibria in vivo seems consistent with the ability

of gold drugs like Myochrysine to inhibit sulphydryl-disulphide

exchange reactions (22).

The gold drugs listed in Table 1.2.1 are administered by weekly

injection. Researchers at Smith, Kline and French Laboratories have developed a new compound, triethylphosphinegold(I) 2,3,4,6-tetra-0-acetyl-1-thio-β-D-glucopyranoside (Ridaura[TM] or auranofin), with the aim of avoiding the necessity and potentially toxic side effects of weekly injections (see Figure 1.2.1).

$$CH_2OAc \quad S-Au-P(CH_2CH_3)_3$$
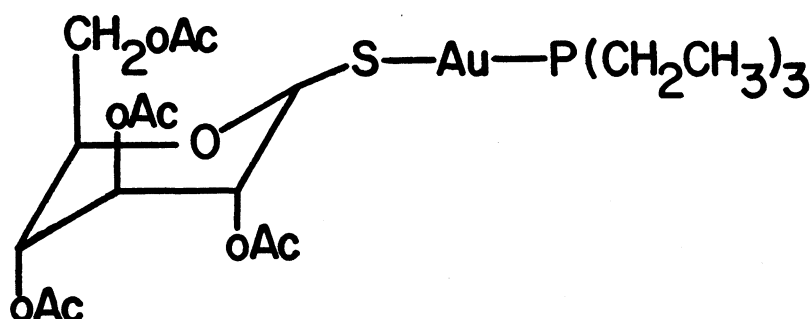
Figure 1.2.1   Auranofin

In fact, auranofin has been found to be effective against RA after oral administration (23). Unlike Myochrysine, which hereafter will be representative of 'injectable' gold drugs, auranofin contains the triethylphosphine ligand as well as the standard thiol group. It is monomeric and has been fully characterized chemically including a determination of its structure by X-ray diffraction (24).

1.3 Inorganic Chemistry of Gold;

The inorganic chemistry of gold has been covered extensively in several review articles (16,17,25,26). Some of the chemistry as it pertains to gold drugs is summarized here.

The biologically relevant oxidation states of gold are 0, I and III. Colloidal gold has been used on a limited basis for arthritis

treatment, however, it tends to be phagocytosed and deposited into

'aurosomes' (27) as opposed to being metabolized and biochemically

mobilised (16,17). Gold(III) has interested researchers because of its

similarity electronically (d^8) and structurally (majority of complexes

are square planar) to platinum(II) which has an established

chemotherapeutic role in the treatment of cancer (28). However, EXAFS

and XANES studies by Elder et al., where gold(I) was recovered from the

kidneys of rats into which sodium gold tetrachloroaurate had been

injected, suggest that +3 is an unlikely oxidation state for gold in

vivo at least when coordinated to chloride ligands (29). The oxidation

state diagram for gold illustrated in Figure 1.3.1 confirms that tetra-

chloroaurate is a relatively strong oxidizing agent. In fact, in a

biological system, which is generally mildly reducing at -0.5 to 0.0v,

gold(III) complexes of secondary and chelating amines surpass

$Au(CN)_2I_2^-$ in redox stability. The large drop in redox couple

potential from Au^{3+} to $Au(CN)_2I_2^-$ and $Au(pip)_4^{3+}$ demonstrates the

ability of certain ligands to stabilize this oxidation state.[1]

The diagram is also consistent with the susceptibility of

gold(I) salts to disproportionate in aqueous solution with the

thermodynamically favourable formation of elemental gold as the driving

---

[1] It should be noted that Elder's study was concerned with
oxidation state of gold deposited in aurosomes of rats' kidneys.
Aurosomes contain particles which after electron diffraction (EDS)
analysis are confirmed to be Au and S. Although EDS does not reliably
quantitate second row elements, it is able to detect P. In aurosomes
produced after introduction of gold phosphine complexes, Au and S were
again the only elements present (33). It has thus been postulated that
these aurosomes contain deposits of Au_2S as a common, thermodynamically
stable byproduct of decomposition of gold complexes. Elder studied
Au_2S-containing aurosomes only, therefore his sample was not
necessarily representative of gold in the serum or the kidney as a whole.
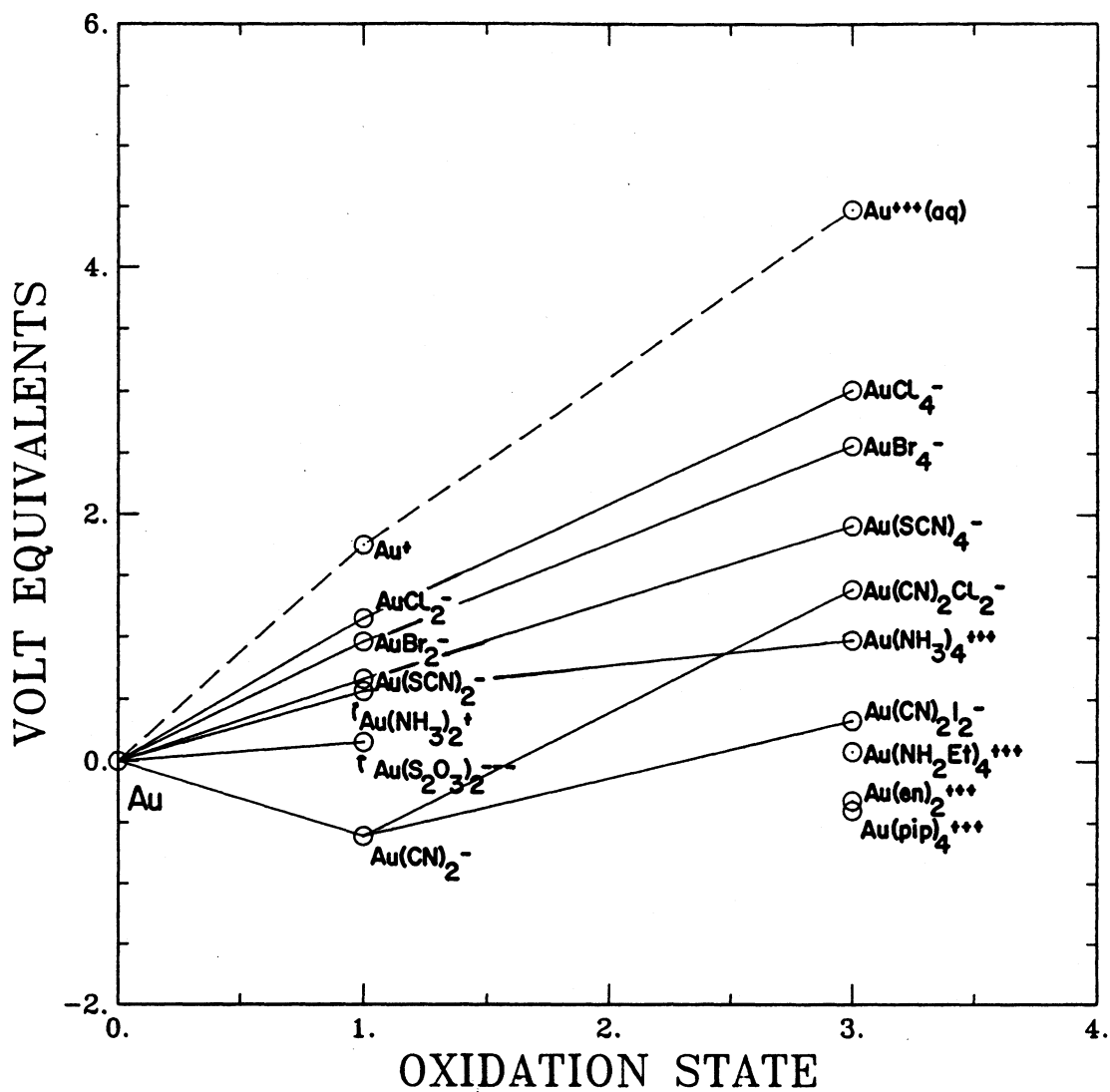
Figure 1.3.1 Oxidation state diagram for gold in aqueous solution.
E^O for $Au^+(aq)$ is a calculated value (31). Data taken
from (30,31,32). NH_2Et = ethylamine,
en = ethylenediamine and pip = piperidine.

force (16,17). The redox chemistry of gold(I) species can, however, be altered by the incorporation of stabilizing ligands such as $S_2O_3^{2-}$ and CN^-. Other examples of polarizable or 'soft' ligands, which stabilize gold(I) are those containing sulphur or phosphorus. This information has practical implications in the synthesis of gold(I) compounds; for example, simple substitution reactions of $AuCl_2^-$ are impossible. Complexes analogous to the gold drugs are usually prepared _via_ one of three routes:

scheme 1 $KAu(CN)_2 + RSH \longrightarrow AuSR + 2CN^- + H^+ + K^+$

scheme 2 $AuCl_4^- + 3RSH \longrightarrow AuSR + RSSR + 3HCl + Cl^-$

scheme 3 $AuCl_4^- + 2S(CH_2CH_2OH)_2 \longrightarrow ClAuS(CH_2CH_2OH)_2 + OS(CH_2CH_2OH)_2$

$ClAuS(CH_2CH_2OH)_2 + RSH$ or $L \longrightarrow AuSR$ or $LAuCl + S(CH_2CH2OH)_2$
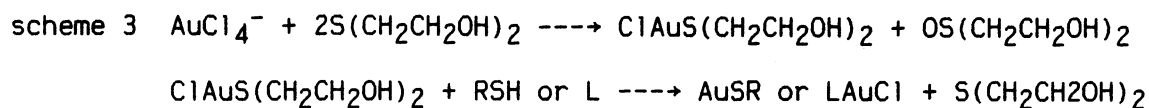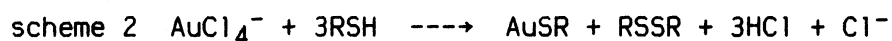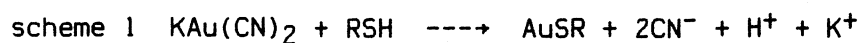
In scheme 1, elemental gold is the starting material and it is oxidized to gold(I) to form the stable cyanide complex which can be used in further reactions with thiols (34). In schemes 2 and 3, gold(III) is reacted with a reducing agent. Since desirable ligands for gold(I) are often reducing agents, (phosphines are also used to this end), excess ligand is often employed and the reaction follows scheme 2 (35). Scheme 3 involves prior reduction of gold(III) to an intermediate thioether complex (36) (ascorbic acid has also been used as a reducing agent (37)). The thioether is a better leaving group than chloride and is replaced during subsequent ligand addition. This method has particular application when the desired ligand is not a reducing agent or when it is preferable to economize on the ligand (15).

The general preparation of the injectable drugs follows scheme 2. Chlorotriethylphosphine gold(I) (Et$_3$PAuCl) is the synthetic precursor of auranofin where the chloride is eventually replaced by the thioglucose derivative. Et$_3$PAuCl can be synthesized by a route analogous to scheme 2 but better yields and cleaner products are obtained with the method of scheme 3 where the phosphine is represented by L in general.

Consistent with its soft nature is the pronounced tendency of gold(I) to form covalent rather than ionic metal-ligand bonds. Trends in increasing thermodynamic stability of anionic and cationic complexes are partially summarized as follows (16);

$$CNO^- < SCN^- \cong Cl^- < Br^- < I^- << CN^- \qquad \text{(anionic)}$$

$$Ph_3PO < Me_2S < py < Ph_3As < NH_3$$

$$< C_6H_{11}NH_2 << Ph_3P < MeCN < Ph_2MeP < PhMe_2P \quad \text{(cationic)}$$
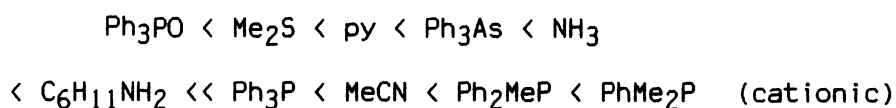
Along with being classified as a soft ion, gold(I) is also relatively electron-rich with a set of filled d orbitals and low oxidation state. For this reason, it may be expected that ligands with good π-acceptor capabilities are necessary to make the most stable complexes. The general π-acceptor series for ligands bound to transition metals is as follows (38);

$$NO^+ > CO > RNC > CN^- \cong PF_3 > PCl_3 > PCl_2OR > PCl_2R >>$$

$$P(OR)_3 > PR_3 \cong SR_2 > RCN > NH_3$$
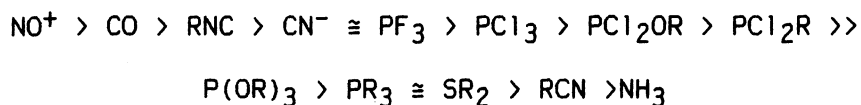
It is apparent from these two contrasting series that π-acceptor quality is, curiously, not a prerequisite. Gold(I) binds well to good σ-donor ligands. Possibly the d orbitals of the metal are too

different in energy to allow appreciable interaction with the empty π^*

orbitals of second and third row elements listed in the series.

Gold(I) has a d^{10} electronic configuration which results in a

ligand field stabilization energy of zero and is thus kinetically

labile. Reported examples of facile ligand exchange include the

following experiments: 1) ^{35}S-labelled thiourea substitutes a

coordinated ligand on bis(thiourea)gold(I) complexes (39); 2)

resolution of dissymmetric tetrahedral salts such as bis-(2-butenyl-

diethylphosphine)bis(diethyl-2-propenylphosphine)gold(I) is not

possible (40); 3) ^{1}H and ^{13}C NMR studies suggest that gold sodium

thiomalate (GST) exchanges with glutathione such that in one to one

ratios, approximately half the coordinated thiomalate is displaced and

that excess thiomalate added to aqueous solutions of aurothiomalate at

pH7 is in fast exchange with bound thiomalate (41,42); and 4) ^{1}H NMR

studies of (trimethylphosphine)methylgold(I) in benzene solution show

that exchange of free and bound phosphine occurs at the methylgold

centre in the presence of excess phosphine. The postulated mechanism

for this reaction involves the formation of a three-coordinate

intermediate (43). Evidence for this type of intermediate is readily

obtained as three and four coordinate gold(I) complexes with phosphine

ligands have been structurally characterized (44,45,46). Stable tris

and tetrakis thiolato complex formation is less likely because of

energetically unfavourable negative charge buildup

(i.e. $Au(SR)_4^{3-}$) (17).

Linear gold(I) complexes, like others of the late second and

third row transition elements, are subject to the _trans_ influence which

causes ligands to be bonded more or less tightly depending on the group opposite them (17). The _trans_ effect is closely related to the _trans_ influence in that, in the transition state, groups may be more or less labilized to displacement by the opposite ligand (38). The _trans_ influence of ligands bound to gold(I) must be assessed in some cases on the basis of results from other metals since, for example, few structures of gold(I) complexes with a thiolate ligand have been determined. It may be assumed that thiols are slightly weaker ligands than phosphines but these two types generally exert a strong _trans_ influence according to the following series (38);

$$CN^- \cong CO \cong NO \cong H^- > CH_3^- \cong PR_3 \cong SC(NH_2)_2 \cong SR_2 > SO_3H^- > NO_2^- \cong I^-$$

$$\cong SCN^- > Br^- > Cl^- > py > RNH_2 \cong NH_3 > OH^- > H_2O$$
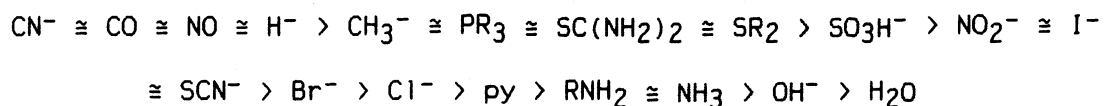
1.4 in vivo Chemistry;

A comparison of the metabolism of injectable and oral gold drugs can be made on the basis of similarities and differences in their chemistry. A summary of the metabolic properties of the compounds is found in Table 1.4.1. First of all, the origin of labelling the gold drugs as oral or injectable has metabolic implications. Why can gold sodiumthiomalate (GST) not be absorbed across the gut (47)? The answer may lie in the solubility properties of the two compounds. GST is a water-soluble, charged species where auranofin is hydrophobic and neutral. Biological membranes consist of phospholipid bilayers through which neutral compounds, of small enough size, may travel passively where active transport is required for charged species (48).

Table 1.4.1 Metabolic properties of oral vs. injectable gold

	ORAL	INJECTABLE
serum concentration		
bioavailability	• 25% of administered dose	• >95% of administered dose
steady-state	• 0.9 mg/L after 60-120 days following 6 mg/day schedule	• 3-5 mg/L after 35-70 days following 50 mg/week schedule
concentration ratio blood:synovial fluid	• 1.7:1	• 1.66:1
compartmentalization in serum	• 40-66% associated with cells remainder largely bound to albumin	• >90% albumin-bound ≅10% globulin-bound small molecular weight fraction
body retention	• 15% total dose eliminated via kidneys • <5% total body retention after 100 days	• 70% total dose eliminated via kidneys • >50% total body retention after 100 days

In support of this argument are inverted gut experiments performed by Tepperman et al. where auranofin was shown to pass through the membrane with the Et_3PAu moiety virtually intact although exchange of the thiol group was apparent (49). Decomposition of the compound into charged fragments did not occur in the acid medium of the stomach where only deacetylation of the sugar ligand has been observed (50). The trans influence of the phosphine ligand has been implicated where substitution of the thiolate is expedited and the Et_3PAu species moves across a chain of translocases whose function is to transport substrates through the membrane (48). Strength of binding of the thiosugar compared with the chloride ligand is also apparent in metabolic studies. Et_3PAuCl can be absorbed across the gut as well and is effective in treatment of adjuvant arthritis (23), but because chloride is a better leaving group, the compound is expected to be more reactive. This may be the source of reported gastro-intestinal discomfort experienced by patients in drug trials (23).

Because injectable gold drugs are introduced directly into the blood, serum levels are at their peak almost immediately after administration (51). A higher steady-state concentration is achieved with GST as larger quantities of gold are actually administered and body clearance is slower than with auranofin although percentage of serum gold which enters the synovial fluid is constant (52).

Albumin is a transport protein of unknown structure (though it has been sequenced (53)) found in high concentrations (0.65 mM) in serum (54). It contains a single cysteine thiol group thought to be located in a crevice approximately 0.95 nm deep, thus it is not

surprising that gold in either oral or injectable form with its affinity for thiols and labile nature would be found bound to albumin after thiol ligand substitution (16). Evidence for gold binding to albumin is supplied by Gerber who found that GST alters the heat and urea denaturation of serum albumin by preventing the formation of inter-protein disulphide bonds (55).

Auranofin has demonstrated its ability to bind to the surface of erythrocytes and even to penetrate the red blood cell (RBC) membrane in in vitro radio-labelling and ^{31}P NMR studies using whole blood (56-58). Once inside the cell, a likely binding site would be glutathione, a tripeptide present in approximately 5 mM concentration, which also contains a sulphydryl group (48). Gold from GST has also been reported to penetrate RBC's but this tends to occur in cases where the patient is a smoker. It is postulated that the presence of relatively more cyanide ion in the blood of smokers enhances formation of $Au(CN)_2^-$ which is capable of crossing RBC membranes (40). It is not known whether the ability of gold to enter RBCs is relevant to arthritis but it does lend insight into the differential biochemistry of the two types of anti-arthritic compounds.

In terms of toxicity, oral gold is better tolerated than injectable gold. Kidney toxicity is one the most potentially lethal side effects of gold treatment. Seventy percent of injectable gold is cleared from the blood by the kidneys where it enjoys relative longevity (58). Kidneys contain large amounts of the protein metallothionein which has several available sulphydryl sites implicated in the storage and intracellular homeostasis of metals such as copper

and zinc (59). Substantial quanities (35%) of GST administered to rats were found bound to metallothioneins in the cytosol (60). In comparison, only fifteen percent of the oral dose passes through the kidney (61). It has also been speculated that the passage of oral gold through the kidney is aided by the trans influence of the phosphine ligand allowing gold to transfer more readily from one thiol to the next (16).

In general, differences in the administration and chemical nature of the two types of drugs lead to distinct pharmacological properties. To summarize, orally absorbed gold administered daily in lower doses than the injectable form leads to more stable blood and tissue concentrations with less associated toxicity. However, results of clinical trials have shown that, although both gold drugs are significantly better than placebo, GST is the more effective drug in RA treatment (62-64).

1.5 Methods of observation of gold(I) complexes:

Elder has described gold(I) as a spectroscopically quiet nucleus (29); it is diamagnetic with a full d-shell giving rise to no useful ESR, magnetic or UV/VIS measurements. Although the [197]Au isotope is NMR-active, its large quadrupole moment precludes observation of a signal even with the highly symmetric AuF_6^- ion (65). [195]Au radio-labelling experiments have proven useful in the biological milieu where sensitive techniques are required to overcome difficulties associated with low concentrations. For example, the body retention statistics summarized in Table 1.4.1 were acquired from total body radiation

measurements on patients after administration of [195]Au-labelled oral or injectable drug (3,63). Studies using double-labelled GST ([199]Au and ^{35}S) in mice demonstrated dissociation of GST in vivo into protein-bound gold and free thiomalate (66). Similarly, investigations of radio-labelled auranofin with rat and dog blood indicate drug metabolism after oral ingestion. The postulated products are thioglucose, triethylphosphine oxide and protein-bound gold. This led to subsequent tests on adjuvant arthritic rats which suggest that the non-gold decomposition products of auranofin have no anti-inflammatory effect (23,67). Such results indicate that the therapeutic activity of the drugs resides in the gold component itself even though the thiolate ligands show marked similarity to the antirheumatoid drug d-penicillamine which has no metal component (68). Remarkably, radio-tracer studies have indicated that 90% of the Et_3P in auranofin is converted to the corresponding oxide within three days after drug administration (57).

1.5.1 Moessbauer spectroscopy;

The use of [197]Au Moessbauer spectroscopy in characterizing gold compounds has been reviewed (12). Because gold(I) has a full d-shell, isomer shift (IS) and quadrupole splitting (QS) parameters reflect directly the population of the 6s and 6p orbitals respectively. IS values are a measure of total s-electron density at the gold nucleus and those for QS give insight into the imbalance of electronic charge distribution about gold. An increase in the magnitude of each parameter is indicative of better electron donor ligands and an increased covalency in the bonds to neighbouring atoms. The lowest IS

and QS values are found for the gold(I) halides and get progressively larger as the ligand donor atom changes from nitrogen to sulphur to phosphorus to carbon. An effectively linear correlation is found between IS and QS parameters which suggests that parameters for mixed ligand complexes are the average of those for the two corresponding bis ligand complexes (12).

Moessbauer spectroscopy has not yet been used to its full capacity in the elucidation of structure of gold compounds. A case in point is the observation of Moessbauer parameters for "chloro(pyridine)gold(I)" and similar compounds for which the peak linewidths (Γ) are reported to be larger than those for other gold(I) compounds (69). Since the Moessbauer parameters were first reported for the pyridine compound, the correct structure has been determined (70), but no attempt has been made to refit Moessbauer data for the complex which is now known to contain two distinct gold sites.

1.5.2 ^{1}H and ^{13}C NMR spectroscopy;

Gold sodiumthiomalate (GST) has been characterized to a certain extent using NMR spectroscopy. The most dramatic coordination shift from free to gold-bound thiomalate is that experienced by the CH carbon adjacent to the sulphur atom which moves 5.32 ppm downfield (13). The populations of the three rotomeric isomers of thiomalate have been investigated by analysis of ^{1}H-^{1}H and ^{1}H-^{13}C three-bond NMR coupling constants. The results indicate that at pH7, the most populated rotomer is that in which the carboxylate groups are trans to each other. The effect of gold(I) coordination on the conformation of

thiomalate is small at low ionic strength. At high ionic strength or at low pH (i.e. 1) neutralization of carboxylate charges by added cations allows closer approach of components in solution and concomitant broadening of NMR peaks is suggestive of the formation of high molecular weight polymers with up to three different thiomalate environments. This is reversible upon dilution or neutralization (13).

Parallel studies of non-polar arenethiolate gold(I) complexes show that apparent equivalence of the organic groups is readily achieved by a rapid exchange process at 120°C (15). Three sets of signals in the ^1H NMR (ca.1:2:2) were resolved at ambient temperature. On the basis of the relative intensity ratio, a five-membered ring structure has been proposed. (An intramolecular exchange process such as ring flexing by inversion at the sulphur atoms is consistent with the pentameric formulation.) There is little concentration dependence of peak coalescence temperatures which supports an intramolecular mechanism. A connection is implied between the three ligand environments observed in solution of the non-polar gold thiolates and the similar behaviour of the polar gold thiolates in solutions of high ionic strength (15).

The formation of a new complex has been observed by Sadler in ^{13}C NMR upon reaction of excess thiomalate with GST and $Au_4(SR)_7^{3-}$ has been suggested as the ultimate product (71). Shaw has interpreted the results otherwise suggesting $Au(SR)_2^-$ is the ultimate product on the basis of the tendency of gold(I) to be two-coordinate (20).

Further studies in this vein are concerned with monitoring thiol exchange rates with use of ^{13}C NMR. For GST with excess free

thiol at pH7 the following order of binding strength is observed: ·cysteine methylester $\cong$ D-penicillamine $>$ β-D-thiolglucose $>$ N-acetylcysteine $>$ glutathione $\cong$ thiomalate $\cong$ mercaptoacetate. This trend reflects the order of pK_{SH} where the most strongly bound thiols are those with the lowest pK_{SH} values (72).

The bis phosphine species $(Et_3P)_2AuCl$ (also an anti-rheumatic drug) is ionized in aqueous solution and ^1H and ^{13}C NMR spectra of $(Et_3P)_2Au^+$ indicate that Et_3P exchange is slow in that the effects of virtual coupling are observed. In $CDCl_3$ or MeOD, exchange is slow only at low temperatures thus lability of the non-polar phosphine group is solvent dependent (50).

1.5.3 ^{31}P NMR

The introduction of gold-phosphine derivatives as anti-arthritic agents also supplied the research field with ^{31}P NMR spectroscopy as a tool for observation of drug chemistry.

Initial studies of the reaction of auranofin with whole blood confirmed previous experiments in that the gold phosphine moiety was partitioned between plasma (45%) and red cells (55%) (57). ^{31}P chemical shift values indicated that gold was bound to a thiol which may or may not be the original thiosugar of the drug (58). In fact, two different sites were observed and deduced to be glutathione and haemoglobin (cysβ93). The latter is present in RBCs at concentrations on the order of 4 mM (73). Both new peaks were shifted downfield from those of the free complex (42.2 and 40.2 ppm from 37.6 ppm relative to 85% H_3PO_4 with a 15% D_2O internal lock) (58).

A peak at 50.3 ppm arose when Et_3PAuCl was mixed with a relatively concentrated solution of glutathione (GtSH) (10 mM) in $D_2O/3\%$ MeOH and has been attributed to $(Et_3P)_2AuCl$ formed _via_ disproportionation (58).

$$ClAuPEt_3 + GtSAuPEt_3 \longrightarrow (GtSAu)_n + ClAu(PEt_3)_2$$
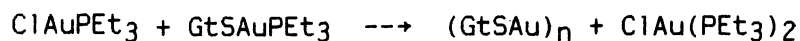
This peak assignment has been questioned by Shaw _et al._ who observed a similar resonance (41.1 ppm _vs._ $OP(OMe)_3$) in the reaction of albumin (AlbSH) or the S-protected AlbSSCy with Et_3PAuCl. An oligomer of AlbSH analogous to $(GtSAu)_n$ is not likely (20).

The bis complex has demonstrated its ability to denature albumin, probably by a redox reaction with the albumin disulphide link releasing a phosphine group which becomes oxidized to triethylphosphine oxide (Et_3PO) (68.5 ppm _vs._ $85\%H_3PO_4/15\%D_2O$ external reference) (58).

Thorough studies of the interaction of auranofin and Et_3PAuCl with albumin have been performed which involve ^{31}P NMR observation of products isolated by gel filtration chromatography in addition to direct analysis of reaction mixtures. Results indicate that both auranofin and Et_3PAuCl react at cys34 of albumin with retention of Et_3P and displacement of the anionic ligand to form $AlbSAuPEt_3$. Integration of the spectra give results in agreement with virtually quantitative gold binding (74,75).

Reaction of excess Et_3PAuCl with albumin gives rise to ^{31}P NMR peaks attributable to gold binding at weaker protein sites (27 and 28 ppm relative to $OP(OCH_3)_3$). Subsequent work suggests that these chemical shifts may indicate Et_3PAu^+ coordination to imidazole, lysine, carboxylate or thioether donor groups of albumin (76).

In chromatographed samples of excess Et_3PAuCl with AlbSH, a ^{31}P resonance at 35.9 ppm is postulated to represent a thiolate-bridged dimeric gold species $[(\mu\text{-}AlbS)(AuPEt_3)_2]^+$ and compares well with the 36.0 ppm resonance of $[(Et_3PAu)_2SATg]^+$. The albumin-digold species is detected only after removal of Cl^- and organic solvents from the reaction mixture. It is possible that the location of albumin's cys34 in a protein crevice may favour the binding of the second Et_3PAu^+ here over more exposed surface locations (74).

Also notable is the ability of auranofin to reverse the 'aging' process of albumin where the SH titer decreases over time. In other words, the oxidized form of AlbSH (probably the sulphinic acid) is slowly reduced and the released thiol from reaction of auranofin is the likely reducing agent. The possibility of Et_3PO as the reducing agent has been ruled out on the basis of ^{31}P NMR results. The amount of Et_3PO generated (<10%) was insufficient to account for additional gold bound to albumin with low SH titer (74).

Displacement of Et_3P and subsequent oxidation to Et_3PO has been established in vitro. It was determined that addition of HSAtg (which has the strongest affinity for gold) resulted in a larger extent of Et_3PO produced than HStg and HSGt in order. Oxygen was not necessary for the reaction. Disulphide bonds with thiols such as cysteine and glutathione comprise 30 to 40% of albumin in vivo and are the probable sources of oxidizing agent for triethylphosphine (77). Also, the phosphine oxide is apparently displaced from the gold-albumin complex but not from auranofin or deacetylated auranofin. The lability of the albumin gold-bound phosphine may be attributed to the exceptional

strength of the gold(I)-albumin bond in another example of trans

influence. The extent of Et_3P displacement is probably small but

subsequent oxidation drives the reaction toward Et_3PO.

1.6 Anti-cancer properties of gold compounds

Since Rosenberg's discovery of the antitumour properties of

cis-diamminedichloroplatinum(II) (cisplatin) (78-80), the possibility

of other metal complexes giving similar results has inspired extensive

investigation including the systematic examination of gold complexes

for their antitumour activity (81). During the course of continuous

screening a series of mono- and diphosphine gold complexes were

prepared and evaluated for DNA binding (by gel electrophoresis),

cytotoxicity and in vivo antitumour activity. Monophosphine complexes

such as Et_3PAuCl_3 showed DNA binding but were only marginally active in

vivo. Auranofin itself has demonstrated limited activity against He-La

cells, p388 lymphocytic leukemia and sarcoma 180 tumours in mice (82-

85) but not against other tumours (86). Recently, the thiolate bridged

complex $(Ph_3PAu)_2\mu\text{-}DTE$ (DTE=dithioerythritol) was tested and showed

significant activity in mice against the Erlich-Ascites tumour cell

(87). Analogous trialkylphosphine complexes of gold(I) are active;

potency depends on the phosphine group and is maximized by use of a

thiosugar as the second ligand (88). The gold(I) complexes of

1,2(diphenylphosphino)ethane (DIPHOS) $[(DIPHOS)AuCl_2]Cl$ and

$DIPHOS(AuCl)_2$ significantly cured p388 leukemia in mice (81). Thiolate

complexes containing the DIPHOS ligand i.e.$DIPHOS(AuTg)_2$ were also

tested and found to be active. This complex apparently reacts readily

with serum (perhaps with albumin) and the product is the bis(DIPHOS)

gold salt.   It has been postulated that this is in fact the actual

antitumour compound (89).   The ligand alone is cytotoxic to cancer cell

lines but cells made resistant to DIPHOS are killed by exposure to the

gold complex (89).   In fact, the DIPHOS ligand is likely the antitumour

agent and the gold complex is effective against DIPHOS-resistant cells

only because of a difference in carrier properties since analogous

copper compounds are also active (89).

Because of the electronic and structural similarity to Pt(II),

Au(III) could serve as a model for reactions of cisplatin with nucleic

acid constituents.   Interestingly, the cation $[Au(5-diazouracil)_2Cl_2]^+$

itself has been reported to posess antitumour activity in mice (90)

although the source of this activity is likely the 5-diazouracil

ligand.   In light of the strong oxidizing ability of $AuCl_4^-$, there are

reservations concerning the viability of Au(III) in a biological milieu

(see section 1.3), however, with the coordination of appropriate

ligands this oxidation state may become stabilized.   In the hard-soft-

acid-base context of Pearson (91), Au(III) should favour the relatively

harder N-donor ligands in contrast to gold(I) which forms strong bonds

with the softer S- and P-donors.   Thus the DNA bases could constitute

suitably relevant binding sites for Au(III) in vivo and investigations

of such binding have been carried out by the following experiments: 1)

viscometry and UV studies of $AuCl_4^-$ and DNA (92),

2) chromatographic investigations of gold(III)-adenine adducts (93), 3)

IR studies of Au(III) complexes with cytidine, uridine, AMP and GMP

(94), 4) synthesis and partial characterization of gold(III) and

gold(I) complexes with nucleosides such as inosine, guanosine and their triacetyl derivatives and cytidine (37) and gold(I) compounds with adenine, guanine, theobromine, theophylline, azaguanine and cytosine by conductivity, IR, ^{1}H NMR and Moessbauer measurements (95,96), 5) ^{1}H NMR studies comparing the interaction of gold(III) and platinum(II) or palladium(II) with cytosine (97), 6) X-ray crystallographic analysis of trichloro(1-methylcytosine)gold(III) (98) and 7) several experiments involving gel electrophoresis of pBR322 plasmid DNA after incubation with a variety of gold(III) and gold(I) compounds (99,100).

Other investigations involving gold(I) interaction with nucleobases have been restricted to in situ observation by UV and CD spectroscopies of Et$_3$PAuCl and nucleobases (101) and the crystal structure determination of the N(9)-bound adeninatotriphenylphosphine gold(I) (102). Recently, the preferred DNA binding site for the complex Et$_3$PAuBr$_3$ has been pinpointed as N(7) of guanine since alkylation at N(7) by dimethylsulphate is inhibited in the presence of this complex (103).

1.7 Objectives

The initial aim of the work reported in the following chapters was to synthesize and characterize compounds of gold(I) having the general formula L-Au-X where L=Et$_3$P and X=tetracetylthioglucose or chloride in the case of auranofin or its precursor. Substitution of L by ligands having comparable properties to Et$_3$P provide a means of studying gold(I) chemistry as well as the potential to examine the role, by comparison, of the phosphine ligand itself. Ligands

incorporated to this end included isocyanides, heterocyclic aromatic nitrogen donors and triphenylphosphine. Particular emphasis has been placed on the interaction of gold(I) compounds with DNA spurred by reports of the antitumour properties of auranofin (82-85). A discussion of these results is found in Chapter 3, Part A. Part B is devoted to some DNA binding studies of a number of gold(III) compounds.

The remainder of the thesis focusses on the chemical properties of compounds of the ligand tris-2-pyridylphosphine (TPP, see Figure 1.7.1). This ligand was chosen as a substitute for Et_3P for several reasons of which the most compelling is the availability of the relatively harder pyridyl nitrogen sites for binding to other metals in addition to the phosphorus site to which gold(I) is bound.

Syntheses of a variety of transition metal complexes of TPP and chloro(tris-2-pyridylphosphine)gold(I) (ClAuTPP) are reported in Chapter 5. When possible, characterization of these compounds was
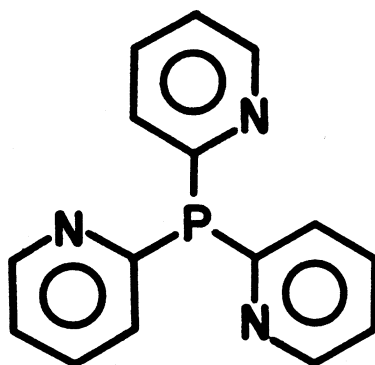
Figure 1.7.1 tris-2-pyridylphosphine (TPP)

carried out by single crystal X-ray diffraction techniques. Other techniques such as Moessbauer, electronic absorption, electron spin resonance and infrared spectroscopies have proven valuable to fill in the gaps where X-ray crystallography was not possible.

CHAPTER 2

EXPERIMENTS

2.1 Compound Preparation and Analysis

Details of compound preparation and purification will be given in subsequent chapters. Elemental analyses were performed by Atlantic Microlab, Atlanta, GA. Cultivation of crystals suitable for single crystal work involved either slow evaporation of solvent or crystallization from the appropriate sealed solvent mixture at 0°C.

Gold was obtained from two sources. Used electrodes were obtained and cleaned by scrubbing and bathing in concentrated HCl. The other source of gold was laboratory residue which was collected, treated with hydrazine, then filtered and washed with water. The resulting solid was ignited in a porcelain crucible over a Meker burner followed by heating in a 800°C oven overnight. The cleaned gold from either route was dissolved in aqua regia ($1HNO_3:4HCl$) which was heated, stirred and evaporated to low volume under an air stream. HCl was added with subsequent concentration of the solution. The HCl procedure was repeated twice more at which time, the solution was taken to dryness carefully to avoid thermal reduction of gold to the metal. The above is a modification of the procedure for recovery of platinum from laboratory residues (104).

2.2 X-RAY CRYSTALLOGRAPHY

The following discussion will focus on aspects of the crystallographic experiment which have had direct practical application in the solution and refinement of the structures presented in this thesis. The theoretical basis of single crystal X-ray crystallography as well as a broader description of a practical nature is treated by Buerger (105), Stout and Jensen (106), Luger (107) and Glusker and Trueblood (108).

2.2.1 Crystal Preparation;

Crystals to be used in the diffraction experiment were chosen on the basis of size, shape and homogeneity. Acceptable specimens were no larger than 0.5 mm to ensure uniform bathing of X-irradiation during data colection. Where possible, crystals were shaped by grinding to cylinders with use of emery paper to prevent inherent absorption effects of irregular shapes (see section 2.2.3.1). When crystals were soft and powdered on attempted grinding, they were either used as found or cut to approximately uniform dimensions. Suitable samples were then examined by rotation under a polarizing microscope where complete extinction every 90° indicated homogeneity. Crystals were mounted by wedging them in 0.2 mm or 0.3 mm diameter Lindemann capillaries or by gluing to the end of a fibre. The crystal of trichloro(chloro(tris-2-pyridylphosphine-P)gold(I)-N,N′,N")chromium(III) ((ClAuTPP)CrCl$_3$) required sealing within a capillary in the presence of mother liquor since crystals were prone to decomposition upon loss (by evaporation) of lattice solvent. Density measurements were made by suspending crystals in a mixture of two solvents, one less and one more dense than

the crystal itself. Density measurements used in conjunction with elemental analyses aided in the choice of the correct cell and space group (see eqn 2.2.1) determined by X-ray precession photography.

$$\rho = \frac{M \times Z}{0.6022 \times V(\text{\AA}^3)} \qquad \text{eqn 2.2.1}$$

where M is the molecular weight, Z is the number of molecules in the unit cell and V is the volume of the unit cell.

Verification of triclinic symmetry was accomplished by Delaunay reduction (179). Crystals were then transferred to a Syntex $P2_1$ or Nicolet P3 diffractometer and centered optically; the crystal was mounted, if possible, with its long dimension along the 2θ-ω axis to minimize errors in absorption correction (see Figure 2.2.1). A polaroid photograph of the crystal undergoing full θ-rotation was taken, generating vertical and horizontal 2-fold axes on the film relating Friedel pairs. Horizontal and vertical distances between symmetry related spots were converted to χ and 2θ values for the reflection. A centering routine was used to determine the location of each reflection more accurately. The set of reflections thus obtained was used to generate 30 indexed vectors in an arbitrary cell. Lengths of the vectors and the angles between them were used to assign unit cell parameters. The angles of properly indexed reflections were entered into a least-squares program to determine the orientation matrix which relates the crystal axes to the unit cell axes and diffractometer angles. This orientation matrix was used to drive the diffractometer angles to the appropriate locations for incremental **hkl** data collection.
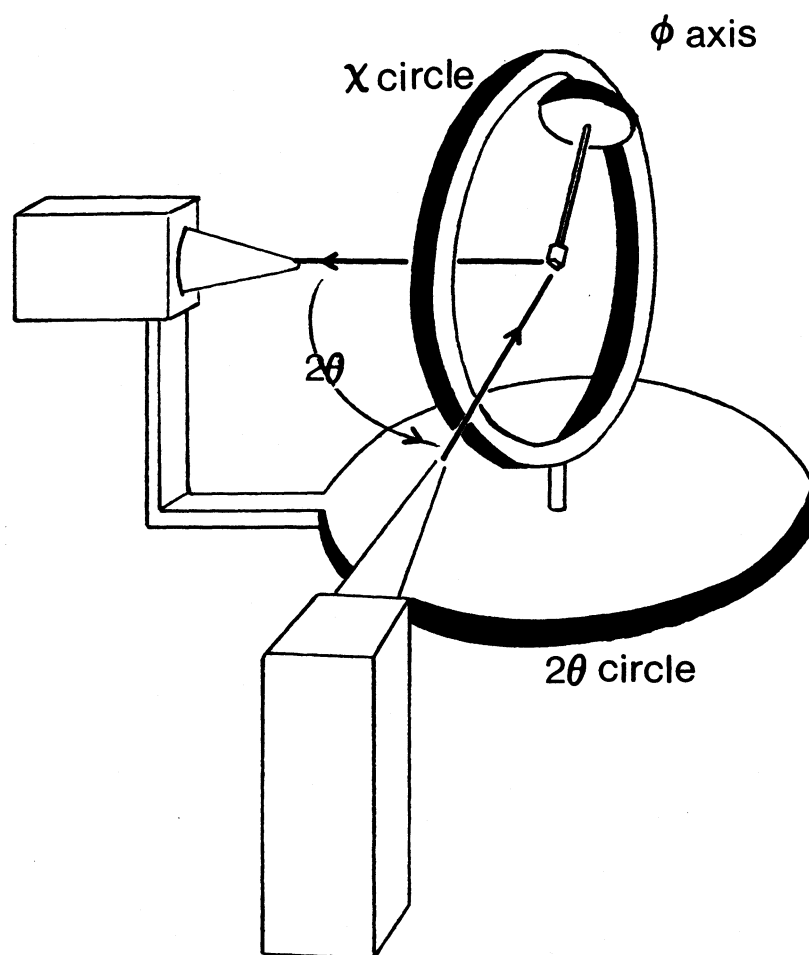
Figure 2.2.1   The four-circle diffractometer

2.2.2 Data Collection;   All data, with the exception of those for

(ClAuTPP)CrCl$_3$, were measured at room temperature. Low temperature

adaptation of the P3 required the introduction of a stream of cold

nitrogen gas passed along the ϕ axis (see Figure 2.2.1). To prevent

frosting on the capillary, a heater was used at the stream outlet to

warm the cold stream perimeter and another after the stream had passed

the crystal to disperse the cold gas. Software was programmed to

transform reflections with $75° \leqslant \chi \leqslant 90°$ to their Friedel equivalents to

avoid collision between the χ-circle and the low temperature equipment.

Intensities were measured with use of graphite monochromatized

MoKα radiation ($\lambda 0.71069$ Å) and a coupled θ(crystal)-2θ(counter) scan.

The minimum scan rate for a reflection was set at 5.0°/min.; limits for

the choice of scan rate for each reflection have been described in

detail elsewhere (109,110).

Intensities were measured with an upper 2θ limit of 45 - 55°.

The range of θ-values depended on the relative size (thus scattering

power) of the crystal. The range of **h,k,** and **l** was determined by

crystal symmetry and the lengths of the cell edges such that $2\theta_{max}$ was

the restricting value. Space group possibilities dictated what

fraction of available reciprocal space was required to make up a full

set of unique |Fo| data; at least two octants were collected in all

cases. Crystal stability was monitored throughout the course of data

collection by observation of two standard reflections (oriented at

approximately 90° to each other in ϕ) every 48 reflections. Intensity

(I) and its error (σI) were calculated according to procedures outlined

in the Nicolet reference manuals.

2.2.3 Preliminary Data Treatment;   Reflections with $3\sigma_I > I > -3\sigma_I$ were

treated by the method of French and Wilson (111) in all structures,

except 1-methylthyminato(triphenylphosphine)gold(I) and chloro(t-butyl-

isocyanide)gold(I).   Intensities were reduced to a more convenient

form, the structure factor modulus ($|Fo|$), by the following equation:

$$|Fo| = \left| \frac{(KIAbs)^{1/2}}{(Lp)^{1/2}} \right| \qquad \text{eqn 2.2.3}$$

In eqn 2.2.3, the term Abs represents the correction factor for an

observed intensity as a result of absorption, L is the Lorentz factor,

p is a polarization term and K is a scaling factor. These are

discussed below.

<u>2.2.3.1 Absorption;</u>   The effect of absorption on the intensity of X-

rays is

$$I = I_o e^{-\mu\tau} \qquad \text{eqn 2.2.4}$$

where I_o is the incident beam intensity, τ is the thickness of the

crystal, and μ is the linear absorption coefficient which depends on

the atomic absorber at a given radiation wavelength. The absorption

problem is compounded with crystals of irregular shape. This

introduces systematic errors into observed intensities. These errors

are expressed in terms of A^* - a transmission factor which is the

correction required to convert an observed intensity to its true value.

Values for A^* have been determined analytically for cylindrical

crystals and are listed as a function of $\mu/\rho R$ (R=crystal radius) and θ

by Bond in The International Tables for X-ray Crystallography (112).

In general, a range of A^*, calculated from maximum and minimum tracks

(R) through the crystal, which corresponded to variation in intensity

larger than 10%, was taken as criterion of the need to correct for absorption. This was done empirically with use of the program PSISCAN (113) whose operation involves the breakdown of A* into empirical and analytical components, thus $A^* = A_\psi^* A_\theta^*$. A_ψ^* is determined by monitoring the intensity variation of a given reflection of moderate intensity as the crystal is rotated 360° in 10° increments, about $\phi corr$ – the normal to the reflecting plane ($\phi corr = \phi - \omega \cos\chi$). Thus in each 2θ region studied, (up to 20 values spanning the data set), a curve of intensity vs. $\phi corr$ was plotted. Interpolating these curves, a value of A_ψ^* for each reflection was obtained. The effect of such data modification was to take the reflections obtained from an irregularly-shaped crystal and produce a set of reflections representing a hypothetically cylindrical crystal for which the Bond (112) correction (A_θ^*) could be applied.

2.2.3.2 Polarization: In general, an X-ray beam is partially polarized by reflection from a crystal plane; wave vector components parallel to the reflecting plane are unaffected by angle of incidence but the perpendicular component is dependent on 2θ. Corrections must be made for this polarization. The corrections vary with the geometry of the measuring system. In the present case, the correction for polarization of the monochromator as well as the sample crystal is given in the Nicolet diffractometer manual.

2.2.3.3 Lorentz factor: The Lorentz factor, applied in DATARDN (117), arises because the time required for a reciprocal lattice point to pass through the Ewald sphere depends on its position in reciprocal space and the direction from which it approaches the sphere.

2.2.3.4 Merged reflections; Symmetry equivalent reflections were averaged and an indication of discrepency is given by the figure of merit $R_{internal}$ (R_{int}) given in equation 2.2.5.

$$R_{int} = \frac{(\Sigma(N \times \Sigma(w(\langle F\rangle - F)^2)))^{1/2}}{(\Sigma(N-1)\Sigma wF^2)^{1/2}} \qquad \text{eqn 2.2.5}$$

where the inner summations are over N equivalent reflections averaged to give $\langle F\rangle$ and outer summations are over all unique reflections. The weighting factor $w = \sigma_c^{-2}(Fo)$ and σ_c is the estimated standard deviation in Fo from counting statistics (116).

2.2.4 Structure Solution and Refinement; The structure factor $|Fc|$, is a quantity which can be calculated on the basis of the model of electron density within the crystal. The structure factor is defined as the sum of all waves scattered in the direction of the hkl reflection from the atoms in the structure such that

$$Fc_{hkl} = \sum_j f_j e^{i\delta_j} \qquad \text{eqn 2.2.6}$$

The amplitude of the scattering factor, f_j, is the scattering power for the jth atom with respect to that of a single hypothetical electron and $\delta_j = 2\pi(hx + ky + lz)$ is the phase of the reflected wave relative to the origin of the cell. The scattering factor is a function of atom type and $(\sin\theta/\lambda)$. Scattering power decreases at larger angles as rays scattered from one part of an electron cloud are to an increasing extent out of phase with scattered rays from another part. This effect

increases for atoms with larger atomic numbers because corresponding

electron clouds are increasingly diffuse (see Figure 2.2.2).

Scattering factors were supplied by Cromer and Waber in Table 2.2A of

the International Tables (114).

Scattering factors for heavy atoms were corrected for anomalous

dispersion effects where

$$f = f_o + \Delta f' + \Delta f''$$ eqn 2.2.7

Anomalous dispersion occurs when the frequency of the X-ray beam falls

near a natural absorption frequency of an element causing a phase

change to occur during scattering by electrons associated with the

absorption edge. Values for $\Delta f'$ and $\Delta f''$ were taken from Cromer and

Ibers (Table 2.3.1 of the International Tables) (115).

Scattering factors are calculated on the basis of electron

distribution in a stationary atom when, in fact, the effect of thermal

motion is to spread the electron cloud over a larger volume and cause

the real scattering power to fall off more quickly than in the ideal

atom; an effect reflected by the expression $\exp(-B(\sin^2\theta)/\lambda^2)$.

$$B = 8\pi^2 u^2$$ eqn 2.2.8

where u is the mean square amplitude of atomic vibration and is more

explicitly described in three dimensions at the final stages of

refinement by the equation of an ellipsoid.

$$T = \exp[-2\pi^2(U_{11}h^2a^{*2} + U_{22}k^2b^{*2} + U_{33}l^2c^{*2} + 2U_{12}hka^*b^*\cos\gamma^*$$

$$+ 2U_{13}hla^*c^*\cos\beta^* + 2U_{23}klb^*c^*\cos\alpha^*)]$$ eqn 2.2.9

where U_{ij}'s are anisotropic thermal parameters expressed in terms of
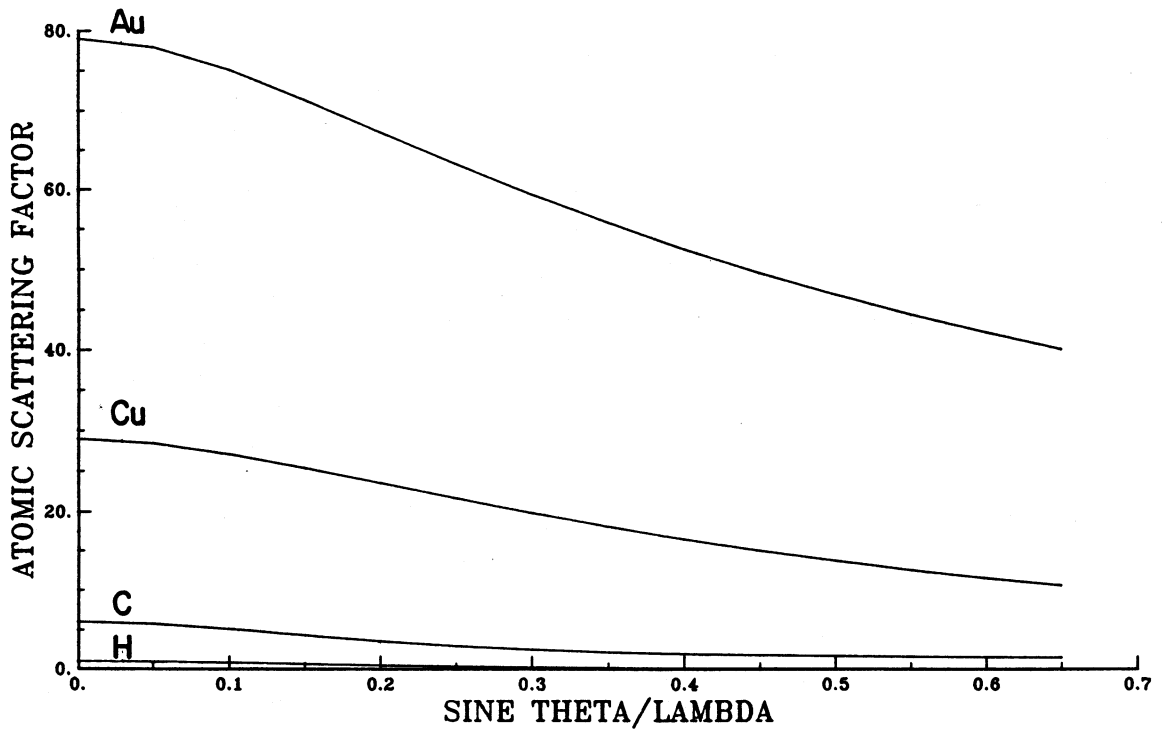
Figure 2.2.2   The relationship between atomic scattering factor and
sine θ/λ for gold, copper, carbon and hydrogen.

mean square amplitude of vibration along the principle axes of the
ellipsoid ($i=j$) and the ellipsoid orientation ($i\neq j$). **a***, **b***, and **c***
are the reciprocal cell axes. Thus the structure factor may be
explicitly expressed as

$$F(\mathbf{hkl}) = \underset{hkl}{\Sigma\Sigma\Sigma} (f_{j,2\theta} + \Delta f' + \Delta f'') \exp(i\delta_j) \exp(-T_j) \quad \text{eqn 2.2.10}$$

Measured intensities contain only the amplitude of the
structure factors (Fo^*) thus phase (δ_{hkl}) must be derived from a model
structure. Because the arrangement of atoms in the model structure
(and the actual one) is periodic, the image of the structure is
obtained from a Fourier transform of the structure factor such that

$$\rho_{(xyz)}=(1/V) \underset{hkl}{\Sigma\Sigma\Sigma} Fo^* \exp(-2\pi i(hx + ky + lz) \quad \text{eqn 2.2.11}$$

where $\rho_{(xyz)}$ is the electron density at the point xyz and V is the unit
cell volume.

As a result of Friedel's law which states that $|F_{\mathbf{hkl}}|=|F(\mathbf{\overline{hkl}})|$,
eqn 2.2.11 collapses to

$$\rho_{(xyz)}=(1/V) \underset{hkl}{\Sigma\Sigma\Sigma} |Fo| \cos(2\pi(hx + ky + lz) - \delta_{hkl}) \quad \text{eqn 2.2.12}$$

An approximate solution to the Fourier series is obtained for a
model structure where identities and estimated positions of atoms are
used to calculate structure factor amplitude and phase. The Patterson
method was used to this end in all but the case of bis(chloro(tris-2-
pyridylphosphine)gold(I))copper(II) dinitrate (($ClAuTPP)_2Cu$) to arrive

at positional parameters for relatively heavy atoms present in the unit

cell. The method consists of evaluation of a Fourier series for which

$|F^2|$ (i.e. intensity) for each reflection is used.

$$P(uvw)=(1/V) \sum_{hkl}\sum\sum |F^2| \cos(2\pi(hu + kv + lw)) \qquad \text{eqn 2.2.13}$$

where u,v,w is a vector between points of electron density. When

electron density at points x,y,z and x+u,y+v,z+w is large (i.e. where

heavy atoms are located), Patterson density at u,v,w is also large.

Solution of a Patterson map requires knowledge of the symmetry

operations relating heavy atoms so that their position may be deduced

from corresponding u,v,w vectors.

The direct phasing method of SHELX (116) was employed for the

solution of the structure of $(ClAuTPP)_2Cu$ which contains two gold and

two copper atoms in the asymmetric unit.

Further development of trial structures was accomplished with

use of difference syntheses. Phases calculated from the model

structure were applied to $|Fo|$ as well as $|Fc|$ and the Fourier

transform of ΔFj (ΔFj = $|Fo|exp(i\delta_{hkl})$ - $|Fc|exp(i\delta_{hkl})$) was obtained

to give information on electron density insufficiently accounted for.

For example, unassigned electron density would show up as a peak in the

difference map. Hydrogen atom positions were calculated and fixed for

all structures except those of dichloro[bis-N,N-(2-hydroxyethyl-

dithiocarbamato-S,S'-]gold(III) where hydrogen atoms located and fixed

and tris-2-pyridylphosphine where hydrogen atoms were located and

refined. Refinement of atomic positional and thermal parameters (which

influence $|Fc|$) involved the method of least-squares minimizing the
quantity $\Sigma w(|Fo|-|Fc|)^2$. Structure solution was considered complete
when a comparison of final $|Fo|$ and $|Fc|$ values yielded suitable (<0.10
in most cases) figures of merit R and Rw summed over all reflections.

$$R = \frac{\Sigma(|Fo|-|Fc|)}{\Sigma|Fo|} \quad , \quad Rw = \frac{(\Sigma w(|Fo|-|Fc|)^2)^{1/2}}{(\Sigma w|Fo|^2)^{1/2}} \qquad \text{eqn 2.2.14}$$

where w is a weighting parameter equal to $(\sigma_c^2(Fo) + gFo^2)^{-1}$. The
parameter, g, represents errors from sources other than counting
statistics such as instrument and crystal instability, and is normally
given a value of the same order as the square of the deviation of the
standard reflections since these are used to monitor such
instabilities.

Other criteria for judging satisfactory structure completion
were used in combination with R values. S (error in observation of unit
weigh) is an assessment of the weighting scheme and for an ideal case
approaches unity.. It is calculated by the equation

$$S = \frac{(\Sigma w(|Fo|-|Fc|)^2)^{1/2}}{(m-n)^{1/2}} \qquad \text{eqn 2.2.15}$$

where the summation is over all reflections, m is the number of
reflections and n is the number of parameters (116). Least-squares
refinement was considered finished when maximum and average
shifts/error of atomic parameters had reached values <0.1. Residual
peaks and valleys in the difference map were examined. Minor

variations (<1.0 eÅ^{-3}) normally arise from series termination errors. Peaks greater than this were examined to see whether they could be assigned as an atom (or the result of a misplaced atom). In all cases they were found near the heavy atoms in the structure.

In the case of acentric structures (1-methylthyminato-N^3-triphenylphosphinegold(I) and dichloro[N,N-bis(2-hydroxyethyl)-dithiocarbamato-S,S']gold(III)) alternative refinements were tested where atomic position x,y,z were replaced by -x,-y,-z. R values (|Fo| and |Fc|) were compared to confirm assignment of the correct hand for the structure made possible because of anomalous dispersion effects.

Lists of |Fo| and |Fc| for each structure are found in the microfiche appendix of this volume.

2.2.5 Computer Programs

Computations were performed on CYBER 170/730 and 815 and VAX 8600 and 8650 mainframe computers. The programs DATCO5 and DATARDN from the XRAY76 package (117) and STARTX, DIFDAT, SORTREF and ADDREF from the XTAL program suite (118) were used for preliminary data treatment. Structure solution and refinement was accomplished with use SHELX (116), geometry calculations employed MOLGEOM (119), NRC 22 (120), LSQPL (118) and CHEMX (121), and diagrams were prepared with use of ORTEP II (122) and SNOOPI (123).

2.3 Vibrational Spectroscopy

Most samples for infrared spectroscopy (4000-250 cm^{-1}) were prepared as KBr pellets (5-10% w/w). Liquid samples and nujol mulls

were held between NaCl discs. Spectra were recorded on a Perkin Elmer 283 spectrometer with use of polystyrene film calibrant. Spectra in the 500-100 cm^{-1} range were obtained on an indene-calibrated Nicolet 7199 FT-IR spectrometer as nujol mulls between polyethylene plates. Raman spectra were obtained from powdered samples. A Coherent Radiation Argon Laser Model 52 generated the λ514.5 nm exciting line. Spectra were calibrated against powdered $HgCl_2$ and recorded on a SPEX 14018 recorder with a reproducibility of $\pm$ 3 cm^{-1}.

2.4 NMR Spectroscopy

^1H and natural abundance ^{13}C magnetic resonance spectra were recorded on a Bruker WM-500 spectrometer. Additional proton spectra were obtained on a Varian EM 390 spectrometer with use of TMS or TSP as an internal reference. ^{13}C spectra were recorded on a Bruker WP-80 FT-NMR spectrometer with use of D_2O as an external lock. ^{31}P spectra were recorded on a Bruker WM-250 FT-NMR spectrometer with use of D_2O as an external lock and 85% H_3PO_4 in D_2O as an external reference.

2.5 Electron Spin Resonance Spectroscopy

Spectra were recorded on a Bruker ER 100D spectrometer equipped with a Variable Temperature Unit. The TE4101 microwave cavity was used with a Bruker ER 040 X microwave bridge. Spectra were calibrated externally with use of Mn^{2+}.

2.6 Ultraviolet/Visible Spectroscopy

Spectra were obtained in the 800-200 nm range on a Perkin Elmer

Lamda 9 UV/VIS/NIR spectrometer.

2.7 Moessbauer Spectroscopy

Moessbauer spectra were recorded with an Elscint MFG-N-5 Moessbauer function generator, Elscint MDF-N-5 Driver/Generator and an MVT-4 transducer operating in sinusoidal waveform mode. Transmitted radiation was detected by an Aptec (500 mm^2 x 10 mm) planar germanium detector and processed with use of a Canberra 2022 linear amplifier and CMTE Multichannel Data Processor controlled by an IBM PC/AT microcomputer.

The source used for ^{197}Au spectra was ^{197}Pt foil (14-20 mCi) produced by irradiation of ^{196}Pt (86%) for 4-6 hours at ca. 1.5 x 10^{13} $cm^{-2}s^{-1}$ neutron flux in the McMaster University Nuclear Reactor. Powdered absorber samples contained 0.05-0.15 gcm^{-2} of ^{197}Au and both sample and source were cooled to 4.2K with use of a Janis Research Corp. cryostat. Isomer shifts were referenced to Au foil (0.025 mm thickness) obtained from Ventron Corp.

^{57}Fe spectra were run at 77K with use of a Technology Systems cryostat. The source used was ^{57}Co/Rh (25 mCi) obtained from Amersham International. Isomer shifts were referenced to Fe foil.

A standard Fe foil absorber and the ^{57}Co/Rh source were used to calibrate the velocity scale for experiments on both nuclei.

Folded spectra were computer-fitted with use of the program GMFP (124) to either single lines or quadrupole doublets in the Lorentzian approximation.

2.8 Agarose Gel Electrophoresis

Compounds to be tested were dissolved in DMSO or DMF and diluted with deionized water to nanomolar concentrations. Samples of P63 and PuC119 plasmid DNA were obtained from Dr. C.Harley, Department of Biochemistry, McMaster University. They were diluted with water to 10^{-3} μg/mL concentrations. 10 μL of this DNA solution were mixed with 10 μL of tricine buffer (50 mM solution, pH 8.1) and incubated at 37°C with varying amounts of compound solution.

Electrophoresis buffer (5X) consisted of the following mixture; 54 g tris base, 27.5 g boric acid, 3.72 g EDTA (pH 8.0), in 1 L of water. This buffer was diluted with water in 1:4 proportions to make 1X buffer which was used as the actual electrophoresis medium.

Gels were prepared by dissolving 1.2 g of electrophoresis grade agarose in 25 mL of 5X buffer and 100 mL water (10% agarose). Boiling of the mixture was necessary for dissolution of the agarose. The solution was allowed to cool to 55°C before pouring into the electrophoresis apparatus.

DNA solutions were loaded into wells in the stiffened gel after addition of 10 μL of a loader solution (0.1% bromphenol blue, 40% sucrose, and 10^{-5} M NaN_3).

Gels were run at 4°C at varying voltages (35-80 v) for varying lengths of time (3-12 hours). They were developed by soaking in a solution of 250 μL of 10 mg/mL aqueous ethidium bromide and 250 mL of 1X buffer. Exposure of the developed gel was then achieved by irradiation with UV light. In each experiment, at least one lane containing only DNA, tricine and loader was reserved for control.

2.9 Ames Assays (125)

Ames assays were carried out with use of the Salmonella typhimurium TA102 strain of bacteria. This line of cells has been cultivated such that, because of mutation, bacteria are deficient in the enzyme required for production of the amino acid histidine. Normal S. typhimurium can synthesize their own while the TA102 strain must be supplied with histidine in order to survive. In the presence of a mutagenic compound, TA102 cells may undergo further mutation restoring function to the altered gene and resulting in cells which can now survive without an external source of histidine. These cells, having recovered their normal viability, will grow and produce colonies of "revertants". Numbers of revertants are dependent upon concentration of added mutagen and well as its potency.

TA102 cells are susceptible to DNA frame shift and base substitution types of mutations and is capable of detecting cross linking agents which are poorly recognized by other more common tester strains. This sensitivity is attributed to the A=T base pairs at the site of mutation rather than the more stable G≡C pairs. An acceptable range of spontaneous reversion for TA102 is 240-320 revertants per plate while incubation with cisplatin gives rise to >1000 revertants at concentrations comparable those used for the gold compounds described below and in Table 3.4.A.

Minimal glucose plates were prepared under sterile conditions in batches of approximately 350 plates (100 x 15mm). Agar (14 g) was added to each of 12 conical flasks containing 710 mL of water. Dissolution was accomplished during autoclaving at 121°C for 30

minutes. Sterile 40% D-glucose solution (40 mL) and Vogel-Bonner
Medium E (50 mL) were mixed into each flask and solutions were allowed
to cool before plates were poured under standard sterile conditions.
Plates were stored at 4°C until used.

Bacteria were innoculated into Oxoid Growth Media (2.5% Oxoid
Medium) and agitated at 37°C for approximately 12 hours. Concentration
of cells was 1-2 x 10^9 cells/mL measured by optical density at λ650 nm
to ensure sufficient bacterial growth for the experiment. Aliquots of
100 μL of bacteria were incubated at 37°C on the prepared plates with
varying amounts of gold compounds (previously dissolved in sterile DMSO
or water to concentrations of approximately 1 mg/mL) and 2 mL of a
solution of top agar containing histidine. After three days, the
plates were counted with use of a New Brunswick Scientific Plate
Counter. A positive (cisplatin or adriamycin) and negative (DMSO)
control was run as a parallel assay in each experiment.

CHAPTER 3

THE INTERACTION OF GOLD COMPLEXES WITH DNA

3.1 General Introduction

The possible use of gold salts as anti-tumour agents has been investigated only to the extent of systematic compound screening in several animal cancer cell lines such as HeLa, p388 leukemia, sarcoma 180, Erlich-ascites tumours and murine tumours. Of the compounds screened all those reported to have any activity, with the exception of [(5-diazauracil)$_2$AuCl$_2$]Cl, contained a phosphine ligand. Other ligands incorporated into these complexes were limited to chloride or thiols. It has been shown by NMR studies (see section 1.5.2) that these ligands are quickly replaced in solution as a result of a) poor affinity for the metal in the case of chloride, b) lability of gold(I) in general and c) the trans effect of the phosphine ligand (16,17). Interestingly, easy displacement by hydrolysis of the chloride ligands of cisplatin within a tumour cell is thought to be necessary to its activity (126). NMR studies have also shown that the phosphine ligand itself is eventually displaced from gold (50). The subsequent oxidation to the phosphine oxide may have toxic effects in vivo.

A study of the possible anti-cancer effects of gold compounds was undertaken with the aim of A) synthesizing gold(I) compounds such that the phosphine ligand is replaced by less potentially harmful ligands and observation of the interaction of these complexes with DNA, B) examining possible models for gold(I) binding to DNA and C) investigating the interaction of gold(III) complexes with DNA.

PART A

GOLD(I) COMPOUNDS ANALOGOUS TO AURANOFIN

3.2.1 Introduction

The preparation of gold(I) compounds analogous to those which

show anticancer properties involved replacement of the phosphine by

those ligands which have similar electronic properties. Phosphines are

known to be good electron donors, good π-acceptors, good _trans_

directors, relatively polarizable (soft), and neutral (38). Isocyanide

ligands also meet these criteria and synthesis of the chlorogold(I)

complexes of t-butylisocyanide, phenylisocyanide and

diphenylaminocarbene as well as bis(t-butylisocyanide)gold(I)PF$_6$ and

bis(phenylisocyanide)PF$_6$ are reported in section 3.2.2.

The N-donor ligands guanine, theophylline, cytosine, and

nicotinamide were also employed as phosphine-substitutes. The

synthetic approach to these compounds was based on the patented

preparation for chloro(pyridine)gold(I) (127). The rationale behind

the choice of ligands such as the above was that these would be

biologically non-toxic upon displacement from the metal _in vivo_.

3.2.2 Preparations

(t-butylisocyanide)chlorogold(I); The method used to prepare this

compound is different from those reported by McCleverty and da Mota

(128) and Eggleston _et al._ (129) to avoid the necessity of working with

excess isocyanide.

HAuCl$_4$ (1.5261 g, 6.8 mmol) was dissolved in 40 mL of water at

0°C. Thiodiglycol (0.725 mL, 13 mmol) in 2 mL of ethanol was added

dropwise to the stirred gold solution. A transient yellow precipitate formed during this addition, followed by the production of an orange gum which settles out of a pale yellow solution. (This was a common observation for all preparations involving thiodiglycol reduction of $HAuCl_4$ in aqueous solution). T-butylisocyanide (0.410 mL, 6.8 mmol) in 10 mL of ethanol was added dropwise. The colourless product precipitated immediately but stirring was continued until the orange gum was consumed (ca. 30 minutes). The precipitate was filtered and dried on a vacuum line. The product was dissolved in acetone and reprecipitated by the addition of hexanes to yield 1.45 g (4.6 mmol) of a white crystalline solid (67.6%). Analysis required for C_5H_9AuClN:

C;19.0, H;2.9, N;4.4, Cl;11.3%. Found: C;19.1, H;2.9, N;4.4, Cl;11.3%.

IR: νCN; 2248, $\nu Au-Cl$; 353, 345 cm^{-1}

^1H NMR ($CDCl_3$)(EM390): 1.6 ppm(s)

^{13}C NMR ($CDCl_3$)(WP80): 30.08 ppm(s), 53.41 ppm(t;J_{CN} 5.0 Hz),

153.33 ppm (t;J_{CN} 3.6 Hz).

^{197}Au Moess: δ; 3.46(2) mm/sec, Δ; 7.86(5) mm/sec, Γ; 1.85(8) mm/sec.

bis(t-butylisocyanide)gold(I) hexafluorphosphate; According to the method of McCleverty and da Mota (128), 0.3594 mL (1.1 mmol) of t-butylisocyanide was added to a stirred solution of 1.0025 g (1.1 mmol) of (t-butylisocyanide)chlorogold(I) in 40 mL of acetone. A 10 mL acetone solution of 1.7 g (10 mmol) of NH_4PF_6 was then added to produce an immediate white precipitate. The reaction mixture was allowed to stir for 45 minutes at which time the precipitate was filtered and washed with water until no chloride could be detected in the washings. Analysis required for $C_{10}H_{18}AuF_6N_2P$: C;23.6, H;3.6, N;5.5%. Found:

C;23.8, H;3.6, N;5.5%.

IR: νCN; 2251, νPF; 830 cm-1

chloro(phenylisocyanide)gold(I); Phenylisocyanide was prepared according to literature methods (130). The synthesis of the gold(I) complex was analogous to that for the t-butylisocyanide complex.

IR: νCN; 2233, νAuCl; 355, 346 cm-1.

chloro[bis(phenylamino)carbene]gold(I); Similar to the preparation of chloro[bis(p-tolylamino)carbene]gold(I) (131), 0.0831 g (0.25 mmol) of chloro(phenylisocyanide)gold(I) was suspended in 10 mL of diethyl ether. Aniline (0.045 mL, 0.5 mmol) was added and the mixture stirred for 7 days. The white precipitate produced was filtered and purified by dissolving it in CH_2Cl_2 followed by reprecipitation with hexanes to give 0.092 g of product (86% yield). Analysis required for $C_{13}H_{12}AuClN_2$: C;36.4, H;2.8, N;6.5, Cl;8.3%. Found: C;36.4, H;2.8, N;6.5, Cl;8.3%.

IR: νNH; 3260, νAuCl; 328 cm-1

chloro(nicotinamide)gold(I); This complex was prepared by a modification of that reported for chloro(pyridine)gold(I) (127). $HAuCl_4$ (0.4861 g, 1.2 mmol) was dissolved in 20 mL of water at 0°C. After thiodiglycol reduction (addition of 0.247 mL (2.4 mmol) in 1 mL of ethanol), 1.5 g (6.2 mmol) of nicotinamide in 20 mL of ethanol was added (ca. 5-fold excess). After 30 minutes, the solution was evaporated under reduced pressure to 10 mL. The white precipitate was filtered and washed with water, then dried under vacuum in the dark. Analysis required for $C_6H_6AuClN_2O$: C;20.3, H;1.7, N;7.9, Cl;10.0%. Found: C;20.3, H;1.7, N;7.9, Cl;10.0%.

3.2.3 Discussion of the syntheses;

Attempts were made to modify the patented synthesis of chloro(pyridine)gold(I) in the preparations of guanine, theophylline, cytosine and nicotinamide complexes in order to avoid problems in the work-up associated with excess starting material. Stoichiometries of 1:1 N-donor ligand:gold were used with other factors remaining constant, but products thus obtained were highly unstable to decomposition and rapidly turned grey as metallic gold was deposited. Excess ligand in the reaction mixture was necessary to overcome this decomposition, possibly in order to stabilize the complexes in solution rather than leaving the bare AuCl moiety to disproportionate irreversibly.

An excess of ligand was not required in the preparation of the t-butylisocyanide or phenylisocyanide complexes and 1:1 stoichiometry was sufficient for the isolation of stable complexes.

Conclusions may, therefore, be drawn as to the relative strength and stability of the gold(I)-isocyanide bond compared to gold(I)-aromatic nitrogen. The implications of this are discussed further in section 3.2.5.

Other unsuccessful synthetic reactions give insight into the chemistry of gold(I) complexes. For example, removal of chloride with $AgNO_3$, $AgClO_4$ or $AgPF_6$ from the chloro(phosphine)gold(I) complexes R_3PAuCl (R=Ph,Et) yields stable cationic salts. Similar reactions with the isocyanide complexes result in unstable cations which rapidly decompose. Also, auranofin is prepared through substitution of the chloride in Et_3PAuCl with tetra-O-acetylthioglucose (132) but during

analogous reaction with isocyanide complexes the volatile isocyanide is also replaced to form a gold-tetra-O-aceteylthioglucose polymer.

3.2.4 The crystal and molecular structure of (t-butylisocyanide)chloro gold(I):

Crystal data and other details of data collection and structure refinement are summarized in Table 3.2.1. Atomic positional parameters and anisotropic temperature factors are listed in Table 3.2.2 and 3.2.A respectively. The molecule is illustrated in Figure 3.2.1 and selected interatomic distances and angles are given in Table 3.2.3. All data are comparable to those reported in the concurrent structure determination published by Eggleston et al. (129).

The coordination environment of the gold atom is linear and the Cl, Au, C(1), N, C(2), C(4), and H(4) atoms lie on a crystallographic mirror plane. The Au-Cl distance (2.248(4) Å) is typical of Au(I)-Cl bonds (68). The Au-C(1) distance (1.92(1) Å) is identical within error to that reported by Eggleston et al. (129) who attribute its length to a certain amount of back-donation of electron density onto the t-butylisocyanide ligand as compared to the Au-C(isocyanide) distance in cyano(methylisocyanide)gold(I) (1.98(5) Å) (133). Although the two Au-C distances indeed appear different, this difference is only marginal after consideration of experimental errors and the infrared results discussed in section 3.2.5 indicate that there is, in fact, very little, if any, back-donation into the C=N bond.

The angles around C(2) (C(4)-C(2)-C(4′) 115(1)° and C(3)-C(2)-C(4) 110.9(9)°) are evidence for considerable sp^2 character exhibited

Table 3.2.1 Crystal Data for chloro(t-butylisocyanide)gold(I)

Formula	C_5H_9AuClN
Formula weight	315.5
Crystal size and shape	0.2mm radius sphere
Systematic absences (Pnma)	h00;h=2n hk0;h=2n
	0k0;k=2n 0kl;k+l=2n
	00l;l=2n
Space group	Pnma
Diffractometer	P3
Temperature	22°C
Unit cell parameters	a=12.964(3)Å V=1116.2(5)Å^3
	b=6.622(2)Å Z=4
	c=9.725(2)Å
ρ_{calc},ρ_{obs}	2.51, 2.53gcm^{-1}; ZnBr$_2$(aq)
Range of **hkl**	0<h<16, 0<k<8, -12<l<12
Maximum 2θ	55°
Number of reflcns measured	2191
Number of independent reflcns	993
Standard reflcns(e.s.d)	4 1 3 (1.2%), 2 2 0 (1.2%)
R_{int}	0.0292
Final R,Rw	0.0715, 0.0607
Final shift/error max(ave)	0.104(0.013)
Error in obs of unit weight	S=1.3736
Highest peak, lowest valley	2.0eÅ^{-3},-2.0eÅ^{-3}
Weighting	w=(σ^2(F) + 0.000769 F^2)$^{-1}$
F(000)	827.86
Linear Absorption coefficient	μ=183.8cm^{-1}
Absorption Coefficient limits	29.7<A*<67.8*
Number of Variables	47

* absorption correction applied

Table 3.2.2 Positional parameters ($\times 10^4$) and U_{eq} ($\mathring{A}^2 \times 10^3$) for chloro(t-butylisocyanide)gold(I).

Atom	x	y	z	U_{eq}
Au	5181.8(2)	2500	4190.7(6)	58.4
Cl	3735(3)	2500	2917(5)	82.1
C(1)	6463(14)	2500	5203(17)	61
N	7237(11)	2500	5750(13)	60
C(2)	8215(11)	2500	6496(16)	59
C(3)	8760(10)	617(25)	6108(15)	97
C(4)	7945(17)	2500	8021(19)	91
H(4)	8691	2500	8712	
H(44)	7663	1197	8160	
H(3)	9382	377	6622	
H(33)	8955	903	5305	
H(333)	8459	-500	6346	

$U_{eq} = 1/3(U_{11} + U_{22} + U_{33})$

Hydrogen atoms were located and fixed with isotropic temperature factors of $U = 0.06 \mathring{A}^2$.

Table 3.2.3 Selected Bond Distances (Å) and Angles (°) for
chloro(t-butylisocyanide)gold(I)

Au-Cl	2.248(4)	Au-C(1)	1.93(2)
C(1)-N	1.14(2)	N-C(2)	1.46(2)
C(2)-C(3)	1.48(2)	C(2)-C(4)	1.52(2)
Au····Au	3.696()		
Cl-Au-C(1)	177.2(5)	Au-C(1)-N	177(2)
C(1)-N-C(2)	178(2)	N-C(2)-C(3)	106.7(9)
N-C(2)-C(4)	107(1)	C(3)-C(2)-C(4)	110.9(9)
C(4)-C(2)-C(4')	115(1)		

Figure 3.2.1   A molecule of (t-butylisocyanide)chlorogold(I) showing
the atom numbering.   Those atoms with a prime affix were
generated by the symmetry of the mirror plane.
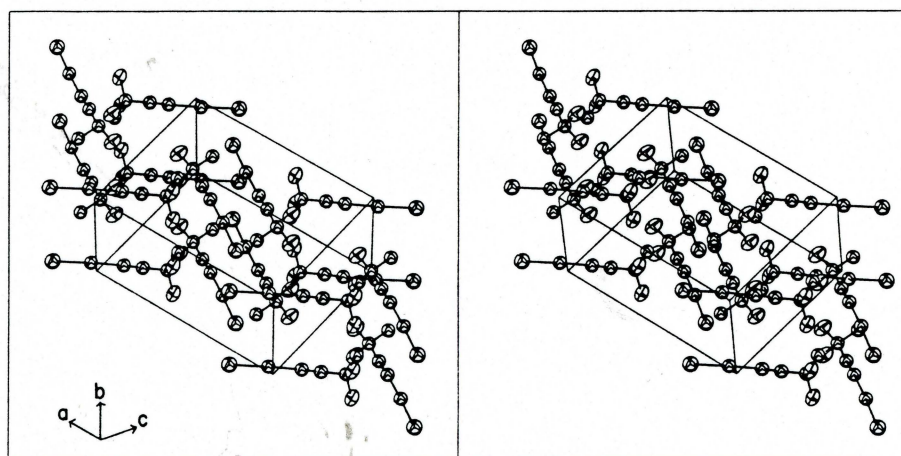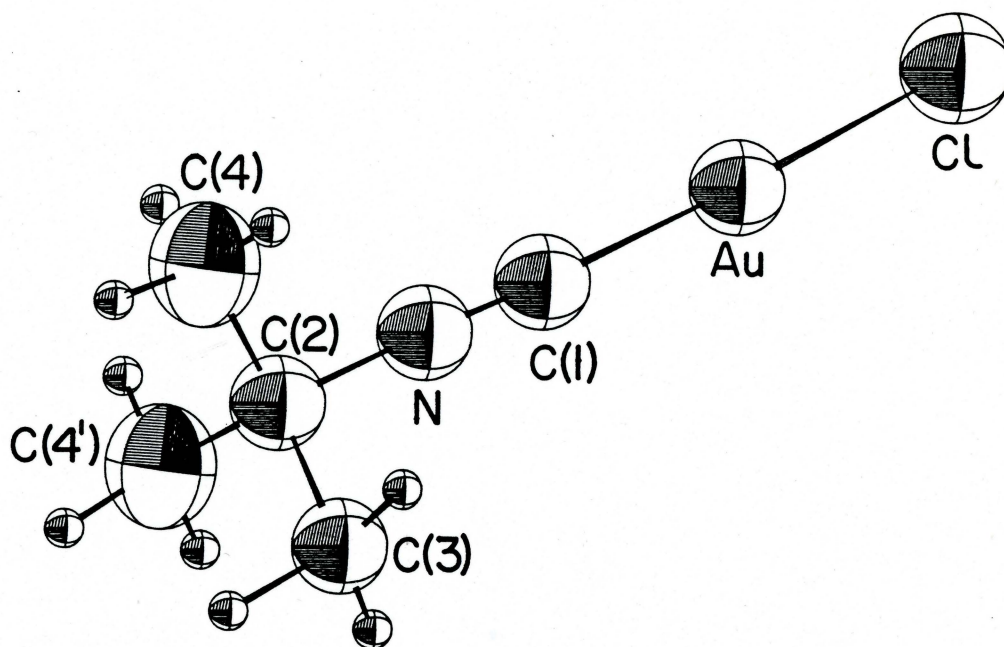
Figure 3.2.2   A stereoview of the crystal packing of (t-butyl
isocyanide)chlorogold(I).

by C(2) suggesting some polarization of electron density towards the triple bond and the gold atom.

A stereoview of the packing in the unit cell is illustrated in Figure 3.2.2. Molecules are arranged in alternating dipole sequences such that those aligned with the [1 0 1] and [-1 0 -1] directions are related by inversion centers at 1/2,0,0, 1/2,0,1/2, and 1/2,1/2,1/2 and those along the [1 0 -1] direction are located at the unit cell corners and are related by inversion centers at 0,0,1/2, 0,1/2,1/2 and 1/2,1/2,1/2,. Packing is dominated by a combination of dipole alternation effects and the space requirements of the t-butyl groups. Although packing occurs in such a way as to allow the closest approach of gold atoms to each other, the Au-Au distance of 3.69(1) Å is longer than the sum of Van der Waals radii (134), thus no intermetallic bonding is indicated.

3.2.5 Vibrational Spectroscopy

Stretching frequencies and some tentative peak assignments for the isocyanide-derived complexes are listed in Table 3.2.B and those for gold compounds of the N-donor ligands discussed in this section are given in Table 3.2.C. These are summarized in section 3.2.2 with the corresponding preparations.

The implications of the _trans_ influence allow the easily discernible νAu-Cl stretch to be used as a probe for the relative strength of the ligand-gold bond located opposite. This stretch occurs at 354 cm^{-1} in the isocyanide complexes compared to 328 cm^{-1} in phosphine complexes. The relatively lower frequency stretch of the

phosphine complex implies a weaker Au-Cl bond explained by the greater

trans influence of the phosphine ligand. Comparison of the Au-Cl bond

length in (t-butylisocyanide)chlorogold(I) (2.247(4) Å) with that in

chloro(triphenylphosphine)gold(I) (2.274(1) Å) (135) offers further

evidence for phosphine trans influence.

Upon binding to gold(I) the νC=N frequencies of both phenyl-

isocyanide (2119 cm^{-1}) and t-butylisocyanide (2120 cm^{-1}) were observed

to increase to 2233 cm^{-1} and 2248 cm^{-1} respectively. If back-donation

occurs from the monopositive gold onto the ligand, νC=N would be

expected to shift to lower frequency. The observed shift to higher

frequency indicates that little or no back-donation occurs and the

shift to higher frequency is explained by the exertion of inductive

effects of the metal ion (136).

Complete characterization of complexes of the N-donor ligands

has proven difficult because of low compound solubility in the case of

the nicotinamide complex and decomposition of others. Some conclusions

can, however, be drawn from vibrational data.

As stated in section 3.2.2, chloro(nicotinamide)gold(I) was

prepared by a modification of the patented preparation of

chloro(pyridine)gold(I) (127). More recently, a crystal structure

determination (69) has shown that this complex was not correctly

formulated as a monomer. It, in fact, exists as a salt composed of

bis(pyridine)gold(I) cations and dichloroaurate anions. The anion

exhibits its asymmetric Au-Cl stretch at 349 cm^{-1} in the infrared. The

Raman frequency of the corresponding symmetric stretch is reported to

be 329 cm^{-1} (137).

The analytical data available for"chloro(nicotinamide)gold(I)",

suggest 1:1:1 ligand:gold:chloride stoichiometry but these data alone

are not sufficient to predict its structure. Importantly, the Raman

spectrum shows no evidence of a symmetric Au-Cl stretch resulting from

the dichloroaurate anion. As well, the infrared shows no evidence of

νAuCl from either $AuCl_2^-$ or an L-Au-Cl species. It is therefore

postulated that the chloride is not bound.

Other information as to the structure of this complex comes

from the shift in frequency of the ring breathing mode of nicotinamide

which results in an absorption at 992 cm^{-1} in the free ligand and

increases to 1022 cm^{-1} in the complex. This is suggestive of metal

binding to the pyridine nitrogen atom (see section 6.2). Furthermore,

the band at 3380 cm^{-1} attributed to νNH is shifted to lower frequency

(3320 cm^{-1}) in the complex. A shift to lower frequency is expected if

the metal binds to the NH_2 group, but not a shift of this magnitude

(137). Hydrogen bonding may also be involved. At the same time, the

peak assigned as νC=O shifts from 1690 cm^{-1} to 1720 cm^{-1}. Such a shift

may be explained after consideration of electron delocalization within

the amide group in the free ligand depicted in Figure 3.2.3.
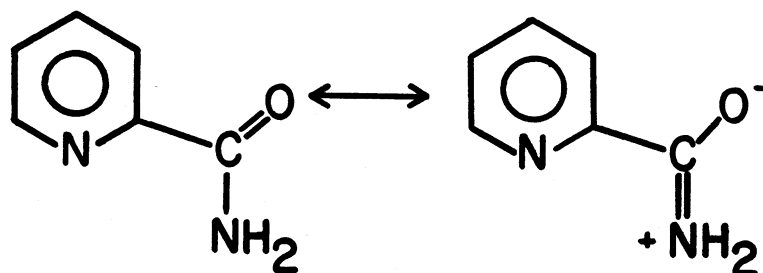
Figure 3.2.3 Possible resonance forms of nicotinamide

If the NH_2 group is involved in metal interaction, the above resonance

would be disrupted such that the C-O bond assumes more double bond

character and νCO would shift to higher frequency. These results are evidence against the formulation of "chloro(nicotinamide)gold(I)" as having a similar structure to the pyridine salt. Not enough information is available to determine whether nicotinamide is acting in a chelating fashion or whether the complex has a polymeric structure.

3.2.6 DNA binding studies

Preliminary studies concerned with the interaction of chloro (t-butylisocyanide)gold(I) with DNA were carried out in similar fashion to that established by Blank and Dabrowiak (101). Representative UV/VIS spectra of guanosine and a solution containing guanosine and the above gold complex in 1:4 ratio are illustrated in Figure 3.2.4.

Guanosine was chosen for this experiment since it offers a binding site (N7) which is considered to be softer than any on other nucleobases and therefore the most likely to show interaction with a soft metal ion such as gold(I) (139).

Chloro(triethylphosphine)gold(I) has been shown to shift the 252 and 274 nm absorptions characteristic of guanosine to 259 and 276 nm (as well as the 271 nm peak of cytidine to 277 nm) at a 1:4 nucleoside:gold ratio (101). Under identically buffered conditions, chloro(t-butlyisocyanide)gold(I) shifts the guanosine absorptions to 256 and 280 nm giving evidence of the potential for this complex to bind to DNA.

Studies were extended to agarose gel electrophoresis of plasmid P63 DNA. Binding of (t-butylisocyanide)chlorogold(I) and chloro(triphenylphosphine)gold(I) to DNA occured, as evidenced by the
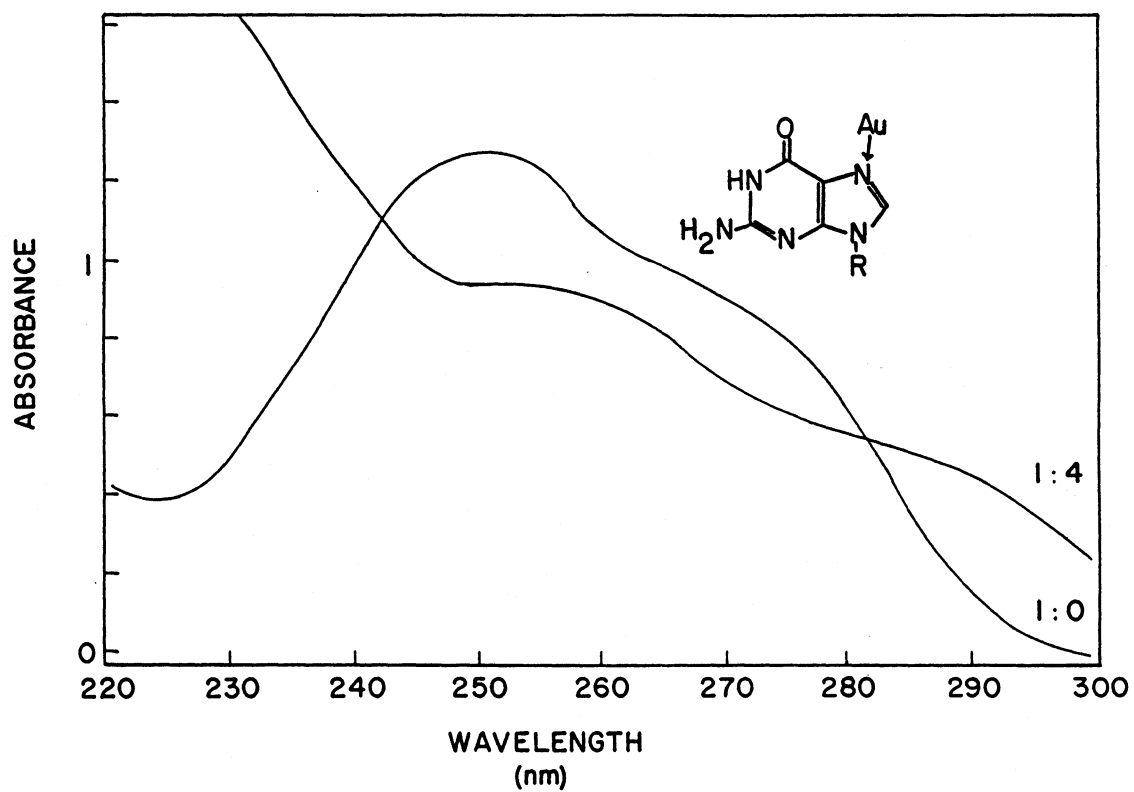
Figure 3.2.4   The UV/Visible spectrum of guanosine and a 1:4 mixture of
guanosine and (t-butylisocyanide)chlorogold(I)

alteration in electrophoretic mobility of the plasmid, under conditions

outlined in section 2.8. Similar experiments with auranofin failed to

show any such alteration suggesting that DNA binding occurs for

complexes which have relatively easily replaced ligands such as halides

but occurs much more slowly (if at all) when the leaving group is

poorer (i.e. thiol). Other work in the same vein has been reported

where (1,2-bis(diphenylphosphino)methane)bis(chlorogold(I)) causes an

alteration in the mobility of pBR322 DNA while auranofin had no

effect (99).

Ames tests performed on bis(pyridine)gold(I)dichloroaurate(I),

(t-butylisocyanide)chlorogold(I) and auranofin gave interesting if

inconclusive results. At low concentrations, the compounds had no

effect on TA102 cells relative to DMSO control runs. Toxicity was

apparent at higher concentrations in that colony counts were smaller

than those achieved by background controls. As concentration

increased, it became obvious by the absence of a background "lawn" that

cell death was occurring soon after complex introduction to the cells.

A background lawn is expected in Ames assays because of the nature of

the experiment. Histidine-requiring cells are incubated in a top-agar

medium containing histidine which allows them to survive through the

first few cell divisions. If mutation occurs during this time,

colonies continue to grow and are counted and those which do not

mutate, die when histidine is exhausted giving rise to the "lawn". The

absence of the lawn suggests that cells did not survive even the first

periods of growth. In addition, plates took on a pink colouration

indicative of gold sol (Au^0) formation.

3.2.7 Conclusions

Gold(I) complexes containing heterocyclic nitrogen ligands have been shown, in general, to be somewhat unstable as they require excess ligand during their preparation and they decompose under ambient conditions after being isolated. The most viable complex in this respect is that incorporating the nicotinamide ligand. Insolubility of this compound has precluded its recrystallization for X-ray experiments as well as preventing other analyses such as conductivity or molecular weight determinations.

Although t-butyl- and phenylisocyanide form chlorogold(I) complexes relatively less sensitive to light and air, products of chloride substitution reactions are unstable in that the isocyanide is also lost during isolation procedures (see section 3.2.3). It has proven possible to use the reaction of the t-butylisocyanide complex with disodiumthiomalate as a method to synthesize purer GST than that presently marketed as a drug. This has also led to good yield in the synthesis of each of the R and S forms of GST. Preliminary studies have shown that complexes of t-butylisocyanide otherwise behave in a similar fashion to that of triethylphosphine in its interaction with DNA bases.

Furthermore, none of the compounds tested, including auranofin itself, remained intact during _in vivo_ Ames experiments as evidenced by pink agar plate colouration at high compound concentrations.

PART B

MODELLING GOLD(I) BINDING TO DNA

3.3.1 Introduction

The evidence for anti-cancer activity in in vivo testing of auranofin (82-86,140) has prompted further investigation of the interaction of auranofin and analogous gold compounds with DNA both in vivo and in vitro (100,141,142).

A number of gold(I) complexes with nucleobases have been prepared by Hadjiliadis et al. and partially characterized by Moessbauer, NMR and infrared spectroscopies (37,96,143).

Bonati et al. (90) have studied a series of (triphenylphosphine)gold(I)-nucleobase compounds as a continuation of previous studies of gold(I) complexes of pyrazole and imidazole derivatives (144-147).

Beck et al. (102) have solved the only gold(I)-nucleobase structure yet reported, namely that of (adeninato-N^9-)-(triphenylphosphine)gold(I). The information obtained is of limited use as an in vivo model because the metal binds to the deprotonated N(9) position, a site occupied by the sugar group in biological systems.

The (1-methylthyminato-N^3-)(triphenylphosphine)gold(I) complex was synthesized and characterized by a variety of spectroscopic techniques as well as X-ray crystallography and its relevance as a model for metal binding to DNA will be discussed in subsequent sections.

3.3.2 Preparations

1-methylthymine (Fluka) was used without further purification.

Analyses were performed by Atlantic Microlab, Atlanta, Georgia.

Potassium 1-methylthyminate; 1-methylthymine (0.2 g) was dissolved in

15 mL of distilled water. The pH of this solution was raised to 12 by

addition of 5 N KOH. After heating for several minutes, the solvent

was evaporated under reduced pressure and the residue was dried _in_

vacuo at 80°C for 3 hours. The resulting solid was used in infrared

spectroscopy without further purification.

Chloro(triphenylphosphine)gold(I); $HAuCl_4 \cdot 3H2O$ (1.00 g, 2.5 mmol) was

dissolved in 20 mL distilled water and cooled in an ice bath. To this

was added, dropwise, a solution of 500 µL (5.0 mmol) of thiodiglycol in

1 mL ethanol. An ethanol solution (20 mL) of 0.70 g (2.5 mmol)

triphenylphosphine was added and the mixture was stirred for 30 min.

The product was filtered and dried _in vacuo_ for 12 hours then

recrystallized twice from dichloromethane/hexane to yield 1.06 g of a

white crystalline solid (86%).

1-Methylthyminato-N³-triphenylphosphinegold(I); 1-methylthymine (0.70

g, 5.0 mmol) was dissolved in 20 mL of distilled water and the pH was

raised to 11.1 by addition of 0.5 N NaOH. A methanol solution (20 mL)

of chloro(triphenylphosphine)gold(I) (2.47 g, 5.0 mmol) was added and

the covered solution was stirred. After 6 hours, all but 10 mL of the

solvent were removed under reduced pressure and the resulting

suspension was filtered, the precipitate washed with cold water and

dried _in vacuo_ to yield 2.21 g of a white solid (74%). Crystals

suitable for diffraction were obtained by slow recrystallization from

methanol/water (50/50 v/v) at 4°C.

Analysis required for $C_{24}H_{22}AuN_2O_2P$: C;48.2, H;3.7, N;4.7%.

Found: C;48.3, H;3.9, N;4.6%.

3.3.3 The crystal and molecular structure of (1-methylthyminato-N³) triphenylphosphinegold(I)

Crystal data and other details of data collection and structure refinement are summarized in Table 3.3.1. Atomic positional parameters and anisotropic temperature factors are listed in Tables 3.3.2 and 3.3.A respectively. The molecule is illustrated in Figure 3.3.1. Selected interatomic distances and angles are given in Table 3.3.3 and a summary of best planes, dihedral and torsional angles is given in Table 3.3.4.

Bond lengths and angles involving gold, phosphorus and the phenyl rings (C-C ave. 1.42(3) Å range 1.35(4)-1.52(4) Å, C-C-C ave. 119(9)°, range 112(3)-125(2)°) are consistent with results for chloro(triphenylphosphine)gold(I) (135). The Au-N(3) distance is significantly longer (2.20(1) Å) than those reported in the following structures; 3,5-dimethylpyrazoletriphenylphosphinegold(I) tetra-fluoroborate (2.00(2) Å) (145), (tricylohexylphosphine)(2-isopropyl-imidazolato)gold(I) (2.019(5) Å) (147), chloro(piperidine)gold(I) (2.068(18) Å) (148), (adeninato-N⁹-)triphenylphosphinegold(I) (2.038(4) Å) (102), and one of the distances in the bis(pyridine)gold(I) cation (2.08(3) and 2.10(4) Å) (69). The unexpectedly longer Au-N distance in the title compound, even though coordinated to an anionic ligand, is explained by electronic effects associated with the carbonyl oxygen

Table 3.3.1 Crystal data for (1-methylthyminato-N^3-)
            triphenylphosphinegold(I)

Formula	$C_{24}H_{22}AuN_2O_2P$
Formula weight	598.37
Crystal size and shape	0.13x0.13x0.16mm^3 cylinder
Systematic absences	hkl;h+k=2n+1
Space group	$C222_1$ (no. 20)
Diffractometer	$P2_1$
Temperature	22°C
Unit cell parameters	a=12.760(1)Å
	b=11.530(2)Å V=4692(3)Å^3
	c=31.893(5)Å Z=8
ρ_{calc}, ρ_{obs}	1.694, 1.69; $ZnCl_2$(aq)
Reflections measured	h,k,±l
Maximum 2θ	55°
Number of reflcns measured	6629
Number of independent reflcns	4760
Standard reflcns(e.s.d)	-3 1 3 (1.6%), 2 0 8 (1.7%)
R_{int}	0.0306
Final R,Rw	0.1117, 0.0761
Final shift/error max(ave)	0.155(0.011)
Error in obs of unit weight	S=1.3575
Highest peak, lowest valley	4.2eÅ^{-3}, -3.4eÅ^{-3}
Weighting	w=(σ^2(F) + 0.0004F^2)$^{-1}$
F(000)	2301
Linear Absorption coefficient	μ=65.74cm^{-1}
Absorption Coefficient limits	2.029<A*<2.897*
Number of Variables	271

---

* absorption correction was not applied introducing a maximum error in
  Fo of ≅8%.

Table 3.3.2 Atomic positional parameters and U_{eq} ($A^2 \times 10^4$) for
(1-methylthyminato-N^3-)triphenyphosphinegold(I)

Atom	x	y	z	U_{eq}
Au	2849.0(5)	6644.6(6)	3665.8(2)	47.4
N(1)	2065(15)	3107(12)	3359(6)	74
C(1)	1596(23)	2139(18)	3561(11)	132
C(2)	2266(15)	4157(15)	3591(6)	52
O(2)	1980(16)	4239(13)	3950(5)	92
N(3)	2648(10)	5098(11)	3383(4)	41
C(4)	2904(15)	5018(16)	2949(6)	54
O(4)	3234(11)	5953(11)	2759(5)	77
C(5)	2784(18)	3910(16)	2751(6)	58
C(5')	3157(18)	3792(19)	2285(7)	85
C(6)	2419(14)	3020(16)	2955(8)	64
P	3108(3)	8351(5)	3985(1)	42
C(7)	3862(13)	9336(14)	3669(6)	45
C(8)	3912(19)	10507(23)	3783(7)	87
C(9)	4431(28)	11395(38)	3543(15)	160
C(10)	4986(29)	10956(30)	3216(13)	125
C(11)	4986(16)	9758(36)	3071(8)	113
C(12)	4371(16)	8921(21)	3321(8)	82
C(13)	1907(15)	9097(13)	4094(6)	50
C(14)	1027(14)	8902(15)	3795(6)	63
C(15)	90(16)	9536(17)	3877(8)	71
C(16)	-5(20)	10301(20)	4223(7)	82
C(17)	817(22)	10467(17)	4489(8)	92
C(18)	1800(17)	9897(17)	4442(6)	73
C(19)	3797(15)	8188(14)	4488(5)	50
C(20)	3205(21)	7570(21)	4797(7)	92
C(21)	3660(24)	7296(30)	5193(12)	129
C(22)	4626(37)	7799(26)	5246(8)	136
C(23)	5294(20)	8470(23)	4937(10)	116
C(24)	4790(17)	8659(16)	4542(6)	64

$U_{eq} = 1/3 (U_{11} + U_{22} + U_{33})$

Table 3.3.3 Selected Interatomic Distances (Å) and Angles (°) for
(1-methylthyminato-N^3-)triphenylphosphinegold(I)

Au-P	2.240(5)	Au-N(3)	2.20(1)	N(1)-C(2)	1.44(2)
C(2)-N(3)	1.36(2)	N(3)-C(4)	1.42(2)	C(4)-C(5)	1.43(2)
C(5)-C(6)	1.30(2)	C(6)-N(1)	1.37(2)	N(1)-C(1)	1.42(3)
C(2)-O(2)	1.20(2)	C(4)-O(4)	1.31(2)	C(5)-C(5′)	1.57(3)
Au····O(2)	3.12(2)	Au····O(4)	3.04(2)		
P-C(7)	1.80(2)	P-C(13)	1.79(2)	P-C(19)	1.84(2)
C(7)-C(8)	1.40(3)	C(13)-C(14)	1.49(2)	C(19)-C(20)	1.43(3)
C(8)-C(9)	1.44(5)	C(14)-C(15)	1.42(3)	C(20)-C(21)	1.42(2)
C(9)-C(10)	1.36(5)	C(15)-C(16)	1.42(3)	C(21)-C(22)	1.37(5)
C(10)-C(11)	1.46(5)	C(16)-C(17)	1.36(4)	C(22)-C(23)	1.52(4)
C(11)-C(12)	1.48(3)	C(17)-C(18)	1.42(3)	C(23)-C(24)	1.43(3)
C(12)-C(7)	1.37(3)	C(18)-C(13)	1.45(2)	C(24)-C(19)	1.39(2)

P-Au-N(3)	178.7(4)	Au-P-C(7)	112.3(6)
Au-N(3)-C(2)	122(1)	Au-P-C(13)	112.5(6)
Au-N(3)-C(4)	118(1)	Au-P-C(19)	112.1(6)
C(6)-N(1)-C(2)	119(2)	N(1)-C(2)-N(3)	119(2)
C(2)-N(3)-C(4)	120(1)	N(3)-C(4)-C(5)	118(2)
C(4)-C(5)-C(6)	121(2)	C(5)-C(6)-N(1)	122(2)
C(6)-N(1)-C(1)	121(2)	C(1)-N(1)-C(2)	120(2)
N(1)-C(2)-O(2)	120(2)	O(2)-C(2)-N(3)	121(2)
N(3)-C(4)-O(4)	118(2)	O(4)-C(4)-C(5)	124(2)
C(4)-C(5)-C(5′)	118(2)	C(5′)-C(5)-C(6)	121(2)
C(13)-P-C(7)	105.3(7)	C(19)-P-C(7)	107.4(9)
C(19)-P-C(13)	106.8(8)	P-C(7)-C(8)	119(2)
P-C(13)-C(14)	117(1)	P-C(19)-C(20)	114(2)
C(7)-C(8)-C(9)	125(3)	C(13)-C(14)-C(15)	116(2)
C(19)-C(20)-C(21)	120(3)	C(8)-C(9)-C(10)	113(4)
C(14)-C(15)-C(16)	122(2)	C(20)-C(21)-C(22)	112(3)
C(9)-C(10)-C(11)	127(4)	C(15)-C(16)-C(17)	120(2)
C(21)-C(22)-C(23)	130(3)	C(10)-C(11)-C(12)	117(3)
C(16)-C(17)-C(18)	123(2)	C(22)-C(23)-C(24)	113(2)
C(11)-C(12)-C(7)	117(2)	C(17)-C(18)-C(13)	117(2)
C(23)-C(24)-C(19)	117(2)	C(12)-C(7)-C(8)	122(2)
C(18)-C(13)-C(14)	121(2)	C(24)-C(19)-C(20)	126(2)
C(12)-C(7)-P	119(1)	C(18)-C(13)-P	122(1)
C(24)-C(19)-P	120(2)		

Table 3.3.4   Best planes, dihedral and torsional angles for
(1-methylthyminato-N^3-)triphenylphosphinegold(I)

Plane	Distance of atom from plane (Å)
1.N(1),C(2),N(3),C(4),C(5),C(6)	N(1);0.06(2),C(2);0.04(2), N(3);0.01(1),C(4);0.03(2), C(5);0.01(2),C(6);0.04(2), C(1);0.13(3),O(2);0.02(2), O(4);0.10(1),C(5′);0.09(2), Au;0.006(1).
2.C(7),C(8),C(9),C(10),C(11),C(12)	C(7);0.00(2),C(8);0.03(2), C(9);0.04(4),C(10);0.03(4), C(11);0.00(2),C(12);0.02(2), P;0.015(4).
3.C(13),C(14),C(15),C(16),C(17),C(18)	C(13);0.00(2),C(14);0.00(2), C(15);0.00(2),C(16);0.00(2), C(17);0.00(2),C(18);0.00(2), P;0.054(5).
4.C(19),C(20),C(21),C(22),C(23),C(24)	C(19);0.01(2),C(20);0.03(2), C(21);0.03(3),C(22);0.02(3), C(23);0.00(3),C(24);0.00(2), P;0.057(5).

5.Au,P,C(7)

6.Au,P,C(13)

7.Au,P,C(19)

8.C(7),C(13),C(19)

Dihedral angles (°)

1 - 2	19(2)	1 - 3	87(2)	1 - 4	120(2)	2 - 3	79(2)
2 - 4	106(2)	3 - 4	108(2)	2 - 5	14(2)	3 - 5	77(2)
4 - 5	120(2)	2 - 6	57(2)	3 - 6	30(2)	4 - 6	93(2)
2 - 7	115(2)	3 - 7	51(2)	4 - 7	64(2)	2 - 8	77(2)
3 - 8	117(2)	4 - 8	32(2)				

Torsional angles (°)

C(2)-N(1)-P-C(7)	155(2)	C(4)-N(1)-P-C(7)	11(2)
C(2)-N(1)-P-C(13)	82(2)	C(4)-N(1)-P-C(13)	112(2)
C(2)-N(1)-P-C(19)	32(2)	C(4)-N(1)-P-C(19)	133(2)

Figure 3.3.1 A molecule of (1-methylthyminato-N^3-)-
triphenylphosphinegold(I). Carbon atoms of the phenyl
rings are denoted by their numbers only.
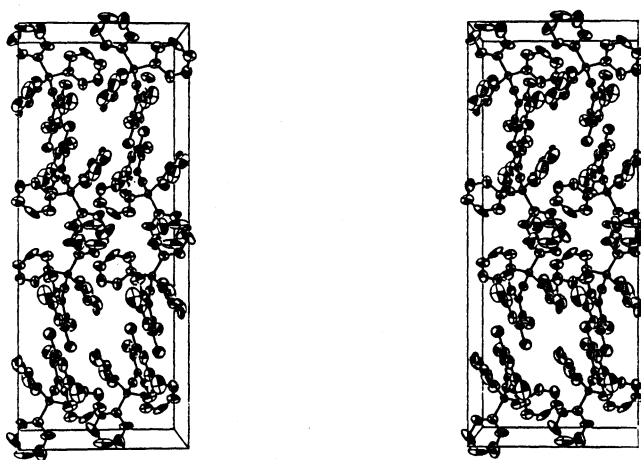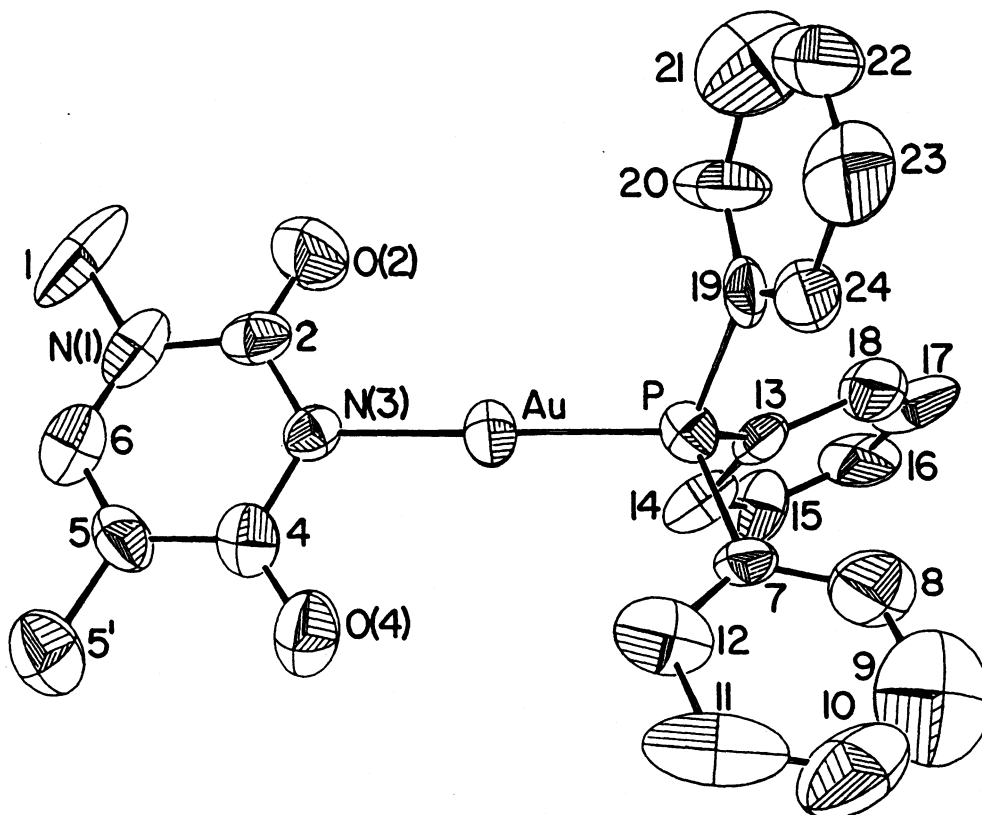
Figure 3.3.2 Stereoview of the unit cell down the **b** axis

atoms O(2) and O(4) and their 3.12(2) and 3.04(2) Å approach to gold.
The gold-oxygen distance is close to van der Waals (3.20 Å) (134)
suggesting negligible interaction.

Coordination to (triphenylphosphine)gold(I) which involves
deprotonation at N3 has the effect on 1-methylthymine of lengthening
the C(4)-O(4) bond distance to 1.31(2) Å in the thyminate complex
vs. 1.237(4) Å in 1-methylthymine (149). In neutral 1-methylthymine,
C(4)=O(4) is involved in hydrogen bonding and is therefore already a
relatively long bond (cf C(2)=O(2) 1.20(2) Å). The C(5)-C(6) distance
in the gold complex is shortened (1.30(2) Å) compared to that for
1-methylthymine (1.346 Å (149)). Other effects of gold binding on
interatomic distances are the lengthening of the N(3)-C(4) (1.42(2) Å
vs. 1.375(4) Å (149)) and N(1)-C(2) (1.44(2) Å vs. 1.379(4) Å (149))
distances. The C(4)-N(3)-C(2) angle (126.2(4)° in 1-methylthymine
(149)) narrows to 122(2)° in the complex. Other angles (C(6)-N(1)-
C(2), N(1)-C(2)-N(3), N(3)-C(4)-C(5), C(4)-C(5)-C(6)) in the ring open
to compensate. (Triphenylphosphine)gold(I) is apparently more able to
stabilize N(3) in an sp^2 form than the proton as it is a poorer
electron acceptor. It has been observed for platinum(II) binding to
cytosine that angle opening is not as great as that caused by
protonation (150).

The packing is shown in Figure 3.3.2. The chirality of the
structure arises as a result of the propeller-like packing arrangement
of the phenyl rings. The molecules are arranged in sets of bilayers
parallel to the **ab** plane. Within a given bilayer, molecules are
oriented such that the N-Au-P dipole is roughly in the **b** direction

which will maximize any dipole-dipole interaction. In the adjacent
bilayer in the c direction, dipoles are in the opposite direction along
the b axis. The molecules are inclined from the b direction, however,
such that there are hydrophobic layers formed by the phenyl groups at
z=0,1/2 and hydrophilic layers formed by the thyminate groups at
z=1/4,3/4.

The question arises as to why this crystal is chiral (as is the
crystal of the starting compound, chloro(triphenylphosphine)gold(I))
(135), since the preparative reaction should give a racemic product.
Surprisingly, in a compound with so many aromatic rings, there is very
little evidence of any π-π interaction of the rings (see section 4.3),
except for the small interaction of the thyminate group in one molecule
with the C(7-12) ring of the adjacent molecule in the a direction
related by the C centering operation. This interaction may be
responsible for the rather small Au-P-C(7) - ring(C(7)) dihedral angle
of 14º, but it is then unlikely to be the main cause of the chirality,
since when the dihedral angle is 0º the phenyl ring exerts no selective
force on the other rings in determining their configuration. Indeed,
apart from the above interaction, there is no evidence of any
interactions, other than van der Waals, which could cause the crystal
to be chiral and we can see no good reason why the chiral space group
is preferred.

3.3.4 1H and 13C NMR spectroscopy

The proton and carbon-13 NMR data for 1-methylthymine,
potassium 1-methylthyminate and 1-methylthyminato-N3-

triphenylphosphinegold(I) are given in Table 3.3.5. The positions of the peaks arising from methyl protons are similar in the three compounds. Small upfield shifts occur in the methyl resonances of the 1-methylthyminate ion (1.77 to 1.68 ppm and 3.24 to 3.15 ppm) compared to 1-methylthymine. On the other hand, (triphenylphosphine)gold(I) appears to be somewhat electron withdrawing as the methyl peaks of the complex are shifted slightly downfield compared to those of the neutral ligand (1.77 to 1.86 ppm and 3.24 to 3.27 ppm). The effect of removal of the H(3) proton and its substitution by gold is more pronounced for H(6), the proton bound to C(6) than for the methyl groups. An upfield shift is observed (7.36 to 7.17 ppm) on deprotonation. In the gold substituted case, however, a further upfield shift (to 6.88 ppm) is observed, opposite to that noticed for the methyl groups external to the ring. It is speculated that the downfield shift of the methyl resonances upon gold binding is an inductive effect caused by the electronegativity of the (triphenylphosphine)gold(I) cation, whereas the upfield shift of H(6) is a result of increased electron density at the para position. Complexation to gold has also affected the electronic structure of thymine enough to eliminate the small coupling (^4J 1 Hz) between H(6) and the C(5') methyl protons observed in both neutral and anionic 1-methylthymine spectra. This is precedented in reported spectra of cytosine with (dibenzylsulphide)chlorogold(I) (97).

Assignment of peaks in the ^{13}C NMR spectrum of 1-methyl-thymine in D_2O is in agreement with literature assignments for DMSO-d_6 solutions (151,152). The positions of peaks arising from C(5'), C(1), and C(5) change very little in the three compounds. The C(6) signal

Table 3.3.5 Nuclear Magnetic Resonance Data pertaining to the interaction of chlorotriphenylphosphinegold(I) with 1-methylthymine

	1-methylthymine[a]			1-methylthyminate[b]			1-methylthyminato-N[3]-triphenylphosphinegold(I)		
	Chem. Shift(ppm)	Mult.(J in Hz)	Assignment	Chem. Shift(ppm)	Mult.(J in Hz)	Assignment	Chem.Shift(ppm)	Mult.(J in Hz)	Assignment
^{1}H NMR	1.7709	d(^{4}J 1.00) CH$_3$(5')-H(6)	CH$_3$(5')[d]	1.6757	d(^{4}J 1.00) CH$_3$(5')-H(6)	CH$_3$(5')	1.8616	s	CH$_3$(5')
	3.2413	s	CH$_3$(1)	3.1464	s	CH$_3$(1)	3.2714	s	CH$_3$(1)
	7.3560	q(^{4}J 1.00) H(6)-CH$_3$(5')	H(6)	7.1707	q(^{4}J 1.00) H(6)-CH$_3$(5')	H(6)	6.8765	s	H(6)
							7.4140	m	C(7)-C(12)[e]
							7.5620	m	"
	12.32	s	C(5')	13.40	s	C(5')	13.45	s	C(5')
	36.80	s	C(1)	37.57	s	C(1)	36.67	s	C(5')
	111.44	s	C(5)	111.62	s	C(5)	110.93	s	C(5)
^{13}C NMR	145.32	s	C(6)	144.48	s	C(6)	140.27	s	C(6)
	154.00	s	C(2)	159.99	s	C(2)	157.71	s	C(2)
	168.17	s	C(4)	175.92	s	C(4)	172.06	s	C(4)
				168.37	s	K$_2$CO$_3$[f]	129.25	d(^{3}J 11.31) P-C(9)	C(9)C(1)
							129.38	d(^{1}J 61.56) P-C(7)	C(7)
							131.74	s	C(10)
							134.40	d(^{2}J 13.82) P-C(8)	C(8)C(12)

[a] sample run in D$_2$O

[b] sample run in D$_2$O made basic with K$_2$CO$_3$ (pH 11)

[c] sample run in CDCl$_3$

[d] see numbering scheme in Figure 3.3.1 (molecule)

[e] refers to carbons listed in this table and their equivalents on the other two phenyl rings (see Fig. 3.3.1)

[f] K$_2$CO$_3$ in D$_2$O (pH 11) was run alone to confirm this peak assignment

shows a significant upfield shift in the gold complex compared to the neutral and anionic species which is further evidence of the shielding power of electron density from the gold atom at the <u>para</u> position. Deprotonation has a marked effect on the resonance of C(2) and C(4). The electronegativity of the oxygen atoms appears to increase and deshield these carbon atoms. Complexation with gold partially compensates for the absence of the N(3) proton. C(4) is the carbon which shows the greatest sensitivity to changes in the electronic structure.

3.3.5 Vibrational Spectroscopy

The vibrational spectra of 1-methylthyminato-N^3-triphenyl-phosphine gold(I) and related species are summarized in Table 3.3.6. Assignments were facilitated by previous vibrational analyses by Susi and Ard (153) on 1-methylthymine, Guay <u>et al.</u> (154) on 1-methylthyminate, Whiffen (155) on monosubstituted benzenes, Shobatake <u>et al.</u> (156) on metal triphenylphosphines and MacKay <u>et al.</u> (157) on triphenyl compounds of group Va elements. Deprotonation at N(3) of 1-methylthymine, or substitution of this proton by a heavy metal ion, is expected to result in the disappearance of the N(3)-H modes (νN(3)-H at 3155 cm^{-1} and γN(3)-H at 897 cm^{-1}) of 1-methylthymine. Potassium thyminate bands occuring in the 2800 cm^{-1} to 3100 cm^{-1} region, caused by various C-H stretches, are unaffected by deprotonation or binding to gold.

The three peaks for 1-methylthymine in the 1600-1700 cm^{-1} region assigned to νC(2)=O(2) (1698 cm^{-1}), νC(4)=O(4), νC(5)=C(6)

Table 3.3.6. Vibrational Spectra of 1-Methylthyminato-N[3]-triphenylphosphine gold(I) and related species

K thyminate		chloro(triphenylphosphine)gold(I)		1-methylthyminato-N[3]-triphenylphosphinegold(I)		assignment
infrared[a]	Raman[b]	infrared	Raman	infrared	Raman	
		3080m	3060(37)			νC-H(ph)[c]
3062m	3052(10)	3060m	3052(29)	3050w	3056(4)	νC-H(ph), νC(6)-H
3020m	3027(5)					νaNC-H3, νaCC-H3
2980sh	2980(5)					νC-H3
2960m	2959(7)					.
2940m	2938(7)					.
2924w	2921(7)			2920		νaCC-H3
2900vw	2904(10)					νC-H3
2840w						
		1980w		1980w		νC=C(ph),
		1900w		1900w		phenyl ring
		1820w		1820w		overtones
1702w						
1663br	1659(22)			1655s	1648(13)	νC(2)=O(2)
1610s	1624(41)			1590s	1586(52)	in phase,νC(4)=O(4),νC(5)=C(6)
		1585w	1590(53)		1586(52)	νC=C(ph)
			1573(10)		1574(10)	νC=C(ph)
1570s				1580s		out of phase, νC(4)=O(4),νC(5)=C(6)
1525vs	1525(20)					"alternate bonds stretch"
		1480m	1479(2)	1479m	1481(8)	νC=C(ph)
1460s	1480(7)			1454w		νaC-CH3, νaN-CH3
		1439s	1435(3)	1432s	1432(2)	νC=C(ph)
		1432s		1425sh		νC=C(ph)
1430s	1431(20)					δa C-CH3, δa N-CH3
1415s	1417(20)			1418s		δsNCH3,ν-ring(thy)[d]
		1381m		1381m	1380(8)	
1375m	1372(10)			1360sh		δs C-CH3
1352s	1356(50)			1354m	1359(10)	δs N-CH3, ν-ring(thy)
1327s	1323(10)			1323m		δ CH(ph), ν-ring(thy)
1277m	1278(10)			1274w		
1232w				1240w	1244(13)	ν-ring(thy)
1200s				1213m		ν-skel(thy)
		1179m	1182(5)	1184w	1183(10)	δ CH(ph) (in-plane)
1158s	1158(7)		1160(10)	1163m	1160(6)	ν-skel(thy)
		1100m	1100(38)	1101s	1100(39)	ν P-C (q-vib)[e]
1060m	1060(10)			1060w		r N-CH3
1040mw						
		1021s	1028(20)	1026w	1027(32)	δ CH(ph) (in-plane)
			1024(30)			δ CH(ph) (in-plane)
1002m	1002(10)					r C-CH3
		995m	996(100)	996m	999(100)	ring breathing, ν C=C(ph)
				984sh		
948w						
900m	900(35)			922vw	920(10)	ν-skel(thy)
888s	882(5)			896v		ν-ring(thy)
780s	777(86)			773m	781(20)	γCH,δ,ν-ring(thy)
758sh				761m		δ,ν-ring(thy),γCH
		750m	745(10)	745m		δ CH(ph) (out-of-plane)
		741s		743m		δ CH(ph) (out-of-plane)
		736m		721m		δ CH(ph) (out-of-plane)
		705s	711(6)	705s	709(5)	r-vib
697m				690sh		
689s	689(33)	688s	689(12)	688s	692(13)	δ-ring(thy), r-vib
657m	661(7)			655vw	660(5)	δ C-O (in-plane)
		615vw	615(14)		612(17)	δ-ring(thy), δ C-C-C(ph)(in-plane)
548w	543(90)					δ-ring(thy)
		545m	540(4)	548s	537(15)	y-vib
		505s	520	511m		y-vib
		500s	505	503m		y-vib
468vs	466(23)					δ-ring(thy)
455m		452w		458s	457(7)	t-vib
		448w	450	452w		t-vib
		438w	438	444m		
426vs	421(10)	390w	393	435w	430(5)br	δ C-O (in plane)
				354w		δ C-CH3
	325(7)	325m	327(30)	330mw	328	ν Au-^{35}Cl
		316m	319(20)			ν Au-^{37}Cl
283w	283(10)			285m		δ N-CH3
			272(10)		261(10)	ν Au-N, ν Au-P, x-vib
			262(10)			
			253(20)	256w	257(20)	ν Au-N, ν Au-P, x-vib
254w						δ-ring(thy)
			229(16)		224(10)	
217vw	216(15)	218w	216(10)	194w	194(6)	u-vib
		205vw	203(22)			u-vib
186m	192(10)					δ-ring(thy)
			181(23)			δ AuCl
157m	149(13)		158(3)	164w	156(11)	δ PAuN
131m	122(13)			128w	123(10)	δ PAuN

[a]   abbreviations: s=strong, m=medium, w=weak, v=very, sh=shoulder,br=broad.

[b]   Raman peak intensity relative to strongest peak taken as 100.

[c]   (ph) refers to phenyl rings of triphenylphosphine.

[d]   (thy) refers to the thymine ring.

[e]   for definition of q,r,t,u,y and x-vib (155) see Figure 3.3.3.

in-phase (1654 cm^{-1}), νC(4)=O(4), νC(5)=C(6) out-of-phase (1638 cm^{-1})

(153) are all shifted to lower frequency (1663, 1610 and 1570cm^{-1}

respectively) upon N(3) deprotonation. This can be explained by a

decrease in double bond character because of electron delocalization

throughout the O-C-N-C-O system, resulting from N(3) deprotonation.

The peak at 1525 cm^{-1} assigned to the "alternate bond stretch"

(158) shows a very large increase in intensity in the infrared and

Raman spectra of the anion compared to 1-methylthymine and agrees with

results previously obtained (159). A similar assignment was made for

the 1462 cm^{-1} peak in uracil (158). The increase in absorption is

probably a result of a large dipole moment being created upon loss of

the proton. Further changes in the frequencies of these bands are

observed when gold is bound to 1-methylthyminate. It is expected that

binding a heavy metal to N(3) would result in the release of electron

density into the thymine ring, increasing the basicity of the carbonyl

groups in agreement with NMR results. For the purpose of comparison,

spectra of potassium 1-methylthyminate are more suitable than those of

the neutral ligand, since 1-methylthymine exists in the solid as a

dimer whose hydrogen bonding affects the nature of its conjugated

bonds. At 1580 cm^{-1}, the peak arising from the νC(4)=O(4), νC(5)=C(6)

out-of-phase mode is found 10 cm^{-1} higher in the complex than in the

anion. The shift of νC(4)=O(4) to 1580 cm^{-1} in the complex from 1610

cm^{-1} in the anion and 1654 cm^{-1} in 1-methylthymine is consistent with

the observed lengthening of the C(4)-O(4) bond in the complex. The

extent of lowering of the νC(2)=O(2) frequency (1663 cm^{-1} in

1-methylthyminate to 1655 cm^{-1} in the complex from 1698 cm^{-1} in neutral

1-methylthymine) is somewhat surprising in light of the C(2)=O(2) bond

length. Such shifts indicate more single bond character in both the

1-methylthyminate ion and the ion bound to gold. It must be remembered,

however, that the structure reported here is not particularly accurate,

and the errors are such that the C(2)-O(2) bond in the complex may well

be sufficiently longer than in the neutral molecule to explain the

shift. There is no close interaction between Au and O(2) and O(4), as

there is in the Ag complex (160).

As an approximation, certain bands in the vibrational spectra

of triphenylphosphine, chloro(triphenylphosphine)gold(I) and the

thyminato complex can be interpreted in terms of the spectra of

monosubstituted benzene. Whiffen (155) has categorized the bands of

monosubstituted benzenes into those vibrations which are and are not

affected by changes in the substituent group. Six of the fundamental

modes (Whiffen's q, r, t, u, y and x bands, depicted in Figure 3.3.3

are
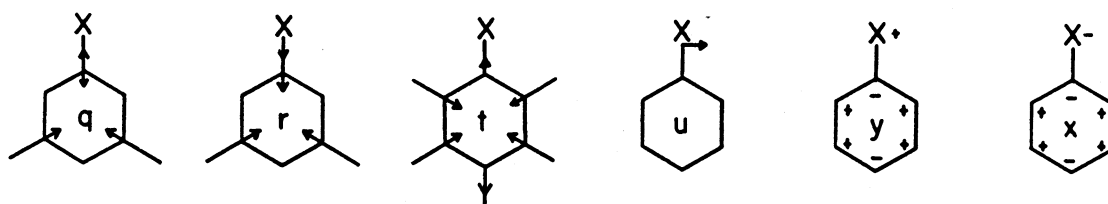
Figure 3.3.3 The substituent-sensitive modes of benzene (155)

sensitive to substituent change. In the q, r and t modes, there is

vibration along the Ph-X bond (X=substituent), whereas u, y and x are

Ph-X bending vibrations. When triphenyphosphine is coordinated to

either chlorogold(I) or 1-methylthyminato-N^3-gold(I), the q, r and t

bands are shifted to higher frequency, while the u, y and x bands are

not significantly shifted. The q-band at 1089 cm^{-1} in triphenyl-

phosphine shifts to 1100 cm^{-1} in chloro(triphenylphosphine)gold(I), the

r-bands shift from 688, 680 cm^{-1} to 705, 688 cm^{-1} and the t-bands shift

from 425, 413 cm^{-1} to ≅450, 440 cm^{-1}. Of these, the t-bands show the

larger shift.

In general, it is difficult to assign metal-phosphorus

stretching bands because triphenylphosphine itself exhibits a number of

bands in the low frequency region. In the past, the metal isotope

substitution technique has been used for some complexes; for example,

trans-Pd[P(C$_6$H$_5$)$_3$]$_2$Cl$_2$, and the bands having the larger isotopic shifts

have been assigned to Pd-Cl and Pd-P stretching vibrations (161). The

latter at 191 and 155 cm^{-1} seem to be very low and are possibly more

typical of metal-chlorine bending motions. Indeed, force constant

analyses have shown that bending vibrations can have a larger isotopic

shift than stretching vibrations, depending on the interactions of

force constants and the potential energy distribution (162). In the

present work no bands can be assigned to purely Au-P or Au-N stretching

modes. It is expected that the Au-P modes will be strongly coupled to

the vibrations of the triphenylphosphine ligand, and because the phenyl

rings are "tilted" there will be a component of motion along the Au-P

bond even for the ligand bending vibrations. The ligand t-band is

essentially a P-phenyl stretch, and it will be coupled to the Au-P and

Au-N stretching vibrations. In the ligand x-vibration, two of the

phenyl rings contribute a component of motion along the P-Au-N axis and

hence one can assume Au-N as well as Au-P coupling. It is reasonable for this "out-of-plane" phenyl ring bend to be at higher wavenumber than the "in-plane" u-vibration because it contains more phenyl-phenyl ring interaction.

The band at 181 cm^{-1}, absent in the thyminate complex, is typical of metal chlorine bending vibrations, and is so assigned. Other low frequency bands are likely δNAuP, in-plane and out-of-plane motions (with respect to the plane of thyminate ring).

3.3.6 Conclusions

Gold(I) is considered a soft or class b metal ion (91,163) and likely to interact with the relatively soft sites on DNA bases. In studies involving cisplatin, platinum(II) binds preferentially at the N(7) position of guanine residues (139). However, in other experiments, when attempts are made to strip platinum off the DNA strand with cyanide ion, the small fraction of the metal which remains is bound to thymine residues (164). Reaction of platinum(II) with deprotonated thymine is apparently not reversible as with other bases. The pH at which this reaction occurs in vitro is higher than physiological pH and whether the reaction with thymine can occur in vivo is not known. Nevertheless, the possibility of metal assisted pK shifts or enzyme assistance can not be ruled out. It has been shown that interactions of DNA bases with metals at one site can markedly affect the pK of another site. Thus the interaction of platinum(II) with N(7) of guanine causes an acid shift of the N1 proton of 1.6 pK units and platinum(II) can bind at pH 7 to the exocyclic O(4) or N(4)

groups of 1-methylthymine, 1-methylcytosine and 1-methyluracil by a process of deprotonation, even though the pK of the NH_2 group in 1-methylcytosine is formally >12. (The pK's of the OH groups in the enol forms of 1-methyluracil and 1-methylthymine are unknown.) This reaction apparently involves initial binding of another platinum(II) atom at N3 of cytosine (165). Because of evidence for the stability of a platinum-thyminate interaction, it was expected that gold would also form a stable compound, and it does.

It is apparent that gold(I) can bind to DNA bases at similar positions to platinum(II) although, because of geometric requirements, any interactions with more than one base on a DNA strand will be different to those for cisplatin.

INTERACTION OF GOLD(III) COMPOUNDS WITH DNA

3.4.1 Introduction

Investigations of the interaction of gold(III) compounds with

DNA were sparked by the development of cisplatin as an anti-cancer drug

whose activity is thought to be associated with its ability to bind to

and produce lesions in cell DNA (28). These investigations were based

on two closely related aims. The study of gold(III) compounds, which

share a number of chemical and structural characteristics with platinum

drugs, is used for comparison purposes to lend further insight into the

details of action of cisplatin and analogous second generation drugs.

There is also the possibility of developing a gold anti-cancer drug

effective in its own right.

The biological relevance of gold's +3 oxidation state has been

questioned in light of XANES studies by Elder et al. (29). Certainly,

tetrachloroaurate, a relatively strong oxidant (see Figure 1.3.1), is

subject to almost quantitative reduction in vivo. However with

sufficient ligand stabilization, the possibility of obtaining a complex

with the potential to remain biologically intact can not be ruled out.

This is supported by studies carried out by Gibson et al. (166) who

synthesized adenine adducts of gold(III) in the interests of examining

their use as a biological stain. In contrast to the apparent reduction

of gold ions (ie. hydroxychloroaurate) by sugars and amino acids, the

gold(III)-adenine adduct was found to be effective as a positive stain

for chromatin, nucleoli and ribosomes without the characteristic

granular depositions left after gold salt staining.

A number of in vitro assays have been carried out on complexes such as trichloro(pyridine)gold(III) (99,100), trichloro- and tribromo(triethylphosphine)-gold(III) (100,103) and trichloro(2-hydroxyethylpyridine)gold(III) (141) confirming the ability of gold(III) to bind to plasmid DNA and alter its electrophoretic mobility and that the N(7) position of guanine residues is particularly susceptible to gold(III) interaction (103) (as it is to platinum(II) (139)).

Agarose gel electrophoresis was also performed on compounds 6 to 13 listed in Table 3.4.1 and the effects of their binding to plasmid DNA is compared to those of cisplatin and the gold(III) compounds already examined.

Results of these in vitro experiments were extended to the living system of the TA102 strain of Salmonella bacteria with the series of gold(III) compounds listed in Table 3.4.1. All but two of the compounds contain the chloride ligand, deemed a good leaving group. The exceptions are compounds 13 which has bromide and 9 which has no halide leaving group. With cisplatin it is postulated that once inside the cell, the complex is hydrolysed because of relatively low chloride ion concentration and the resulting aquo complex is more likely to bind to its target DNA base (126). It has also been established in cisplatin research that neutral compounds are necessary - probably to allow penetration of the complex across cell membranes (139). Two of the four compounds which do not fulfill this requirement are dichloro(1,10-phenanthrolene)gold(III)chloride and

Table 3.4.1 Description of compounds 1 - 13
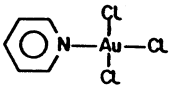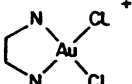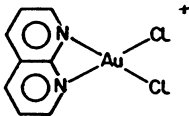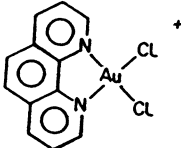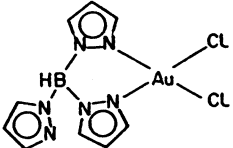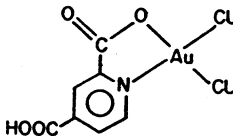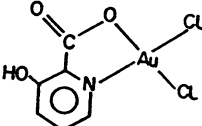
	Complex	Name	Ref.
	1	trichloro(pyridine)- gold(III)	(169)
	2	dichloro(ethylenediamine)- gold(III) chloride	(170)
	3	(2,2'-bipyridine)dichloro- gold(III) chloride	(171)
	4	(1,10-phenanthrolene)dichloro- gold(III) chloride	(172)
	5	dichloro[hydrotris(1-pyrazolyl- borate-N,N'-)gold(III)	(173)
	6	dichloro(4-carboxypicolinato- N,O-)gold(III)	
	7	dichloro(3-hydroxypicolinato- N,O-)gold(III)	

Table 3.4.1 continued

	Complex	Name
	8	dichloro(5-carboxypicolinato-N,O-)gold(III)
	9	bis(picolinato-N,O-)gold(III) diperchlorate
	10	dichloro[N,N'-bis(2-hydroxyethyl)-dithiocarbamato-S,S'-]gold(III)
	11	dichloro(2-hydroxymethyl-O-pyridine-N-)gold(III)
	12	dichloro(2-hydroxyethyl-O-pyridine-N-)gold(III)
	13	dibromo(2-hydroxypicolinato-N,O-)gold(III)

dichloro(bipyridine)gold(III)chloride whose N-donor ligands are potential DNA intercalators. Complexes of these ligands have been shown to be active even though they are charged (167,168).

3.4.2 Preparations

Methods used to synthesize complexes 1 to 5 have been reported in the literature and references are given in Table 3.4.1 alongside the respective compounds. Complexes 6 to 13 were synthesized by R.V.Parish, University of Manchester Institute of Science and Technology, Manchester, England, M60 1QD for the purpose of biochemical testing discussed in section 3.4.3.

3.4.3 Agarose gel electrophoresis and Ames Assays

Covalently closed circular plasmid DNA has been used to model the interaction of cisplatin with DNA. At increasing concentrations, cisplatin decreased and subsequently restored the electrophoretic mobility of pSM-1 and pM2 DNA (174). It has been postulated that the drug generates torsion in the DNA duplex (175,176) through intrastrand cross-linking (177) or local denaturation mechanisms (178). The resulting torsion would be consistent with dose dependent relaxation of the supercoiled plasmid followed by positive supercoiling and concomitant restoration of electrophoretic mobility. (py)AuCl$_3$, (Et$_3$P)AuBr$_3$ and (Et$_3$P)AuCl$_3$ alter the conformation of pBR322 DNA in a similar manner to cisplatin although higher concentrations were required to achieve the same effects (99,100,103).

A representative photograph, Figure 3.4.1, shows that the interaction of compounds 11,12 and 13 with PuC119 DNA resulted in an initial decrease in electrophoretic mobility followed by restoration of

Figure 3.4.1   A representative gel after electrophoresis of PuC119 DNA
               incubated with compounds 11, 12, 13 and cisplatin.

               The plasmid control (250 ng in each lane) is marked with
               an arrow.

               The key to complexes and their concentration in each lane
               is as follows:

complex 11   complex 12

i h g f e d c b a   ↓   i h g f e d c b a
- - - - - - - -   - - - - - - - -

- - - - - - - -   - - - - - - - -
i h g f e d c b a   ↑   i h g f e d c b a

complex 13   cisplatin

quantity of complex (nmol)

a; 1000
b; 100
c; 10
d; 1.0
e; 0.1
f; 0.01
g; 0.001
h; 0.0001
i; 0.00001
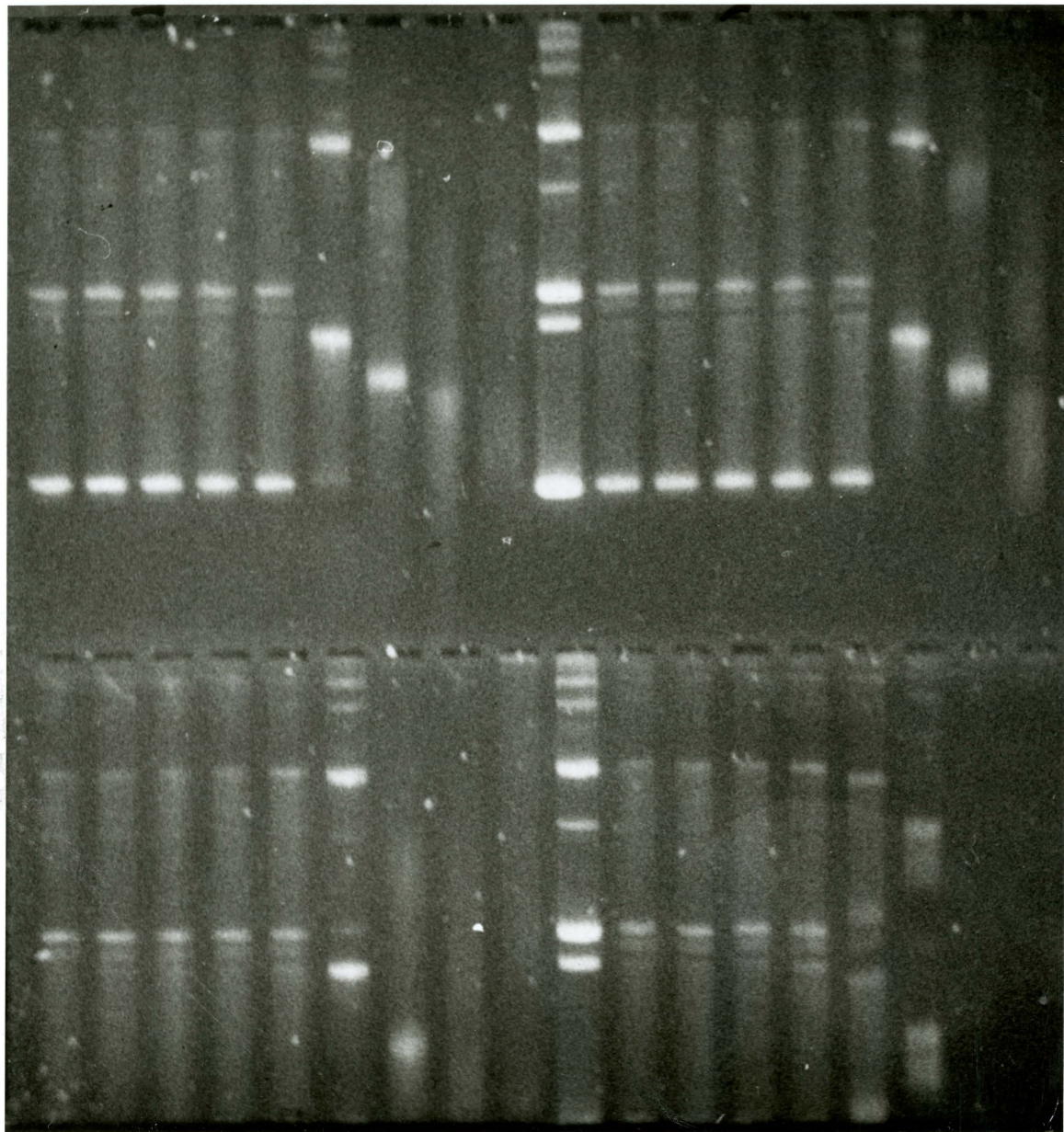
mobility as concentration was increased for both supercoiled plasmid (lower band) and supercoiled dimer (upper band). In accord with the literature (174-178), the observations are explained by an initial relaxation of the plasmid supercoil to a relatively less dense form - possibly closed circular. As compound concentration is increased, DNA-shortening, described previously, is apparent as evidenced by increasing electrophoretic mobility. At concentrations of 250 molecules of compound per base pair, smearing of bands is indicative of DNA degradation giving, essentially, a continuum of bands in the electrophoresis experiment.

With the exception of compound 10 (see Table 3.4.1), which almost completely degrades DNA even at low concentration, compounds tested showed similar ability to alter plasmid mobility and this ability is reminiscent of the effects of cisplatin although lower concentrations for the platinum complex were sufficient. Thus the mode of interaction of these complexes with DNA appears to be similar to that of cisplatin. However, compound 9, which unlike the other complexes has no halide leaving group, also gives similar results in the electrophoresis experiment. Therefore, an intercalative mechanism of DNA interaction was considered as all compounds tested (except 10) are planar. An X-ray structural determination of compound 10 has been carried out to examine the details of its non-planarity and this is discussed in section 3.4.4.

Further electrophoresis experimentation is necessary to study the mechanism of compound interaction with plasmid DNA. This work is beyond the scope of this thesis.
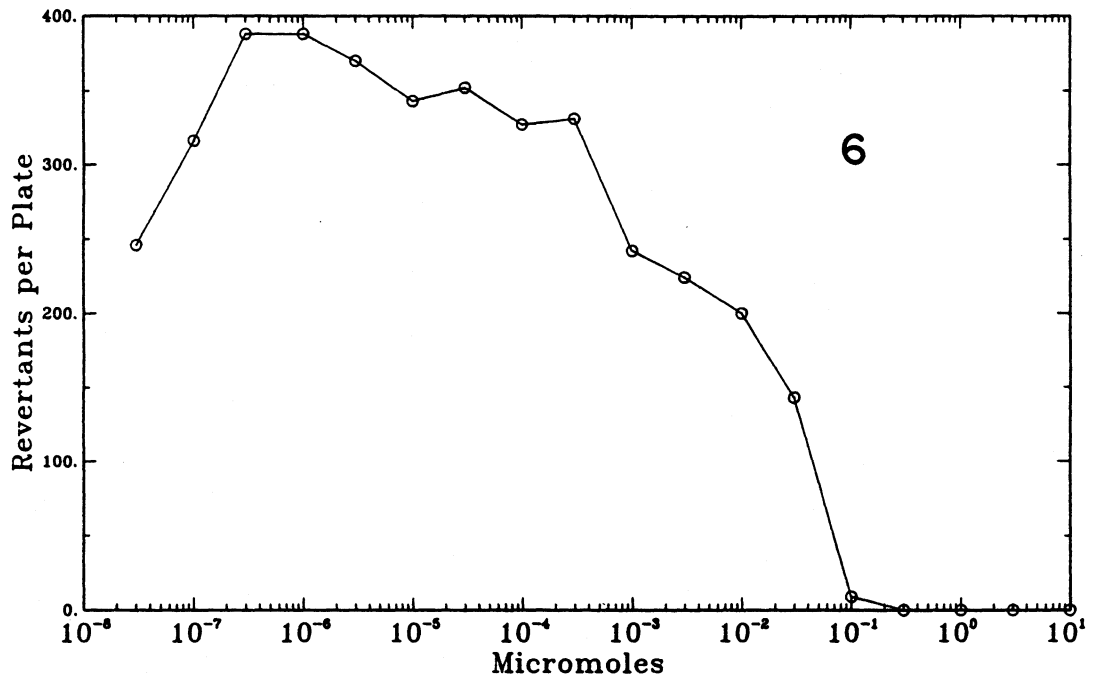
Figure 3.4.2 A representative plot of revertants per plate vs. concentration from TA102 Ames experiments on compound 6 (see Table 3.4.1).

Without exception the compounds were cytotoxic rather than mutagenic when tested in Ames assays of TA102 Salmonella bacteria (118) at concentrations of maximum cisplatin mutagenic activity.

The effect of changing concentration on number of revertants in the Ames tests is summarized in Table 3.4.A and plots for each compound and are illustrated in Figure 3.4.A. A representative example (compound 6) is shown as Figure 3.4.2. All graphs show that at higher concentrations, the compounds are cytotoxic. If this cytotoxicity is related to mutagenicity, it should be possible to observe an increase in number of revertants at lower compound concentration. This is, however, not the case as number of revertants never significantly exceeds that for DMSO controls even at extremely low complex concentration suggesting that mutation is not the source of cytotoxicity.

3.4.4 The Crystal and molecular structure of dichloro[bis(hydroxyethyl)dithiocarbamato-S,S']gold(III) (10)

Crystal data and other information pertinent to data collection and structure solution are given in Table 3.4.2. Atomic positional parameters and anisotropic temperature factors are listed in Tables 3.4.3 and 3.4.B. The origin for the unit cell was chosen according to Hahn (179). The molecule is shown in Figure 3.4.3 and interatomic distances and angles are listed in Table 3.4.4. The geometry of the gold atom is square planar, distorted as a result of the typical restricting chelate angle (S-Au-S 75.5(1)o) of the dithiocarbamate ligand (180-182). The main portion of the molecule is roughly planar. A summary of least-squares planes is given in Table 3.4.5. There are

Table 3.4.2 Crystal data for dichloro[N,N-bis(2-hydroxyethyl-
            dithiocarbamato-S,S'-]gold(III)

Formula	$C_5H_{10}AuCl_2NO_2S_2$
Formula weight	448.135
Crystal size and shape	$0.50 \times 0.10 \times 0.15 mm^3$ cylinder
Systematic absences	h00;h=2n
	0k0;k=2n
	00l;l=2n
Space group	$P2_12_12_1$
Diffractometer	P3
Temperature	22°C
Unit cell parameters	a=7.446(2)Å
	b=11.434(4)Å V=1325.5(4)Å³
	c=13.110(3)Å Z=4
ρ_{calc}, ρ_{obs}	2.67, 2.65gcm⁻³; $CHCl_3/CHBr_3$
Range of hkl	0<h<8, 0<k<13, -15<l<15
Maximum 2θ	50°
Number of reflcns measured	2259
Number of independent reflcns	1974
Standard reflcns(e.s.d)	0 -5 2(1.7%), 4 0 -5(1.6%)
R_{int}	0.0107
Final R,Rw	0.0432, 0.0397
Final shift/error max(ave)	0.039(0.017)
Error in obs of unit weight	S=1.4550
Highest peak, lowest valley	1.89eÅ⁻³, -2.11eÅ⁻³
Weighting	$w=(\sigma^2(F) + 0.0004F^2)^{-1}$
F(000)	784.2
Linear Absorption coefficient	μ=144.0cm⁻¹
Absorption Coefficient limits	3.148<A*<9.818*
Number of Variables	118

* absorption correction was applied

Table 3.4.3 Positional parameters ($\times 10^4$) and U_{eq} ($\text{Å}^2 \times 10^3$) for dichloro[N,N-bis(2-hydroxyethyl)dithiocarbamato-S,S'-]gold(III)

Atom	x	y	z	U_{eq}
Au	5469.4(6)	7735.3(4)	-830.7(3)	34.5
Cl1	5441(6)	9738(3)	-564(3)	51
Cl2	5347(5)	7914(3)	-2597(2)	55
S1	5622(4)	7224(3)	868(2)	39
S2	5561(5)	5736(3)	-840(2)	45
C1	5748(17)	5809(10)	456(9)	37
N	5917(13)	4897(9)	1058(8)	39
C2	6263(17)	3714(12)	586(9)	42
C3	4562(24)	3037(12)	396(11)	59
O1	3890(17)	2492(10)	1266(8)	80
C4	6073(20)	5016(15)	2181(10)	52
C5	4322(24)	5270(13)	2682(10)	57
O2	3069(16)	4389(10)	2489(8)	69
H2	705	387	12	
H22	733	361	112	
H3	497	220	8	
H33	355	363	5	
H4	707	565	229	
H44	673	436	219	
H5	367	618	251	
H55	502	511	324	
H99	314	296	156	

$U_{eq} = 1/3(U_{11} + U_{22} + U_{33})$

Hydrogen atoms were located and fixed.
The hydrogen atom attached to O2 was not located.

Table 3.4.4 Selected interatomic distances (Å) and angles (o) for
dichloro[N,N-bis(2-hydroxyethyl)dithiocarbamato-S,S'-]
gold(III)

Au-Cl1	2.316(3)	Au-Cl2	2.325(3)
Au-S1	2.305(3)	Au-S2	2.287(3)
S1-C1	1.71(1)	S2-C1	1.71(1)
C1-N	1.31(2)	N-C2	1.51(2)
N-C4	1.48(2)	C2-C3	1.51(2)
C4-C5	1.49(2)	C3-O1	1.39(2)
C5-O2	1.40(2)	O1-H99	0.87(1)
Au···S1	3.610(3)	Au···S1	3.838(3)
O1···O2	2.77(2)	O2···Cl1	3.35(1)
O1-H99	0.87	H99···O2	2.04
Cl1-Au-Cl2	93.6(1)	Cl1-Au-S1	96.0(1)
Cl1-Au-S2	171.5(1)	Cl2-Au-S1	170.4(1)
Cl2-Au-S2	94.8(1)	S2-Au-S1	75.5(1)
Au-S1-C1	86.4(4)	Au-S2-C1	87.0(4)
S1-C1-S2	110.9(7)	S1-C1-N	125(1)
S2-C1-N	125(1)	C1-N-C2	119(1)
C1-N-C4	122(1)	C2-N-C4	118(1)
N-C2-C3	113(1)	N-C4-C5	113(1)
C2-C3-O1	113(1)	C4-C5-O2	111(1)
Au···S1···Au	177.3(1)	C3-O1···2	101.7(1)
C5-O2···Cl1	99.4(1)	O1-H99···O2	141

Table 3.4.5   Best Planes and dihedral angles for
dichloro[N,N-bis(2-hydroxyethyldithiocarbamato-S,S'-]
gold(III)

Plane	Distance of atom from plane (Å)
1. Cl1,Cl2,Au,S1,S2	Cl1;0.020(6), Cl2;0.010(5), Au;-0.0006(6), S1;0.006(4), S2;0.012(5), C1;-0.08(1), N;0.15(1), C2;0.40(1), C3;-0.88(2) O1;1.43(1), C4;0.20(2), C5;-1.11(2) O2;-2.06(1).
2. Au,S1,S2,C1	Au; 0.0000(6), S1;-0.003(5), S2;-0.005(5), C1;0.06(1), Cl1;0.038(6), Cl2;0.019(5), N;0.119(1), C2;0.36(2), C3;-0.93(2), O1;-1.49(2), C4;0.17(2), C5;-1.15(2), O2;-2.10(1).
3. S1,S2,C1,N	S1;0.000(5), S2;0.000(5), C1;0.01(1), N;0.00(1), Cl1;0.23(2), Cl2;0.21(2), Au;0.105(9), C2;0.20(2), C3;-1.11(2), O1;-1.73(2), C4;0.19(2), C5;-1.32(2), O2;-2.30(2).
4. C1,N,C2,C4	C1;0.02(2), N;-0.04(1), C2;0.02(2), C4;0.04(2), Cl1;0.54(5), Cl2;0.24(5), Au;0.22(3), S1;0.16(2), S2;-0.07(2), C3;-1.35(2), O2;-1.97(2), C5;-1.22(3), O2;-2.29(2).

Dihedral angles (°)

1 - 2	0.5(1)	1 - 3	3.6(3)
1 - 4	7.6(4)	2 - 3	3.2(3)
2 - 4	7.1(4)	3 - 4	5.3(5)

Figure 3.4.3 A molecule of dichloro[N,N-bis(2-hydroxyethyl)-
dithiocarbamato-S,S'-]gold(III). The intramolecular
hydrogen bond is shown by the broken line.
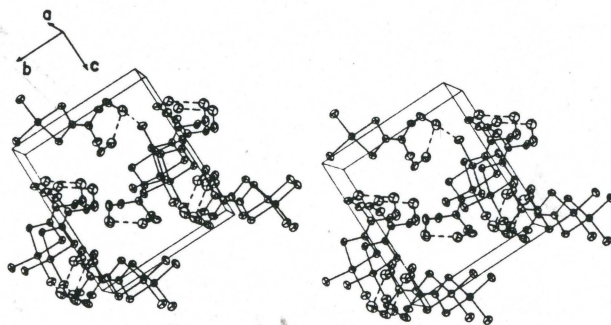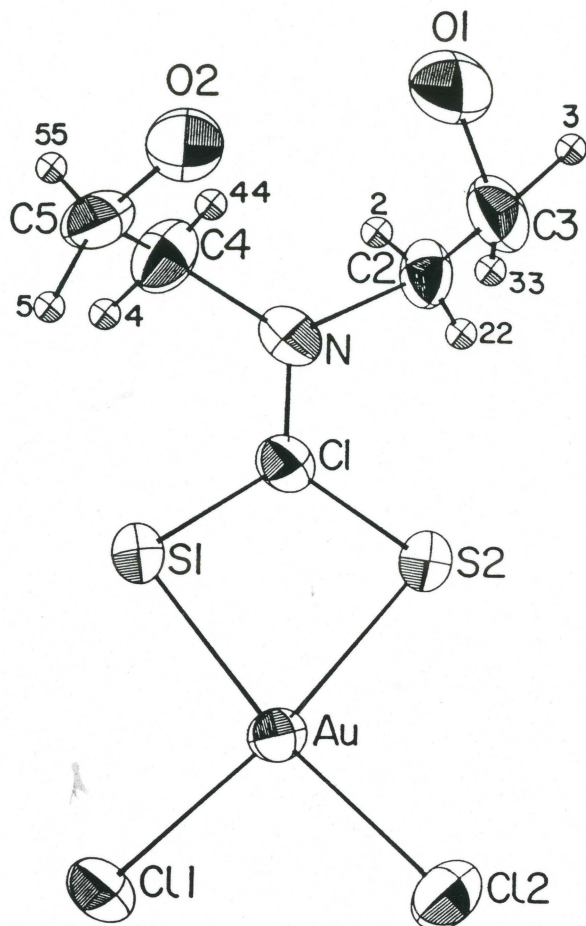
Figure 3.4.4 Stereoview of the packing. Hydrogen bonding is depicted
by broken lines.

small distortions of the square plane towards square pyramidal geometry such that the gold atom lies roughly 0.01 Å out of the ligand atom plane. The S1,S2,C1,N plane lies at 3.6(3)° to the square plane and the C1,N,C2,C4 plane is bent a further 4.0(4)° away from the square plane, although a slight twist has developed such that the dihedral angle between S1,S2,C1,N and C1,N,C2,C4 is 5.3(5)° rather than 4.0(4)°. The N-CH$_2$-CH$_2$ planes are almost at right angles to these planes and are arranged such that the CH$_2$OH units lie on the same side of the square plane. They are arranged in this manner because of an intramolecular hydrogen bond (O1···O2, 2.77(2) Å; O1-H99, 0.87 Å; H99···O2, 2.04 Å; O1-H99···O2, 141°; C3-O1···O2, 101.7(4)°). The asymmetry introduced here is responsible for the twist mentioned above. Thus the carbon atoms of the -CH$_2$OH groups lie 0.88(2) Å (C3) and 1.11 Å (C5) and the oxygen atoms 1.43(1) (O1) and 2.06(1) Å (O2) out of the square plane such that overall, the molecule is markedly non-planar.

The Au-Cl bonds are relatively long but this is because of the _trans_ influence of the sulphur atoms. The strong _trans_ influence of a ligand sulphur atom compared to chlorine has been shown in the structure of trichloro(thianthrene)gold(III) (183) where the Au-Cl distance _trans_ to the thianthrene ligand is 2.31(2) Å and that _trans_ to the chlorine atom is 2.27(4) Å. The Au-Cl and Au-S bond lengths agree well with those observed in similar Au(III) structures (180,181,184).

Angles within the dithiocarbamate group are consistent with an sp^2 hybridization scheme for C1 (S1-C1-S2 110.9(7)°, S1-C1-N 125(1)°, S2-C1-N 125(1)°). The shortness of the C1-N bond length (1.31(2) Å) compared to the other C-N bond lengths (1.51(2), 1.48(2) Å) suggests

considerable double bond character in the Cl-N bond as reported in crystallographic and infrared studies of a diethylthiocarbamato-nickel(II) complex (182).

A stereoview of the packing is shown in Figure 3.4.4. The molecules related by the 2_1 axis parallel to **a** are arranged such that the square planes are coplanar with **bc** and stack one above the other in the **a** direction. The result is that the gold atom in one molecule lies directly above and below S1 of adjacent molecules. If there is an Au····S interaction it is extremely weak as Au···S1 distances (3.610(6), 3.838(6) Å) are greater than the sum of van der Waals radii (approximately 3.5 Å) (134). The S1···Au···S1' chain is rectilinear (S1···Au···S1', 177.9(1)°). Within a given chain, pairs of -CH$_2$OH units project in the same direction from the main planes of the molecules and are hydrogen bonded to Cl1 (through O2···Cl1, 3.35(1) Å) in molecules in an adjacent chain in which the -CH$_2$OH units project from the main planes in the opposite direction. The resultant hydrogen bonded molecules form a helix generated by the 2_1 axis in the **c** direction and are the source of chirality in the structure.

3.4.5 Conclusions: Even though compounds 6 to 13 have shown their ability to interact with DNA and are thus potentially mutagenic, in a living system they exert a cytotoxic effect before DNA interaction can take place. Furthermore, reduction of the gold(III) complexes _in vivo_ likely occurs and it is this reaction which is the probable cause of cell death. The N,O-chelate ligands incorporated in all but compound 10 are apparently not sufficiently able to stabilize gold(III) in a biological milieu.

CHAPTER 4

TRIS-2-PYRIDYLPHOSPHINE AND CHLORO(TRIS-2-PYRIDYLPHOSPHINE-P-)GOLD(I)

4.1 Introduction

The tris-2-pyridylphosphine ligand is somewhat novel from the point of view of coordination chemistry. As outlined in section 1.7, two chemically different sites on TPP are available for binding to metals, namely, the relatively polarizable phosphorus atom to which the soft gold(I) ion coordinates as well as the aromatic nitrogen sites which are relatively harder and available for binding to harder metals. It was originally hypothesized that transition metal ion coordination to these pyridines would provide a means of tuning electronic effects at the phosphorus site which could extend to the gold(I) complexes formed. In addition, the incorporation of other metals into TPP offers the possiblility of altering solubility properties of the typically hydrophobic phosphine complex. Furthermore, not only can ^{31}P NMR be used to probe the fate of these compounds in vivo, but more sensitive techniques would become available, for example, electron spin resonance spectroscopy of paramagnetic metal ions such as copper(II).

Aspects of transition metal complex studies are discussed in Chapter 5. For the purposes of future comparison with transition metal complexes, properties of TPP and chloro(tris-2-pyridylphosphine)gold(I) (ClAuTPP) will be described in the following sections of this chapter. The comparative ability of TPP to serve as a sufficiently stabilizing ligand in complexes analogous to auranofin will also be discussed in section 4.5 in light of preliminary ^{1}H and ^{31}P NMR results.

99

4.2 Preparations

tris-2-pyridylphosphine (TPP); The ligand was made on one tenth scale according to the method of Boggess and Zatko (185).

chloro(tris-2-pyridylphosphine)gold(I) (ClAuTPP); 300 μL (3 mmol) of thiodiglycol in 1 mL of ethanol was added dropwise to a solution of 0.589 g (1.5 mmol) of $HAuCl_4 \cdot 3H_2O$ at 0°C and stirred for 20 minutes. To this was added a solution of 0.4 g (1.5 mmol) of tris-2-pyridylphosphine in 10 mL of ethanol. A white precipitate began to form immediately. The reaction mixture was allowed to stir for 45 minutes after which the precipitate was filtered and dried _in_ _vacuo_ over night. The product was recrystallized twice from CH_2Cl_2/hexanes (1:1) to yield 0.488 g of a colourless crystalline solid (65%). Analysis required for $C_{15}H_{12}AuClN_3P$: C; 36.2, H; 2.4, N; 8.4, Cl; 7.1%. Found: C; 35.2, H; 2.4, N; 8.1, Cl; 7.9%.

^{197}Au Moess: δ; 3.92(2) mm/sec, Δ; 7.44(8) mm/sec, Γ; 1.88(13)mm/sec.

[2,3,4,6-tetra-O-acetylthioglucopyranosato-S-](tris-2-pyridylphosphine)gold(I) (TATGAuTPP); Tetracetylthioglucose (1.385 g, 0.38 mmol) was dissolved in 15 mL of ethanol to which had been added an aqueous solution of K_2CO_3 (5 mL) such that pH was ca. 7.5. An equimolar ethanol (20 mL) solution of ClAuTPP was added and the mixture allowed to stir at 0°C for three hours during which time more K_2CO_3 was added to bring the pH to 8. The solvent was then removed under reduced pressure and the residue extracted with CH_2Cl_2 (10 mL). The fraction of product which was insoluble in CH_2Cl_2 dissolved in water and precipitated AgCl on addition of aqueous $AgNO_3$. Addition of hexanes to the CH_2Cl_2 solution produced a gummy solid which could not be filtered.

Infrared spectra of the residue (Table 4.2.A) as well as ^{1}H NMR spectra
(Table 4.5.1) support the formulation of the product as the title
compound.

4.3 The crystal and molecular structure of TPP

Crystal data and other details of data collection and structure
refinement are listed in Table 4.3.1. Atomic positional parameters and
anisotropic temperature factors are given in Tables 4.3.2 and 4.3.A
respectively. The molecule is illustrated in Figure 4.3.1 and bond
lengths and angles are listed in Table 4.3.3.

Bond lengths and angles at the phosphorus atom are normal and
comparable to those reported in the structure of triphenylphosphine (P-
C; 1.837(4) Å (ave.) for TPP vs. 1.828(9) Å (ave.) for
triphenylphosphine and C-P-C; 101.5(2)° (ave.) for TPP vs. 103(4)°
(ave.) for triphenylphosphine) (186). The phosphorus atom is in a
roughly trigonal pyramidal environment; the pyridine rings assume a
propeller-like arrangement although dihedral angles between rings are
distorted from the 120° angles expected for a C_3 propeller. A list of
best planes and dihedral angles is given in Table 4.3.4. Bond lengths
within the rings are normal, angles are slightly distorted from 120° as
a result of perturbation by the nitrogen atom such that angles at N are
relatively small (N1;116.5(2), N2;116.7(2), N3;117.4(2)°) and, to
compensate, those at C5 are relatively large (C51;124.9(3),
C52;123.7(3), C53;124.0(3)°).

A diagram of the packing is given in Figure 4.3.2. The packing
in this lattice is dominated by two types of intermolecular

Table 4.3.1 Crystal data for tris-2-pyridylphosphine

Formula	$C_{15}H_{12}N_3P$
Formula weight	265.25
Crystal size and shape	$0.26\times0.27\times0.48mm^3$ cylinder
Systematic absences	h0l;l=2n
	0k0;k=2n
	00l;l=2n
Space group	$P2_1/c$
Diffractometer	P3
Temperature	22°C
Unit cell parameters	a=9.172(2)Å $\quad$ β=100.99(1)°
	b=9.169(2)Å $\quad$ V=1325.5(4)$Å^3$
	c=16.057(3)Å $\quad$ Z=4
ρ_{calc},ρ_{obs}	1.329, 1.34 gcm^{-3}; $ZnCl_2(aq)$
Range of **hkl**	0<h<10,0<k<10,-18<l<18
Maximum 2θ	50°
Number of reflcns measured	2481
Number of independent reflcns	2341
Standard reflcns(e.s.d)	0 1 -4(1.4%),0 2 1(1.5%)
R_{int}	0.0067
Final R,Rw	0.0694,0.0548
Final shift/error max(ave)	0.004(0.001)
Error in obs of unit weight	S=1.4775
Highest peak, lowest valley	$0.6eÅ^{-3},-0.3eÅ^{-3}$
Weighting	$w=(\sigma^2(F) + 0.000219F^2)^{-1}$
F(000)	552.3
Linear Absorption coefficient	$\mu=2.0cm^{-1}$
Absorption Coefficient limits	1.047<A*<1.075*
Number of Variables	208

* absorption correction was not applied introducing a maximum error
 in Fo of ≅0.7%

Table 4.3.2. Positional parameters ($\times 10^4$) (hydrogen atoms $\times 10^3$) and Ueq ($\times 10^3$) for tris-2-pyridylphosphine.

Atom	x	y	z	U_{eq}
P	6163(1)	7131(1)	3745.4(4)	40.6
C11	7416(3)	7949(3)	3113(1)	35
C21	6880(3)	9097(3)	2580(2)	42
C31	7785(3)	9721(3)	2086(2)	47
C41	9183(3)	9183(3)	2129(2)	50
C51	9620(3)	8028(3)	2663(2)	49
N1	8789(2)	7402(2)	3156(1)	42
C12	6698(3)	8120(3)	4758(1)	40
C22	5717(3)	8088(3)	5310(2)	55
C32	6070(4)	8811(4)	6071(2)	64
C42	7357(4)	9568(3)	6249(2)	58
C52	8270(4)	9580(3)	5665(2)	59
N2	7969(3)	8869(2)	4922(1)	52
C13	7048(3)	5349(3)	3990(1)	38
C23	7920(3)	4935(3)	4747(2)	51
C33	8473(4)	3528(4)	4831(2)	63
C43	8105(4)	2580(3)	4166(2)	59
C53	7234(3)	3075(3)	3437(2)	52
N3	6698(2)	4426(2)	3333(1)	45
H21	591(3)	944(3)	258(2)	
H31	739(3)	1055(3)	175(1)	
H41	984(3)	963(3)	179(1)	
H51	1061(3)	761(3)	271(1)	
H22	492(3)	755(3)	515(2)	
H32	541(3)	879(3)	646(2)	
H42	765(3)	1014(3)	675(2)	
H52	920(3)	1010(3)	579(1)	
H23	807(3)	561(3)	516(2)	
H33	898(3)	327(3)	532(2)	
H43	842(3)	158(3)	422(1)	
H53	696(3)	238(3)	294(1)	

$Ueq = 1/3(U11 + U22 + U33 + 2Cos\beta U13)$

Hydrogen atoms were located and their positions were refined with isotropic temperature factors fixed at 0.06 Å^2.

Table 4.3.3 Bond Lengths (Å) and Angles (o)
for tris-2-pyridylphosphine

P-C11	1.832(2)	P-C12	1.844(2)	P-C13	1.835(3)
C11-C21	1.386(3)	C12-C22	1.378(3)	C13-C23	1.375(3)
C21-C31	1.378(3)	C22-C32	1.375(4)	C23-C33	1.383(4)
C31-C41	1.364(4)	C32-C42	1.352(4)	C33-C43	1.369(4)
C41-C51	1.378(4)	C42-C52	1.371(4)	C43-C53	1.363(4)
C51-N1	1.330(3)	C52-N2	1.341(3)	C53-N3	1.331(3)
N1-C11	1.346(3)	N2-C12	1.335(3)	N3-C13	1.343(3)
C21-H21	0.94(2)	C22-H22	0.88(3)	C23-H23	0.90(2)
C31-H31	0.97(2)	C32-H32	0.95(2)	C33-H33	0.87(2)
C41-H41	0.98(2)	C42-H42	0.95(2)	C43-H43	0.96(3)
C51-H51	0.97(3)	C52-H52	0.96(2)	C53-H53	1.01(2)
C11-P-C12	101.4(1)	C11-P-C13	100.6(1)	C12-P-C13	102.5(1)
P-C11-C21	117.8(2)	P-C12-C22	117.4(2)	P-C13-C23	126.4(2)
C11-C21-C31	119.3(2)	C12-C22-C32	119.3(3)	C13-C23-C33	119.0(3)
C21-C31-C41	119.0(3)	C22-C32-C42	118.9(3)	C23-C33-C43	118.9(3)
C31-C41-C51	118.1(2)	C32-C42-C52	118.8(3)	C33-C43-C53	118.4(3)
C41-C51-N1	124.9(3)	C42-C52-N2	123.7(3)	C43-C53-N3	124.0(3)
C51-N1-C11	116.5(2)	C52-N2-C12	116.7(2)	C53-N3-C13	117.4(2)
N1-C11-P	119.9(2)	N2-C12-P	120.2(2)	N3-C13-P	111.3(2)
N1-C11-C21	122.2(2)	N2-C12-C22	122.5(2)	N3-C13-C23	122.2(2)
C11-C21-H21	118(2)	C12-C22-H22	115(2)	C13-C23-H23	116(2)
H21-C21-C31	123(2)	H22-C22-C32	125(2)	H23-C23-C33	125(2)
C21-C31-H31	117(1)	C22-C32-H32	120(2)	C23-C33-H33	118(2)
H31-C31-C41	124(1)	H32-C32-C42	121(2)	H33-C33-C43	123(2)
C31-C41-H41	120(1)	C32-C42-H42	124(1)	C33-C43-H43	121(2)
H41-C41-C51	122(1)	H42-C42-C52	118(2)	H43-C43-C53	121(2)
C41-C51-H51	121(1)	C42-C52-H52	120(1)	C43-C53-H53	119(1)
H51-C51-N1	114(1)	H52-C52-N2	117(1)	H53-C53-N3	117(1)

Table 4.3.4   Best planes and dihedral angles for
tris-2-pyridylphosphine

Plane	Distance of atom from plane (Å)
1. C11,C21,C31,C41,C51,N1	C11;0.004(3),C21;-0.006(3),C31;0.001(4) C41;0.007(4),C51;-0.006(3),N1;-0.000(2)
2. C12,C22,C32,C42,C52,N2	C12;0.007(3),C22;-0.011(4),C32;0.006(4) C42;0.004(4),C52;-0.005(4),N2;-0.002(3)
3. C13,C23,C33,C43,C53,N3	C13;0.001(3),C23;-0.006(4),C33;0.008(4) C43;0.006(4),C53;0.000(4),N3;0.001(3)
4. C11,C22,C33	P;0.822(2)

Dihedral angles (o)

1 - 2	97.0(1)	1 - 4	60.0(1)
1 - 3	97.4(1)	2 - 4	58.0(1)
2 - 3	91.8(1)	3 - 4	47.2(1)

Figure 4.3.1   A molecule of tris-2-pyridylphosphine showing atom
labelling
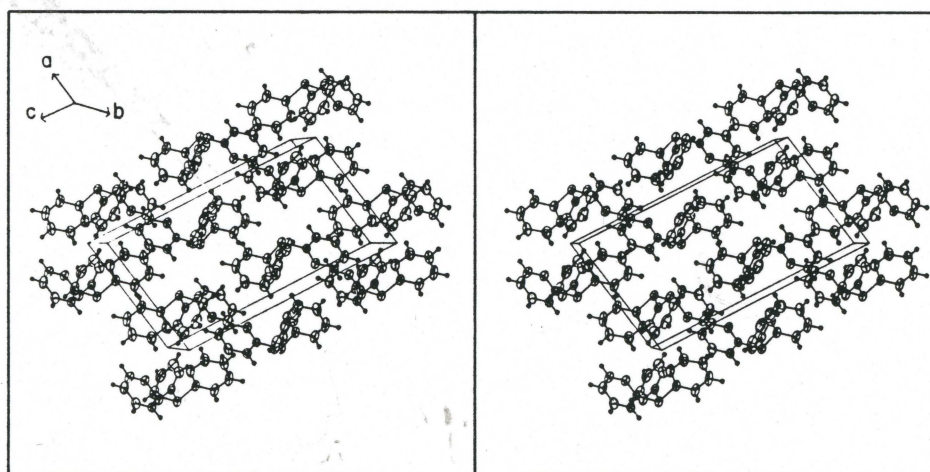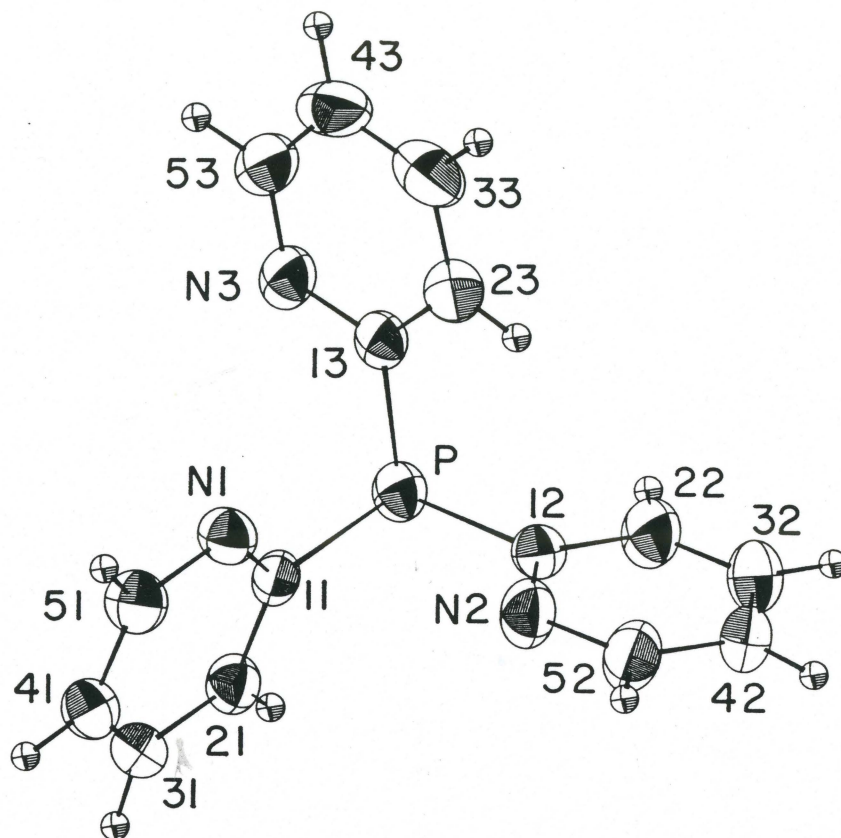
Figure 4.3.2   Stereoview of the unit cell

interactions. The first is dipolar attraction where molecules are
stacked with their approximate C_3 axes parallel to the $\underline{a}$ axis such that
molecular dipoles oppose one another in adjacent chains of molecules
parallel to the $\underline{c}$ direction and related by the $\underline{c}$-glide plane. The
other source of lattice energy exerted in the packing of this molecular
solid are van der Waals interactions which can be further specified as
π-π interactions. These interactions arise, for example, as a
consequence of the attraction between nuclei in an aromatic ring with
the negatively charged π-electron cloud of an adjacent ring. As with
other van der Waals attractions, the energy of such an interaction
falls off as a function of $1/r^6$. Calculations performed on the benzene
lattice have determined that energy associated with such π-π
interactions ranges from 6 to 9 kcal/mol (187) which is similar in
magnitude to a strong hydrogen bond ($\cong 6$ kcal/mol in ice (38)). Energy
is maximized when two rings are completely overlapped but parallel
rings which have undergone slight sideways slippage still experience
significant intermolecular attraction. Energies fall off as rings
deviate from coplanarity. In the title structure, π-π interactions are
evident about the inversion centers at 1/2,0,1/2 (ring-ring distance
3.7 Å) and 1/2,1/2,0 (ring-ring distance also 3.7 Å) involving ring 2
and its symmetry-related equivalent. Figure 4.3.3 is a photograph of
the CHEMX-generated (121) view of overlapping van der Waals shells in
the π-π interaction between adjacent molecules related by the inversion
center at 1/2,0,1/2 in the present structure. This is the only
apparent interaction between adjacent chains. Other π-π interactions
occur beween neighbouring molecules within the chain which involve
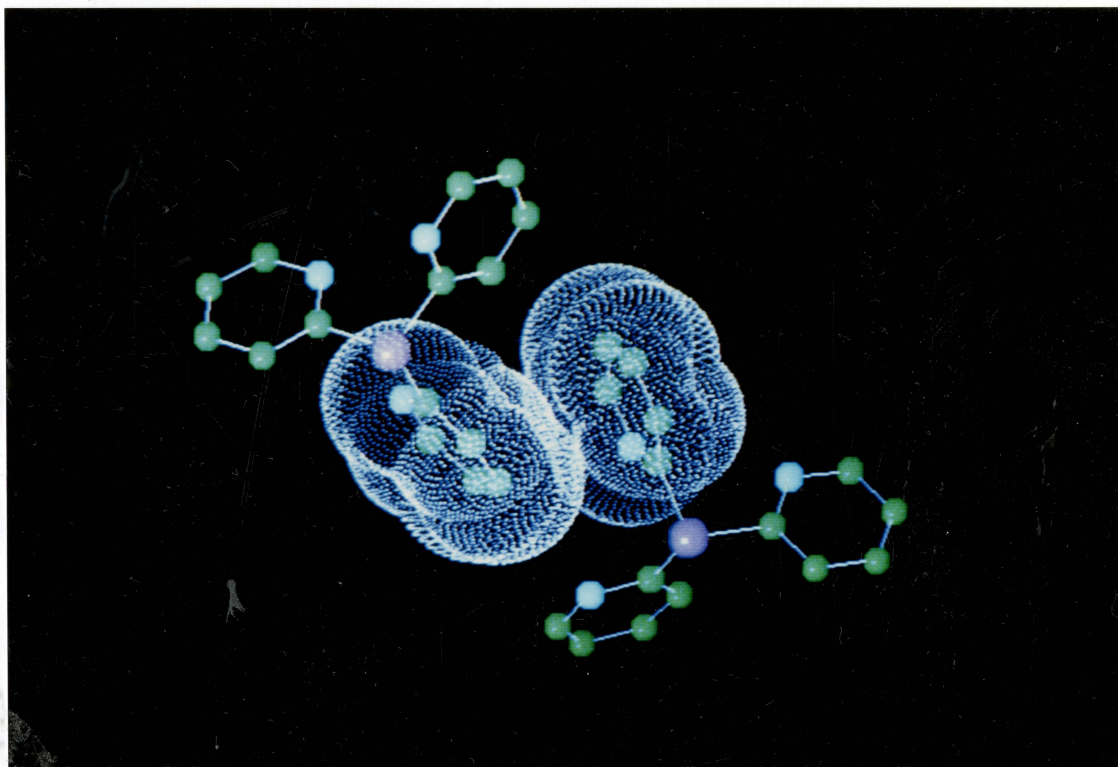
Figure 4.3.3 The overlapping van der Waals shells in the π-π
           interaction about 1/2,0,1/2 in the lattice of TPP
           generated by the CHEMX (121) program

rings 1 and 2 (ring 1 - ring 2 distance 3.73 Å).

Considerable distortion is experienced by ring 3 as a result of packing effects. The bending of this ring is evident in comparison of dihedral angles between the rings and the C11-C12-C13 plane. For a strictly C_{3v} molecule, these angles would be 90°. Ring 3 makes and angle of only 47.2(1)° while those for rings 1 and 2 are 60.0(1) and 58.0(1)° respectively. As well, angles surrounding C1 of each ring where P-C11-C21 is 117.8(2)°, P-C11-N1 is 119.9(2)°, P-C12-C22 is 117.4(2)° and P-C12-N2 is 120.2(2)° but P-C13-C23 is 126.4(2)° and P-C13-N3 is 111.3(2)° indicate a tilting of ring 3 toward its nitrogen atom. Ring 3 is also distinguished from rings 1 and 2 according to the position of the nitrogen atom with respect to the apical phosphorus atom. If phosphorus is considered to be the top of the molecule, rings 1 and 2 are positioned so that their respective nitrogen atoms are at the bottom of the molecule and C12 and C22 are toward the top while ring 3 is turned so that N3 is on the upper side. The opposite orientation of ring 3 has implications in the packing of molecules in the lattice. Ring 3 bends upward in order to avoid steric interactions of the hydrogen attached to C23 (H23) with hydrogen atoms from rings in the next layer. N1 and N2 in the equivalent positions on the other rings have no such hydrogen atom and are not subject to the same potential steric effects.

4.4 The crystal and molecular structure of ClAuTPP

The title compound crystallizes in two distinct phases which are designated as structures **A**, with four molecules, and **B** with two

molecules in their triclinic cells. Crystal data for both phases and
other information pertinent to structure solution are given in Table
4.4.1. Atomic positional parameters of structure **A** are listed in Table
4.4.2 and Table 4.4.3 summarizes those for **B**. Lists of anisotropic
temperature factors are given in Tables 4.4.A and 4.4.B for **A** and **B**
respectively. Molecule 1 from **A** is shown in Figure 4.4.1 (the other
molecules are very similar) and selected bond lengths and angles are
given in Table 4.4.4. The same numbering scheme is maintained in all
three molecules, except that atoms in the second molecule of **A** have a
prime affix. The general geometry of the molecule is very like that
observed for chlorotriphenylphosphinegold(I) (135) and chloro(2-
pyridyl)diphenylphosphinegold(I) (174). The P-Au-Cl unit is
essentially linear in all three molecules. The Au-Cl bond distances
are similar to those in other structures (135,188) but are shorter than
the bridging Au-Cl distances in $((C_6H_5)_3PAu)_2Cl^+$ (2.328(5), 2.340(5) Å)
and marginally shorter than the terminal Au-Cl distances in Cl-
$Au((C_6H_5)_2P(CH_2)_2P(C_6H_5)_2)Au-Cl$ (2.299(5), 2.289(5) Å) (188). The
distances and angles within the phosphine do not differ from
corresponding values in $(C_6H_5)_2(C_5H_4N)P$ complexes of silver and gold
(135). The effect of gold binding at the phosphorus atom is to
increase the C-P-C angles in the free ligand (C11-P-C12, 101.4(1), C11-
P-C13, 100.6(1) and C12-P-C13, 102.5(1)°) to C11-P-C12; 103.9(6)(**A**),
102.1(7)(**A′**), 103.6(3)(**B**), C11-P-C13; 106.3(8)(**A**), 110.7(8)(**A′**),
105.9(3)(**B**) and C12-P-C13; 105.3(6)(**A**), 105.0(7)(**A′**) and 106.5(3)(**B**).
The effect of C-P-C angle opening is perhaps better reflected by a
comparison of phosphorus distances from the C11,C12,C13 plane. (A

Table 4.4.1 Crystal data for chloro(tris-2-pyridylphosphine)-
gold(I) cells **A** and **B**

	A	**B**
Formula	$C_{15}H_{12}AuClN_3P$	$C_{15}H_{12}AuClN_3P$
Formula weight	497.68	497.68
Crystal size	$0.097 \times 0.210 \times 0.258mm^3$	$0.129 \times 0.226 \times 0.613mm^3$
shape	plate	plate
Systematic absences	none	none
Space group	$P\bar{1}$	$P\bar{1}$
Diffractometer	$P2_1$	$P3$
Temperature	22°C	22°C
Unit cell parameters	a=13.050(1)Å	a=8.611(2)Å
	b=14.276(2)Å	b=9.118(2)Å
	c=11.263Å(2)	c=11.186(3)Å
	α=115.86(1)°	α=94.86°
	β=92.10(1)°	β=112.22(2)°
	γ=118.80(1)°	γ=94.96(2)°
	V=1571.5 Å³	V=803.4 Å³
	Z=4	Z=2
ρ_{calc}, ρ_{obs}	2.10,2.1 3gcm⁻¹; ZnBr₂(aq)	
Reflections collected	h,k,±l	h,k,±l
Maximum 2θ	45°	55°
Number of reflcns measured	4349	3889
Number of independent reflcns	3861	3486
R_{int}	0.026	0.009
Final R,Rw	0.0584,0.0645	0.0399,0.0394
Final shift/error max(ave)	0.036(0.007)	0.022(0.005)
Error in obs of unit weight	S=1.1366	S=1.2955
Highest peak	1.0eÅ⁻³	1.0eÅ⁻³
Lowest valley	-0.84eÅ⁻³	-0.87eÅ⁻³
Weighting	$w=(\sigma^2(F) + 0.001493F^2)^{-1}$	$w=(\sigma^2(F) + 0.000528F^2)^{-1}$
F(000)	966.8	483.4
Linear Absorption coefficient	μ=99.4cm⁻¹	μ=99.4cm⁻¹
Absorption Coefficient limits	2.20<A*<7.73*	3.19<A*<11.2*
Number of Variables	379	190

* absorption correction applied

Table 4.4.2. Positional parameters and Ueq ($\times 10^3$) for chloro(tris-2-pyridylphosphine)gold(I), cell **A**.

Atom	x	y	z	U_{eq}
Au	369.50(5)	696.93(5)	655.57(5)	24.3
Cl	445.1(4)	789.4(4)	-469.9(4)	39
P	296.1(3)	605.7(3)	-223.7(3)	23
C11	376(1)	708(1)	-35(1)	25
C21	436(1)	838(1)	23(1)	34
C31	485(1)	908(1)	170(2)	38
C41	482(1)	853(2)	243(2)	37
C51	420(2)	728(2)	174(2)	43
N1	370(1)	657(1)	38(1)	31
C12	134(1)	549(1)	-238(1)	23
C22	96(1)	578(1)	-122(2)	37
C32	-31(2)	533(2)	-145(2)	49
C42	-108(1)	462(2)	-283(2)	45
C52	-59(1)	435(2)	-390(2)	41
N2	65(1)	480(1)	-367(1)	39
C13	304(1)	470(1)	-279(1)	22
C23	208(1)	356(1)	-301(1)	29
C33	224(1)	257(1)	-353(2)	36
C43	331(1)	275(1)	-372(2)	35
C53	425(1)	392(1)	-344(2)	39
N3	411(1)	489(1)	-295(1)	37
Au'	149.04(5)	883.12(5)	970.34(5)	27.1
Cl'	222.2(4)	837.3(4)	-212.7(4)	39
P'	79.3(3)	937.8(3)	148.6(3)	22.6
C11'	-91(1)	842(1)	98(1)	25
C21'	-163(1)	888(1)	108(2)	34
C31'	-293(1)	801(2)	56(2)	43
C41'	-336(2)	676(2)	7(2)	42
C51'	-252(1)	638(2)	1(2)	42
N1 '	-130(1)	724(1)	46(1)	37
C12'	124(1)	916(1)	286(1)	25
C22'	210(2)	885(2)	283(2)	37
C32'	244(2)	876(2)	398(2)	50
C42'	186(2)	895(2)	497(2)	41
C52'	107(1)	929(1)	493(1)	32
N2'	73(1)	940(1)	387(1)	33
C13'	139(1)	1107(1)	237(1)	28
C23'	260(2)	1184(2)	251(2)	48
C33'	306(2)	1314(2)	319(2)	67
C43'	231(2)	1353(2)	360(2)	48
C53'	111(2)	1262(2)	343(2)	51
N3'	70(1)	1142(1)	276(1)	44

$U_{eq}=1/3(U_{11}+U_{22}+U_{33}+2\cos\alpha U_{23}+2\cos\beta U_{13}+2\cos\gamma U_{12})$

Table 4.4.3. Positional parameters (x10^4) and Ueq (x10^3) for
chloro(tris-2-pyridylphosphine)gold(I), cell **B**.

Atom	x	y	z	U$_{eq}$
Au	1722.3(3)	3185.4(2)	1489.2(2)	38.8
Cl	2609(3)	4463(2)	154(2)	57.7
P	902(2)	1915(2)	2802(1)	36.8
C11	1649(7)	90(6)	2952(5)	38
C21	1173(10)	-828(8)	1835(6)	58
C31	1667(11)	-2217(9)	1921(9)	70
C41	2695(10)	-2629(8)	3102(9)	66
C51	3170(11)	-1595(9)	4162(8)	68
N1	2653(9)	-230(7)	4102(6)	63
C12	-1381(7)	1488(6)	2269(6)	41
C22	-2447(9)	2273(8)	1389(8)	56
C32	-4162(10)	1953(10)	1037(9)	68
C42	-4768(10)	873(11)	1575(10)	72
C52	-3609(11)	118(11)	2446(10)	81
N2	-1931(8)	410(7)	2803(6)	64
C13	1669(8)	2873(6)	4453(6)	39
C23	981(12)	2491(10)	5334(8)	76
C33	1676(12)	3246(11)	6589(8)	89
C43	3023(11)	4350(9)	6884(7)	62
C53	3614(10)	4626(8)	5958(7)	59
N3	2957(7)	3922(6)	4737(5)	50

$U_{eq}=1/3(U_{11}+U_{22}+U_{33}+2\cos\alpha U_{23}+2\cos\beta U_{13}+2\cos\gamma U_{12})$

Table 4.4.4. Selected Interatomic Distances (Å) and Angles (°)
for chloro(tris-2-pyridylphosphine)gold(I)

	A	A′	B
Au-Cl	2.277(5)	2.272(5)	2.274(1)
Au-P	2.214(4)	2.218(4)	2.220(1)
P-C11	1.84(1)	1.86(1)	1.834(6)
C11-C21	1.42(2)	1.36(3)	1.344(8)
C21-C31	1.42(2)	1.42(2)	1.37(1)
C31-C41	1.37(3)	1.40(3)	1.39(1)
C41-C51	1.34(3)	1.43(4)	1.36(1)
C51-N1	1.32(2)	1.35(2)	1.36(1)
N1-C11	1.30(3)	1.32(2)	1.324(8)
P-C12	1.84(2)	1.84(2)	1.820(6)
C12-C22	1.39(2)	1.38(3)	1.370(9)
C22-C32	1.42(3)	1.43(4)	1.37(1)
C32-C42	1.40(3)	1.37(3)	1.36(1)
C42-C52	1.38(3)	1.35(3)	1.38(1)
C52-N2	1.39(2)	1.36(3)	1.34(1)
N2-C12	1.30(2)	1.34(2)	1.333(8)
P-C13	1.82(2)	1.86(2)	1.821(6)
C13-C23	1.39(2)	1.37(2)	1.381(9)
C23-C33	1.40(3)	1.42(3)	1.39(1)
C33-C43	1.34(3)	1.35(4)	1.39(1)
C43-C53	1.39(2)	1.41(3)	1.35(1)
C53-N3	1.36(3)	1.32(3)	1.343(9)
N3-C13	1.31(2)	1.23(3)	1.321(7)

Table 4.4.4 continued

	A	A′	B
Cl-Au-P	179.5(1)	176.5(2)	178.9(1)
Au-P-C11	114.4(5)	112.8(4)	113.0(2)
Au-P-C12	114.0(6)	115.0(6)	114.4(2)
Au-P-C13	112.2(5)	110.7(5)	112.6(2)
C11-P-C12	103.9(6)	102.1(7)	103.6(3)
C11-P-C13	106.3(8)	110.7(8)	105.9(3)
C12-P-C13	105.3(6)	105.0(7)	106.5(3)
P-C11-C21	118(1)	124(1)	115.8(5)
C11-C21-C31	113(2)	118(2)	117.2(6)
C21-C31-C41	122(2)	117(2)	121.4(7)
C31-C41-C51	117(2)	121(2)	116.7(7)
C41-C51-N1	125(2)	120(2)	122.8(7)
C51-N1-C11	119(2)	119(2)	117.8(6)
N1-C11-C21	124(1)	126(1)	124.1(6)
N1-C11-P	119(1)	109(1)	120.0(4)
P-C12-C22	121(1)	120(1)	120.6(5)
C12-C22-C32	116(1)	116(2)	119.1(7)
C22-C32-C42	119(2)	117(2)	119.6(8)
C32-C42-C52	119(2)	122(2)	117.8(7)
C42-C52-N2	122(2)	123(2)	123.7(8)
C52-N2-C12	117(2)	116(2)	116.9(7)
N2-C12-C22	127(1)	126(2)	122.9(6)
N2-C12-P	112(1)	114(1)	116.5(5)
P-C13-C23	124(1)	115(2)	122.2(5)
C13-C23-C33	118(2)	116(2)	118.5(7)
C23-C33-C43	120(2)	120(2)	117.9(7)
C33-C43-C53	119(2)	117(2)	118.9(6)
C43-C53-N3	122(2)	121(2)	124.3(6)
C53-N3-C13	119(1)	121(2)	116.7(5)
N3-C13-C23	123(2)	125(2)	123.6(6)
N3-C13-P	114(1)	120(1)	114.3(4)

Table 4.4.5. Best planes, dihedral angles and torsional angles for
chloro(tris-2-pyridylphosphine)gold(I), cells **A** and **B**.

Plane	Distance of atom from plane (Å)

Cell A Molecule 1

1. C11,C21,C31,C41,C51,N1   C11,0.00(2);C21,0.01(2);C31,-0.01(2);
    C41,0.01(2);C15,-0.01(2);N1,-0.02(2).

2. C12,C22,C32,C42,C52,N2   C12,0.01(2);C22,-0.01(2);C32,0.00(3);
    C42,0.01(3);C52,-0.01(2);N2,0.00(3).

3. C13,C23,C33,C43,C53,N3   C13,-0.02(2);C23,0.02(2);C33,0.01(2);
    C43,0.00(2);C53,0.00(2);N3,0.01(2).

4. C11,C22,C33   P,0.73(1)

Cell A Molecule 2

1. C11;C21;C31;C41;C51;N1'   C11;0.01(2);C21;0.01(2);C31;-0.03(2);
    C41;0.02(2);C51;0.01(2);N;-0.01(2).

2. C12;C22;C32;C42;C53;N2'   C12;-0.01(2);C22;0.01(2);C32;0.02(3);
    C42;-0.02(2);C52;0.00(2);N2;0.01(2).

3. C13;C23;C33;C43;C53;N3'   C13;0.01(2);C23;0.00(2);C33;0.01(3);
    C43;-0.02(2);C53;0.03(3);N3;-0.01(2).

4. C11,C22,C33   P,0.72(1)

Cell B

1. C11,C21,C31,C41,C51,N1   C11,-0.01(1);C21,0.03(1);C31,-0.01(1);
    C41,-0.01(1);C51,0.01(1);N1,0.01(1).

2. C12,C22,C32,C42,C52,N2   C12,0.00(1);C22,0.00(1);C32,0.00(1);
    C42,0.01(1);C52,0.00(1);N2,0.00(1).

3. C13,C23,C33,C43,C53,N3   C13,0.00(1);C23,0.00(1);C33,0.00(1);
    C43,0.01(1);C53,-0.01(1);N3,0.00(1).

4. C11,C22,C33   P,0.723(4)

All molecules

5. Au,P,C11(')
6. Au,P,C12(')
7. Au,P,C13(')

Table 4.4.5 continued

	A	A'	B
Dihedral angles (°)			
1 - 2	124.4(8)	103.4(7)	100.6(3)
1 - 3	122.0(7)	157.0(9)	105.3(3)
2 - 3	134.7(6)	100.0(8)	133.7(3)
1 - 4	81.2(9)	67(1)	38.2(3)
2 - 4	31.4(8)	88.6(7)	73.7(3)
3 - 4	40.0(7)	90(1)	75.6(3)
1 - 5	17(1)	71.0(6)	60.0(2)
2 - 5	38(1)	57(1)	54.0(3)
3 - 5	50.0(5)	53.4(6)	69.6(3)
1 - 6	54.3(8)	78.8(9)	86.2(2)
2 - 6	12.9(4)	2(3)	18.4(2)
3 - 6	57.3(5)	82(2)	51.3(3)
1 - 7	25.0(8)	78.0(7)	56.7(2)
2 - 7	77.4(9)	76.2(9)	88.6(3)
3 - 7	62.5(6)	55.6(7)	18.1(3)
Torsional angles (°)			
Cl-Au-P-Cl1	130.2(3)	101.4(3)	-28.3(2)
Cl-Au-P-Cl2	-110.5(3)	-142.1(3)	-146.6(2)
Cl-Au-P-Cl3	9.0(3)	-23.3(3)	91.7(2)

Figure 4.4.1   A molecule of chloro(tris-2-pyridylphosphine)gold(I)
                showing atom labelling

CELL A

CELL B
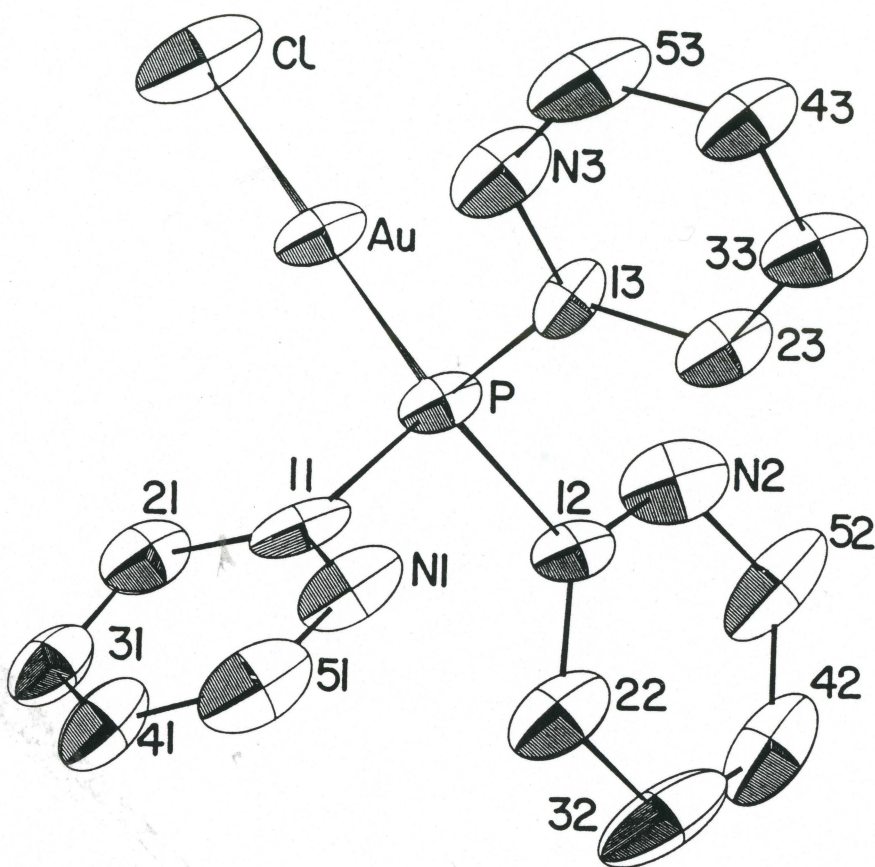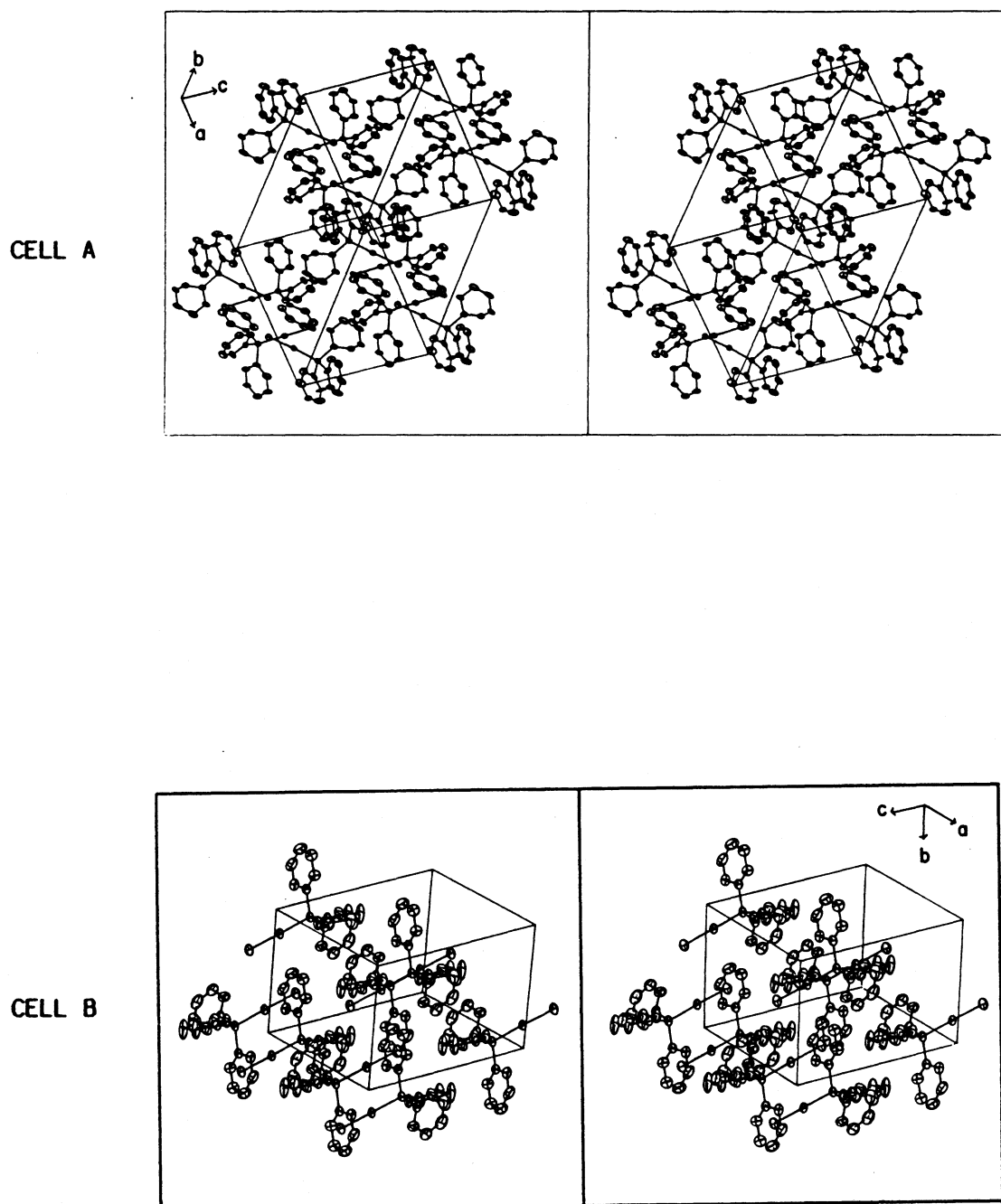
Figure 4.4.2   Stereoviews of the packing in cells **A** and **B**

summary of least-squares planes, dihedral and torsional angles is given

in Table 4.4.5). This distance decreases from 0.822(2) Å in TPP to

0.73(1)(**A**), 0.72(1)(**A'**) and 0.723(4) Å (**B**) in ClAuTPP and is consistent

with removal of sterically demanding lone pair electron density from

the phosphorus atom when gold is bound. The Au-P distances are short.

They lie below Au-P values found for gold-phosphine clusters (range:

2.267(2)-2.42(1) Å) (188), two coordinate Au(I) complexes (range,

2.226(4)-2.389(6) Å) (188) and the long distances in three and four

coordinate Au(I) complexes (range, 2.359(6)-2.610(9) Å) (188) as well

as the Au-Cl distance in chloro(triphenylphosphine)gold(I) (2.235(3)

(135).

The 2-pyridyl rings in the phosphines of **A** (first molecule) and

B are arranged so that the geometry is markedly distorted from C$_3$

(dihedral angles, (Au-P-Cli)-(Ring i), **A**, i=1, 17(1); 2, 12.9(4); 3,

62.5(6)°; **A**, i=1', 71.0(6); 2', 52.4(3); 3', 55.6(7); **B**, i=1, 60.0(2);

2, 18.4(2); 3, 18.1(3)°). This is caused by the intermolecular

interactions of the packing.

The packing of **A** and **B** are shown in Figure 4.4.2. In **B** the

molecular P-Au-Cl axis lies roughly along [1 1 -1] and because of the

inversion centre all are parallel and dipolar interactions cancel. The

small dihedral angle of ring 2, noted above, is a consequence of a π-π

interaction between equivalent rings in molecules related by the

inversion centre at 1/2,0,0. Apart from this interaction the

intermolecular ring-ring contacts are normal van der Waals interactions

and are arranged primarily about the z=1/2 plane, whereas the chlorine

atoms lie close to the z=0 plane.

The prime difference between the packing in **A** and **B** is that in **A** the P-Au-Cl axes are not all parallel and this is caused by the much greater extent of π-π ring interactions. The second (primed) molecular axis is roughly parallel to **c** while the molecular axis of the first molecule lies roughly along [1 1 -1]. There is a double stack of phenyl rings centered around the **b** axis. Along this line the sequence of pairs of rings is: Rings 1 and 3 from **A'**; Rings 3 and 1 from the centrosymmetrically (0,0,0) related **A'**; Rings 3 from **A** and its centrosymmetrically (0,0,1/2) related pair; Rings 1 and 3 from **A'**; etc. This packing arrangement explains why rings 1 and 3 in **A'** are close to coplanar (dihedral angle 157.0(9)o).

4.5 ^{1}H and ^{31}P NMR

The ^{1}H NMR spectrum of TATGAuTPP is very similar to that reported by Sadler (189) for auranofin. Chemical shift data and assignments are listed in Table 4.5.1. Only the C(1) proton resonance experiences a significant shift upon gold binding. That shift occurs from 4.756 ppm in TATG to 5.119 ppm in auranofin and 5.13 ppm in TATGAuTPP.

Phosphorus chemical shift data are given in Table 4.5.2. The shift for (1-methylthyminato-N^{3-})triphenylphosphinegold(I) has been included for comparison. The downfield shift in ^{31}P NMR resonance of TPP (-0.33 ppm) to 33.06 ppm (CDCl$_3$) in ClAuTPP is explained by the electron withdrawing effect of the gold(I) ion. The subsequent upfield shift in the 33 ppm resonance of the gold complex upon interaction with thiols such as glutathione (21.26 ppm) and TATG (21.08 ppm) are

Table 4.5.1 ^{1}H NMR chemical shifts (CDCl$_3$) for tetracetylthioglucose

TATG[a]	Auranofin[a]	TPPAuTATG	assgmt
4.756	5.119	5.13	C(1)H
4.902	5.15	5.13	C(2)H
2.051	2.016	1.98	C(2)Me
5.235	5.15	5.13	C(3)H
2.036	2.058	2.00	C(3)Me
5.042	4.983	5.13	C(4)H
2.002	2.083	2.04	C(4)Me
3.875	3.730	3.78	C(5)H
4.249	4.224	4.28	C(6)Ha
4.099	4.131	4.23	C(6)Hb
1.966	1.988	1.90	C(6)Me

[a] ref (189)

Table 4.5.2 ^{31}P NMR data for the interaction of chloro(tris-2-pyridylphosphine)gold(I) with sulphur containing ligands

system	solvent	chemical shift[a]
TPP	$CDCl_3$	-0.33
TPPAuCl	DMSO	33.66
TPPAuCl	$CDCl_3$	33.09
Ph_3-Au-thyminate	$CDCl_3$	32.71
TPPAuCl + d-pen[b] disulphide	D_2O	32.02
TPPAuCl + glutathione	D_2O	21.26
TPPAuCl + tetracetylthioglucose	$CDCl_3$	21.08
TPPAuCl + albumin	D_2O/NH_4HCO_3	36.77 30.22
Et_3AuCl + glutathione	D_2O	33.1[c]
Et_3AuCl + TATG	D_2O	34.3[c]
Et_3AuCl + ergothioneine	D_2O	31.9[c]
Et_3AuCl + albumin	D_2O	36.1[c]
Et_3AuCl + oxidized albumin	D_2O/NH_4HCO_3	26.7, 25.1, 22.2[d]

[a] in ppm relative to H_3PO_4 (85% in D_2O)

[b] d-penicillamine

[c] Chemical shift values reported vs. $OP(OCH_3)_3$ (74) have been converted in this table by subtraction of 2.74 ppm.

[d] Same comment as (c) (75)

consistent with relative shielding effects of these ligands compared to the chloride ligand. In support of this explanation is the almost insignificant upfield shift from 33.06 ppm upon interaction with a poorer sulphur-containing ligand such as d-penicillamine disulphide (32.02 ppm). The chemical shift is also similar when chloride is replaced by the thyminate ligand (32.71 ppm).

The above trend is opposite to that reported by Shaw et al. where pK_{SH} of the sulphur ligand was related to ^{31}P NMR chemical shifts of triethylphosphinegold(I) complexes such that pK_{SH} decreased with increasing thiol affinity for gold(I) and this in turn was accompanied by larger ^{31}P downfield shifts (74). These observations were supported by competition studies where albumin was able to displace TATG and glutathione from gold(I) but the reverse reaction did not occur. Changing from one thiol ligand to another has a larger influence on the ^{31}P chemical shift for triethylphosphine than is observed for the tris-(aromatic ring) ligand.

Notably, resonances associated with the interaction of ClAuTPP with albumin suggest binding to weaker protein sites than the anticipated βcys-34 thiol. Thiol titre was measured according to the method of Ellman (190) to ensure that albumin aging had not occurred to the extent that only the weak sites were available for gold binding. It seems unlikely that the pyridyl rings are so sterically restrictive that they prevent penetration of the gold into the crevice thought to accomodate the thiol site (54). Further experimentation is required before conclusions can be drawn about either electronic or the steric effects of TPP.

CHAPTER 5

COMPLEXES OF TRIS-2-PYRIDYLPHOSPHINE

5.1 Introduction

Tris-2-pyridylphosphine is a member of a series classified as tripod ligands which have the ability to chelate metal ions and constrain them to coordination geometries not necessarily achieved by comparable unrestricted ligands.

This property of tripods (and other multidentate ligands of fixed geometry) has been used in an approach to the construction of models for metalloprotein active sites. The tertiary structure of proteins also places constraints on the metal coordination sphere by holding potential ligands in certain geometries to which metal ions must mold. In fact, TPP and similar ligands have been studied, for example, as models for the active site of human carbonic anhydrase (191,192) (see section 5.2) and the oxygen carrying protein haemerythrin (193) (see section 5.4).

Thus the point of view for study of TPP is not restricted to reactions which take place at the phosphorus binding site and the changes which can be affected by N-bound metal ions but is extended to focus as well on coordination of other metals at the nitrogen sites with the possibility of observing the effect of co-coordination of gold(I).

Syntheses, X-ray crystallographic and spectroscopic studies of zinc(II) (section 5.2), copper(II) (section 5.3), cobalt(III) (section 5.5), iron(II) and iron(III) (section 5.4) and chromium(III) (section

5.5) complexes with TPP and ClAuTPP are discussed in the following sections of this chapter and a summary of crystallographic parameters and infrared data is given in Chapter 6.

5.2 Zinc complexes

5.2.1 Introduction

The preparation and properties of complexes of zinc with TPP and ClAuTPP will be discussed in this section. The zinc(II) ion has a d^{10} electronic configuration thus spectroscopic techniques available for studying the chemistry of its complexes are somewhat limited. This metal was chosen on the basis of its diamagnetic properties, however, because its complexes (particularly those with ClAuTPP and those resulting from their interaction with thiol ligands) could be studied with use of NMR spectroscopy.

Zinc complexes of TPP have also previously been examined as potential models for human carbonic anhydrase (HCA) (192). The active site of HCA is known to contain zinc coordinated to three imidazole groups from histidine residues in the protein. The fourth binding site in the distorted tetrahedral zinc(II) coordination sphere is thought to be held by a water or hydroxide ligand (194,195). It has previously been shown that a complex of zinc(II) with tris(4,5-diisopropyl-imidazol-1-yl)phosphine also possesses the capability of catalyzing the conversion of CO_2 to HCO_3^- and is thus a good model of the protein active site (196).

5.2.2 Preparations

triaquo(tris-2-pyridylphosphine)zinc(II) dinitrate trihydrate

([TPPZn(H$_2$O)$_3$](NO$_3$)$_2$); TPP (0.7768 g, 2.9 mmol) was dissolved in 20 mL of ethanol. An ethanol solution (20 mL) of 0.8597 g (2.9 mmol) of Zn(NO$_3$)$_2$·6H$_2$O was added to the TPP solution slowly and stirred overnight. The ethanol was removed under reduced pressure and the residue was stirred in acetone for 30 minutes after which time a white solid was filtered off, washed with acetone and air dried. The colourless solid was recrystallized from 10:90 H$_2$O:ethanol to yield 0.794 g (52%) of product. Crystals used in the X-ray diffraction experiment were obtained by slow evaporation of an aqueous solution. Analysis required for C$_{15}$H$_{12}$N$_5$O$_6$PZn: C; 39.6, H; 2.7, N; 15.4%. Found: C; 39.2, H; 2.8, N; 15.1%.

^{31}P NMR; -43.29(s) ppm

[(chloro(tris-2-pyridylphosphine)-P-gold(I))-N,N',N"-]zinc(II)

dinitrate ([(ClAuTPP)Zn](NO$_3$)$_2$); An aqueous solution (10 mL) containing 0.044 g (0.15 mmol) Zn(NO$_3$)·6H$_2$O was added to 0.0736 g (0.15 mmol) (ClAuTPP in 10 mL of acetone and stirred for 2 hours. The solvent was removed under reduced pressure to leave an oily residue which produced a white solid when stirred with acetone. The product was soluble in water but attempts at recrystallization resulted in decomposition of the zinc complex by precipitation of ClAuTPP. It was therefore necessary to carry out spectroscopic (see Chapter 6) measurements on the crude material.

bis(tris-2-pyridylphosphine-N,N',N"-)zinc(II)diperchlorate

([(TPP)$_2$Zn](ClO$_4$)$_2$); was prepared according to the method of Boggess

5.2.2 Preparations

triaquo(tris-2-pyridylphosphine)zinc(II) dinitrate trihydrate

([TPPZn(H$_2$O)$_3$](NO$_3$)$_2$); TPP (0.7768 g, 2.9 mmol) was dissolved in 20 mL

of ethanol. An ethanol solution (20 mL) of 0.8597 g (2.9 mmol) of

Zn(NO$_3$)$_2$·6H$_2$O was added to the TPP solution slowly and stirred

overnight. The ethanol was removed under reduced pressure and the

residue was stirred in acetone for 30 minutes after which time a white

solid was filtered off, washed with acetone and air dried. The

colourless solid was recrystallized from 10:90 H$_2$O:ethanol to yield

0.794 g (52%) of product. Crystals used in the X-ray diffraction

experiment were obtained by slow evaporation of an aqueous solution.

Analysis required for C$_{15}$H$_{12}$N$_5$O$_6$PZn: C; 39.6, H; 2.7, N; 15.4%. Found:

C; 39.2, H; 2.8, N; 15.1%.

^{31}P NMR; -43.29(s) ppm

[triaquo(chloro(tris-2-pyridylphosphine)-P-gold(I))-N,N',N"-]zinc(II)

dinitrate ([(ClAuTPP)Zn(H$_2$O)$_3$](NO$_3$)$_2$); An aqueous solution (10 mL)

containing 0.044 g (0.15 mmol) Zn(NO$_3$)·6H$_2$O was added to 0.0736 g (0.15

mmol) (ClAuTPP in 10 mL of acetone and stirred for 2 hours. The

solvent was removed under reduced pressure to leave an oily residue

which produced a white solid when stirred with acetone. The product was

soluble in water but attempts at recrystallization resulted in

decomposition of the zinc complex by precipitation of ClAuTPP. It was

therefore necessary to carry out spectroscopic (see Chapter 6)

measurements on the crude material.

bis(tris-2-pyridylphosphine-N,N',N"-)zinc(II)diperchlorate

([(TPP)$_2$Zn](ClO$_4$)$_2$); was prepared according to the method of Boggess

and Zatko (185).

bis(chloro(tris-2-pyridylphosphine-P-)gold(I)-N,N′,N″)zinc(II)

dinitrate ([(ClAuTPP)₂Zn](NO₃)₂); A solution of 0.1075 g (0.36 mmol)

of $Zn(NO_3)_2 \cdot 6H_2O$ in 10 mL of ethanol was added to 0.3597 g (0.72 mmol)

of ClAuTPP in 20 mL of acetone. A precipitate formed immediately. The

reaction mixture was stirred overnight and the product was filtered and

air dried. This compound was subject to the same decomposition problem

described for $[(ClAuTPP)Zn](NO_3)_2$ and infrared data (Chapter 6) are

reported for the crude material.

5.2.3 The crystal and molecular structure of TPPZn(H₂O)₃(NO₃)₂·3H₂O

The molecule is illustrated in Figure 5.2.1. Crystal data and

other parameters relevent to data collection are given in Table 5.2.1.

Atomic positional parameters and anisotropic temperature factors are

listed in Tables 5.2.2 and 5.2.A respectively. Interatomic distances

and angles are given in Table 5.2.3. The zinc atom is approximately

octahedral with _facial_ coordination to the three pyridyl nitrogen atoms

as well as three oxygen atoms from bound water molecules. In

comparison, the coordination of the similar but more sterically

hindered ligand tris-(4,5-diisopropylimidazol-2-yl)phosphine to zinc

results in a tetrahedral complex with chloride as the fourth ligand

(197). The octahedral shape is somewhat distorted although this does

not appear to result directly from chelate restrictions imposed by the

tripod ligand since the N-Zn-N angles deviate least from the 90° angles

expected in an octahedral complex. The participation of the

coordinated water molecules in extensive intermolecular hydrogen

Table 5.2.1 Crystal Data for triaquo(tris-2-pyridylphosphine-N,N',N"-) zinc(II) dinitrate monohydrate

Formula	$C_{15}H_{12}ZnN_5O_6PZn \cdot H_2O$
Formula weight	526.704
Crystal size and shape	0.29x0.26x0.39mm^3 cylinder
Systematic absences	h0l; h+l=2n
	0k0;k=2n
	00l;l=2n
Space group	$P2_1/n$
Diffractometer	P3
Temperature	22°C
Unit cell parameters	a=9.031(2)Å β=91.85(2)°
	b=16.923(4)Å V=2151.6(9)Å^3
	c=14.086(3)Å Z=4
ρ_{calc}, ρ_{obs}	1.626,1.63(6); CHCl$_3$/CHBr$_3$
Range of hkl	0<h<10, 0<k<20, -16<l<16
Maximum 2θ	50°
Number of reflcns measured	3999
Number of independent reflcns	3811
Standard reflcns(e.s.d)	-3 -6 -2(1.7%), 4 4 -2(1.9%)
R_{int}	0.0093
Final R,Rw	0.0635,0.0553
Final shift/error max(ave)	0.004(0.001)
Error in obs of unit weight	S=1.3714
Highest peak, lowest valley	0.8eÅ^{-3},-0.4eÅ^{-3}
Weighting	$w=(\sigma^2(F) + 0.000537\ F^2)^{-1}$
F(000)	1081.8
Linear Absorption coefficient	μ=13.152cm^{-1}
Absorption Coefficient limits	1.34<A*<1.59*
Number of Variables	313

* absorption correction applied

Table 5.2.2 Positional parameters (x10⁴) and Ueq (x10³) for triaquo(tris-2-pyridylphosphine-N,N′,N″-)zinc(II) dinitrate hydrate.

Atom	x	y	z	U_{eq}
Zn	-487.4(5)	1294.3(3)	7273.4(3)	32.2
P	20.8(1)	-686.7(6)	7599.3(8)	45
N4	5428(4)	1872(2)	9840(2)	45
N5	-5331(5)	2222(2)	5280(3)	58
O1	5992(4)	1426(2)	9247(2)	58
O2	4827(4)	2502(2)	9580(2)	63
O3	5452(4)	1682(2)	10694(2)	57
O4	5097(5)	1984(2)	4509(3)	76
O5	-6561(4)	2517(2)	5350(3)	78
O6	-4498(4)	2186(3)	6004(3)	112
O7	927(3)	2258(2)	7211(2)	41
O8	-1729(4)	2056(2)	8177(2)	47
O9	-1614(4)	1799(2)	6086(2)	46
O10	3763(3)	2065(3)	7610(3)	77
C11	945(4)	-19(2)	8530(3)	39
C21	1753(5)	-347(3)	9275(3)	49
C31	2373(5)	141(3)	9968(3)	54
C41	2181(5)	946(3)	9896(3)	47
C51	1353(5)	1237(2)	9129(3)	42
N1	740(4)	774(2)	8451(2)	36
C12	1058(5)	-220(2)	6567(3)	40
C22	2005(5)	-679(2)	6043(3)	48
C32	2753(5)	-349(3)	5303(3)	55
C42	2511(5)	440(3)	5100(3)	53
C52	1530(5)	872(3)	5643(3)	44
N2	812(4)	552(2)	6367(2)	39
C13	-1750(5)	-378(2)	7472(3)	37
C23	-2801(6)	-964(3)	7513(3)	50
C33	-4282(6)	-763(3)	7450(3)	62
C43	-4675(5)	30(3)	7361(3)	56
C53	-3555(5)	585(3)	7321(3)	44
N3	-2114(4)	393(2)	7373(2)	36

$U_{eq}=1/3(U_{11}+U_{22}+U_{33}+2Cos\beta U_{13})$

Table 5.2.2 continued

Hydrogen positional parameters

Atom	x	y	z
H1	123	190	910
H2	267	132	1045
H3	300	-128	1056
H4	167	-97	918
H7	220	-131	621
H8	351	-69	489
H9	310	73	452
H10	137	152	547
H12	-253	-160	760
H13	-517	-120	749
H14	-584	21	731
H15	-387	123	724
H71	171(6)	223(3)	729(4)
H72	82(5)	253(3)	671(3)
H81	-114(6)	238(3)	858(3)
H82	-210(7)	194(4)	851(4)
H91	-97(6)	195(3)	574(3)
H92	-253(6)	185(3)	605(3)
H101	-562(5)	225(3)	712(3)
H102	414(6)	219(3)	811(3)

* Hydrogen positions with no standard errors were calculated by the SHELX (115) program and fixed. Those with standard errors were located and their positions varied with temperature factors fixed at 1.5x that of the oxygen to which they were attached.

Table 5.2.3 Bond distances (Å) and angles (°) for triaquo(tris-2-pyridylphosphine-N,N′N″)zinc(II)dinitrate monohydrate.

Zn-N1	2.153(3)	Zn-N2	2.164(3)	Zn-N3	2.126(3)
Zn-O7	2.075(3)	Zn-O8	2.152(3)	Zn-O9	2.110(3)
P-C11	1.839(4)	P-C12	1.844(4)	P-C13	1.847(4)
C11-C21	1.376(6)	C12-C22	1.386(6)	C13-C23	1.375(6)
C21-C31	1.382(6)	C22-C32	1.378(6)	C23-C33	1.380(7)
C31-C41	1.377(6)	C32-C42	1.380(6)	C33-C43	1.392(7)
C41-C51	1.384(6)	C42-C52	1.396(6)	C43-C53	1.383(6)
C51-N1	1.341(5)	C52-N2	1.340(5)	C53-N3	1.341(5)
N1-C11	1.358(5)	N2-C12	1.352(5)	N3-C13	1.351(5)
N4-O1	1.247(4)	N4-O2	1.245(4)	N4-O3	1.244(4)
N4-O4	1.232(5)	N5-O5	1.224(5)	N5-O6	1.249(5)
N1-Zn-N2	86.6(1)	N1-Zn-N3	89.7(1)	N1-Zn-O7	93.0(1)
N1-Zn-O8	93.1(1)	N1-Zn-O9	177.7(1)	N2-Zn-N3	90.7(1)
N2-Zn-O7	94.9(1)	N2-Zn-O8	178.4(1)	N2-Zn-O9	91.4(1)
N3-Zn-O7	174.0(1)	N3-Zn-O8	90.9(1)	N3-Zn-O9	91.6(1)
O7-Zn-O8	83.6(1)	O7-Zn-O9	86.0(1)	O8-Zn-O9	88.8(1)
C11-P-C12	98.5(2)	C11-P-C13	102.6(2)	C12-P-C13	102.9(2)
P-C11-C21	117.8(3)	P-C12-C22	117.3(3)	P-C13-C23	116.9(3)
C11-C21-C31	119.4(4)	C12-C22-C32	120.0(4)	C13-C23-C33	119.2(4)
C21-C31-C41	119.5(4)	C22-C32-C42	118.1(4)	C23-C33-C42	119.2(5)
C31-C41-C51	118.2(4)	C32-C42-C52	119.5(4)	C33-C43-C53	118.3(4)
C41-C51-N1	123.3(4)	C42-C52-N2	122.4(4)	C43-C53-N3	122.9(4)
C51-N1-C11	117.9(3)	C52-N2-C12	118.0(4)	C53-N3-C13	118.2(4)
C52-N1-Zn	120.0(3)	C52-N2-Zn	119.9(3)	C53-N3-Zn	119.6(3)
Zn-N1-C11	122.1(2)	Zn-N2-C12	121.7(3)	Zn-N3-C13	122.3(3)
N1-C11-C21	121.9(4)	N2-C12-C22	122.1(4)	N3-C13-C23	122.3(4)
N1-C11-P	120.3(3)	N2-C12-P	120.6(3)	N3-C13-P	120.8(3)
O1-N4-O2	120.3(4)	O1-N4-O3	119.7(4)	O2-N4-O3	120.0(4)
O4-N5-O5	121.1(4)	O4-N5-O6	120.4(4)	O5-N5-O6	118.5(4)

Bond distances and angles associated with hydrogen bonding

O7-H71	0.71(5)	H71··O10	1.92(5)	O7···O10	2.624(5)	O7-H71··O10	174(5)
O7-H72	0.85(5)	H72··O3	1.98(5)	O7···O3	2.813(5)	O7-H72··O3	169(5)
O8-H81	0.94(5)	H81··O4	2.01(5)	O8···O4	2.945(5)	O8-H81··O4	176(5)
O8-H82	0.61(5)	H82··O1	2.22(6)	O8···O1	2.801(4)	O8-H82··O1	159(7)
O9-H91	0.80(5)	H91··O2	2.04(5)	O9···O2	2.787(4)	O9-H91··O2	155(5)
O9-H92	0.84(5)	H92··O6	1.86(5)	O9···O6	2.685(5)	O9-H92··O6	169(5)
O10-H101	0.96(5)	H101··O6	1.89(5)	O10···O6	2.803(5)	O10-H101··O6	157(4)
O10-H102	0.80(5)	H102··O2	2.21(5)	O10···O2	3.000(5)	O10-H102··O2	171(5)

Table 5.2.4. Best planes, dihedral angles and torsional angles for
triaquo(tris-2-pyridylphosphine-N,N',N"-)zinc (II)
dinitrate monohydrate.

Plane	Distance of atom from plane (Å)
1. C11,C21,C31,C41,C51,N1	C11;0.000(5),C21;-0.001(6),C31;0.003(6), C41;-0.003(6),C15;0.001(5),N1;0.000(4).
2. C12,C22,C32,C42,C52,N2	C12;0.005(5),C22;-0.007(6),C32;0.002(6), C42;0.004(6),C52;-0.003(5),N2;-0.001(4).
3. C13,C23,C33,C43,C53,N3	C13;0.003(5),C23;0.002(6),C33;-0.007(7), C43;0.006(7),C53;0.000(5),N3;-0.002(4).
4. C11,C22,C33	P;0.828(3)
5. N4,O1,O2,O3	N4;0.004(4),O1;-0.001(5), O2;-0.001(5),O3;-0.001(5).
6. N5,O4,O5,O6	N5;-0.009(5),O4;0.003(6), O5;0.002(5),O6;0.005(8)
7. O7,O8,N2,N3	O7;-0.022(4),O8;0.029(5),Zn;0.021(2), N2;0.023(5),N3;-0.024(4)
8. O7,O9,N1,N3	O7;0.063(4),O9;-0.076(4),Zn;-0.033(2), N1;-0.065(4),N3;0.070(4)
9. O8,O9,N1,N2	O8;0.004(5),O9;-0.003(4),Zn;-0.027(2), N1;-0.003(4),N2;0.003(4)
10. O7,O8,O9	

Dihedral angles (°)

1 - 2	108.3(1)	2 - 3	128.5(2)	1 - 3	123.0(2)
1 - 4	89.8(2)	2 - 4	87.7(2)	3 - 4	92.0(2)
4 - 5	43.0(2)	1 - 7	87.6(1)	2 - 7	140.0(1)
3 - 7	136.5(1)	1 - 8	130.3(1)	2 - 8	83.6(1)
3 - 8	133.9(1)	1 - 9	132.4(1)	2 - 9	131.4(1)
3 - 9	90.8(2)	4 - 10	35.2(2)	5 - 10	104.0(2)

Torsional angles (°)

Zn-N1-C11-P	1.7(2)	O9-Zn-N1-C11	17.5(2)
Zn-N2-C12-P	3.1(2)	O8-Zn-N2-C12	79.8(2)
Zn-N3-C13-P	3.8(2)	O7-Zn-N3-C13	53.8(2)

Figure 5.2.1　The triaquo(tris-2-pyridylphosphine-N,N′,N″-)-
zinc(II) cation
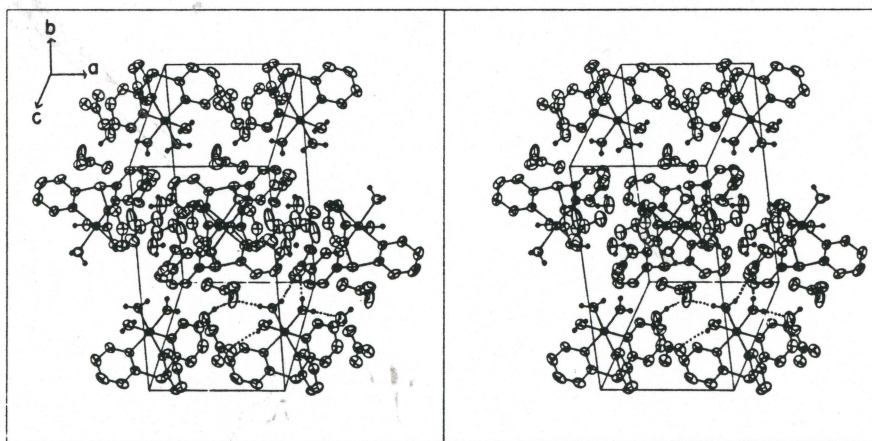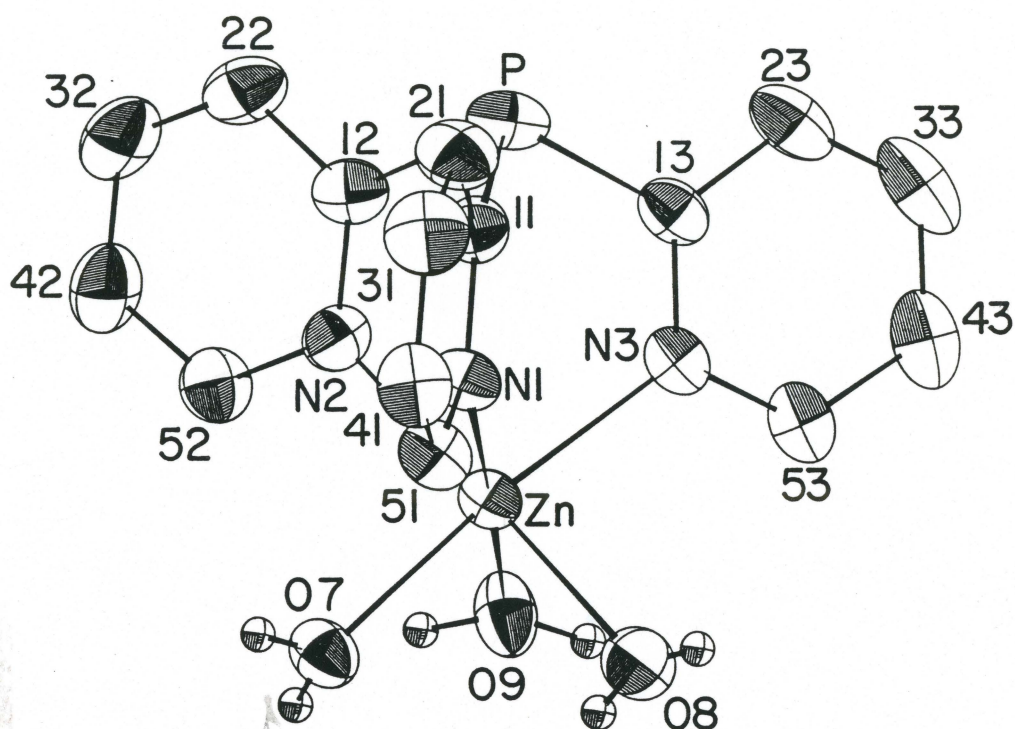
Figure 5.2.2　A stereoview of the unit cell.　Dotted lines depict
hydrogen bonding.

bonding is in fact responsible for distortion of the complex from octahedral symmetry.

The Zn-N distances are within range of those reported in similar structures (Zn-N; 2.092(10) Å in tetraaquobis(2-sulphonato-pyridine)zinc(II) (198), 2.18(1) and 2.15(1) Å in 1,1,1-tris(pyridine-2-aldiminomethyl)ethanezinc(II) perchlorate (199), and 2.214(5) Å in tris(2-picolylamine)zinc(II) dichloride) (200). The Zn-N3 distance (2.126(3) Å) is shorter than the other two (Zn-N1; 2.153(3) Å and Zn-N2; 2.164(3) Å).

Comparison with distances reported by Hathaway et al. (2.131(9) and 2.140(9) Å) (198) suggest that Zn-O8 and Zn-O9 bond lengths are normal (2.152(3) and 2.110(3) Å respectively), but Zn-O7 at 2.075(3) Å is short. It is interesting that it is the relatively short Zn-O7 bond which is located opposite to the relatively short Zn-N3 bond. It would seem that exertion of any trans influence is outweighed by crystal packing effects.

The Zn-N bond lengths are apparently affected to some extent by crystal packing since ring 3 is the only ring not involved in a π-π interaction. As well, the N1-Zn-N2 angle of 86.6(1)° is significantly smaller than N1-Zn-N3 (89.7(1)°) and N2-Zn-N3 (90.7(1)°).

Tris-2-pyridyl phosphine P-C bond lengths and C-P-C angles remain unchanged from the free ligand and the only effect of binding to zinc is the constraint placed on the ring-ring dihedral angles which are 90.5° (ave.) in the free ligand and 119.9° (ave.) in the zinc complex. Least-squares planes, dihedral and torsional angles are listed in Table 5.2.4. Bond lengths and angles about the nitrogen

atoms within the pyridyl rings may be changed with coordination to zinc but errors preclude certainty. Average N-C bonds are longer (Ni-Cli; 1.341(5), Ni-C5i; 1.334(3)Å (ligand) vs. Ni-Cli; 1.354(5), Ni-C5i; 1.341(5)Å (complex)). The internal angle at nitrogen (116.9(8)° in the free ligand) is increased to 118.0(1)° in the complex with concomitant narrowing of the adjacent N-C5-C4 angle (124.2(5)° (ave. for free ligand), 122.9(4)° (ave. complex)).

Read and James (197) make a point of reporting the Zn···P distance (3.283(2) Å) in the structure of chloro(tris(4,5-diisopropyl-imidazol-2-yl)phosphine)zinc(II). This distance is much longer in the structure of $TPPZn(H_2O)_3^{2+}$ (3.438(1) Å) although according to ^{31}P NMR results, the shielding effect of electron density at the zinc center is felt by the phosphorus atom whose resonance is shifted to -43.29 ppm compared with -0.33 ppm for the free ligand.

Bond lengths and angles about N4 are identical within error indicating a symmetric nitrate anion. The other nitrate ion is asymmetric; N5-O5 is short (1.224(5)Å) whereas the average N-O distance in the other five N-O bonds is 1.243(6)Å. Coincidentally, O5 is the only oxygen which is not involved in hydrogen bonding. The O5-N5-O4 (121.4(4)°) and O5-N5-O6 (118.5(4)°) angles deviate from an expected symmetric 120° angle as a consequence of hydrogen bonding which is dealt with below.

A stereoview of the packing is shown in Figure 5.2.2. Molecules pack in the unit cell with their dipoles roughly parallel to the **b** direction and form a series of alternating hydrophilic and hydrophobic layers coplanar with **ac**. The hydrophobic layers, located

roughly at b=0 and 1/2, consist of stacked pyridyl rings with π-π interactions (3.7Å) relating ring 1 with its equivalent about inversion centers at 0,0,0 and 1/2,1/2,1/2 and ring 2 with its equivalent about 0,0,1/2 and 1/2,1/2,0 (3.8Å). Ring 3 is positioned to bisect rings 1 and 2 in adjacent molecules of the same layer. Hydrophilic layers are located roughly at b=1/4 and 3/4. Details of the extensive intermolecular hydrogen bonding are summarized in Table 5.2.3. All three coordinated water molecules act as hydrogen donors to nitrate oxygens; O7 donates one hydrogen to the lattice water. The N5,O4,O5,O6 nitrate lies at 35.2(2)° to and slightly above the plane formed by the three coordinated oxygen atoms and serves as a hydrogen bonded link through O4 and O6 between adjacent molecules in the same layer. The N4,O1,O2,O3 plane lies at 43.0(2)° to the other nitrate plane and 104.0(2)° to the O7,O8,O9 plane. O2 bridges O10 from one layer and O9 in the next layer in **b**.

5.2.4 Conclusions

The aqueous solubility of zinc complexes with ClAuTPP have presented a barrier to further solution studies in that, as discussed in section 5.2.2, they are unstable in aqueous solution. This is explained as an artifact of the zinc d^{10} electronic configuration which offers no crystal field stabilization, thus complexes are labile. In the case of ClAuTPP, which alone has very low aqueous solubility, zinc's lability allows dissociation with irreversible ClAuTPP precipitation.

After consideration of the molecular structure of

[TPPZn(H$_2$O)$_3$](NO$_3$)$_2$ in comparison with that of chloro(4,5-diisopropyl-imidazol-1-ylphosphine)zinc(II) chloride (197), the question persists as to why TPP is not an effective model of the HCA active site (192). It is assumed that in aqueous solution, the chloride ligand is readily displaced by water so that under the catalytic conditions reported, the compound closely mimics the HCA active site. The steric demands of the isopropyl groups in this complex are such that zinc must adopt a tetrahedral geometry. No such demands are exerted by TPP and three coordination sites can be occupied by water ligands to form an octahedral complex instead of one. In [TPPZn(H$_2$O)$_3$](NO$_3$)$_2$, all the ligands are essentially identical to those required by the protein, it is only the quantity of water ligands which is different. It has been shown that with slight modifications to the 3,7,11,17-tetraazabicyclo[11.3.1]heptadeca-1-2,11,13,15-pentane ligand the coordination number of zinc(II) complexes can be reduced from six to five (201). Reduction in coordination number is accompanied by a reduction in the pKa of the Zn-OH$_2$$^{++}$ group from 10 or greater to 9.1 and an increase in catalytic rate. It has been suggested that further reduction in coordination number to four would increase the rate of CO$_2$ hydration to enzymic order (201). It appears that a nucleophilic Zn-OH$^+$ species is necessary for the catalytic reaction whose mechanism is postulated to involve an attack on a C=O double bond of CO$_2$ (196).

5.3 Copper complexes

5.3.1 Introduction

Many studies have been undertaken attempting to establish a correlation between the electronic properties (in particular, electronic absorption (UV/VIS) and electron spin resonance (E.S.R.) parameters) of copper(II) complexes and the local stereochemistry and geometry of the ion present (202). On the basis of previous findings, it may then be possible to predict structure using the information available from physical techniques such as UV/VIS and E.S.R. The incorporation of tripod ligands such as TPP into copper(II) complexes open an avenue for comparison with complexes of ligands such bipyridine and 1,10-phenanthrolene which have been previously examined in terms of the above correlation (203). It is also possible to compare TPP to pyridine which forms copper(II) complexes of varied stoichiometry preferring trans and meridional isomers in cases of two- and three-coordination respectively (204,205). Although the hexakispyridine complex has been reported (206,207), a reinvestigation of its synthesis concluded that the compound was incorrectly formulated and was, in fact, the tetrakis species with two molecules of lattice pyridine also present, the hexakis salt being too sterically crowded to be stable (204).

The following sections (5.3.3 and 5.3.4) include discussions of the structures of mono- and bis-coordinated copper(II) complexes of TPP and ClAuTPP. These compounds were further characterized by UV/VIS absorption (5.3.5) and E.S.R (5.3.6) spectroscopies.

5.3.2 Preparations

dinitrato(tris-2-pyridylphosphine-N,N′,N″-)copper(II) (TPPCu(NO$_3$)$_2$)

Method A; was prepared through the reaction of 0.3183 g (1.2 mmol) of
TPP in methanol (10 mL) with 0.290 g (1.2 mmol) of Cu(NO$_3$)$_2$·3H$_2$O in 10
mL methanol (2 hours, 22°C). The solvent was removed under reduced
pressure and the residue extracted into dichloromethane (30 mL). The
resulting blue-green dichloromethane solution was filtered and allowed
to evaporate to 5 mL to yield a blue precipitate. Crystals were
obtained after slow evaporation of an aqueous solution at 22°C yielding
0.255 g (47%). Analysis required for C$_{15}$H$_{12}$N$_3$PCu(NO$_3$)$_2$: C;39.7, H;2.7,
N;15.4%. Found: C;39.4, H;2.7,N; 15.1%.

Although the crystal used for diffraction studies was prepared
by the above method, it is suspected that it was not representative of
the bulk sample which after recrystallization from aqueous solution,
may be expected to give the aquo complex. This assumption is based on
infrared results which are discussed in detail in Chapter 6. An
alternative route to the preparation of TPPCu(NO$_3$)$_2$ was also used and
is described in Method B.

Method B; Cu(NO$_3$)$_2$·3H$_2$O (0.1040 g, 0.43 mmol) was dissolved in 40 mL
of a 1:1 2,2′-dimethoxypropane:ethanol mixture and refluxed for 7
hours. An ethanolic (10 mL) solution of 0.1142 g (0.43 mmol) of TPP
was then added to produce an immediate blue precipitate. The reaction
mixture was stirred for a further 8 hours with gentle heating. The
precipitate was filtered and used without further purification in the
infrared experiment described in Chapter 6.

bis[chloro(tris-2-pyridylphosphine-P-)gold(I)-N,N',N"]copper dinitrate dihydrate ([(ClAuTPP)$_2$Cu](NO$_3$)$_2$); Crystals used in the X-ray experiment were first prepared in an attempt to make the mono-ligated copper species, (ClAuTPP)Cu(NO$_3$)$_2$. ClAuTPP (0.060 g, 0.12 mmol) in methanol/acetone (5 mL, 50:50) was added to an acetone solution (5 mL) of Cu(NO$_3$)$_2\cdot$3H$_2$O (0.029 g, 0.12 mmol) and stirred for 2 1/2 hours. The solvent was removed under reduced pressure and the residue extracted with dichloromethane. The dichloromethane-insoluble portion of the residue was filtered off and recrystallized from water giving very low yields (0.016 g, 11%) of the crystals used for diffraction work. Analysis required for C$_{30}$H$_{24}$N$_3$P$_2$Cl$_2$Au$_2$Cu(NO$_3$)$_2$.4H$_2$O: C;28.7, H;2.6, N;8.9, Cl;5.6%. Found: C;28.6, H;2.3, N;9.0, Cl;5.6%. Better yields (84%) were obtained through the 2:1 reaction of chlorotris-2-pyridylphosphine gold(I) and Cu(NO$_3$)$_2\cdot$3H$_2$O in the same solvent system. [197]Au Moess: δ; 3.75 mm/sec, Δ; 7.45(9) mm/sec, Γ; 1.77(15) mm/sec.

bis[tris(2-pyridylphosphine-N,N',N"-]copper(II) dinitrate ([(TPP)$_2$Cu](NO$_3$)$_2$; A methanol solution (15 mL) containing 0.265 g (1.0 mmol) of TPP was added to a solution of 0.1208 g (0.5 mmol) of Cu(NO$_3$)$_2\cdot$3H$_2$O also dissolved in methanol (5 mL). The reaction mixture was allowed to stir for 10 hours after which all the solvent was removed under reduced pressure and the residue extracted into dichloromethane. The dichloromethane evaporated slowly to yield a crop of blue crystals which were recrystallized from aqueous solution at 22oC to yield 0.219 g (0.31 mmol) of product (61%). Analysis required for C$_{30}$H$_{24}$N$_6$P$_2$Cu(NO$_3$)$_2$: C;50.2, H;3.4, N;15.6%. Found: C;49.6, H;3.5, N;15.5%.

5.3.3 The crystal and molecular structure of TPPCu(NO₃)₂

Crystal data and other information related to data collection

are given in Table 5.3.1. Atomic positional parameters and anisotropic

temperature factors are listed in Tables 5.3.2 and 5.3.A respectively.

Bond lengths and angles are given in Table 5.3.3 and the molecule is

illustrated in Figure 5.3.1. The copper atom may be described as being

octahedrally coordinated to three pyridyl nitrogen atom in _facial_

orientation as well as three oxygen atoms from one monodentate and one

asymmetric bidentate nitrate ligand. A large distortion of the

octahedron occurs as a result of the 53.4(2)° O4-Cu-O5 angle imposed by

chelate restrictions of the bidentate nitrate ligand. Distorted square

pyramidal coordination may also be used to describe the copper

environment where N2 is the apex atom and O4, N1, N3 and O2 form a

plane located 0.249(3) Å below the Cu atom and the Cu-O5 bond is given

only secondary consideration in view of the long Cu-O5 distance

(2.540(5) Å). Similarly, the structure of nitrato-tris(2-(2-

pyridyl)ethyl)amine copper(II) nitrate is pentacoordinate and square

pyramidal (208). In this structure, one Cu-N(pyridyl) bond length is

longer (2.202(11) Å) than the other two (2.100(11) Å) and this nitrogen

atom is assigned as the apex atom. With square pyramidal distortion of

octahedral geometry, d orbital degeneracy has been sufficiently

removed so that typical six-coordinate Jahn-Teller axial elongation is

not observed.

The Cu-N distances are all different (Cu-N1; 2.034(3), Cu-N2;

2.109(3) and Cu-N3; 2.069(5) Å) and longer than those reported for

other Cu-pyridine structures (1.931(5) and 1.940(6) Å in μ-(nitrato-

Table 5.3.1   Crystal data for dinitrato(tris-2-pyridylphosphine-N,N',N"-)copper(II)

Formula	$C_{15}H_{12}CuN_5O_6P$	
Formula weight	452.8	
Crystal size and shape	$0.1 \times 0.23 \times 0.32 mm^3$ plate	
Systematic absences	none	
Space group	$P\bar{1}$	
Diffractometer	$P2_1$	
Temperature	22^oC	
Unit cell parameters	$a=8.573(1)Å$	$\alpha=103.11(2)^o$
	$b=9.983(1)Å$	$\beta=121.90(1)^o$
	$c=16.105(2)Å$	$\gamma=113.41(1)^o$
	$V=881.3(3)Å^3$	$Z=2$
ρ_{calc}, ρ_{obs}	1.706, 1.69 $CHCl_3/CHBr_3$	
Range of hkl	$0 < h < 12, -15 < k < 15, -20 < l < 20$	
Maximum 2θ	50°	
Number of reflcns measured	3352	
Number of independent reflcns	2948	
Standard reflcns(e.s.d)	2 -1 -6 (1.7%), 1 -4 4 (1.9%)	
R_{int}	0.0082	
Final R,Rw	0.0588,0.0575	
Final shift/error max(ave)	0.014(0.003)	
Error in obs of unit weight	S=1.4618	
Highest peak, lowest valley	$0.8eÅ^{-3}, -0.53eÅ^{-3}$	
Weighting	$w=(\sigma^2(F) + 0.000765F^2)^{-1}$	
F(000)	458.9	
Linear Absorption coefficient	$\mu=14.26$ cm^{-1}	
Absorption Coefficient limits	$1.13 < A^* < 1.19^*$	
Number of Variables	253	

* an absorption correction was applied

Table 5.3.2 Positional parameters and U_{eq} ($\times 10^4$) for
dinitrato(tris-2-pyridylphosphine-N,N',N"-)copper(II)

Atom	x	y	z	U_{eq}
Cu	-619.8(9)	-214.5(7)	7442.2(4)	18.1
P	-1908(2)	1965(2)	8524(1)	20.6
C11	-3724(7)	-454(6)	7803(4)	19
C21	-5558(9)	-1247(7)	7737(4)	27
C31	-7202(9)	-3095(8)	7051(5)	31
C41	-6901(9)	-4084(7)	6490(5)	28
C51	-4968(8)	-3214(6)	6639(4)	22
N1	-3429(6)	-1445(5)	7262(3)	18
C12	1169(7)	2815(5)	9538(3)	18
C22	2755(9)	4366(6)	10652(4)	25
C32	5113(9)	5129(7)	11410(4)	29
C42	5826(8)	4316(6)	11051(4)	26
C52	4185(8)	2792(6)	9947(4)	23
N2	1877(6)	2047(5)	9182(3)	18
C13	-2179(6)	2007(5)	7313(4)	18
C23	-2874(8)	2944(6)	6936(4)	22
C33	-2986(9)	3085(6)	6069(4)	24
C43	-2425(7)	2253(6)	5600(4)	21
C53	-1797(7)	1310(6)	5999(4)	19
N3	-1645(6)	1182(5)	6845(3)	17
N4	721(8)	-1896(6)	8650(4)	40
N5	-9913(12)	-1051(8)	6010(5)	36
O1	494(9)	-1183(6)	9266(4)	42
O2	228(8)	-1743(6)	7780(3)	34
O3	1368(10)	-2788(7)	8814(5)	53
O4	1353(7)	307(5)	7033(4)	35
O5	-1919(10)	-2200(8)	5534(5)	56
O6	900(13)	-1125(10)	5609(6)	74
H21	-5847	-476	8168	
H31	-8690	-3764	6963	
H41	-8145	-5550	5957	
H51	-4757	-4048	6154	
H22	2186	5006	10942	
H32	6399	6339	12292	
H42	7702	4913	11648	
H52	4794	2156	9656	
H23	-3305	3631	7317	
H33	-3524	3821	5757	
H43	-2539	2322	4897	
H53	-1335	634	5598	

$U_{eq} = 1/3(U_{11} + U_{22} + U_{33} + 2\cos\alpha U_{23} + 2\cos\beta U_{13} + 2\cos\gamma U_{12})$
Hydrogen positions were calculated and fixed.

Table 5.3.3   Bond lengths (Å) and angles (°) for dinitrato-
(tris-2-pyridylphosphine-N,N',N"-)copper(II)

Cu-N1	2.034(3)	Cu-N2	2.109(3)	Cu-N3	2.069(5)
Cu-O2	1.985(6)	Cu-O4	2.050(7)	Cu-O5	2.540(5)
P-C11	1.835(5)	P-C12	1.842(5)	P-C13	1.851(7)
C11-C21	1.38(1)	C12-C22	1.392(6)	C13-C23	1.376(9)
C21-C31	1.393(8)	C22-C32	1.381(9)	C23-C33	1.39(1)
C31-C41	1.37(1)	C32-C42	1.38(1)	C33-C43	1.38(1)
C41-C51	1.38(1)	C42-C52	1.367(6)	C43-C53	1.371(9)
C51-N1	1.335(6)	C52-N2	1.353(7)	C53-N3	1.340(8)
N1-C11	1.352(9)	N2-C12	1.345(9)	N3-C13	1.351(9)
N4-O1	1.23(1)	N4-O2	1.299(9)	N4-O3	1.22(1)
N5-O4	1.282(8)	N5-O5	1.22(1)	N5-O6	1.18(2)

N1-Cu-N2	99.4(2)	N1-Cu-N3	88.9(2)	N1-Cu-O2	94.4(2)
N1-Cu-O4	160.3(1)	N1-Cu-O5	107.0(2)	N2-Cu-N3	88.4(2)
N2-Cu-O2	99.2(2)	N2-Cu-O4	100.2(2)	N2-Cu-O5	153.5(2)
N3-Cu-O2	171.1(2)	N3-Cu-O4	90.2(2)	N3-Cu-O5	93.4(2)
O2-Cu-O4	83.9(3)	O2-Cu-O5	77.7(3)	O4-Cu-O5	53.4(2)
C11-P-C12	105.8(3)	C12-P-C13	97.6(3)	C11-P-C13	97.8(2)
P-C11-C21	117.1(5)	P-C12-C22	116.9(6)	P-C13-C23	117.7(5)
P-C11-N1	121.8(5)	P-C12-N2	121.3(3)	P-C13-N3	120.6(4)
N1-C11-C21	120.9(5)	N2-C12-C22	121.7(5)	N3-C13-C23	121.7(6)
C11-C21-C31	119.7(8)	C12-C22-C32	119.0(7)	C13-C23-C33	119.6(7)
C21-C31-C41	118.7(7)	C22-C32-C42	119.2(5)	C23-C33-C43	118.6(7)
C31-C41-C51	118.9(5)	C32-C42-C52	119.1(6)	C33-C43-C53	118.8(6)
C41-C51-N1	122.8(7)	C42-C52-N2	122.6(7)	C43-C53-N3	123.5(7)
C51-N1-C11	119.0(6)	C52-N2-C12	118.4(4)	C53-N3-C13	117.9(5)
Cu-N1-C11	119.5(3)	Cu-N2-C12	119.0(3)	Cu-N3-C13	120.1(4)
Cu-N1-C51	121.5(5)	Cu-N2-C52	122.5(5)	Cu-N3-C53	122.0(5)
O1-N4-O2	120.1(7)	O2-N4-O3	117.7(8)	O1-N4-O3	122.1(8)
O4-N5-O5	115(1)	O4-N5-O6	120.0(7)	O5-N5-O6	125.4(7)

Table 5.3.4   Best planes, dihedral and torsional angles for
dinitrato(tris-2-pyridylphosphine-N,N',N"-)copper(II)

Plane	Distance of atom from the plane (Å)
1.C11,C21,C31,C41,C51,N1	C11;0.013(8),C21;0.022(9),C31;0.01(1), C41;0.017(9),C51;0.019(8),N1;0.017(6)
2.C12,C22,C32,C42,C52,N2	C12;0.007(8),C22;0.004(9),C32;0.01(1), C42;0.002(9),C52;0.009(8),N2;0.008(7)
3.C13,C23,C33,C43,C53,N3	C13;0.006(7),C23;0.009(8).C33;0.002(9), C43;0.007(8),C53,0.009(8),N3;0.001(6)
4.N5,O4,O5,O6	N4;0.09(1),O4;0.048(8), O5;0.25(1),O6;0.52(1)
5.N4,O1,O2,O3	N5;0.006(8),O1;0.00(1) O2;0.002(9),O3;0.00(1)
6.O2,O4,N1,N3	O2;0.145(8),O4;-0.121(8), N1;-0.079(7),N3;0.080(7), Cu;0.249(3)
7.O4,O5,N1,N2	O4;-1.33(7),O5;1.27(1), N1;-0.319(7),N2;0.862(7), Cu;-0.600(3)
8.C11,C12,C13	P;0.849(4)

Dihedral angles

1 - 2	137.7(2)	1 - 3	113.1(2)	2 - 3	108.8(2)	1 - 4	149.2(3)
2 - 4	166.5(2)	3 - 4	97.7(3)	1 - 5	108.0(3)	2 - 5	114.1(3)
3 - 5	173.6(3)	4 - 5	102.5(4)	1 - 6	50.5(2)	2 - 6	82.0(2)
3 - 6	39.0(2)	4 - 6	45.2(3)	5 - 6	29.6(4)	1 - 7	99.4(2)
2 - 7	110.5(2)	3 - 7	68.2(2)	4 - 7	70.2(3)	5 - 7	51.7(3)
6 - 7	52.0(2)	1 - 8	94.9(3)	2 - 8	89.5(3)	3 - 8	89.8(2)

Torsional angles

P-C11-N1-Cu	8.8(2)	C11-N1-Cu-O4	-142.1(2)
P-C12-N2-Cu	-1.7(2)	C12-N2-Cu-O5	145.3(2)
P-C13-N3-Cu	2.0	C13-N3-Cu-O2	160.5(2)

Figure 5.3.1   A molecule of dinitrato(tris-2-pyridylphosphine-N,N',N"-copper(II)
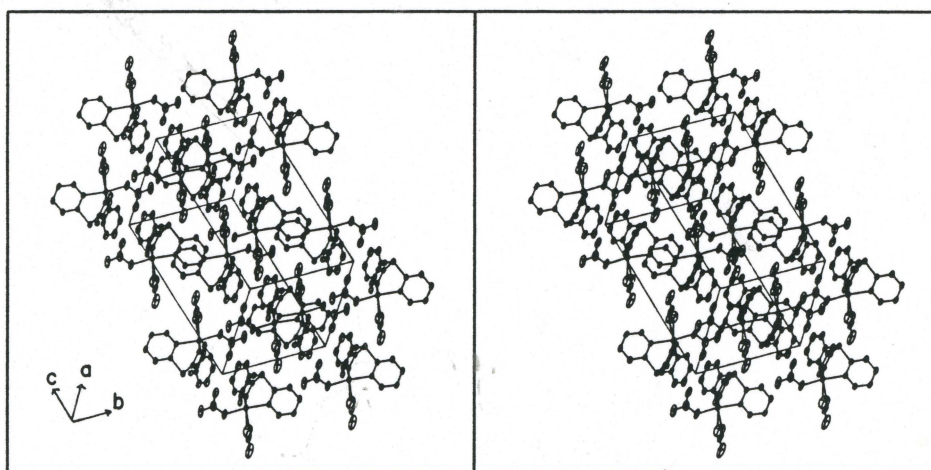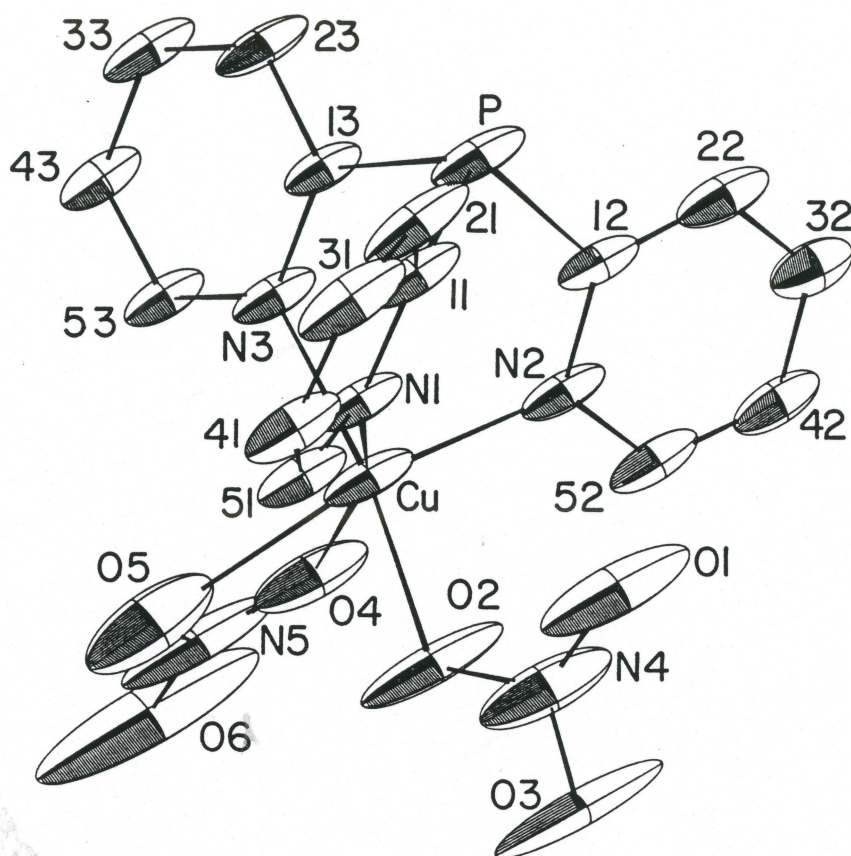
Figure 5.3.2   A stereoview of the packing in the unit cell

0,0'-)bis(nitrato-O-)(N,N,N',N'-tetrakis[(1-methyl-2-benzimidazolyl)methyl]dicopper(II) dinitrate (209), 1.964(4) Å in (cis,trans-2-pyridylmethylketazine)copper(II)dinitrate (210) and 2.020(13) and 2.028(12) Å in nitrato(tris(2-(2-pyridyl)-ethyl)aminecopper(II) (208) although the last structure also has a long bond from copper to the pyridyl fragment located at the apex of the square pyramid (2.202(12) Å). Cu-N bond lengths are similar to those reported for meridionally coordinated tris(pyridine) species (2.018(8) and 2.064(0) Å) (205). The Cu-O2 (1.985(6) Å) and Cu-O4 (2.050(7) Å) distances are the same within error and are in range of similar Cu-O(NO$_3$) distances (2.000(4) Å (209), 2.154(3) Å (210) and 2.044(11) Å (208)). The long Cu-O5 distance (2.540(5) Å) is also in range of those previously observed (2.41(4) and 2.626(5) Å (209) and 2.764(5) Å (210)).

Unlike in the zinc complex, the C-P-C ligand angles experience some distortion relative to the free ligand although P-C bond lengths remain constant. The relatively large C11-P-C12 angle of 105.8(3)° compared to the other C-P-C angles (C12-P-C13; 97.6(3)° and C11-P-C13; 97.8(2)°) coincides with the open N1-Cu-N2 angle (99.4(2)°) and the large ring 1 - ring 2 dihedral angle (137.7(2)°) compared to 113.1(2)° and 108.8(2)° for the ring 1 - ring 3 and ring 2 - ring 3 dihedral angles respectively.

Bond lengths within the pyridyl rings are the same as in the free ligand. The C1-N-C5 angles are relatively less open (ave. 118.4(9)° vs. 123.0° for the ligand itself) and are because the nitrogen atom has increased its coordination. This effect is well

established (150).

Nitrate bond lengths N4-O1(1.23(1) Å), N4-O3 (1.22(1) Å, N5-O5 (1.22(1) Å) and N5-O6 (1.18(2) Å) do not differ and are normal. N4-O2 (1.299(9) Å) and N5-O4 (1.282(8) Å) are also equivalent within error and longer than the other N-O distances, indicative of weaker N-O bonds involving oxygen atoms coordinated to copper. Notably, the N5-O5 distance is typical of N-O lengths where the oxygen atom is not coordinated. This plus the long Cu-O5 distance (2.540(5) Å) and the O4-N5-O5 angle (115(1)°) which is maintained close to the trigonal value of 120° suggests that the Cu-O5 bond is very weak. The monodentate nitrate is essentially coplanar with ring 3 (dihedral angle; 173.6(3)°) which is coordinated opposite to it. With such an orientation, it is able to bisect the angle between rings 1 and 2 (72.0(3) and 65.9(3)° dihedral angles respectively) in an effort to minimize steric effects.

A stereoview of the packing is shown in Figure 5.3.2. Molecules are arranged such that the pyridyl rings align to form hydrophobic layers parallel to [-1 1 1] which alternate with hydrophilic nitrate layers at [-2 2 2]. The hydrophobic layer consists of chains in which adjacent molecules are held together by alternating sets of π-π interactions. The ring 3 - ring 3 π-π interaction occurs about the 1/2,0,1/2 inversion center. The rings are approximately 3.4 Å apart. A double π-π interaction is located at 0,0,0 involving rings 1 and 2 of one molecule with rings 2 and 1 respectively of the adjacent symmetry-related molecule. Because of the restrictions imposed by coordination to copper, the overlap of the rings is not expected to be

as good as in cases where the rings are parallel. The large ring 1 -
ring 2 dihedral angle (137.7(2)°) appears to be an attempt by the
molecule to allow maximum interaction between the rings. Ring 2 is
also involved in a π-π interaction (3.4 Å apart) with ring 2 of the
molecule related by the inversion center at 1/2,1/2,0. This is the
only apparent force holding adjacent chains together to form the
hydrophobic layers mentioned above.

While the pyridyl rings are involved in one (chains) and two
dimensional (layers) interactions, the nitrate ligands are responsible
for the third dimension in packing as they are involved in π-π-type
interactions which hold adjacent layers together. In particular, the
inversion center at 0,0,1/2 relates the bidentate nitrate to itself in
a slipped (only N5 and O6 form the overlap) π-π interaction in which
the nitrate planes are 1.6 Å apart. The distance between monodentate
nitrates located about 1/2,0,0 is too great (4.6 Å) to suggest any
interaction.

5.3.4 The crystal and molecular structure of [(ClAuTPP)$_2$Cu](NO$_3$)$_2$

Crystal data and other information pertaining to data collection
and structure solution are given in Table 5.3.5. Lists of atomic
positional parameters and anisotropic temperature factors are found in
Tables 5.3.6 and 5.3.B respectively. Interatomic distances and angles
are given in Table 5.3.7 and molecule A of the structure is illustrated
in Figure 5.3.3 to show atom labelling. Molecule B has similar
geometry. In both molecules, the copper atom is located on an
inversion center (0,0,1/2 (A) and 0,1/2,0 (B)). References made to

atoms generated by an inversion center are distinguished by a prime affix.

Bond lengths involving the gold atom (Au-Cl; 2.275(3) Å (**A**), 2.267(4) Å (**B**), and Au-P; 2.222(3) Å (**A**), 2.217(3) Å (**B**)) are the same as those found in chloro(tris-2-pyridylphosphine)gold(I) (Au-Cl; 2.277(5), 2.272(5), 2.274(1) Å and Au-P; 2.214(4), 2.218(4), 2.220(1) Å). The coordination geometry at gold is almost rectilinear (P-Au-Cl; 174.3(2)°(**A**) and 176.3(2)°(**B**)). The deviation from linearity in the case of molecule **A** is a result of packing interactions which are discussed subsequently.

Molecules **A** and **B** are described as distortion isomers (211). The observation of distortion isomers has been described as a reflection of dynamic Jahn-Teller effects or the fluxionality of the non-spherical d^9 electron configuration of Cu(II) (212,213). The dynamic nature of the molecules in the structure of bis[hydrotris(pyrazol-1-yl)borate]copper(II) has been studied by an analysis of root-mean-square displacements along the Cu-N bond directions where thermal ellipsoids with long axes parallel to the bond reflect motion along that bond such that the X-ray experiment averages molecules in different distortion geometries (212). Unfortunately, such an analysis of the present structure is precluded by relatively large errors and a tendency for the temperature factor for N3(**B**) to become non-positive definite during anisotropic refinement.

Other than the expected Jahn-Teller type of distortion, very little deviation from octahedral geometry about the copper atom is apparent in that angles about copper are all roughly 90° (N1-Cu-N2;

Table 5.3.5 Crystal data for bis[chloro(tris-2-pyridylphosphine-P-)
gold(I)-N,N',N"-]copper(II) dinitrate dihydrate

Formula	$C_{30}H_{24}AuCl_2CuN_8O_6P\cdot 2H_2O$
Formula weight	1218.9
Crystal size and shape	$0.1\times 0.19\times 0.42mm^3$ plate
Systematic absences	none
Space group	$P\bar{1}$
Diffractometer	P3
Temperature	22°C
Unit cell parameters	a=10.083(5)Å $\quad$ α=93.42(3)°
	b=11.253(4)Å $\quad$ β=115.25(3)°
	c=18.709(8)Å $\quad$ γ=102.71(3)°
	V=1874(2) $\quad$ Z=4
ρ_{calc}, ρ_{obs}	2.195, 2.13 $CHCl_3/CHBr_3$
Range of hkl	0<h<15,-16<k<16,-23<l<23
Maximum 2θ	50°
Number of reflcns measured	4990
Number of independent reflcns	4385
Standard reflcns(e.s.d)	0 -4 5 (2.7%), 2 -1 0 (2.0%)
R_{int}	0.0110
Final R,Rw	0.0628, 0.0582
Final shift/error	
$\quad$(block refinement) max(ave)	0.026(0.004) and 0.012(0.003)
Error in obs of unit weight	S=1.4246
Highest peak, lowest valley	$2.19e\text{Å}^{-3}, -2.36e\text{Å}^{-3}$
Weighting	$w=(\sigma^2(F) + 0.000639F^2)^{-1}$
F(000)	1149.6
Linear Absorption coefficient	$\mu=90.65\ cm^{-1}$
Absorption Coefficient limits	2.10<A*<5.66*
Number of Variables (block refnmt)	278, 278

* an absorption correction was applied

Table 5.3.6 Positional parameters and U_{eq} ($\times 10^3$) for
bis(chloro(tris-2-pyridylphosphine-P-)gold(I)
N,N',N"-)copper(II) dinitrate dihydrate.

Atom	x	y	z	U_{eq}
Molecule A				
Au	8409.0(8)	5058.1(4)	5244.1(3)	33.2
Cu	10000	0	5000	25.9
Cl	763.6(4)	305.8(2)	537.0(1)	40.8
P	903.0(4)	705.6(2)	518.0(1)	29.8
C11	792(2)	790.7(9)	545.0(6)	29
C21	696(2)	7319(1)	575.0(7)	17
C31	617(2)	802(1)	599.8(8)	48
C41	639(2)	927(1)	588.1(9)	51
C51	734(2)	975(1)	555.5(6)	35
N1	813(1)	907.7(8)	535.0(5)	27
C12	1097(2)	789.8(9)	585.9(6)	23
C22	1192(2)	736(1)	643.4(6)	33
C32	1340(2)	803(1)	695.6(7)	40
C42	1391(2)	925(1)	686.2(7)	44
C52	1290(2)	974(1)	627.6(7)	37
N2	1146(1)	911.0(8)	578.9(5)	31
C13	880(2)	735.7(9)	418.4(6)	25
C23	824(2)	636(1)	358.2(6)	32
C33	814(2)	656(1)	283.2(7)	43
C43	864(2)	776(1)	273.9(7)	37
C53	916(2)	873(1)	338.5(6)	33
N3	924(1)	851.1(7)	409.5(5)	27
Molecule B				
Au	946.7(8)	10818.5(4)	1374.0(3)	33.1
Cu	0	5000	0	25.9
Cl	154.4(5)	915.0(2)	192.3(2)	51.6
P	46.0(4)	1244.3(2)	80.0(1)	28.2
C11	81(2)	1382.9(9)	147.6(6)	29
C21	121(2)	1378(1)	228.5(7)	36
C31	141(2)	1482(1)	279.1(7)	38
C41	125(2)	1589(1)	247.3(7)	33
C51	89(2)	1589.6(9)	168.5(6)	28
N1	65(1)	1488.1(8)	118.0(5)	28
C12	164(2)	1294.1(9)	29.0(6)	24
C22	257(2)	1222(1)	23.7(8)	41
C32	344(3)	1259(1)	-16(1)	63
C42	339(2)	1371(1)	-47.8(8)	59
C52	245(2)	1436(1)	-38.0(8)	42
N2	158(1)	1398.1(8)	-0.1(5)	32

Table 5.3.6 continued

C13	-147(2)	1222(1)	3.2(7)	39
C23	-260(2)	1108(1)	-15.8(8)	39
C33	-408(2)	1094(1)	-75.4(8)	40
C43	-434(2)	1192(1)	-116.2(7)	46
C53	-316(2)	1301(1)	-93.1(9)	46
N3	-175(2)	1318.1(8)	-33.3(5)	8
N7	811(2)	92(2)	187.9(9)	66
O1	768(2)	-20(1)	165.0(9)	96
O2	930(2)	127(1)	255.0(8)	83
O3	744(2)	163(1)	151.3(9)	107
N8	471(2)	457(2)	255(1)	83
O4	500(2)	435(2)	320(1)	140
O5	453(2)	561(2)	242.1(9)	106
O6	439(3)	379(3)	198(1)	221
O11	693(2)	388(1)	157.9(7)	88
O22	1503(2)	1247(2)	634(1)	148

$U_{eq} = 1/3(U_{11} + U_{22} + U_{33} + 2\cos\alpha U_{23} + 2\cos\beta U_{13} + 2\cos\gamma U_{12})$

Table 5.3.7 Selected interatomic Distances (Å) and Angles (°) for
bis(chlorotris-2-pyridylphosphine-P-gold(I)-N,N',N")-
copper(II) dinitrate hydrate.

	A	B		A	B
Au-Cl	2.275(3)	2.267(4)	Au-P	2.222(3)	2.217(3)
Cu-N1	2.31(1)	2.04(1)	Cu-N2	2.08(1)	2.16(1)
Cu-N3	2.061(9)	2.24(1)			
P-C11	1.82(2)	1.82(1)	C11-C21	1.39(3)	1.40(2)
C21-C31	1.43(3)	1.38(2)	C31-C41	1.42(2)	1.39(2)
C41-C51	1.38(3)	1.36(2)	C51-N1	1.36(2)	1.35(2)
N1-C11	1.32(1)	1.35(2)	P-C12	1.81(1)	1.84(2)
C12-C22	1.38(2)	1.40(3)	C22-C32	1.38(2)	1.39(3)
C32-C42	1.41(2)	1.42(2)	C42-C52	1.39(2)	1.39(3)
C52-N2	1.34(2)	1.36(3)	N2-C12	1.38(2)	1.32(2)
P-C13	1.84(1)	1.81(2)	C13-C23	1.37(2)	1.43(2)
C23-C33	1.40(2)	1.40(2)	C33-C43	1.39(2)	1.39(2)
C43-C53	1.41(2)	1.40(2)	C53-N3	1.34(2)	1.34(2)
N3-C13	1.32(1)	1.33(2)			
N7-O1	1.22(2)	N7-O2	1.28(2)	N7-O3	1.22(3)
N8-O4	1.17(3)	N8-O5	1.25(3)	N8-O6	1.22(4)
O11···O3	2.70(3)	O11···O6	2.94(4)	O22···O5	2.89(3)
Cl-Au-P	174.3(2)	176.3(2)	N1-Cu-N2	90.6(5)	90.7(5)
N1-Cu-N3	90.2(4)	91.1(4)	N2-Cu-N3	89.8(4)	87.8(5)
Au-P-C11	112.7(4)	115.5(4)	Au-P-C12	115.1(4)	112.2(5)
Au-P-C13	113.7(3)	115.7(4)	C11-P-C12	103.0(6)	104.2(6)
C11-P-C13	106.7(6)	103.9(7)	C12-P-C13	104.7(6)	103.9(7)
P-C11-C21	119(1)	119.7(9)	C11-C21-C31	118(1)	120(1)
C21-C31-C41	117(2)	118(1)	C31-C41-C51	121(2)	120(1)
C41-C51-N1	122(1)	123(1)	C51-N1-C11	118(1)	118(1)
N1-C11-P	116(1)	118.9(9)	C51-N1-Cu	121.0(8)	118.2(8)
Cu-N1-C11	121(1)	123.5(8)	P-C12-C22	121.3(9)	119(1)
C12-C22-C32	120(1)	118(1)	C22-C32-C42	118(1)	119(2)
C32-C42-C52	119(1)	117(2)	C42-C52-N2	122(1)	123(1)
C52-N2-C12	118(1)	119(1)	N2-C12-P	117.5(9)	119(1)
C52-N2-Cu	119.5(9)	118.6(9)	Cu-N2-C12	122.0(9)	122(1)
P-C13-C23	117.9(9)	121(1)	C13-C23-C33	119(1)	119(1)
C23-C33-C43	118(1)	117(1)	C33-C43-C53	119(1)	119(1)
C43-C53-N3	122(1)	125(1)	C53-N3-C13	119(1)	117(1)
C53-N3-Cu	118.4(7)	120.5(9)	N3-C13-P	118.7(8)	116(1)
Cu-N3-C13	122.6(9)	123.0(9)			
O1-N7-O2	114(2)	O2-N7-O3	123(2)	O1-N7-O3	123(1)
O4-N8-O5	118(2)	O5-N8-O6	118(2)	O4-N8-O6	124(3)
O6··O11··O3	110.0(9)	O11-O6-N8	113(2)	O11-O3-N7	147(1)
O22-O5-N8	122(2)				

Table 5.3.8 Best planes, dihedral and torsional angles for
            bis[chloro(tris-2-pyridylphosphine-P-)gold(I)
            -N,N',N"-)copper(II) dinitrate dihydrate

Plane	Distance of atom from the plane (Å)

Molecule A

1.C11,C21,C31,C41,C51,N1

C11;0.00(1),C21;-0.02(2),C31;0.02(2),
C41;0.00(3),C51;-0.02(2),N1;0.01(2)

2.C12,C22,C32,C42,C52,N2

C12;-0.01(2),C22;-0.01(2),C32;0.02(2),
C42;-0.01(2),C52;-0.01(2),N2;0.01(2)

3.C13,C23,C33,C43,C53,N3

C13;0.01(2),C23;-0.02(2),C33;-0.01(2),
C43;0.02(2),C53;-0.01(2),N3;-0.00(2)

4.N1,N1',N2,N2'

N1;0.19(2),N2;-0.16(2),
N1';0.17(2),N2';-0.24(2),Cu;-0.060(7)

5.N1,N1',N3,N3'

N1;-0.06(2),N3;0.04(2),
N1';-0.04(2),N3';0.05(2),Cu;0.042(6)

6.N2,N2',N3,N3'

N2;0.24(2),N3;-0.21(2),
N2';0.29(2),N3';-0.20(2),Cu;-0.205(7)

7.C11,C12,C13

P;0.74(1)

Molecule B

1.C11,C21,C31,C41,C51,N1

C11;-0.00(2),C21;0.01(2),C31;-0.01(2),
C41;-0.01(2),C51;0.01(2),N1;-0.01(2)

2.C12,C22,C32,C42,C52,N2

C12;-0.01(2),C22;0.01(3),C32;-0.01(3),
C41;-0.00(3),C51;0.00(3),N3;0.00(2)

3.C13,C23,C33,C43,C53,N3

C13;-0.02(2),C23;-0.01(3),C33;0.03(2),
C43;-0.02(3),C53;-0.02(3),N3;0.02(2)

4.N1,N1',N2,N2'

N1;0.00(2),N2;0.00(2),
N1';0.00(2),N2';0.00(2),Cu;0.000(7)

5.N1,N1',N3'N3'

N1;0.00(2),N3;0.00(2),
N1';0.00(2),N3';0.00(2),Cu;0.000(7)

6.N2,N2',N3,N3'

N2;0.00(2),N3;0.00(2),
N2';0.00(2),N3';0.00(2),Cu;0.000(7)

7.C11,C21,C31

P;0.75(1)

Table 5.3.8 continued

8.N7,O4,O5,O6	N7;0.01(2),O4;-0.00(2), O5;-0.00(3),O6;-0.00(3)
9.N8,O1,O2,O3	N8;0.04(3),O1;-0.02(3) O2;-0.01(3),O3;-0.02(4)

Dihedral angles (o)

	A	B		A	B
1 - 2	110.6(6)	126.0(6)	1 - 3	127.4(6)	118.0(6)
2 - 3	121.8(6)	115.7(7)	1 - 4	50.0(6)	44.2(5)
2 - 4	36.7(5)	45.5(5)	3 - 4	97.6(5)	88.8(5)
1 - 5	44.4(5)	43.8(5)	2 - 5	96.7(5)	96.1(5)
3 - 5	37.9(5)	42.7(6)	1 - 6	73.0(5)	87.4(5)
2 - 6	47.2(5)	43.9(6)	3 - 6	36.6(5)	46.7(6)
4 - 5	92.7(4)	92.2(4)	4 - 6	96.6(3)	89.0(4)
5 - 6	74.4(4)	89.3(4)	1 - 7	84.7(6)	93.0(7)
2 - 7	82.6(6)	96.3(7)	3 - 7	95.8(6)	88.4(7)
4 - 7	54.9(5)	58.0(6)	5 - 7	56.8(6)	55.6(6)
6 - 7	66.3(6)	55.4(6)			

Torsional angles (o)

	A	B
Cl-Au-P-C11	-10.3(2)	124.4(2)
Cl-Au-P-C12	107.4(2)	5.2(2)
Cl-Au-P-C13	-131.8(2)	-113.8(2)
Au-P-C11-N1	-6.2(2)	-5.1(2)
Au-P-C12-N2	6.3(2)	7.4(2)
Au-P-C13-N3	-5.0(2)	2.2(2)
P-C11-N1-Cu	-6.9(2)	-1.3(2)
P-C12-N2-Cu	4.7(2)	6.4(2)
P-C13-N3-Cu	-6.0(2)	2.2(2)

Figure 5.3.3 The bis[chloro(tris-2-pyridylphosphine-P-)gold(I)-
N,N'N"]copper(II) cation
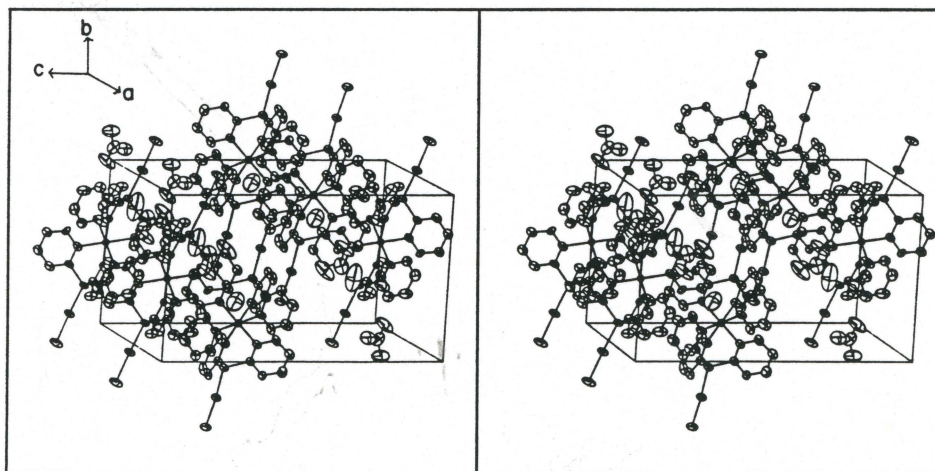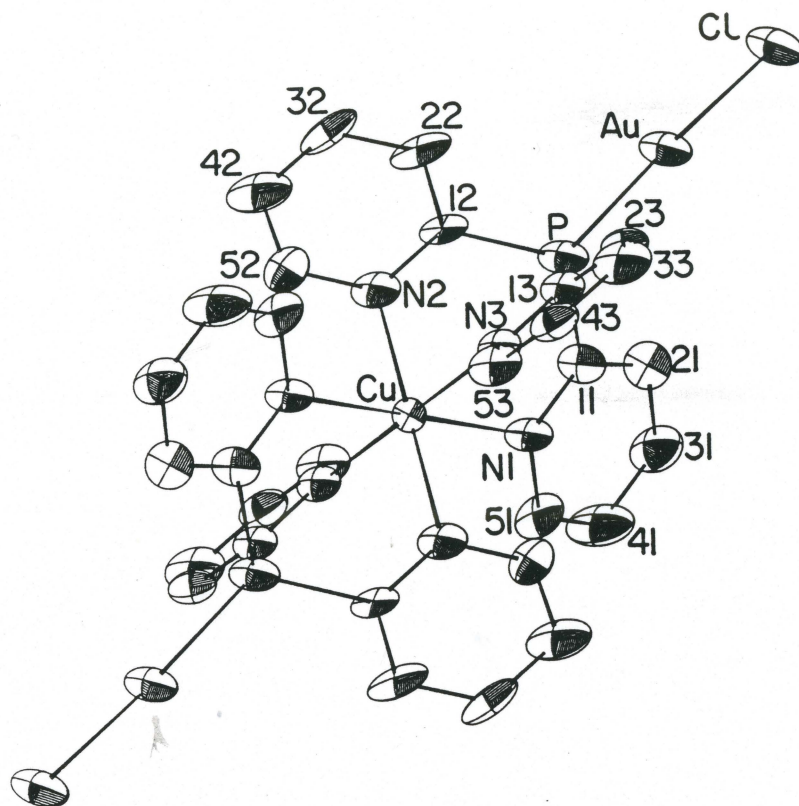
Figure 5.3.4 A steroview of the packing in the unit cell

90.6(5)(**A**), 90.7(5)(**B**), N1-Cu-N3; 90.2(4)(**A**), 91.4(4)(**B**) and N2-Cu-N3;

89.8(4)(**A**), 87.5(5)(**B**)). A list of best planes, dihedral and torsional

angles is given in Table 5.3.8.

Differences in the two crystallographically distinct molecules

in the similar structure of bis[hydrotris(pyrazol-1-yl)-

borate]copper(II) (212) have been evaluated on the basis of the

difference in their tetragonalities T (T=R_S/R_L where R_S=mean equatorial

Cu-N length and R_L=mean axial Cu-N length) (211) which are 0.792 and

0.866. The difference in the tetragonalities of molecules **A** and **B** in

[(ClAuTPP)$_2$Cu]$^{2+}$ are not as pronounced but show the sames trends (T$_A$=

0.896 from bond lengths Cu1-N1; 2.31(1), Cu1-N2; 2.08(1) and Cu1-N3;

2.061(9) Å and T$_B$=0.938 from bond lengths Cu2-N1; 2.04(1), Cu2-N2;

2.16(1) and Cu2-N3; 2.24(1) Å).

Thus the coordination of copper atoms by pyridyl nitrogen atoms

is such that distortions in **A** are considered typical of Jahn-Teller

systems. No distortions are observed in **B** reflecting dynamic Jahn-

Teller effects. Distortion is also apparent in the equatorial plane of

molecule **A** where the copper atom is displaced 0.205(7) Å out of the

plane defined by N2,N2',N3 and N3'. No such distortions are observed

in molecule **B**.

Bond lengths and angles in the tris-2-pyridylphosphine ligands

are normal. This observation, as well as that of regular octahedral

geometry about copper, indicate that very little strain is involved in

coordination of the ligand. On the other hand, the hydrotris(pyrazol-

1-yl)borate ligand has a smaller chelate bite distance and as a result,

ligand distortions have been reported for the Cu(II) complex (212) as

well as elongated rhombic distortion of the metal center.

A stereoview of the packing is given in Figure 5.3.4. Molecules are arranged with their axes roughly parallel to [0 1 0]. An almost linear chain of gold atoms is generated parallel to the a direction although Au-Au distances are too long (Au1··Au1´is shortest at 3.717(2) Å) to suggest any interaction. Because of their nearly parallel orientation, it is not immediately obvious why molecules A and B are crystallographically distinct. It appears that packing of nitrate anions and the associated network of hydrogen bonding interactions lead to small distortions in A and B which distinguish them from one another.

Unlike other structures, no short distances between coplanar pyridyl rings are observed. However, π-π interactions occur between ring 2A and the N7,O1,O2,O3 nitrate which are nearly coplanar (dihedral angle is 25.8(8)º) and which make a closest approach of 3.09(2) Å. This probably has little effect on the geometry of molecule A since the dihedral angle between rings 1 and 2 is the smallest of the three at 110.6(6)º compared to 127.4(6)º (1 - 3) and 121.8(6)º (2 - 3) as is the C11-P-C12 angle (103.0(6)º (vs. C11-P-C13; 106.7(6) and C12-P-C13; 104.7(6)º)). The 110.6(6)º dihedral angle is more likely a result of ring 1A - ring 3A dihedral angle widening to 127.4(6)º which occurs in order to accomodate not only the N8,O4,O5,O6 nitrate but a water molecule as well. The N8,O4,O5,O6 nitrate is involved in an interaction with ring 3A located 2.22(4) Å away at its nearest approach (24.0(9)º dihedral angle). The N8,O4,O5,O6 nitrate is also situated 3.1(1) Å from and coplanar with (2.4(9)º dihedral angle) ring 1B and is

apparently responsible for the relatively large ring 1 - ring 2

dihedral angle of 126.1(6)° in molecule **B**.

Nitrates N7,O1,O2,O3 takes part in hydrogen bonding to O11

through O3 (O11···O3; 2.89(3) Å, N7-O3··O11; 147(1)) and N8,O4,O5,O6 to

both O11 and O22 through O6 and O5 respectively (O11···O6; 2.94(4) Å,

O11··O6-N8; 113(2) and O22···O5; 2.89(3) Å, O22··O5-N8; 122(2)). The

other hydrogen atom from O22 is involved in a weak bond to the chlorine

atom of molecule **A** (O22···Cl; 3.75(3) Å, O22··Cl-Au; 115.5(3)°,

O6··O22··Cl; 117.8(8)°).

5.3.5 Electronic Absorption Spectroscopy

Data from UV/Visible spectroscopic characterization of the

copper complexes of TPP and comparable ligands are listed in Table

5.3.9. Titration of a methanolic solution of $Cu(NO_3)_2 \cdot 6H_2O$ with TPP

was followed in the visible region and the results are shown in Figure

5.3.5. The presence of isosbestic points formed by successive spectra

is evidence that one complex is formed exclusively in each step (214).

Comparison of peak positions at 1:1 and 2:1 TPP:Cu ratios with

independant spectra of $(TPP)Cu(NO_3)_2$ and $(TPP)_2Cu(NO_3)_2$ confirm that

these are, in fact, the products formed in the titration.

The absorption bands at 15,720 cm^{-1} in $[(TPP)_2Cu](NO_3)_2$ and

15,710 in $(ClAuTPP)_2Cu(NO_3)_2$, attributed to the $^2E_g \leftarrow {}^2B_{1g}$ transitions

in octahedral complexes, are somewhat higher than those of other

$Cu(aromatic-N)_6$ compounds reported previously (see Table 5.3.9). This

indicates that TPP has slightly greater ligand field strength compared

to other aromatic nitrogen donors such as 2,2'-bipyridine (bipy) and

Table 5.3.9 Energies of electronic absorptions for Cu(II) complexes

Complex	E $(cm^{-1} \times 10^{-3})$[a]
$Cu(H_2O)_6^{2+}$	12.6 (9.4)
$Cu(en)_3^{2+}$	16.4 (11.8)
$Cu(dien)_2^{2+}$	15.9 (11.8)
$Cu(bipy)_2(H_2O)_2^{2+}$	13.9 (10.5)
$Cu(bipy)_3^{2+}$	14.7 ($\cong$9)
$Cu(phen)_2(H_2O)_2^{2+}$	13.3 (10.2)
$Cu(phen)_3^{2+}$	15.9 ($\cong$8)
$TPPCu(H_2O)_3^{2+}$	14.14
$(TPP)_2Cu^{2+}$	15.72
$(ClAuTPP)_2Cu^{2+}$	15.71

[a] Data for the first seven complexes in this table is from (215)

Figure 5.3.5 UV/Visible Absorption Spectra of TPP complexes with copper(II)
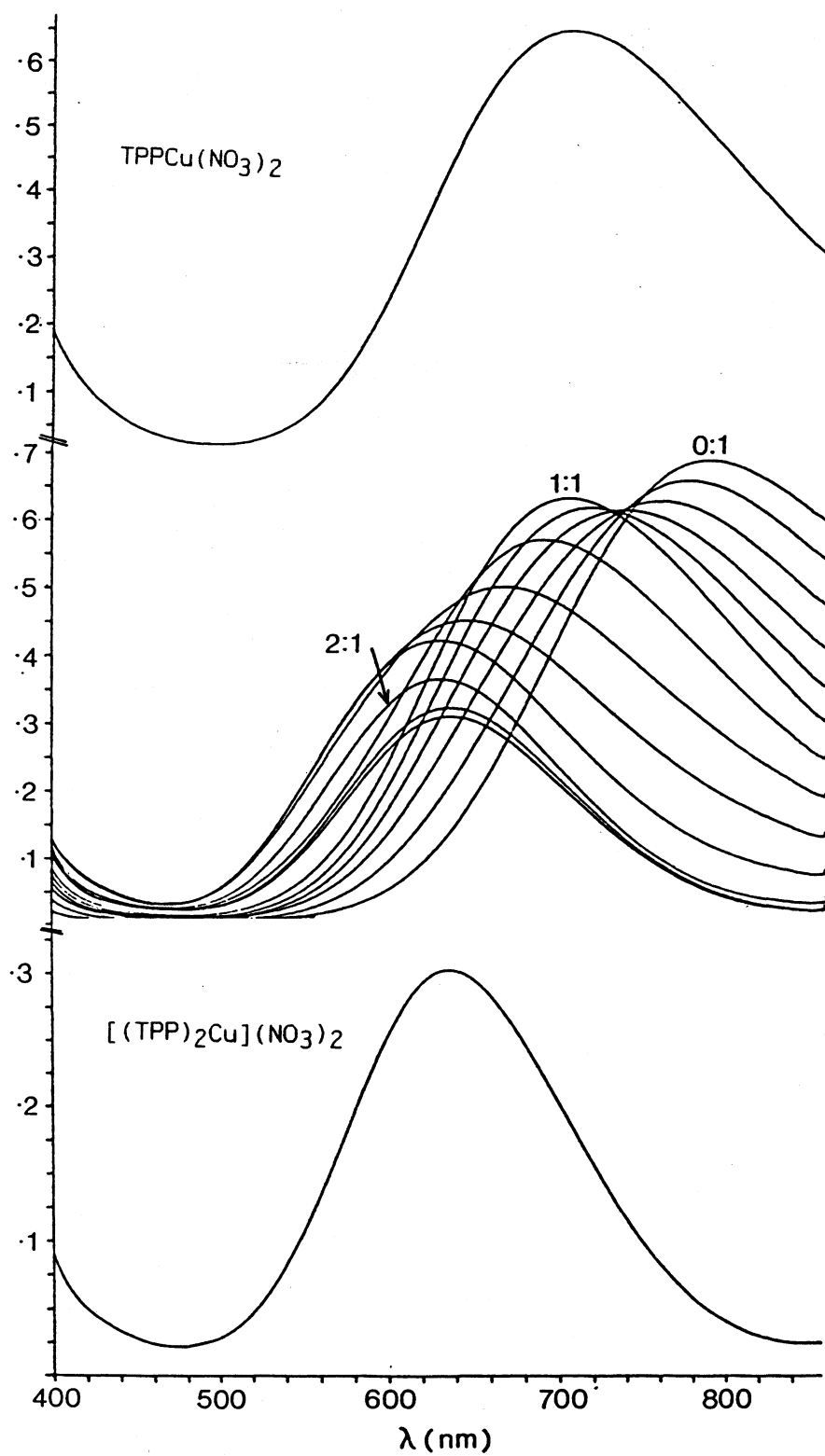
1,10-phenanthrolene (phen) whose tris complexes both absorb at 14,700 cm^{-1} (215). Furthermore, $(TPP)Cu(NO_3)_2$ has three _facially_ coordinated nitrogen atoms and shows a broad absorption band with its maximum at 14,140 cm^{-1}. This is at higher energy than the bands of $Cu(bipy)_2(H_2O)_2$ (13,900 cm^{-1}) and $Cu(phen)_2(H_2O)_2$ (13,300 cm^{-1}), (215), in which four nitrogen donors are coordinated to copper in _cis_ geometry. TPP is, thus, intermediate in ligand field strength between aromatic nitrogen ligands such as bipy and phen and saturated amines such as ethylenediamine (en) and diethylenetriamine (dien) whose complexes exhibit bands at 16,400 cm^{-1} ($Cu(en)_3^{2+}$) and 15,900 cm^{-1} ($Cu(dien)_3^{2+}$ (215)).

A band observed in spectra of copper complexes which are subject to Jahn-Teller distortions is attributed to $^2A_{1g} \leftarrow ^2B_{1g}$ and usually appears as a shoulder on the low energy side of the $^2E_g \leftarrow ^2B_{1g}$ absorption (in parentheses in Table 5.3.9). Complexes experiencing a relatively higher degree of tetragonal distortion exhibit this band at higher energies. Although tetragonal elongation is apparent in the X-ray molecular structure of $[(ClAuTPP)_2Cu](NO_3)_2$, this shoulder was not observed in its electronic absorption spectrum or in that of $[(TPP)_2Cu](NO_3)_2$.

5.3.6 Electron Spin Resonance Spectroscopy

Results of E.S.R. studies of copper complexes of TPP and comparable ligands are listed in Table 5.3.10 and typical anisotropic low temperature spectra are illustrated in Figure 5.3.7. At room temperature, spectra are isotropic and show only four broad features consistent with coupling to the $I=3/2$ copper nucleus. It is possible

Figure 5.3.6   Low temperature Electron Spin Resonance Spectra of
TPP complexes with copper(II)

TPPCu(NO$_3$)$_2$

[(TPP)$_2$Cu](NO$_3$)$_2$

[(ClAuTPP)$_2$Cu](NO$_3$)$_2$

3100 G
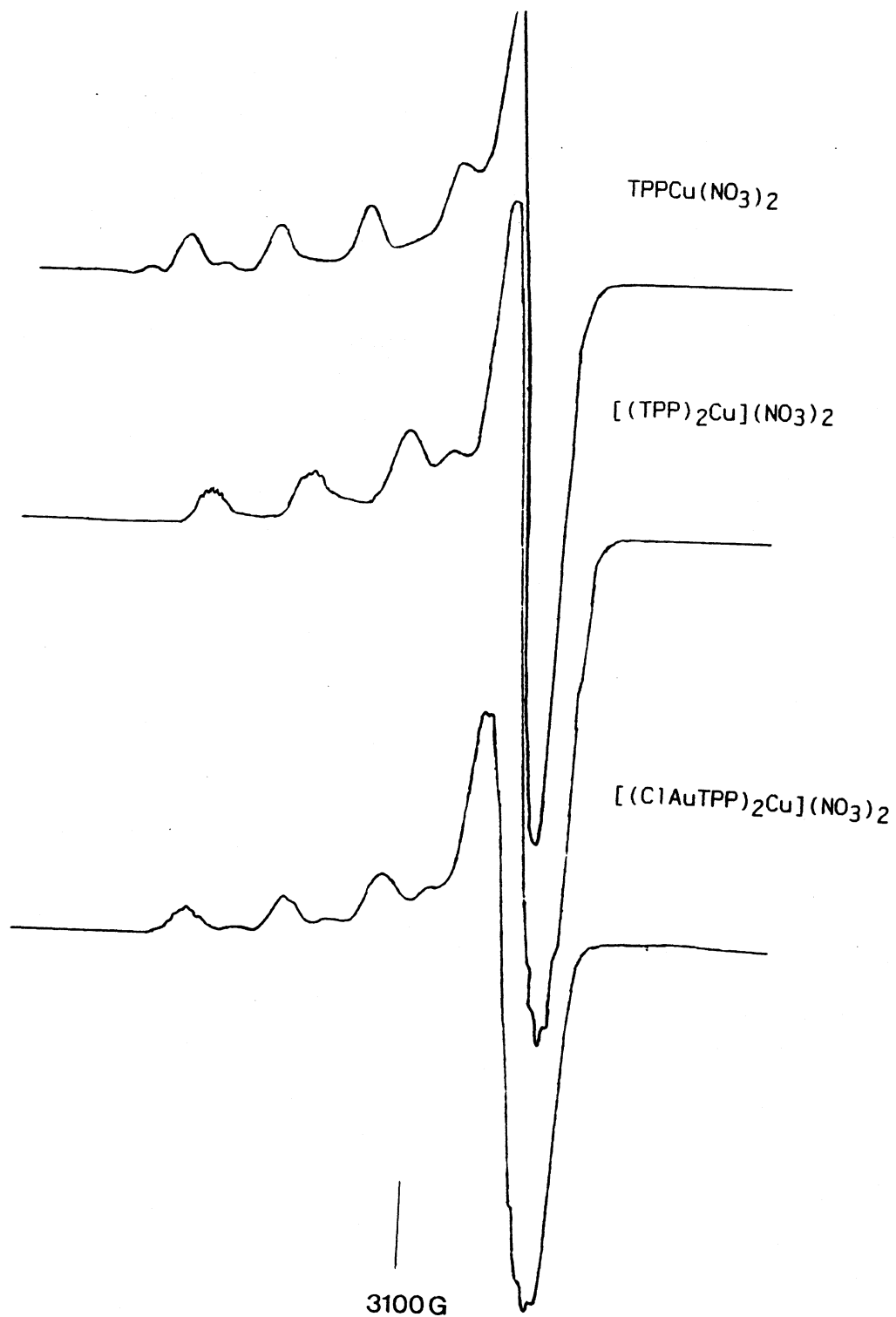
Table 5.3.10. Electron Spin Resonance Data for Copper(II) Complexes

Complex	$g_{\parallel}$	$g_{\perp}$	$A_{\parallel}(Cu)$[a]	$A_{\parallel}(N)$[a]	$A_{\perp}(N)$[a]	ref.
$Cu(TPP)_2^{2+}$ [b]	2.265	2.071	168	10	13	
$Cu(TPPAuCl)_2^{2+}$ [b]	2.268	1.071	167	9	12	
$Cu(bipy)_3^{2+}$ [c]	2.268	2.046	164	9	12	g
$Cu(phen)_3^{2+}$ [c]	2.273	2.062	161	10	12	g
$Cu(N\text{-}MeIm)_6^{2+}$ [d]	2.307	2.065	165		13	h
$Cu(TPP)(NO_3)_2$ [b]	2.310	2.140	159	e	e	
$Cu(py)_3(NO_3)_2$ [d]	g_x= 2.279		A_x= 127	9.4,11.2[f]		i,j
	g_y= 2.151		A_y= 49	12.9,10.9[f]		
	g_z= 2.017		A_z= 78	9.4,15.0[f]		

[a] hyperfine constants $\times 10^{-4}$ cm^{-1}
[b] frozen solution
[c] powder
[d] molecule doped into corresponding zinc complex host lattice
[e] coupling not observed
[f] two $A_{\parallel}(N)$ values for coupling to two crystallographically distinct nitrogen atoms
[g] Allen et al. (203)
[h] Nieuwenhuijse and Reedijk (216)
[i] McPherson and Anderson (217)
[j] work also done by Dudley et al. (218) but no A values reported

to roughly calculate the parallel and perpendicular contributions to the isotropic g value using the following equations;

$$g_\parallel = 2 + 8\frac{|\lambda|}{\Delta}, \quad g_\perp = 2 + 2\frac{|\lambda|}{\Delta}, \quad \text{and } g_{iso} = 2 + 4\frac{|\lambda|}{\Delta}$$

where λ is the spin-orbit coupling constant and Δ is the crystal field splitting of the d-orbitals of the copper atom in an octahedral field (203). In fact, the calculated values for the bis complexes of TPP are in excellent (0.3%) agreement with those observed while values for the mono TPP complex give only moderate agreement (3.0%). The results of these calculations are recorded in Table 5.3.11.

Upon cooling an octahedrally coordinated copper(II) system, dynamic Jahn-Teller effects which allow the system to resonate among three equivalent tetragonal distortions along each octahedral axis, are frozen out such that an anisotropic spectrum arises having two distinct g values (214). These have been labelled $g_\parallel$ and $g_\perp$ where $g_\parallel$ is the value obtained when the field is parallel to the molecular axis and $g_\perp$ when the field is perpendicular. Some effort has been made to correlate the electronic properties of copper(II) complexes with the local stereochemistry of the copper(II) ion present (202). In particular, g values yield information as to the orbital ground state of copper complexes according to the following criteria; $g_\parallel$ values of 2.00 to 2.04 indicate a d_{z^2} ground state rather than a $d_{x^2-y^2}$ (or less commonly d_{xy}) ground state. In general, a $d_{x^2-y^2}$ ground state is associated with a tetragonally elongated octahedral or square pyramidal environment at copper where the d_{z^2} ground state is typical of trigonal bipyramidal geometry (202). Values of $g_\parallel$ for the bis tris-2-pyridylphosphine copper complexes are above 2.04 ((TPP)$_2$Cu; 2.071,

Table 5.3.11 Comparison of Observed and Calculated g-Values

Complex	g_{iso}	Obsvd.		Calc.
$TPPCu(NO_3)_2$	2.155	$g_{\parallel}$	2.310	2.310
		$g_{\perp}$	2.140	2.078
$(TPP)_2Cu^{2+}$	2.130	$g_{\parallel}$	2.265	2.262
		$g_{\perp}$	2.071	2.067
$(TPPAuCl)_2Cu^{2+}$	2.130	$g_{\parallel}$	2.268	2.264
		$g_{\perp}$	2.071	2.066

(TPPAuCl)$_2$Cu^{2+}; 2.071) and tetragonal elongation has been observed in the crystal structure of (TPPAuCl)$_2$Cu thus it is concluded that d$_{x^2-y^2}$ is the common ground state orbital for both species. It is particularly noteworthy to compare data for TPPCu(NO$_3$)$_2$ where g$_\perp$=2.140 and g$_\parallel$=2.310 with the meridionally coordinated Cu(py)$_3$(NO$_3$)$_2$ where g$_z$=2.0250, g$_y$=2.1660 and g$_x$=2.2662. The lowest g value determined from the Cu(py)$_3$(NO$_3$)$_2$ single crystal study (218) and a parallel one involving the study of this molecule doped into a host lattice of the isomorphic zinc complex (217) indicate a trigonal bipyramidal geometry and a d$_{z^2}$ ground state. It is suspected that a single crystal E.S.R. study of TPPCu(NO$_3$)$_2$ would yield different results on the basis of its crystallographically determined square pyramidal structure.

Magnitudes of the hyperfine splitting constants, A, are determined by the size of the nuclear moment and the proximity of the electron to the nucleus (218). In other words, the hyperfine splitting can give an indication as to bond covalency in that decreased coupling to the copper nucleus and the presence of coupling to ligand nitrogen atoms suggests a certain extent of electron delocalization onto the ligands. It is convenient to compare the CuN$_6$ species Cu(bipy)$_3$, Cu(phen)$_3$ (203), Cu(N-MeIm)$_6$ (216) with (TPP)$_2$Cu^{2+} and (ClAuTPP)$_2$Cu^{2+} where similarities in A$_\parallel$(Cu) and A$_\parallel$(N) hyperfine splitting constants (A$_\parallel$(Cu)=168 x 10^{-4} and A$_\parallel$(N)=10 x 10^{-4} cm^{-1} for (TPP)$_2$Cu^{2+} and 167 x 10^{-4} and 9 x 10^{-4} cm^{-1} for (TPPAuCl)$_2$Cu^{2+} compared to A$_\parallel$(Cu)=164, 161 and 165 x 10^{-4} cm^{-1} and A$_\parallel$(N)=9, 10 and 13 x 10^{-1} cm^{-1} for Cu(bipy)$_3^{2+}$, Cu(phen)$_3^{2+}$, and Cu(N-MeIm)$_6^{2+}$ respectively) indicate a similar extent of electron delocalization. The A$_\parallel$(Cu) coupling constant of 159 x 10^{-4}

for the mono-ligated species, TPPCu(NO$_3$)$_2$, is slightly smaller than for

the bis complexes of TPP and coupling with nitrogen atoms is too small

to be resolved. Strictly speaking, the smaller $A_{\parallel(Cu)}$ value is

associated with greater electron delocalization onto the ligands which

is not reflected in $A_{\parallel(N)}$ values. An explanation for the observation

of a smaller $A_{\parallel(Cu)}$ value may be that the unpaired electron of

TPPCu(NO$_3$)$_2$, which has distorted square pyramidal geometry, is in an

orbital which has less s character than that of the other two distorted

octahedral TPP complexes and coupling to the nuclear spin is, in

theory, only possible when the unpaired electron resides in an orbital

which has the capacity for nuclear penetration (220).

5.4 Iron Complexes

5.4.1 Introduction

The use of iron complexes as models for the active sites of

proteins containing oxo-bridged polynuclear centers such as

haemerythrin has been recently reviewed (193).

An X-ray structure solution of azido methaemerythrin (221) has

established details of iron coordination at the active site and this is

illustrated in Figure 5.4.1. Attempts to model the active site with

ligands such as hydro(tris(1-pyrazolyl)borate) (222,223) and

triazacyclononane (224) have been successful as demonstrated by

comparison of their physical properties with those of the protein (in

particular, antiferromagnetic coupling between the two iron nuclei).

The use of the neutral, aromatic TPP as a ligand in these systems would

provide a bridge between the negatively charged, aromatic ligand
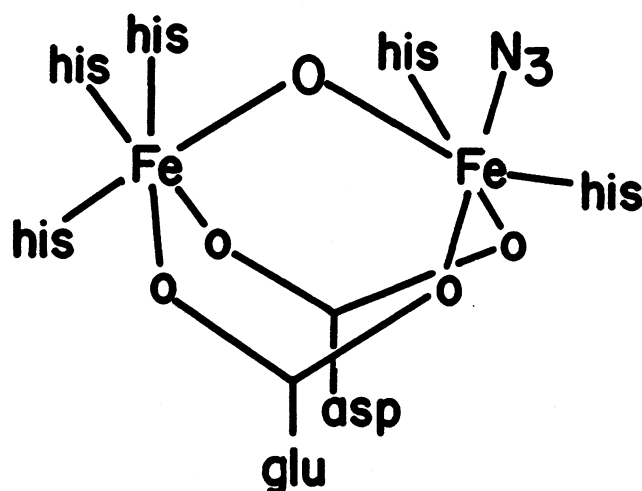
Figure 5.4.1 The active site of metazidohaemerythrin (194)

complexes of HB(pz₃) and the neutral secondary amine sites of TACN.

Furthermore, incorporation of gold(I) into the TPP ligand is possible

and may have an effect on properties such as solubility. A discussion

of synthesis, crystallography and spectra of some iron(II) and

iron(III) complexes of TPP and ClAuTPP appears in the following

sections of this chapter as well as in the summary of crystallographic

and infrared data found in Chapter 6.

5.4.2 Preparations

diaquo(tris-2-pyridylphosphine-N,N',N"-)sulphatoiron(II) trihydrate

(TPPFe(SO₄)(H₂O)₂; Fe(SO₄)·7H₂O (0.217 g, 0.78 mmol) was dissolved in

10 mL of water. An ethanol solution (15 mL) containing 0.207 g (0.78

mmol) of TPP was added dropwise to the aqueous solution and stirred for

12 hours. All but 5 mL of solvent was removed under reduced pressure

and the resulting orange precipitate was filtered and recrystallized

from water to yield 0.068 g of product (44%). Analysis required for

$C_{15}H_{16}FeN_3O_6PS \cdot 3H_2O$: C; 35.5, H; 8.3, N; 4.4%. Found: C; 35.2, H; 8.1,

N; 4.1%.

(chloro(tris-2-pyridylphosphine-P)-gold(I))-N,N',N"-)iron(II)sulphate

(ClAuTPP)FeSO₄; ClAuTPP (0.27 g, 0.54 mmol) was dissolved in 50 mL of

methanol/acetone (49:1). A methanol solution (10 mL) containing 0.08 g

(0.54 mmol) of $FeSO_4 \cdot 7H_2O$ was added dropwise and the solution was

stirred for 12 hours. The solvent was removed under reduced pressure

to a volume of 10 mL. The red precipitate (0.156 g) was filtered and

recrystallized from acetone/water in 39% yield. Analysis required for

$C_{15}H_{16}AuClFeN_3O_6PS \cdot 2.8H_2O$; C; 24.5, H; 3.0, N; 5.7, Cl; 4.8%.

Found: C; 24.9, H; 3.1, N; 5.6, Cl; 5.1%.

bis(tris-2-pyridylphosphine-N,N',N"-)iron(II) perchlorate

(TPP)₂Fe(ClO₄)₂; This compound was prepared according to the method of

Boggess and Zatko (185).

bis[chloro(tris-2-pyridylphosphine)-gold(I)-N,N',N"-]iron(II)

perchlorate (ClAuTPP)₂Fe(ClO₄)₂; $Fe(ClO_4)_2$ (0.127 g, 0.25 mmol) was

refluxed for 8 hours in 20 mL of a solution consisting of

2,2'-dimethoxypropane and ethanol (1:1). A solution of 0.25 g (0.5

mmol) of ClAuTPP in 20 mL of ethanol was added to produce an immediate

red precipitate. The reaction mixture was stirred for a further 6

hours at room temperature. The precipitate filtered and recrystallized

from acetone/hexanes to give 0.256 g of product (82% yield). Analysis

required for $C_{30}H_{24}AuCl_4FeN_6O_8P$: C; 28.8, H; 1.9, N; 6.7, Cl; 11.3%.

Found: C; 28.1, H; 1.8, N; 6.5, Cl; 11.6%.

trichloro(tris-2-pyridylphosphine-N,N',N"-)iron(III) (TPPFeCl₃);

TPP (0.2458 g, 0.93 mmol) was dissolved in 10 mL of ethanol. An

ethanol solution containing 0.2505 g (0.93 mmol) of $FeCl_3 \cdot 6H_2O$ was

added to yield a yellow precipitate. The reaction mixture was stirred

over night. The precipitate was filtered and recrystallized from

acetone/hexanes to yield 0.334 g of product (84% yield). Analysis

required for $C_{15}H_{12}Cl_3FeN_3P$: C; 42.1, H; 2.8, N; 9.8, Cl; 24.9%.

Found: C; 41.8, H; 2.6, N; 9.5, Cl; 25.0%.

5.4.3 The crystal and molecular structure of (TPPFe(H$_2$O)$_2$SO$_4$

The molecule is illustrated in Figure 5.4.2. Atomic positional

parameters and anisotropic temperature factors are given in Tables

5.4.1 and 5.4.A and a list of bond distances and angles is found in

Table 5.4.2. The environment of the iron atom is octahedral with

facial Fe-N bonds as well as coordination to a sulphate anion and two

molecules of water. The Fe-N distances (Fe-N1; 2.184(3), Fe-N2;

2.174(3) and Fe-N3; 2.172(3) Å) are equivalent within error and are

typical of those found in similar complexes of high spin iron(II), for

example, Fe-N bond lengths are 2.17(2) Å in

bis(bipyridyl)bisthiocyanatoiron(II) (225), 2.190(4), 2.179(4) and

2.147(4) Å in bis(hydrotris(3,5-dimethylpyrazol-1-yl)borate)

iron(II) (226) and 2.174(4) and 2.157(4) Å in the bis(triaquatris-

(4-ethyltriazole)iron(II) cation (227). In the sterically crowded

hexakis(pyridine)iron(II) cation, Fe-N bond lengths are very long in

comparison and average 2.26(1) Å (228). Such steric effects are not

observed to the same extent in complexes of TPP since the phosphorus

atom has the ability to restrain the pyridine rings in a C_{3v} geometry.

The Fe-OH$_2$ distances in TPPFe (Fe-OH$_2$; 2.112(4) and 2.103(4) Å) are

also comparable to those reported in similar structures (Fe-OH$_2$

distances are 2.099(2) and 2.159(2) Å in tetraquobis(saccharin)iron(II)

Table 5.4.1 Crystal data for diaquo(tris-2-pyridylphosphine-N,N',N")
sulphatoiron(II)trihydrate

Formula	$C_{15}H_{16}FeN_3O_6PS \cdot 3H_2O$
Formula weight	507.23
Crystal size and shape	$0.26 \times 0.27 \times 0.39 mm^3$ cylinder
Systematic absences	none
Space group	$P\bar{1}$
Diffractometer	P3
Temperature	22°C
Unit cell parameters	$a=8.339(2)Å$ $\alpha=99.71(2)°$
	$b=9.489(3)Å$ $\beta=91.31(2)°$
	$c=14.086(3)Å$ $\gamma=102.49(2)°$
	$V=1070.5(5)Å^3$ $Z=2$
ρ_{calc},ρ_{obs}	$1.573,1.59$ $CHCl_3/CHBr_3$
Range of hkl	$0<h<9,-11<k<11,-16<l<16$
Maximum 2θ	50°
Number of reflcns measured	4077
Number of independent reflcns	3797
Standard reflcns(e.s.d)	2 0 1 (1.5%),0 -3 3 (1.9%)
R_{int}	0.0082
Final R,Rw	0.0588,0.0570
Final shift/error max(ave)	0.015(0.001)
Error in obs of unit weight	S=1.8369
Highest peak, lowest valley	$0.56eÅ^{-3},-0.15eÅ^{-3}$
Weighting	$w=(\sigma^2(F) + 0.000387F^2)^{-1}$
F(000)	525.2
Linear Absorption coefficient	$\mu=9.45$ cm^{-1}
Absorption Coefficient limits	$1.53<A^*<1.95^*$
Number of Variables	297

* an absorption correction was applied

Table 5.4.2 Positional parameters (x104) and Ueq (x104) for
diaquo(tris-2-pyridylphosphine-N.N′,N″-)sulphatoiron(II)
trihydrate

Atom	x	y	z	U_{eq}
Fe	5840.1(7)	7409.1(6)	7832.6(4)	314
P	4770(1)	3595(1)	7273.6(9)	407
C11	6026(5)	4546(5)	6413(3)	395
C21	6501(7)	3690(7)	5614(3)	603
C31	7517(8)	4383(11)	4997(4)	808
C41	8019(8)	5853(10)	5167(4)	696
C51	7496(6)	6639(6)	5956(3)	522
N1	6512(4)	6018(4)	6577(2)	384
C12	3073(4)	4559(4)	7408(2)	321
C22	1496(5)	3690(5)	7336(3)	394
C32	174(5)	4369(6)	7444(3)	439
C42	466(5)	5859(5)	7617(3)	428
C52	2061(5)	6662(5)	7690(3)	385
N2	3357(3)	6041(3)	7585(2)	327
C13	6029(4)	4401(4)	8402(3)	327
C23	6526(6)	3464(5)	8945(4)	506
C33	7527(7)	4021(6)	9756(4)	598
C43	8003(6)	5506(6)	10035(3)	518
C53	7489(5)	6408(5)	9476(3)	415
N3	6508(4)	5872(3)	8663(2)	326
O1	5351(4)	8894(4)	6964(3)	708
O2	5127(4)	8553(4)	9104(2)	590
S1	9118(1)	10196(1)	8070.2(8)	371
O3	8231(3)	8674(3)	8095(2)	431
O4	8318(4)	10774(3)	7331(2)	583
O5	10823(4)	10192(4)	7861(3)	672
O6	9113(6)	11115(4)	9002(2)	770
O7	7474(4)	239(4)	484(2)	631
O8	9130(8)	993(6)	5464(4)	412
O9	2489(7)	613(6)	6312(4)	399

$U_{eq}=1/3(U_{11}+U_{22}+U_{33}+2Cos\alpha U_{23}+2Cos\beta U_{13}+2Cos\gamma U_{12})$

176

Table 5.4.2 continued

Hydrogen positional parameters (x104)

Atom	x	y	z
H21	6171	2471	5586
H31	7827	4000	4598
H41	8513	6192	4649
H51	7714	7703	6035
H22	1522	2544	7199
H32	-859	3791	7359
H42	-230	6371	7628
H52	2145	7611	7778
H23	6434	2659	8753
H33	8018	3463	10128
H43	8720	5880	10603
H53	7840	7469	9625
H1	4689	9050	6682
H2	6206	9742	7005
H3	4342	8965	9115
H4	5613	9109	9517
H71	8021	165	947
H72	8223	407	183

Hydrogens were located and fixed with isotropic temperature factors of 0.05 $Å^2$

Table 5.4.3.   Bond lengths (Å) and angles (º) for diaquo(tris-2-
pyridylphosphine)-N,N′,N″)sulphatoiron(II) trihydrate

Fe-N1	2.184(3)	Fe-N2	2.174(3)	Fe-N3	2.172(3)
Fe-O1	2.112(4)	Fe-O2	2.103(3)	Fe-O3	2.082(2)
P-C11	1.843(4)	P-C12	1.840(4)	P-C13	1.838(4)
C11-C21	1.382(5)	C12-C22	1.384(5)	C13-C23	1.380(7)
C21-C31	1.379(8)	C22-C32	1.384(6)	C23-C33	1.361(7)
C31-C41	1.352(1)	C32-C42	1.366(7)	C33-C43	1.362(7)
C41-C51	1.365(7)	C42-C52	1.375(5)	C43-C53	1.377(7)
C51-N1	1.332(6)	C52-N2	1.340(5)	C53-N3	1.345(5)
N1-C11	1.348(5)	N2-C12	1.354(4)	N3-C13	1.350(4)
S-O3	1.480(3)	S-O4	1.463(4)	S-O5	1.459(3)
S-O6	1.453(3)				
N1-Fe-N2	87.8(1)	N1-Fe-N3	85.9(1)	N1-Fe-O1	90.9(1)
N1-Fe-O2	174.2(1)	N1-Fe-O3	92.2(1)	N2-Fe-N3	89.2(1)
N2-Fe-O1	93.7(1)	N2-Fe-O2	89.4(1)	N2-Fe-O3	178.2(1)
N3-Fe-O1	175.6(1)	N3-Fe-O2	89.0(1)	N3-Fe-O3	89.0(1)
O1-Fe-O2	94.3(1)	O1-Fe-O3	88.1(1)	O2-Fe-O3	90.5(1)
C11-P-C12	102.1(2)	C12-P-C13	101.6(2)	C11-P-C13	100.4(2)
P-C11-C21	118.0(3)	P-C12-C22	116.7(3)	P-C13-C23	118.3(3)
C11-C21-C31	119.2(5)	C12-C22-C32	118.9(4)	C13-C23-C33	119.9(4)
C21-C31-C41	119.1(5)	C22-C32-C42	119.6(3)	C23-C33-C43	119.2(5)
C31-C41-C51	119.4(5)	C32-C42-C52	118.7(4)	C33-C43-C53	119.2(4)
C41-C51-N1	123.0(5)	C42-C52-N2	123.2(4)	C43-C52-N3	122.4(4)
C51-N1-Fe	119.1(3)	C52-N2-Fe	119.9(2)	C53-N3-Fe	118.6(3)
C51-N1-C11	118.1(3)	C52-N2-C12	117.9(3)	C53-N3-C13	117.9(3)
Fe-N1-C11	122.8(2)	Fe-N2-C12	122.0(2)	Fe-N3-C13	123.5(2)
N1-C11-P	120.7(3)	N2-C12-P	121.5(2)	N3-C13-P	120.2(3)
N1-C11-C21	121.3(4)	N2-C12-C22	121.8(4)	N3-C13-C23	121.5(3)
O3-S-O4	109.8(2)	O3-S-O5	108.4(2)	O3-S-O6	109.9(2)
O4-S-O5	110.7(2)	O4-S-O6	109.7(2)	O5-S-O6	108.3(2)

Table 5.4.3 continued

Interatomic Distances (Å) and angles (°) associated with hydrogen bonding

---

| O1···O9 | 2.688(6) | O1-H1 | 0.73 | O9···H1 | 1.99 | O9··H1-O1 | 160 |
| O1···O4 | 2.703(4) | O1-H2 | 0.94 | O4···H2 | 1.83 | O4··H2-O1 | 153 |

| O2···O7 | 2.693(7) | O2-H3 | 0.83 | O7···H3 | 1.89 | O7··H3-O2 | 163 |
| O2···O7′ | 2.755(4) | O2-H4 | 0.76 | O7′···H4 | 2.03 | O7′·H4-O2 | 162 |

| O7···O5 | 2.834(7) | O7-H71 | 0.81 | O5···H71 | 2.03 | O5··H71-O7 | 174 |
| O7···O6 | 2.668(5) | O7-H72 | 0.77 | O6···H72 | 1.99 | O6··H72-O7 | 147 |

| O8···O4 | 2.771(6) | O8···O8′ | 2.792(8) |
| O8···O9 | 2.77(4) | O9···O5 | 2.697(7) |

O9··O1-Fe	131.5(2)	O4··O1-Fe	95.9(1)	O4··O1··O9	128.7(2)
O7··O2-Fe	133.1(2)	O7′·O2-Fe	120.2(1)	O7··O2··O7′	101.6(2)
O8··O4-S	130.0(2)	O7··O5-S	109.4(2)	O7··O6-S	124.8(2)
O5··O7··O2	136.7(2)	O5··O7··O2′	113.6(1)	O6··O7··O2	85.7(1)
O6··O7··O2′	114.5(2)	O5··O7··O6	120.6(2)	O4··O8··O8′	117.0(3)
O4··O8··O9	136.6(9)	O9··O8··O8′	152.0(7)	O1··O9··O5	108.2(2)
O1··O9··O8	135.5(3)	O5··O9··O8	115.8(3)	

Table 5.4.4   Best planes, dihedral and torsional angles for
diaquo(tris-2-pyridylphosphine-N,N′,N″-)sulphato-O-
iron(II)

Plane	Distance of atom from the plane (Å)
1.C11,C21,C31,C41,C51,N1	C11;0.006(5,C21;-0.008(7),C31;0.00(1), C41;0.004(9),C51;0.002(7),N1;-0.003(4)
2.C12,C22,C32,C42,C52,N2	C12;-0.037(4),C22;0.002(5),C32;0.003(6), C42;-0.005(6),C52;0.002(5),N2;0.001(4)
3.C13,C23,C33,C43,C53,N3	C13;0.002(4),C23;0.002(6),C33;-0.007(7), C43;0.005(6),C53;0.007(5),N3;-0.002(4)
4.N1,N2,O2,O3	N1;0.035(4),N2;-0.028(4),O2;0.033(4), O3;-0.026(4),Fe;-0.061(2)
5.N1,N3,O2,O1	N1;-0.052(4),N3;0.042(4),O2;-0.046(4), O1;0.071(5),Fe;0.002(2)
6.N2,N3,O3,O1	N2;0.025(4),N3;-0.027(4),O3;0.025(4), O1;-0.048(5),Fe;0.024(2)
7.C11,C12,C13	P;0.827(2)

Dihedral angles (°)

1 - 2	125.9(2)	1 - 3	113.0(2)	2 - 3	120.9(1)	1 - 4	137.0(2)
2 - 4	133.5(1)	3 - 4	92.6(1)	1 - 5	133.8(2)	2 - 5	95.3(1)
3 - 5	131.6(1)	4 - 5	89.0(9)	1 - 6	91.9(2)	2 - 6	136.3(1)
3 - 6	139.0(1)	4 - 6	89.8(9)	5 - 6	90.7(8)	1 - 7	90.6(2)
2 - 7	87.3(2)	3 - 7	89.9(2)	4 - 7	125.9(1)	5 - 7	125.1(1)
6 - 7	123.3(1)						

Torsional angles (°)

P-C11-N1-Fe	-1.45(1)	C11-N1-Fe-O2	15.27(1)	Fe-O3-S-O4	-30.72(1)
P-C12-N2-Fe	-4.09(1)	C12-N2-Fe-O3	-43.45(1)	Fe-O3-S-O5	28.28(1)
P-C13-N3-Fe	1.17(1)	C13-N3-Fe-O1	-89.72(1)	Fe-O3-S-O6	90.44(1)
				N2-Fe-O3-S	22.71(1)

Figure 5.4.2 A molecule of diaquo(tris-2-pyridylphosphine-N,N',N"-)
sulphatoiron(II). The intramolecular hydrogen bond is
depicted by the dotted line.
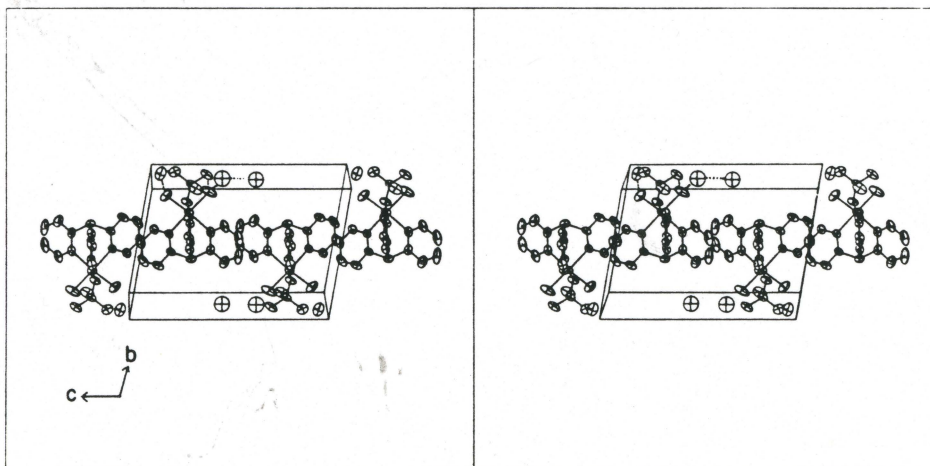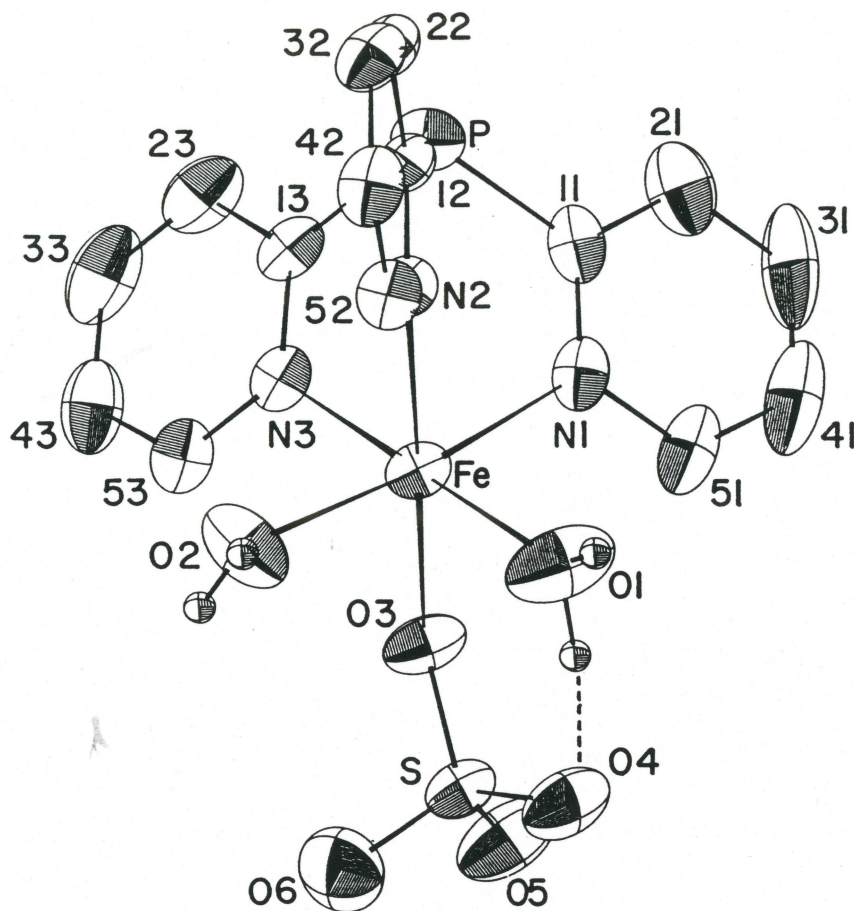
Figure 5.4.3 A stereoview of the unit cell. Hydrogen bonding is
indicated by dotted lines.

(229) and 2.156(4) Å in the bis(triaqua(tris(4-ethyltriazole)iron(II))

cation (227). The Fe-OSO₃ distance (2.082(2) Å) is short in comparison

with those previously reported by Naik and Palinik (230) (2.187(5) and

2.165(4) Å) where the sulphate group bridges two iron atoms.

Angles in the octahedral iron environment are slightly distorted

in that all N-Fe-N angles are less than 90o (N1-Fe-N2; 87.8(1), N1-Fe-

N3; 85.9(1) and N2-Fe-N3; 89.2(1)o). No significant changes in the

geometry of TPP with respect to the free ligand are observed, thus, no

effects of chelate strain are apparent. It is concluded that the TPP

ligand maintains a high degree of rigidity and distortions about the

iron center are a result of the long metal-nitrogen distances required

by the high spin iron system. It is speculated that the N-Fe-N angles

would be closer to 90° in the low spin case as observed for

bis(hydrotris(pyrazol-1-yl)borate)iron(II) where Fe-N bond lengths on

average are 0.119 Å shorter than in the 3,5-dimethylpyrazolyl

derivative which is high spin under identical conditions of

crystallographic data acquisition (226). The small N1-Fe-N3 angle of

85.9(1)o appears to result from packing effects and corresponds to the

small (113.0(2)o) ring 1 - ring 3 dihedral angle (vs. ring 1 - ring 2;

125.9(2) and ring 2 - ring 3; 120.9(1)o) and the relatively small C11-

P-C13 angle of 100.4(2)o compared to 102.1(2)o (C11-P-C12) and

101.6(2)o (C12-P-C13).

Other major deviations from 90o angles at the iron center

involve O1 (N2-Fe-O1; 93.7(1)o and O1-Fe-O2; 94.3(1)o) and may result

from the participation of this atom in hydrogen bonding. A potential

mirror plane in the molecule is destroyed because of the internal

O4...O1 (2.703(4) Å) hydrogen bond depicted by a dotted line in Figure 5.4.1. Such a mirror plane would restrict the N2-Fe-O3-S and Fe-O3-S-O5 torsional angles to values of 0° where, in fact, the sulphate group is tipped in order to accomodate the intramolecular hydrogen bond such that these torsional angles are 22.7(2)° and 28.28(2)° respectively.

A stereoview of crystal packing is illustrated in Figure 5.4.2. Molecules pack such that the Fe-P vectors are roughly parallel to 1 1 0. The lattice is composed of alternating hydrophobic (at b=1/2) and hydrophilic (at b=0,1) layers parallel to the ac plane. The hydrophilic layer consists of the sulphate-water network through which extensive hydrogen bonding occurs. Interatomic distances and angles pertaining to hydrogen bonding are listed in Table 5.4.3. The lattice water molecule containing O7 is involved in four hydrogen bonds, thus its geometry may be described as tetrahedral, though greatly distorted. The six angles about O7 range from 78.4(1) to 136.7(2)°. Because of the large extent of its involvement in hydrogen bonding, anisotropic temperature factors associated with O7 are small in comparison with those of the other two lattice water molecules. This may indicate some degree of disorder in the case of O8 and O9 each of which is hydrogen bonded to only three other oxygen atoms as outlined in Table 5.4.3. Also, as a result of poor definition of O8 and O9, hygrogen atoms attched to these oxygen atoms could not be reliably located as they were for O7.

The packing in the hydrophobic layer consists of only a single π-π interaction between ring 1 and its equivalent by symmetry about the inversion center at 1/2,1/2,1/2 (3.84(8) Å between planes). It appears

that this interaction is the cause of the distortion in dihedral angles involving ring 1 (1-2; 125.9(2) and 1-3 113.0(2)°) which occurs in order to increase ring overlap. Ring 3 is also available for such an interaction but the long distance (4.076 Å) between it and its symmetry related equivalent about 1/2,1/2,0 precludes its consideration as a contributor to packing energy. Ring 2 is not in a position in which such interactions are possible.

5.4.4 Moessbauer Spectroscopy

A list of Moessbauer parameters for the iron complexes is given in Table 5.4.1 and representative spectra are shown in Figure 5.4.1. The complexes $TPPFe(H_2O)_2SO_4$ and $(ClAuTPP)FeSO_4(H_2O)_2$ give rise to doublets in the room temperature Moessbauer spectrum having isomer shifts of 1.1 mm/sec and quadrupole splittings of 1.6 mm/sec. This is typical of iron(II) in its high spin configuration (231). No spin-crossover was observed upon cooling to 77K.

Moessbauer data for $TPPFeCl_3$ indicate that in this complex, the iron(III) ion is also high spin. For a symmetrically coordinated species, this would give rise to a singlet in the Moessbauer spectrum. As no quadrupole splitting was observed (although the line was somewhat broad ($\Gamma=0.74(9)$ mm/sec)), the complex can be considered octahedral and symmetric in spite of the two types of ligands present.

The FeN_6 complexes $(TPP)_2Fe(ClO_4)_2$ and $(ClAuTPP)_2Fe(ClO_4)_2$ are both low spin at room temperature as they give rise to Moessbauer singlets at isomer shifts of 0.34 mm/sec. These values are similar to that reported for bis[hydrotris(1-pyrazolyl)borate]iron(II) (0.45

Table 5.4.5   Summary of Moessbauer parameters for iron complexes of TPP

Complex	T (K)	δ (mm/sec)[a]	Δ (mm/sec)	Γ (mm/sec)
TPPFe(H$_2$O)$_2$SO$_4$[b]	300	1.102(3)	1.567(6)	0.313(8)
	77	1.197(1)	2.541(2)	0.361(3)
(TPP)$_2$Fe(ClO$_4$)$_2$[b]	300	0.369(3)	–	0.325(9)
	77	0.436(2)	–	0.328(7)
TPPFeCl$_3$	300	0.32(3)	–	0.74(9)

[a] relative to iron foil at 300K

[b] Attempts were made to record spectra for the corresponding (ClAuTPP) iron complexes. Data was collected for several days and a preliminary examination of the weak spectra which resulted indicated parameters comparable to TPP iron complexes.

Figure 5.4.4 Representative Moessbauer spectra for complexes of TPP

$TPPFe(H_2O)_2SO_4$
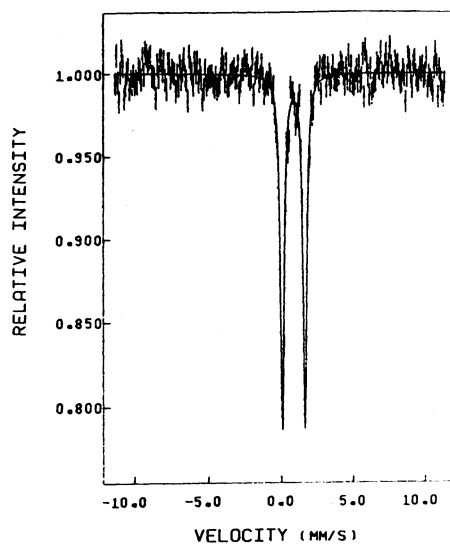
$(TPP)_2Fe(ClO_4)_2$
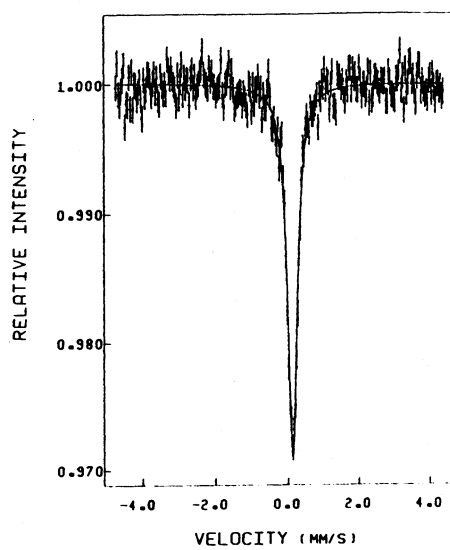
$TPPFeCl_3$
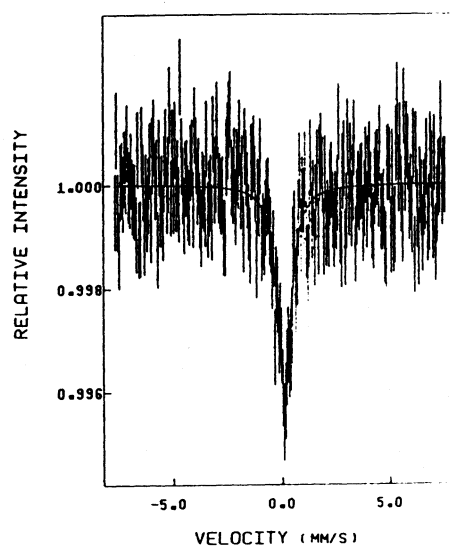
mm/sec) (232) which converts to the high spin species at 398K. It is expected that the bis- complexes of TPP would behave in similar way.

The presence of gold(I) bound at the phosphorus atom appears to have no effect on the Moessbauer parameters of iron after preliminary data treatment.

5.5 Chromium(III) and cobalt(III) complexes

5.5.1 Introduction

The preparations of chromium(III) and cobalt(III) complexes of TPP are combined in this section because of the similar coordinative properties of the metal ions involved. The chromium(III) center has a t_{2g}^3 electronic configuration while the cobalt(III) ion is t_{2g}^6 in its low spin arrangement thus in neither ion is there electron occupation of the e_g^* orbitals. The effect of this is to give rise to compounds which are kinetically inert because of their relatively large ligand field stabilization energies (38) and this introduces certain preparative complications which have been overcome in different ways. In the case of the chromium complexes, trichlorotris(tetrahydrofuran)-chromium(III) was used as the starting material since tetrahydrofuran is weakly coordinated and thus easily substituted by TPP. A different approach was taken for the cobalt(III) complexes where the trinitrito complex was synthesized and used as a precursor to the trichloro compound which formed during the reaction with concentrated HCl outlined in the following scheme.

$(NO_2)_3CoTPP + cHCl \longrightarrow Cl_3CoTPP + HNO_2$
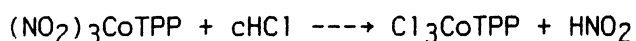
Further reaction of HNO_2 results in the formation of H_2O, NO and NO_2

which drives the reaction to the right.

5.5.2 Preparations

trichloro(tris-2-pyridylphosphine-N,N′,N″-)chromium(III) (TPPCrCl$_3$); A solution containing 0.3759 g of (1 mmol) trichlorotris(tetrahydrofuran) chromium(III) (233) in 30 mL of CH$_2$Cl$_2$ was stirred for 48 hours with 0.269 g (1 mmol) of TPP also dissolved in CH$_2$Cl$_2$. The solution was then filtered and the filtrate evaporated under reduced pressure to yield 0.337 g (79%) of the green solid product which was recrystallized from methanol/ether. Analysis required for C$_{15}$H$_{12}$Cl$_3$CrN$_3$P·3H$_2$O: C; Found: C, 37.1; H, 3.4; N, 8.6; Cl, 21.9%.

trichloro(chloro(tris-2-pyridylphosphine-P-)gold(I)-N,N′,N″-) chromium(III) (ClAuTPP)CrCl$_3$; HAuCl$_4$ (0.1492 g, 0.38 mmol) in 20 mL of water was reduced with 0.076 mL (0.76 mmol) of thiodiglycol added as a 1 mL methanol solution and the mixture stirred for 30 minutes at 0°C. TPPCrCl$_3$ (0.1616 g, 0.38 mmol) was added as a 30 mL methanol suspension and the mixture stirred for 2 hours and then filtered to yield 0.105 g (42%) of the yellow-green solid. Crystals used in the diffraction experiment were grown from DMSO solution and these were also subjected to elemental analysis. Analysis required for C$_{15}$H$_{12}$AuCl$_4$CrN$_3$P·0.1DMSO: C, 27.5; H, 2.1; N, 6.3; Cl, 21.4%. Found: C, 27.7; H, 2.1; N, 6.3; Cl, 21.2%.

trinitrito(tris-2-pyridylphosphine-N,N′,N″-)cobalt(III) (TPPCo(NO$_2$)$_3$); Sodium cobaltinitrite (0.6073 g, 1.5 mmol) was dissolved in 15 mL of water. Upon addition of a solution of 0.3988 g (1.5 mmol) of TPP in 5 mL of methanol an orange solid precipitated. The mixture was heated at

80°C with stirring for 24 hours and filtered to give the 0.548 g of the title compound (79% yield). Recrystallization was accomplished from CH_2Cl_2/hexanes. Analysis required for $C_{15}H_{12}CoN_6O_6P$: C, 39.0; H, 2.6; N, 18.2%. Found: C, 38.8; H, 2.6; N, 17.6%.

trichloro(tris-2-pyridylphosphine-N,N',N"-)cobalt(III) (TPPCoCl$_3$);

$TPPCo(NO_2)_3$ (0.1334 g, 0.29 mmol) was gently heated in 5 mL of conc. HCl for 30 minutes until gas evolution ceased. The resulting mixture consisted of a green precipitate and blue supernatant. The precipitate was filtered and recrystallized from $CHCl_3$/ether to yield 0.03 g of plate-like crystals in fairly low (24%) yield. Analysis required for $C_{15}H_{12}Cl_3Co$: C; 41.8, H; 2.8 N; 9.8, Cl; 24.7%. Found: C; 42.0, H; 2.9, N; 9.9, Cl; 25.1%.

trinitrito(chloro(tris-2-pyridylphosphine-P-)gold(I)-N,N',N"-) cobalt(III) ((ClAuTPP)Co(NO$_2$)$_3$); The procedure used in the preparation of this compound was analogous to that for $TPPCo(NO_2)_3$ with ClAuTPP as the ligand.

trichloro(chloro(tris-2-pyridylphosphine-P-)gold(I)-N,N',N"-) cobalt(III) ((ClAuTPP)CoCl$_3$); Low yields of this compound were obtained by a similar route to that for $TPPCoCl_3$ with use of $(ClAuTPP)CoCl_3$ as the starting material.

Discussion of the syntheses; Attempts to make $TPPCo(NO_2)_3$ <u>via</u> the reaction of 0.2278 g (0.86 mmol) of TPP with a solution containing 0.2503 g (0.86 mmol) of $Co(NO_3)_2 \cdot 6H_2O$ and 0.2622 g (3.8 mmol) of $NaNO_2$ in sodium acetate buffer (0.0691 g NaOH, 0.2074 g acetic acid in 5 mL of water) also yielded the desired product but this appeared to be contaminated with $TPPCo(NO_3)_2$ as a result of incomplete oxidation of

cobalt(II).

Low yields of the trichlorocobalt(III) species were obtained after reaction of the respective compounds with conc. HCl. Evaporation of the blue supernatant produced a blue residue which when taken up in water gave rise to an orange-pink solution. After evaporation of solvent, infrared spectra of the resulting pale orange residue indicated Co(II)-Cl stretches (137). Upon close examination of the crude green precipitate, it was noted that a white material was also present. Other reactions which appear to occur at the same time as the desired reaction are ligand protonation which would result in a white solid and, once this has occured, the reduction of Co(III) to Co(II) by water is imminent (8).

5.5.3 The crystal and molecular structure of (ClAuTPP)CrCl$_3$

Crystal data and information related to data collection are given in Table 5.5.1. Atomic positional parameters and anisotropic temperature factors are listed in Tables 5.5.2 and 5.5.A respectively. Temperature factors for all but Cr, Au, Cl and P were refined isotropically because of their tendency to become non-positive definite. A list of bond lengths and angles is given in Table 5.5.3 and least-squares planes, dihedral and torsional angles are listed in Table 5.5.4. The molecule is illustrated in Figure 5.5.1. The gold atom exists in its typically linear environment (Cl1-Au-P; 178.6(1)o) with Au-Cl (2.268(3) Å) and Au-P (2.222(3) Å) distances similar to those in other ClAuTPP structures (see sections 4.4 and 5.3.4). The octahedral environment of the chromium atom is distorted such that all

Table 5.5.1　　Crystal data for trichloro(chloro(tris-2-pyridylphosphine-P-)gold(I)-N,N′N″-)chromium(III)

Formula	$C_{15}H_{12}AuCl_4CrN_3P \cdot C_6H_{18}O_3S_3$
Formula weight	890.43
Crystal size and shape	$0.097mm^3$ cube
Systematic absences	h0l; h+l=2n
	0k0; k=2n
	00l; l=2n
Space group	$P2_1/n$
Diffractometer	P3
Temperature	-100^oC
Unit cell parameters	a=9.726(2)Å　　　　β=114.35(1)^o
	b=19.414(3)Å　　　　V=3116.1 Å^3
	c=18.114(3)Å　　　　Z=4
ρ_{calc}	$1.90gcm^{-1}$
Range of **hkl**	$0<h<10, 0<k<20, -19<l<17$
Maximum 2θ	45°
Number of reflcns measured	4233
Number of independent reflcns	4103
Standard reflcns(e.s.d)	0 5 2 (1.6%), 0 3 -3 (1.9%)
R_{int}	0.0087
Final R,Rw	0.0820, 0.0605
Final shift/error max(ave)	0.153(0.019)
Error in obs of unit weight	S=1.1688
Highest peak, lowest valley	$1.4eÅ^{-3}, -1.3eÅ^{-3}$
Weighting	$w=(\sigma^2(F) + 0.0004F^2)^{-1}$
F(000)	1735.0
Linear Absorption coefficient	$\mu=58.29cm^{-1}$
Absorption Coefficient limits	$1.42<A^*<1.95^*$
Number of Variables	184

* absorption correction was not applied introducing a maximum error in Fo of ≅8%.

Table 5.5.2 Positional parameters (x10⁴) and U_{eq} (x10⁴) for trichloro(chloro(tris-2-pyridylphosphine-P)gold(I))-N,N',N")chromium(III).

Atom	x	y	z	U_{eq}
Au	2964.9(6)	9758.2(3)	4684.8(3)	211
Cl1	3521(4)	10310(1)	5877(1)	322
P	2458(3)	9235(1)	3509(1)	182
Cr	1725(2)	8424(0)	1731(1)	144
Cl2	3552(3)	8314(1)	1232(1)	240
Cl3	-97(3)	8780(1)	511(1)	237
Cl4	953(3)	7288(1)	1457(1)	216
C11	554(13)	8894(6)	3000(6)	71
C21	-510(12)	8992(5)	3321(6)	64
C31	-1907(13)	8729(6)	2940(7)	86
C41	-2263(13)	8381(6)	2222(7)	90
C51	-1213(13)	8313(6)	1904(6)	78
N1	211(10)	8566(4)	2284(5)	65
C12	3590(12)	8472(5)	3572(6)	44
C22	4627(13)	8245(6)	4344(6)	80
C32	5409(13)	7637(6)	4387(6)	81
C42	5152(13)	7293(6)	3669(7)	91
C52	4142(13)	7553(6)	2935(7)	87
N2	3332(9)	8137(4)	2885(5)	53
C13	2618(11)	9771(6)	2724(6)	57
C23	2959(13)	10460(6)	2875(6)	86
C33	3039(13)	10855(6)	2243(7)	95
C43	2821(14)	10556(6)	1521(7)	103
C53	2487(13)	9862(6)	1425(6)	82
N3	2370(10)	9456(4)	2004(5)	66
S1	6749(3)	5188(1)	3390(2)	111
O1	6268(10)	5883(5)	3019(5)	163
C1	7255(15)	5288(7)	4451(7)	136
C2	8627(16)	5049(6)	3488(8)	137
S2	5811(3)	8055(1)	9942(2)	104
O2	5769(10)	8817(4)	9783(5)	134
C3	3953(14)	7732(6)	9399(7)	111
C4	6632(17)	7651(7)	9345(9)	171
S3	873(4)	9030(1)	5932(2)	133
O3	790(11)	8776(5)	5131(6)	198
C5	-501(17)	8559(7)	6120(9)	173
C6	2535(17)	8620(8)	6673(9)	184

$U_{eq}=1/3(U_{11}+U_{22}+U_{33}+2U_{13}Cos\beta)$

Table 5.5.2 continued

Hydrogen positional parameters ($\times 10^4$)

Atom	x	y	z
H21	-46	9272	3842
H31	-2788	8527	3225
H41	-3292	8251	1814
H51	-1820	8175	1226
H22	4865	8585	4910
H32	6124	7417	5007
H42	5367	6840	3596
H52	3996	7275	2407
H23	3226	10601	3439
H33	3342	11295	2397
H43	2740	10836	967
H53	2373	9627	993

Hydrogen atom positions were calculated and fixed with isotropic temperature factors of 0.06 $\mathring{A}^2$

Table 5.5.3   Bond Lengths (Å) and Angles (o) for trichloro(tris-2-
pyridylphosphine-P-)gold(I)-N,N',N"-)chromium(III).

Au-Cl1	2.268(3)	Au-P	2.222(3)	Cr-Cl2	2.313(3)
Cr-Cl3	2.295(3)	Cr-Cl4	2.317(3)	Cr-N1	2.113(9)
Cr-N2	·2.105(9)	Cr-N3	2.096(9)		
P-Cl1	1.82(1)	P-Cl2	1.82(1)	P-Cl3	1.82(1)
Cl1-C21	1.39(2)	Cl2-C22	1.41(2)	Cl3-C23	1.38(2)
C21-C31	1.35(2)	C22-C32	1.39(2)	C23-C33	1.41(2)
C31-C41	1.38(2)	C32-C42	1.39(2)	C33-C43	1.37(2)
C41-C51	1.37(2)	C42-C52	1.38(2)	C43-C53	1.38(2)
C51-N1	1.36(1)	C52-N2	1.36(1)	C53-N3	1.36(1)
N1-Cl1	1.36(1)	N2-Cl2	1.33(1)	N3-Cl3	1.37(1)
S1-O1	1.49(1)	S2-O2	1.504(9)	S3-O3	1.50(1)
S1-C1	1.79(1)	S2-C3	1.78(1)	S3-C5	1.77(2)
S1-C2	1.78(1)	S2-C4	1.77(2)	S3-C6	1.81(2)
Cl1-Au-P	178.6(1)	Cl2-Cr-Cl3	93.7(1)	Cl2-Cr-Cl4	93.5(1)
Cl3-Cr-Cl4	91.5(1)	N1-Cr-Cl2	174.7(3)	N1-Cr-Cl3	90.3(3)
N1-Cr-Cl4	89.9(3)	N2-Cr-Cl2	89.3(3)	N2-Cr-Cl3	176.4(3)
N2-Cr-Cl4	90.1(3)	N3-Cr-Cl2	88.7(3)	N3-Cr-Cl3	88.7(3)
N3-Cr-Cl4	177.7(3)	N1-Cr-N2	86.6(3)	N1-Cr-N3	87.9(4)
N2-Cr-N3	89.5(3)				
Au-P-Cl1	115.4(4)	Au-P-Cl2	114.9(4)	Au-P-Cl3	115.5(4)
Cl1-P-Cl2	101.4(5)	Cl1-P-Cl3	102.1(5)	Cl2-P-Cl3	105.7(5)
P-Cl1-C21	121.0(9)	P-Cl2-C22	118.8(8)	P-Cl3-C23	119.3(8)
Cl1-C21-C31	120(1)	Cl2-C22-C32	118(1)	Cl3-C23-C33	117(1)
C21-C31-C41	119(1)	C22-C32-C42	118(1)	C23-C33-C43	121(1)
C31-C41-C51	120(1)	C32-C42-C52	121(1)	C33-C43-C53	118(1)
C41-C51-N1	122(1)	C42-C52-N2	122(1)	C43-C53-N3	124(1)
C51-N1-Cr	118.5(7)	C52-N2-Cr	117.3(7)	C53-N3-Cr	119.1(8)
C51-N1-Cl1	117(1)	C52-N2-Cl2	117.6(9)	C53-N3-Cl3	116(1)
Cr-N1-Cl1	124.7(8)	Cr-N2-Cl2	125.0(7)	Cr-N3-Cl3	124.8(8)
N1-Cl1-C21	122(1)	N2-Cl2-C22	124(1)	N3-Cl3-C23	124(1)
N1-Cl1-P	116.9(8)	N2-Cl2-P	117.5(8)	N3-Cl3-P	116.8(8)
O1-S1-C1	106.5(6)	O2-S2-C3	107.5(6)	O3-S3-C5	105.9(7)
O1-S1-C2	107.4(6)	O2-S2-C4	107.5(6)	O3-S3-C6	104.4(7)
O1-S1-C2	95.4(6)	C3-S2-C4	96.7(7)	C5-S3-C6	98.4(7)

Table 5.5.4   Best planes, dihedral and torsional angles for
trichloro(chloro(tris-2-pyridylphosphine-P-gold(I))-
N,N′,N″-)chromium(III)

Plane	Distance of atom from the plane (Å)
1.Cl1,C21,C31,C41,C51,N1	Cl1;-0.02(2),C21;0.01(2),C31;-0.00(2), C41;-0.01(2),C51;0.01(2),N1;0.00(1)
2.Cl2,C22,C32,C42,C52,N2	C12;0.00(1),C22;0.01(2),C32;-0.01(2), C42;0.00(2),C52;0.02(2),N2;0.01(1)
3.C13,C23,C33,C43,C53,N3	C13;0.00(1),C23;0.01(2),C33;-0.01(2), C43;0.01(2),C53;0.00(2),N3;-0.00(1)
4.N1,N2,C12,C13	N1;0.03(1),N2;-0.03(1),C12;0.003(5), O3;-0.003(5),Cr;-0.049(4)
5.N1,N3,C12,C14	N1;0.06(1),N3;-0.07(1),C12;0.006(5), C14;-0.006(5),Cr;-0.043(4)
6.N2,N3,C13,C14	N2;0.01(1),N3;-0.02(1),C13;0.002(5), C14;-0.002(5),Cr;0.052(4)
7.Cl1,C12,C13	P;0.777(8)

Dihedral angles (°)

1 - 2	114.7(4)	1 - 3	116.5(4)	2 - 3	128.8(4)	1 - 4	133.8(3)
2 - 4	130.9(3)	3 - 4	93.4(3)	1 - 5	136.7(3)	2 - 5	92.6(3)
3 - 5	132.6(3)	4 - 5	90.5(2)	1 - 6	90.3(3)	2 - 6	137.9(3)
3 - 6	135.9(3)	4 - 6	89.0(2)	5 - 6	88.8(2)	1 - 7	91.1(4)
2 - 7	89.4(5)	3 - 7	87.7(5)	4 - 7	126.4(4)	5 - 7	126.2(4)
6 - 7	124.3(4)						

Torsional angles (°)

Cl1-Au-P-Cl1	-147.0(3)	Au-P-Cl1-N1	-178.5(4)
Cl1-Au-P-C12	95.5(3)	Au-P-C12-N2	179.2(4)
Cl1-Au-P-C13	27.5(3)	Au-P-C13-N3	177.3(4)
P-Cl1-N1-Cr	-1.0(4)	Cl1-N1-Cr-Cl2	5.4(4)
P-C12-N2-Cr	1.4(4)	C12-N2-Cr-C13	29.1(4)
P-C13-N3-Cr	3.3(4)	C13-N3-Cr-C14	17.7(4)

Figure 5.5.1 A molecule of trichloro(chloro(tris-2-pyridyl-phosphine-P-gold(I)-N,N',N"-)chromium(III)
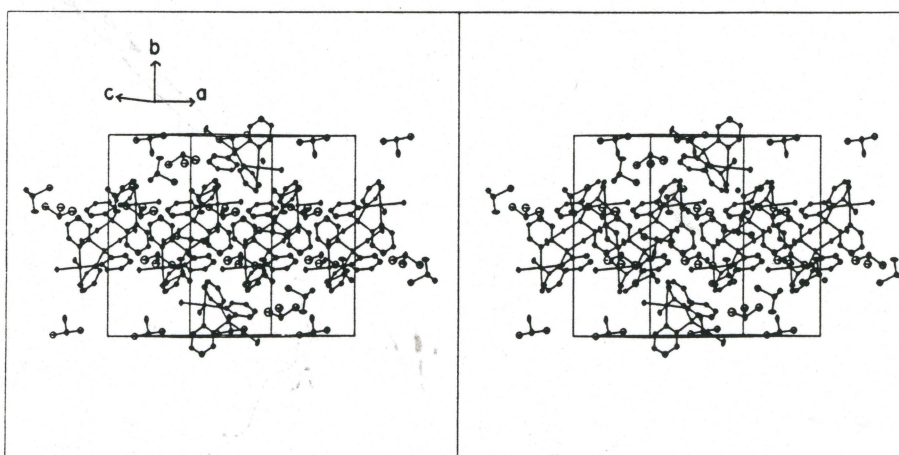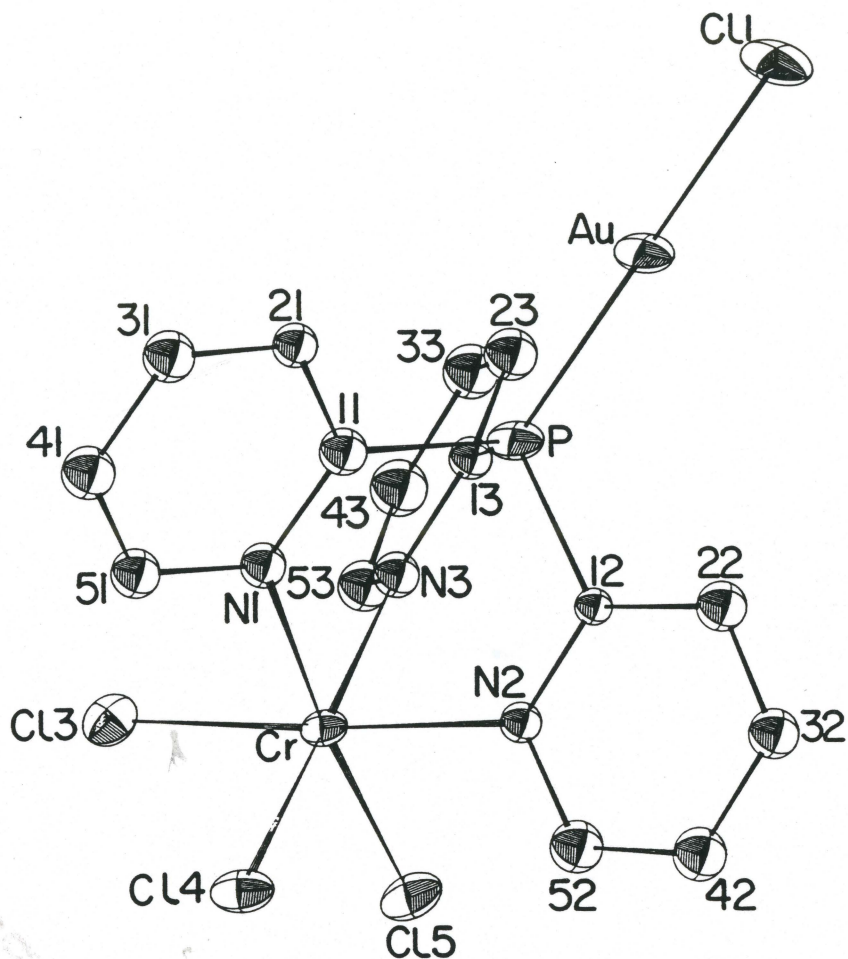
Figure 5.5.2 A stereoview of the packing in the unit cell

N-Cr-N angles are less than 90° (N1-Cr-N2; 86.6(3), N1-Cr-N3; 87.9(4) and N2-Cr-N3; 89.5(3)°) and all Cl-Cr-Cl angles are greater than 90° (Cl2-Cr-Cl3; 93.7(1), Cl2-Cr-Cl4; 93.5(1) and Cl3-Cr-Cl4; 91.5(1)°).

Cr-N distances (Cr-N1; 2.113(9), Cr-N2; 2.105(9) and Cr-N3; 2.096(9) Å) are longer than Cr-N(pyrazole) lengths reported in the structure of dichloro(hydrotris(1-pyrazolyl)borato)pyridine chromium(III) (2.043(3), 2.065(3) and 2.060(3) Å) but are similar to the Cr-N(pyridine) distance (2.108(3) Å) of the same structure (234). Cr-Cl bond lengths (2.313(3), 2.295(3) and 2.317(3) Å) are also similar to the above previously reported structure (2.312(1) and 2.311(1) Å) as well as to those reported for mer-trichloro(dimethylformamide)(1,10-phenanthrolene)chromium(III) (235) and fac-trichloro (diethylenetriamine)chromium(III) (236). The formation of a facial isomer involving coordination of three pyridine molecules is made possible by their bond to phosphorus. Only the meridional isomer of trichlorotris(pyridine)chromium(III) is known and attempts to react this with boiling pyridine fail to produce the tetrakis(pyridine) complex (237).

Dihedral angles between rings give an indication as to deviation from C_{3v} symmetry in that the ring 2 - ring 3 dihedral angle is large (128.8(4)°) where the others are small (1 - 2; 114.7(4), 1 - 3; 116.5(4)°). The apparent twisting of rings 2 and 3 away from each other is also evidenced by the distance of the chromium atom from these planes (Cr-ring 2; 0.16(1), Cr-ring 3; 0.12(1) Å) where chromium lies much closer to the ring 1 plane (0.03(1) Å). As well, the torsional angle involving ring 1 is close to 0° (Cl2-Cr-N1-Cl1;

5.37(4)°) while the Cl3-Cr-N2-Cl2 (29.0(4)°) and Cl4-Cr-N3-Cl3

(17.7(4)°) angles are much larger. Furthermore, the N2-Cr-N3 angle is

the largest of the three though it is still less than 90° (89.5(3)°).

Such a ring twist does not appear to be a result of any intramolecular

effects and may be caused by crystal packing.

A stereoview of the packing is shown in Figure 5.5.2.

Molecules pack such that their approximate C_3 axes are aligned with [1

2 1] and [0 2 1] and their octahedral axes are aligned approximately

with **b** and the two **ac** diagonals. The chromium octahedra form layers

about **b**=1/4 and 3/4 while the gold centers are located at **b**=0 and 1/2.

Molecules are arranged in pairs positioned about inversion centers at

1/2,0,1/2 and 0,1/2,0 such that the chlorine atom of each P-Au-Cl axis

lies between rings 2 and 3 of the other molecule of the pair. Although

this stacking brings gold atoms together, the distance between them is

(3.759(3) Å) longer than the sum of van der Waals radii, therefore no

attractive intermolecular interaction is indicated. The closest

approaches of the chlorine atom to the rings are 3.19(1) Å (Cl1···ring

2) and 3.31(1) Å (Cl1···ring 3) and the effect of this packing

arrangement appears to be the cause of the larger ring 2 - ring 3

dihedral angle. Otherwise, packing in the structure may be described

as featureless and the source of lattice energy is solely van der Waals

forces. The presence of twelve molecules of dimethylsulphoxide in the

unit cell is likely disruptive to any π-π interaction which may

otherwise have resulted.

CHAPTER 6

SUMMARY OF STRUCTURAL AND INFRARED DATA FOR TPP AND ITS COMPLEXES

6.1 Summary of structural data

A summary of salient features obtained from crystallographic determinations of the structures of TPP and its complexes is given in Tables 6.1a and 6.1b. With such information it is possible to establish trends in the effects of P- and N-metal binding on the ligand itself.

Length of the P-C bond is immune to metal binding at either the N- or the P- donor site.

C-P-C angles (although their values are, to some extent, determined by packing effects in individual structures) are generally smaller in the free ligand and N-bound complexes but widen slightly when gold(I) binds to the phosphorus atom. A better indication of this angle widening comes from comparison of distances of the phosphorus atom from the C11-C12-C13 plane (see Figure 4.3.1). In cases where the phosphorus atom is not involved in coordination, these distances are relatively large (0.832(6) Å (ave.)) and decrease to 0.74(2) Å (ave.) when gold(I) binds. This has been explained as a result of removal of sterically demanding lone pair electron density from phosphorus, in turn reducing the effects of lone pair - pyridyl ring repulsions.

A more subtle change which occurs in accordance with the above observation is the fact that N-C1-P angles are consistently larger than 120° (and P-C1-C2 angles are consistently smaller than 120°) in the N-bound complexes TPPZn(H_2O)$_3$, TPPFe(H_2O)$_2SO_4$ and TPPCu(NO_3)$_2$ but

Table 6.1a A summary of structural parameters involving the phosphorus
atom for TPP and its complexes

Complex[a]	P-C(Å)	C-P-C(o)	P-(CCC)	P-C1-N(o)	P-C1-C2(o)	P-M(Å)
TPP	1.832(2)	101.4(1)	0.822(2)	119.9(2)	116.5(2)	-
	1.844(2)	100.6(1)		120.2(2)	116.7(2)	
	1.835(3)	102.5(1)		111.3(2)	117.4(2)	
TPPZn	1.839(4)	98.5(2)	0.828(3)	120.3(3)	117.8(3)	3.438(1)
	1.844(4)	102.6(2)		120.6(3)	117.3(3)	
	1.847(4)	102.9(2)		120.8(3)	116.9(3)	
TPPCu	1.835(5)	105.8(3)	0.849(4)	121.8(5)	117.1(5)	3.336(1)
	1.842(5)	97.6(3)		121.3(3)	116.9(6)	
	1.851(7)	97.8(2)		120.6(4)	117.7(5)	
TPPFe	1.834(4)	102.1(2)	0.827(2)	120.7(3)	118.0(3)	3.481(1)
	1.840(4)	101.6(2)		121.5(2)	116.7(3)	
	1.838(4)	100.4(2)		120.2(3)	118.3(3)	
AuTPP	1.84(1)	103.9(6)	0.73(1)	119(1)	118(1)	-
(A)	1.84(2)	106.3(8)		112(1)	121(1)	
	1.82(2)	105.3(6)		114(1)	124(1)	
	1.86(1)	102.1(7)	0.72(1)	109(1)	124(1)	-
(A′)	1.84(2)	110.7(8)		114(1)	120(1)	
	1.86(2)	105.0(7)		120(1)	115(2)	
	1.834(6)	103.6(3)	0.726(3)	120.0(4)	115.8(5)	-
(B)	1.820(6)	105.9(3)		116.5(5)	120.6(5)	
	1.821(6)	106.5(3)		114.3(4)	122.2(5)	
AuTPPCr	1.82(1)	101.4(5)	0.777(8)	116.9(8)	121.0(9)	3.386(3)
	1.82(1)	102.1(5)		117.5(8)	118.8(8)	
	1.82(1)	105.7(5)		116.8(8)	119.3(8)	
(AuTPP)$_2$Cu	1.82(2)	103.0(6)	0.74(1)	116(1)	119(1)	3.321(3)
(A)	1.81(1)	106.7(6)		117.5(9)	121.3(9)	
	1.84(1)	104.7(6)			117.9(9)	
	1.82(1)	104.2(6)	0.75(1)	118.9(9)	119.7(9)	3.353(3)
(B)	1.84(2)	103.9(7)		119(1)	119(1)	
	1.81(2)	103.9(7)			121(1)	

[a] Complex codes have been abbreviated such that they do not include
the other ligands in the respective metal coordination spheres.

Table 6.1b A summary of structural parameters involving the pyridyl
rings for TPP and its complexes

Complex[a]	ring-ring	N-C5(Å)	N-C1(Å)	M-N	M-N-C5(o)	M-N-C1(o)
TPP	97.0(1)	1.330(3)	1.346(3)	-	-	-
	97.4(1)	1.341(3)	1.335(3)	-	-	-
	91.8(1)	1.331(3)	1.343(3)	-	-	-
TPPZn	108.3(1)	1.341(5)	1.358(5)	2.153(3)	120.0(3)	122.1(2)
	123.0(2)	1.340(5)	1.352(5)	2.164(3)	119.9(3)	121.7(3)
	128.5(2)	1.341(5)	1.351(5)	2.126(3)	119.6(3)	122.3(3)
TPPCu	137.7(2)	1.335(6)	1.352(9)	2.034(3)	121.5(5)	119.5(3)
	113.1(2)	1.353(7)	1.345(9)	2.109(3)	122.5(5)	119.0(3)
	108.8(2)	1.340(8)	1.351(9)	2.069(3)	122.0(5)	120.1(4)
TPPFe	125.9(2)	1.332(6)	1.348(5)	2.184(3)	119.1(3)	122.8(2)
	113.0(2)	1.340(5)	1.354(4)	2.174(3)	119.9(2)	122.0(2)
	120.9(1)	1.345(4)	1.340(5)	2.172(3)	118.6(3)	123.5(2)
AuTPP	124.4(8)	1.32(2)	1.30(3)	-	-	-
(A)	122.0(7)	1.39(2)	1.30(2)	-	-	-
	134.7(6)	1.36(3)	1.31(2)	-	-	-
	103.4(7)	1.35(2)	1.32(2)	-	-	-
(A′)	157.0(9)	1.36(3)	1.34(2)	-	-	-
	100.0(8)	1.32(3)	1.32(3)	-	-	-
	100.6(3)	1.36(1)	1.324(8)	-	-	-
(B)	105.3(3)	1.34(1)	1.333(8)	-	-	-
	113.7(3)	1.343(9)	1.321(7)	-	-	-
AuTPPCr	114.7(4)	1.36(1)	1.36(1)	2.113(9)	118.5(7)	124.7(8)
	116.5(4)	1.36(1)	1.33(1)	2.105(9)	117.3(7)	125.0(7)
	128.8(4)	1.36(1)	1.37(1)	2.096(9)	119.1(8)	124.8(8)
(AuTPP)$_2$Cu	110.6(6)	1.36(2)	1.32(1)	2.31(1)	121.0(8)	121(1)
(A)	127.4(6)	1.34(2)	1.38(2)	2.08(1)	119.5(9)	122.0(9)
	121.8(6)	1.34(2)	1.32(1)	2.061(9)	118.4(7)	122.6(9)
(B)	126.0(6)	1.35(2)	1.35(2)	2.04(1)	118.2(8)	123.5(8)
	118.0(6)	1.36(3)	1.32(2)	2.16(1)	118.6(9)	122(1)
	115.7(7)	1.34(2)	1.33(2)	2.24(1)	120.5(9)	123.0(9)

[a] Complex codes have been abbreviated such that they do not include
the other ligands in the respective metal coordination spheres.

decrease to values less than 120° in those structures where the

phosphorus atom is also involved in coordination (ClAuTPP)CrCl$_3$ and

(ClAuTPP)$_2$Cu). This is the expected result if the ligand framework is

shifted toward the phosphorus atom.

M-N-C5 angles are generally smaller than corresponding M-N-C1

angles in the complexes TPPZn(H$_2$O)$_3$, TPPFe(H$_2$O)$_2$SO$_4$, (ClAuTPP)CrCl$_3$ and

(ClAuTPP)$_2$Cu but this is reversed in the case of TPPCu(NO$_3$)$_2$. Two

factors appear to be relevant to this trend. The first has to do with

the presence of gold for the reasons explained above. The decrease in

P-CCC plane distance is concomitant with a shift of the pyridyl rings

towards the phosphorus atom. Because the metal ion is restricted in

its motion in the same direction because of repulsion by the phosphorus

atom, a change occurs in M-N-C angles. The second factor influencing

these angles is the M-N distance. In complexes with no

P-gold bonding, M-N-C5 angles are smaller than M-N-C1 angles, with

relatively long M-N bonds (2.148(5) Å (ave.) for the zinc complex and

2.177(5) Å (ave.) for the iron complex) whereas the opposite is true in

TPPCu(NO$_3$)$_2$ which has relatively shorter (2.071(5) Å (ave.)) M-N

distances. Thus the metal ion, depending on its size, appears to sit

in the same place under the phosphorus atom while slight changes in

ligand geometry occur around it. M-P distances are comparable to the

sum of van der Waals radii in every case and thus, seems not to be

factor in determining complex geometry.

An obvious change in ring - ring dihedral angles occurs as a

result of metal binding at the nitrogen sites. Dihedral angles in TPP

and ClAuTPP, where pyridyl rings are free, deviate most from 120°,

their values being subject solely to packing effects. Although still subject to packing effects, ring - ring dihedral angles in N-bound complexes are closer to 120°. An examination of cone angles (238) about the phosphorus atom for free and N-bound complexes suggests that the steric requirements of the ligand decrease slightly when metal ions are incorporated and rings are restricted by N-binding.

Changes in N-C1 vs. N-C5 bond lengths and C5-N-C1 angles upon metal binding to nitrogen sites are too small to be considered significant. Thus the effect of metal binding within the pyridine groups is negligible.

6.2 Summary of infrared results

A listing of infrared peaks and their assignments is given in Table 6.2. Spectral assignments were facilitated by previous vibrational analyses of pyridine, 2-substituted pyridines (239-242), as well as those on triphenyl compounds of group VA elements (156,157). Infrared spectra of TPP will be discussed in some detail with reference to these studies as well as observed changes in the spectra as a result of metal binding.

6.2.1 Infrared spectra of tris-2-pyridylphosphine

Infrared spectra of tris-2-pyridyl phosphine have been assigned according to work done by Wilson et al. (239) on pyridine in combination with Whiffen's (155) analysis of substituted benzenes. The notation developed by Whiffen (155) for substituted benzenes will be used for band assignment of pyridine ring modes.

Like spectra reported for 2-alkylpyridines, two bands are

Table 6.2 Summary of infrared data for complexes of tris-2-pyridylphosphine

L	LAu	CuL[a]	CuL$_2$[a]	Cu(LAu)$_2$[a]	ZnL[a]	ZnL$_2$[b]	Zn(LAu)$_2$[a]	FeL[c]	FeL$_2$[b]	Fe(LAu)[c]	Fe(LAu)$_2$[c]	FeL[d]	CoL[d]	Co(LAu)[d]	CrL[d]	Cr(LAu)[d]	assgmt
					3450br		3400br			3370br							υO-H
3050m	3040m	3110w	3090w	3090w	3090sh	3090m	3060w			3090m	3070m	3090w	3115m	3110w	3100w	3100m	υ CH
2985w	2980w	3090w	3050w	3040m					3040w			3070w	3075m	3070w	3070w	3072m	"
		3010vw	3005w	3000w		2990w	2990w		2985w		3000w				2960w	2952m	"
															2920w	2917m	
		2425m															nitrate overtones
		2385m															
1970vw	1975w																
1870w	1870w																
		1762w															nitrate combinations
		1729m															
		1703w	1765sp	1770sp	1769sp												
1670w	1660vw	1635m	1633m	1626m	1640s	1635w	1640s	1640s	1595m	1638m	1630m		1620m	1640m	1630w	1627w	δCH comb i+f[e]
		1610w															
		1603w															
1575s	1572s	1581s	1580s	1583s	1582s	1584s	1587s	1582s	1573m	1584s	1583s	1585s	1590s	1585s	1590s	1588s	υCC in plane
1565sh	1565s	1565w	1562m	1571sh	1579w	1561m		1562m	1560m	1565sh			1558w	1565w	1564w	1584w	"
1560s	1560s		1560w	1562w													"
		1473s															υ NO asym
1456s	1459s	1454s	1454s	1458s	1460s	1461s	1460s	1460s	1463s	1467m	1451s	1452s	1460s	1452s	1455m	1461s	υCC in plane
1452s	1450s																"
		1445sh															"
1429s	1422s	1428sh	1421sh	1423sh	1430s	1430s	1428s	1430s	1428m	1437s	1422s	1423s	1431s	1428s	1421s	1422s	"
1418s																	
1386m	1383m					1386m						1400m			1384m	1387m	
		1375vs	1380vs	1381vs	1380vs		1382vs										υ3N-O2bend
1286m	1284m	1286m	1280m	1287m,br	1280m	1280m	1290m	1290m	1280m		1283m	1274s	1282s	1280s	1278m	1282m	YCH + υNO sym
1279m	1280m								1270m								
1275sh	1275m	1272m													1261w		
1230w	1230w	1235m	1230w	1244w	1236m	1234m		1230m	1232m			1240w	1228m	1229w	1232w	1235w	
											1179m						
1161m	1154m	1169m	1165sh	1162m,br	1165m	1160m	1160m		1160m	1160m		1160m	1170m	1167m	1162m		YCH
1155s		1164m	1159m														"
1148s		1150sh															"
1119w	1123m	1112w	1115w	1132m	1123w		1130m			1132m		1115w	1129w	1134m	1120w	1135m	υP-C
									1110vs		1090vs						υSO4
						1090s			1085vs		1082vs						υClO4
1083m	1084m	1096sh	1095sh	1092m	1092m		1089m					1088m	1094m	1090m	1089m	1093m	P-C
		1089m	1087m														
1046s	1045m	1057m	1057m	1058m	1056m		1059m	1065m		1051m		1056m	1060m	1052m	1056m	1061m	Y CH
		1049m							1050m								
1009w																	
		1021sh	1011m	1018													υNO

Table 6.2 continued

L	LAu	CuL[a]	CuL_2[a]	$Cu(LAu)_2$[a]	ZnL[a]	ZnL_2[b]	$Zn(LAu)_2$[a]	FeL[c]	FeL_2[b]	Fe(LAu)[c]	$Fe(LAu)_2$[c]	FeL[d]	CoL[d]	Co(LAu)[d]	CrL[d]	Cr(LAu)[d]	assgmt
989s	988s	1009s	995m	1004	1011s	1011s	1012s	1010m	1011m	1008m	1010m	1009s	1019m	1011s	1022s	1018s	ring breath.
984s			985sh	986			982w	989m	982m	995w	985m						"
958m		969w	965w		960w												
904m	900w	900w	890w	899w	905w			900w		910w			894w	895w	900w		
892m																	
		837m	832w	819w	835w		828m										ν_2 NO3
		823s	825m	811m	821m												
770s	774s	762s	767s	760s	769s	770s	771s	769s	761s	778s	765s	767s	785m	767s	770s	771s	γ CH f-vib
761s	760s	764sh											769s		765sh		
743s	738s	747m	756m		746m	755m	740m	748m	740m	745m	750w	750w			745m		γ CH r-vib
739s	732s											740w			740m	738m	
		727m,sp															
719w	721m	707w	705w	704w	709w	709w	719m	712w	719m	720m	727s	709w	720m	729m	716w		v-vib
708w	712w													719m			"
613m	612m	627m	638w	635w	633m	640m	639m	640m				631w	642w	631m	642m	638m	s-vib
						620s	631m										ClO4
	552s		620w	622w				610m	618m	610w	616m	625w					
				547vs	550w	550m	559s	549m	549w	561s	570m		552w	572s	574s		
				537sh							549s			561s			
515s	511s	506s	510s	519s	515s	515s	520s	510s	516m	520s	518s	514s	519s	519s	515s	523s	y-vib
506s	505s	490m	490m	501m	500m				500sh								"
498s																	"
432s	462m	434m	434m	444m	460w,br	440m	460w	462m,br	455m	462m,br	465m	442s	465s	462m	457m		t-vib
427s	426m												446s				
409sh	399m	417m	416w	408w	412s	425m	410m	421m		411m	390m	423m		409m	424w	431m	w-vib
404m	393m														420w		"
396m																	
												368m	368m	348s	345s		νCr-Cl
												342m	349m	334s	334s		
	329s			340m						335m	330m				329m	360s	νAu-Cl
	320s			330m													
		310s															νM-O
			301w	308m									300m	297m	296sh	306w	νM-N
												299s					νFe-Cl
												280s					"
293w	278m	289sh	294w	288m		282s	291s	278m		288m	269w				291m	296s	x-vib
270s	258m	281m	282		274w	278s	262w									276m	
258m	250w	260w					253m								262m	263w	
248s	232w	238w			250m	237m	241w	233m						255m		255m	νM-N
		216m															δN-M-O
205m	215w	200m	210vw	208vw		194vs	187m								218s	212m	u-vib

Table 6.2 continued

L	LAu	CuL[a]	CuL$_2$[a]	Cu(LAu)$_2$[a]	ZnL[a]	ZnL$_2$[b]	Zn(LAu)$_2$[a]	FeL[c]	FeL$_2$[b]	Fe(LAu)[c]	Fe(LAu)$_2$[c]	FeL[d]	CoL[d]	Co(LAu)[d]	CrL[d]	Cr(LAu)[d]	assgmt
197m	197w			195m											212sh		"
						180s	180s										υZn-N
						165s	165s										
															172sh	169m	δCl-Cr-Cl
		169w													165s	162m	
		148m		154m													
		131sh															
	115m																

L=tris-2-pyridylphosphine (TPP)

abbreviations: s=strong, m=medium, w=weak, v=very, sh=shoulder, sp=sharp

[a] nitrate salts

[b] perchlorate salts

[c] sulphate complex

[d] chloride complexes

[e] alphabetical labels refer to modes assigned by Whiffen (155) for substituted benzenes

observed in the νCH region of TPP at 3050 and 2985 cm^{-1}. Cook and Church (241) have shown that alkyl substituted pyridines have characteristic absorption bands in the 2000-1650 cm^{-1} region attributed to overtone absorptions which depend on substituent location on the aromatic ring. Bands reported for 2-alkylpyridines are located at 1960 and 1755 cm^{-1} and compare with those for TPP which occur at 1970 and 1870 cm^{-1}. A weak, broad absorption at 1670 cm^{-1} has been assigned to a combination of modes i at 904 and 892 cm^{-1} and f at 770 and 761 cm^{-1}. Similar assignments have been made for the spectra of triphenylarsine (156).

Pyridine shows four bands in the 1650-1350 cm^{-1} region attributable to ring stretches l, m, n and o. Shifts in the frequencies of these bands from those observed in pyridine (1580 cm^{-1}) (243) depend on the nature of the substituent. Katritzky and Hands (240) report bands at 1586 and 1573 cm^{-1} in 2-chloro and 2-bromopyridine respectively and attribute the shift to heavy atom effects. They also observe shifts to lower frequency as electron acceptor quality of the substituent is increased. With strong electron acceptors, the intensity of the peaks decrease. Since the 1575 cm^{-1} peak in the spectrum of TPP is relatively strong, any indication of the ability of phosphorus to act as an electron acceptor is not conveyed and the observed shift is probably a result of substituent mass. The other peaks in this region are at the low end of frequency ranges defined by spectra of 2-substituted pyridines (240) (1560-1575 cm^{-1} vs. 1565 and 1560 cm^{-1} for TPP, 1460-1480 cm^{-1} vs. 1456 and 1452 cm^{-1} for TPP and 1425-1440 cm^{-1} vs. 1429, 1422, and 1418 cm^{-1} for TPP). The

peak multiplicity observed in spectra of TPP arises from lattice effects which lower its potential C_{3v} symmetry.

Four bands attributable to βCH modes are expected in the 1300-1000 cm^{-1} region for monosubstituted pyridines. In TPP these are located at 1286 and 1279 cm^{-1}, 1230 cm^{-1}, 1161, 1155 and 1148 cm^{-1} and 1083 cm^{-1}. An additional weak band at 1119 cm^{-1} has been tentatively assigned as the q-vibration and is one of the six modes described by Whiffen (155) as having some P-pyridine component.

The symmetric ring breathing mode absorbs at 989 cm^{-1} in agreement with frequencies reported for other 2-substituted pyridines (994 ± 4) (240).

The intensities of bands attributed to the j, i and f out-of-plane CH bending modes correspond to those reported for halobenzenes. The f mode in particular is expected to give very strong absorption in the infrared and its frequency (770 cm^{-1}) is within range of similar bands observed in 2-substituted pyridines (780-740 cm^{-1}). Bands at 743 and 739 cm^{-1} are assigned to the r-vibration and contain a contribution from P-pyridine stretching. This band is considerably shifted in frequency from its position in triphenylphosphine (688 and 680 cm^{-1}). Other vibrations in the 800-400 cm^{-1} region are assigned as the v and w vibrations (out-of-plane ring deformation) located at 719, 708 cm^{-1} and 409, 404, 398 cm^{-1} respectively and the s-vibration (in-plane ring deformation) at 613 cm^{-1}. Whereas bands resulting from the w-vibration are weak in spectra of benzene and triphenylphosphine, they have relatively high intensity in TPP.

Out-of-plane modes may be expected to be more sensitive to

lattice effects. This fact has been used as an aid to assignment of peaks in the CH and CC bending region. Consistent with the above assignments is the observation that the extent of band splitting is larger in CH and CC modes with out-of-plane components. Those modes resulting from in-plane vibrations give bands with either smaller or non-existent splittings.

The substituent-sensitive mode gives rise to peaks at 515, 506 and 498 cm^{-1} and like x (293 cm^{-1}) and u (205 and 197 cm^{-1}) is attributed to a certain extent to P-pyridine bending. Of the substituent sensitive vibrations, assigned according to previous studies on triphenylphosphine (156), the t-vibration is expected to show the largest shift as a result of changing substituent (410 cm^{-1} in triphenylphosphine and 432 and 427 cm^{-1} in TPP).

6.2.2 N-bound metal complexes

In general, the frequencies of pyridine ring modes are little affected by metal ion coordination. It has been suggested that the similarity between spectra of its complexes and pyridine itself is an indication of back-donation of electron density from the metal atom to the pyridine ring (244). E.S.R. evidence suggests 2 or 3 % back donation of unpaired electron density delocalizing onto the rings (see section 5.3.6).

In most cases, bands which are split in the spectra of the free ligand or TPPAuCl have become degenerate in the spectra of N-bound metal complexex indicative of the ability of the metal ion to restrain the ligand in a higher (C_{3v}) symmetry conformation.

In an extensive far-infrared study on metal pyridine complexes (245), two metal sensitive pyridine vibrations were monitored, namely the 601 cm^{-1} s-vibration and the 403 cm^{-1} w-vibration, and found to shift invariably to higher frequencies upon metal coordination. In spectra of N-metal complexes of TPP, these peaks shift from 613 and 403 cm^{-1} to 627-642 cm^{-1} and 412-444 cm^{-1}.

A peak which does not receive attention in the summary by Clark and Williams (245) is the ring breathing mode (p) at ca. 989 cm^{-1} in TPP and 984 cm^{-1} in TPPAuCl which consistently shifts to higher frequency (1011-1025 cm^{-1}) upon metal binding although to a lesser extent than the s and w vibrations.

6.2.3 P-bound metal complexes

The overall appearance of the spectrum of TPPAuCl resembles that of the free ligand with particular regard to splittings of peaks observed for transitions whose potential degeneracy has been removed by lattice packing effects.

No significant changes in frequency are observed for bands arising from the in-plane aromatic ring stretching modes which have been reported to be susceptible to changing mass and electronegativity of substituents at the pyridine 2- position.

Tentative assignment of the q-vibration (having a ring-P component) is made for the band located at 1123 cm^{-1} in TPPAuCl compared to its position at 1119 cm^{-1} in the free phosphine. This peak is also shifted to slightly higher frequency in spectra of other phosphorus bound complexes (1135 cm^{-1} in (ClAuTPP)CrCl$_3$, 1132 cm^{-1} in

$(AuClTPP)_2Cu(NO_3)_2$ and 1133 cm^{-1} $(AuClTPP)FeSO_4)$. A shift in the same direction (1089 to 1100 cm^{-1}) was also noted upon gold binding to triphenylphosphine (see section 3.3.5). Other alterations may be expected to occur in peaks resulting from the substituent-sensitive vibrations. Notably the t-vibration located at 432 and 427 cm^{-1} in the free ligand shifts to 462 and 426 cm^{-1} in the gold complex. This trend is also followed in the mixed metal complexes i.e. the t-vibration absorbs at 434 cm^{-1} in mono and bis TPP copper complexes and this shifts to 444 cm^{-1} when gold is also incorporated. Likewise, the band at 423 cm^{-1} in $(TPP)Zn(H_2O)_3(NO_3)_2$ and 425 cm^{-1} in $(TPP)_2Zn(ClO_4)_2$ shifts to 441 cm^{-1} in $(AuClTPP)_2Zn(NO_3)_2$ and the band at 442 cm^{-1} in $(TPP)CrCl_3$ shifts and splits in $(AuClTPP)CrCl_3$ to 457 and 446 cm^{-1}.

The spectra of gold-bound complexes invariably exhibit a peak at ca. 550 cm^{-1}. Because of its proximity to bands resulting from y-mode vibrations at ca. 500 cm^{-1} (metal-sensitive), this peak was at first assigned as a y-band which shifted to higher frequency when the gold atom was bound to phosphorus. Such an assignment, however, is not consistent with the previous observations (156) that the vibration most sensitive to substituent effects is in fact the t-mode. In TPP and its complexes, the magnitude of t-band shifting ranges from 10 cm^{-1} (copper complexes) to 30 cm^{-1} (TPP to TPPAuCl). If the shift to ca. 550 cm^{-1} was attributed to the y-vibration, this would constitute a shift of ca. 50 cm^{-1}, a difference 20 cm^{-1} greater than any observed for a t-vibration. After further consideration, the peak at 552 cm^{-1} in TPPAuCl was tentatively assigned as a combination band involving the Au-Cl stretch located at 329 cm^{-1} and the metal sensitive u-vibration

(215 cm^{-1}). In support of the assignment of a νAu-Cl component in this band is the existence of splitting (547 and 537 cm^{-1}) in the case of (TPPAuCl)$_2$Cu(NO$_3$)$_2$ which may correspond to the isotopic splitting of the Au-Cl stretch at 340 and 330 cm^{-1} with the u-vibration at 208 cm^{-1}. Furthermore, the combination band at 574 cm^{-1} in (AuClTPP)CrCl$_3$ is at a higher frequency than found in the other compounds but can still be shown to correspond to the sum of νAu-Cl and u-vibration peak frequencies. The Au-Cl stretch is also found at higher frequency (360 cm^{-1}) and combines with the u-vibration at 212 cm^{-1}. As a test of the above hypothesis, the spectrum of (BrAuTPP)CrCl$_3$ was recorded and the peak again appeared at 570 cm^{-1}. It appears that this band occurs as a result of some mode which experiences a change in dipole moment upon coordination of gold(I). It remains to be seen to what extent this occurs upon binding of other metals to the phosphorus site.

6.2.4 Nitrate modes

The possibility of using nitrate bands in the infrared spectra near 1750 cm^{-1} for structural diagnosis was initiated by Curtis and Curtis (246) and developed further by Lever et al. (247). This band has been assigned to a combination of the free nitrate (D$_{3h}$) ν_1 symmetric stretch and the ν_4 in-plane bending modes. Local symmetry of the nitrate is reduced to C$_{2v}$ upon coordination and as a result ν_4 splits into two components each of which couple with ν_1, thus the $\nu_1+\nu_4$ combination band also splits. The extent of this splitting has been used to fingerprint monodentate (Δ=5-26 cm^{-1}) and bidentate (Δ=20-66 cm^{-1}) nitrate coordination in ammine complexes of transition metals

summarized by Lever et al. (247). The larger extent of splitting in

the bidentate case is explained by the larger deviation from D_{3h}

symmetry which occurs in bidentate coordination. The spectra of

$TPPZn(H_2O)_3(NO_3)_2$ exhibit the sharp single band at 1769 cm^{-1},

$(TPP)_2Cu(NO_3)_2$ and $(ClAuTPP)_2Cu(NO_3)_2$ at 1765 and 1770 cm^{-1}

respectively, indicative of free nitrate. The spectrum of $TPPCu(NO_3)_2$

on the other hand, has three weak bands in this region at 1762, 1729

and 1703 cm^{-1}. According to Lever et al., complexes with both

monodentate and bidentate nitrate groups may be expected to show four

combination bands - one pair being generated from each coordination

mode (247). In the case of $TPPCu(NO_3)_2$, two of these bands probably

overlap. A simple calculation of the splitting of these bands is

likely not a reliable method of assigning the bands explicitly because

of the asymmetric nature of the bidentate nitrate established in the

crystal structure determination.

6.2.5 Metal - skeletal band assignments

Clark and Williams (245) have reported a range of M-N

stretching frequencies from 214 to 287 cm^{-1} for metal complexes of

pyridine having monomeric octahedral geometry. A more recent study on

nitrato complexes of cobalt, nickel and zinc with varying pyridine

stoichiometries took into consideration the effects of metal isotope

and deuteriopyridine substitution on bands in the 400-100 cm^{-1} region

of the infrared (249). Although these assignments give some indication

of frequencies, none of the previously reported compounds have facial

pyridine coordination geometries with the exception of complexes of

rhodium and iridium (νM-N; 266, 245 cm^{-1} (rhodium), 270, 266 cm^{-1}

(iridium) (245)).

The meridional isomer of Cu(py)$_3$(NO$_3$)$_2$ exhibits peaks at 268,

223, 211 and 156 cm^{-1} which have been assigned to νCu-O, νCu-N, δN-Cu-N

and δN-Cu-O respectively (248). Peaks in the spectrum of (TPP)Cu(NO$_3$)$_2$

which are absent in that of TPP itself are those at 310 and 216 cm^{-1}

and these are tentatively assigned as νCu-O and δN-Cu-O respectively

since they are also absent in spectra of the CuN$_6$ species. In support

of the νCu-O assignment is the observation of strong bands at 322 and

282 cm^{-1} attributed to νCu-O in the spectrum of Cu(py)$_2$(NO$_3$)$_2$. A

corresponding band in the spectrum of (TPP)Cu(NO$_3$)$_2$ at approximately

281 cm^{-1} may be present but coincidental with a ligand absorption.

Bands resulting from the νCu-N mode in the spectra of [hydro

tris(pyrazol-1-yl)borate]copper(II) have been located at 263 and 244

cm^{-1} and [hydro tris(3,4,5-trimethyl)pyrazol-1-yl)borate]copper(II) at

233 cm^{-1} (249). Cu-N stretches in Cu(bipy)$_3^{2+}$ and Cu(phen)$_3^{2+}$ have

been located at 297 and 255 cm^{-1} and 287, 272 and 265 cm^{-1} (250).

Bands in this region are present in spectra of the Cu-TPP complexes but

cannot be definitely assigned as νCu-N since they are also present in

spectra of the free ligand. The zinc complexes exhibit bands at 180

and 165 cm^{-1} for (TPP)Zn(H$_2$O)$_2$(NO$_3$)$_2$ and 180 and 169 cm^{-1} for

(ClAuTPP)$_2$Zn(NO$_3$)$_2$) which have greater intensity with respect to those

in the free ligand. It is possible that νZn-N contributes to their

intensity. Frequencies for the Zn-N modes are also in agreement with

assignments made by Hutchinson et al. (249) for the pyrazolylborate

ligands (227 and 180 cm^{-1} for (HB(pz)$_3$)$_2$Zn, 204 cm^{-1} for

$(HB((Me)_3pz)_3))_2Zn$ and Takemoto et al. (250) for bands at 230 and 184 cm^{-1} in $Zn(bipy)_3^{2+}$ and 198 and 175 cm^{-1} in $Zn(phen)_3^{2+}$. A strong band appears in the spectrum of $(TPP)_2Zn(ClO_4)_2$ but it is overlapped by a broad peak at 194 cm^{-1} tentatively attributed to δN-Zn-N. The Zn-O mode was not assigned but may contribute to the band at 250 cm^{-1}. M-N stretches in the case of the chromium complexes are found at much higher frequency (296 cm^{-1} for $(TPP)CrCl_3$ and 306 cm^{-1} for $(ClAuTPP)CrCl_3$). This is explained by the relatively higher charge on the metal center and the fact that its three d electrons are in orbitals which are oriented between the ligands (t_{2g}^3) whereas in all the other examples for which far infrared data were collected the e_g orbitals are occupied (250).

Frequencies of the νM-Cl modes have been assigned at 347 and 330 cm^{-1} in $(TPP)CrCl_3$, 345 and 334 cm^{-1} in $(ClAuTPP)CrCl_3$, 299 and 280 cm^{-1} in $(TPP)FeCl_3$, 368 and 342 cm^{-1} in $(TPP)CoCl_3$ and 368 and 349 cm^{-1} in $(ClAuTPP)CoCl_3$. The relatively lower frequency of the bands in the iron complex suggest a high spin electronic configuration in accordance with Moessbauer results (see section 5.4.4). Far infrared spectra of the chromium complexes reveal other doublets at 172 and 162 cm^{-1} $((TPP)CrCl_3)$ and 169 and 162 cm^{-1} $((ClAuTPP)CrCl_3)$ which have been assigned to the δCl-M-Cl modes.

CHAPTER 7

GENERAL CONCLUSIONS AND FUTURE CONSIDERATIONS

The development of the oral anti-arthritis compound, auranofin,.
has shown both advantages and disadvantages in its use as a drug.
Among the disadvantages is its possible carcinogenicity which becomes a
greater risk during long-term RA treatment. The source of this
carcinogenicity is likely the phosphine ligand itself and not a result
of gold-DNA interactions similar to those implicated in the series of
platinum(II) anti-cancer drugs (although chloro- complexes of gold(I)
with triphenylphosphine and t-butylisocyanide have shown their ability
to bind to DNA in in vitro experiments). Comparison of the properties
of other gold(I) complexes with respect to their anti-arthritis effects
has potential to lend insight into the nature of the disease itself as
well as its treatment (like the established structure-activity
relationships of platinum(II) complexes in cancer therapy). Attempts
to synthesize compounds analogous to auranofin with ligands other than
phosphine suggest that these complexes are either unstable (i.e.
aromatic nitrogen donor) or are too labile to survive subsequent
reaction with thiols (i.e. isocyanide complexes) to form auranofin-like
species. This lack of stability limits the use of alternative
compounds even for initial clinical comparisons with auranofin and the
injectable gold drugs. Complexes of gold(III) are more similar to
those of platinum(II) and have also shown ability to bind to DNA in
vitro. These, too, are unstable in biological systems where other

215

reactions result in compound decomposition. In summary, it has been difficult to find a ligand which will stabilize gold(I) (or gold(III)) in a biological milieu and which also forms a characterizable complex.

For the purposes of future _in vitro_ and _in vivo_ experiments, complexes of TPP have been prepared and characterized. Among these are complexes with copper(II) (section 5.3) which have also been characterized on the basis of E.S.R. and electronic absorption spectroscopies. These complexes have promising potential as the copper ion provides a relatively sensitive label with which to follow _in vivo_ reactions in future experimentation.

Some effort has been exerted to establish trends in E.S.R. and UV/Visible data to ultimately describe which d orbitals are involved in bonding in copper complexes and thus make predictions as to structure. In order for this to be possible, it is necessary to gather spectral information for which complex structure has been determined crystallographically. The TPP ligand is useful in this respect because it restricts the copper ion to _facial_ geometries. The hydro(tris-1-pyrazolyl)borate ligand places _facial_ restrictions on copper as well, but these are accompanied by rhombic distortions in the bis complex and the mono- ligated species has not been reported.

In general, TPP is intermediate in ligand field strength between aromatic amine ligands such as bipy and phen and primary (and secondary) amines like en and dien.

A preliminary study of E.S.R. parameters for the copper complexes of TPP suggest similarities in electronic structure between CuN_6 species, as expected. The $TPPCu(NO_3)_2$ complex, which gives rise

to relatively large g∥ and g⊥ values, remains to be fully characterized by single crystal E.S.R. work. Its crystallographically determined structure is of distorted square pyramidal geometry. Although Hathaway (202) has included complexes of this geometry in his hypothesis regarding g values and structure, a square pyramidal complex has not yet been tested on these grounds.

TPP has been conceptualized as a protein model, for example, as zinc(II) and iron(II) or iron(III) complexes and a discussion of structural data with respect to this potential has been included in sections 5.2 and 5.4.

In the case of zinc, the octahedral coordination observed is apparently what prevents the complex from catalysing the hydration of carbon dioxide at biological pH for reasons outlined in section 5.2.4. The study of complexes of similar ligands with the pyridine 5- position occupied by groups of ranging steric demands is suggested as a course of possible further work. Examination of the steric properties of tris(imidazole)phosphine derivatives has already begun.

It is unfortunate that the lability of the zinc(II) ion allows decomposition of the $[(ClAuTPP)Zn(H_2O)_3](NO_3)_2$ and $[(ClAuTPP)_2Zn](ClO_4)_2$ complexes in aqueous solution through precipitation of ClAuTPP. The diamagnetic nature of zinc(II) would have been ideal for a study of the reactions of these complexes in NMR experiments. Instead, a kinetically inert diamagnetic ion is required. Development of cobalt(III) complexes has begun for this purpose (see sections 5.5 and 6.2) and work on these systems continues.

Structurally, iron complexes of TPP have shown their potential

as models for the active site of haemerythrin although the actual diiron species has yet to be synthesized.

While, in theory, it may be possible to affect slight changes in the electronic properties of the phosphine site by incorporation of other transition metals at the nitrogen sites, this does not appear to occur in practice as evidenced by comparison of structural properties reported in Chapter 6. The only indications of structural changes result from restrictions placed on the pyridyl rings upon metal binding where they are no longer free to assume a propeller-like arrangement but are forced to adopt C_{3v} symmetry. Distortions in this C_{3v} symmetry have been observed to result from packing effects. Also, gold is able to withdraw lone pair electron density from the phosphorus atom allowing the pyridyl rings to spread out regardless of the presence of N-bound metal ions.

The effect on ring distances and angles of binding transition metals to the pyridyl nitrogen atoms is too slight to suggest any trend. THis observation coincides with infrared results summarized in section 6.2 where pyridine ring frequencies were little affected by metal coordination.

The large quantity of work already reported for benzenes, pyridines and pyridine complexes (155, 239-248) have allowed fairly complete assignments to be made for infrared absorptions of TPP complexes. With the variety of data presented in this thesis, certain trends have surfaced which allow predictions to be made about the structures of complexes.

Evidence for gold(I) binding at the phosphorus atom comes from

the slight shift in frequency of the band assigned as the q-vibration at 1119 cm^{-1} in the spectrum of TPP which is located at higher wavenumber in phosphorus-bound complexes. Also, shifts to higher frequency (Δ=30 cm^{-1}) are apparent for the t-vibration at 432 and 427 cm^{-1} in the free ligand. The most dramatic effect on the infrared spectra of phosphorus-bound complexes is the appearance of a peak at $\cong$550 cm^{-1} absent in spectra of phosphorus-free compounds. An assignment of this peak has yet to be made. It may prove valuable to monitor this peak as a function of other atoms bound at the phosphorus site ranging from oxygen or sulphur to metal ions other than gold(I).

An obvious effect of N-metal coordination on the overall appearance of infrared spectra is the removal of band degeneracy arising from the ability of the metal ion to impose C_{3v} symmetry on the ligand. The 601 cm^{-1} s-vibration and 403 cm^{-1} w-vibration shift invariably to higher frequency upon metal N-binding as does the ring breathing mode located at 989 cm^{-1} in TPP.

As usual, it is difficult to assign M-N and M-O skeletal modes with certainty. It becomes necessary to make a study involving metal and ligand isotopic substitution in order to define bands arising from these modes and even then, bands at low frequencies may contain a large contribution from lattice vibrations.

So far, literature reports of TPP complexes have been concerned only with the tripod nature of the ligand and transition metal-pyridine binding. The availability of phosphorus as a binding site seems to have been overlooked.The phosphorus site may, however, provide these complexes with other properties. Phosphines are prevalent as ligands

in organometallic chemistry and the possibility presents itself, for
example, where the ability to alter compound solubilities by changing
N-metal coordination may prove useful. Also, while protein active site
models thus far discussed exhibit their activity in solution, it may
now be possible to fix, for example, a diiron or a zinc center on to a
surface to provide heterogenous catalysts which perform the same
function as biological enzymes.

REFERENCES

1. E.J.Kamin and C.V.Multz, Calif.Med. <u>110</u>,17 (1969).

2. Empire Rheumatism Council, Ann. Rheum. Dis. <u>20</u>, 315 (1961).

3. R.C.Gerber, H.E.Paulus, R.I.Jennrich, M.Lederer, R.Bluestone, W.H.Blahd and C.M.Pearson, J. Lab. Clin. Med. <u>83</u>, 778 (1974).

4. J.H.Liebfarth and R.H.Persellin, Agents and Actions, <u>11</u>, 458 (1981).

5. P.Stastny, N. Eng. J. Med., <u>298</u>, 869 (1978).

6. B.H.Waksman, C.N.Pearson and J.T.Sharpe, J. Immunol., <u>85</u>, 403 (1961).

7. A.J.Lewis, J.Cottney, D.D.White, P.K.Fox, A.McNeillie, J.Dunlop, W.E.Smith and D.H.Brown, Agents and Actions, <u>10</u>, 63 (1980).

8. F.A.Cotton and G.Wilkinson, "Advanced Inorganic Chemistry", 4th edition, J. Wiley and Sons, New York (1980).

9. W.F.Kean and W.W.Buchanan, Ther. Rev., <u>36</u>, 1557 (1981).

10. S.H.Hong, A.Olin and R.Hesse, Acta Chem. Scand., <u>A29</u>, 583 (1975).

11. I.G.Dance, Inorg. Chim. Acta, <u>25</u>, 47, 1977.

12. R.V.Parish, Gold Bull., <u>15</u>, 51 (1982).

13. A.A.Isab and P.J.Sadler, J. Chem. Soc. Dalton, 1657 (1981).

14. R.C.Elder, K.Ludwig, J.N.Cooper and M.K.Eidsness, J. Am. Chem. Soc., <u>107</u>, 5024 (1985).

15. A.K.H.Al-Sa'ady, K.Moss, C.A.McAuliffe and R.V.Parish, J.Chem. Soc. Dalton, 1609 (1984).

16. P.J.Sadler, Struct. Bonding, <u>29</u>, 171 (1976).

17. C.F.Shaw, Inorg. Persp. Biol. Med., 2, 287 (1979).

18. M.Duarte, D.A.Harvey and C.J.L.Lock, in progress.

19. H.Ruben, A.Zalkin and M.O.Faltens, Inorg. Chem., 13, 1836 (1974).

20. C.F.Shaw, J.Eldridge and M.P.Cancro, J. Inorg. Biochem., 14, 267 (1981).

21. Lorber et al, Gold Bull., 12, 149 (1979).

22. D.T.Walz, M.J.DiMartino, B.M.Sutton and A.Misher, J. Pharm. Exp. Ther., 181, 292 (1972).

23. D.T.Walz, M.J.DiMartino, L.W.Chakrin, B.M.Sutton and A.Misher, J. Pharm. Exp. Ther., 197, 142 (1976).

24. D.T.Hill and B.M.Sutton, Cryst. Struct. Commun., 9, 679 (1980).

25. R.J.Puddephatt,"The Chemistry of Gold", Elsevier, Amsterdam , (1978).

26. H.Schmidbauer, Angew. Chem. Int. Ed. Engl., 15, 728 (1976).

27. F.N.Ghadially, J. Rheumatol. 6, (Suppl. 5), 45 (1979).

28. "Cisplatin; Current Status and New Developments", A.W.Prestayko, S.T.Crooke and S.K.Carter eds., Academic Press (1980).

29. R.C.Elder, M.K.Eidsness, M.J.Heeg, K.G.Tepperman, C.F.Shaw and N.Schaeffer in "Platinum, Gold and Other Metal Chemotherapeutic Agents", (Ed. S.J.Lippard), ACS Symposium Series, 209, American Chemical Society, Washington, D.C., 385 (1983).

30. M.H.Ford-Smith, J.J.Habeeb and J.H.Rawsthorne, J. Chem. Soc. Dalt., 2116 (1972).

31. C.J.Hawkins, OMØnsted and J.Bjerrum, Acta Chem. Scand., 24, 1059 (1970).

32. G.M.Schmid in "Standard Potentials in Aqueous Solution", Eds.

A.J.Bard, R.Parsons and J.Jordan, Marcel Dekker; New York, 313 (1985).

33. W.F.Kean, C.J.L.Lock and Y.Kassam, J. Rheumatol., 14, 209 (1987).

34. D.H.Brown, G.C.McKinley and W.E.Smith, J. Chem. Soc. Dalt., 199 (1978).

35. F.Hermann, Chem. Ber., 38, 2813 (1905).

36. G.P.Paret, G.P. 121, 6296 (1965).

37. N.Hadjiliadis, G.Pneumatikakis and R.Basosi, J. Inorg. Biochem., 14, 115 (1981).

38. J.E.Huheey,"Inorganic Chemistry: Principles of Structure and Reactivity", 2nd edit., Harper and Row; New York, 406 (1978).

39. G.Marcotrigiano, R.Battistazzi and G.Peyronel, Inorg. Nuc. Chem. Lett., 8, 399 (1972).

40. M.Davis and F.G.Mann, J. Chem. Soc., 379 (1964).

41. D.Lewis, H.A.Capell, C.J.MacNiel, M.S.Iqbal, D.H.Brown and W.E.Smith, Ann. Rheum. Dis., 42 ,566 (1983).

42. G.G.Graham, T.M.Haavisto, H.M.Jones and G.D.Champion, Biochem. Pharmacol., 33, 1257 (1984).

43. A.Shiotani. H.-F.Klein and H.Schmidbauer, J. Am. Chem. Soc., 93, 1555 (1971).

44. J.A.Muir, M.M.Muir and E.Lorca, Acta Cryst., 36B, 931 (1980), L.J.Guggenburger, J. Organomet. Chem., 81, 271 (1974).

45. P.G.Jones, Acta Cryst., 36B, 3105 (1980).

46. P.G.Jones, G.M.Sheldrick, A.Fugner, F.Gotzfried and W.Beck, Chem. Ber., 114, 1413 (1981).

47. S.P.Blau, Arth. Rheum., 16, 777 (1973).

48. A.L.Lehninger,"Biochemistry", 2nd edition, Worth; New York (1977).

49. K.Tepperman, R.Finer, S.Donovan, R.C.Elder, J.Doi, D.Ratliff and K.Ng, Science, 225, 430 (1984).

50. M.T.Razi, G.Otiko and P.J.Sadler in "Platinum,Gold and Other Metal Chemotherapeutic Agents", ACS Symposium Series, (Ed. S.J.Lippard), American Chemical Society, Washington, D.C. 370 (1983).

51. H.M.Rubenstein and A.A.Dietz, Ann. Rheum. Dis., 32, 128 (1973).

52. N.L.Gottlieb, J. Rheumatol., 9, (Suppl. 8), 99 (1982).

53. J.R.Brown in "Albumin: Structure, Function and Uses, (Eds. V.M.Rosenor, M.Oratz, and M.A.Rothschild), Pergamon Press; New York, 27 (1977).

54. T.Peters, Clin. Chem., 23, 1 (1977).

55. D.A.Gerber, J. Pharm. Exp. Ther., 143, 137 (1964).

56. A.P.Intocchia, T.L.Flanagan, D.T.Walz, L.Gutzait, J.E.Swagzdis, J.Flagiello, B.Y-H.Hwang, R.H.Dewey and N.Noguchi in "Bioinorganic Chemistry of Gold Coordination Compounds", (Ed. B.M.Sutton), Smith Kline and French Laboratories, Philadelphia, PA, 21 (1983).

57. N.S.Malik, G.Otiko and P.J.Sadler, J. Inorg. Biochem., 12, 317 (1980).

58. N.L.Gottlieb, P.M.Smith and E.M.Smith, Arth. Rheum., 15, 582 (1972).

59. K.L.N.Blocka, Clin. Pharmakokinetics, 11, 133 (1986).

60. R.W.Mason, R.P.Sharma and E.G.McQueen in "Trace Elements in the Pathogenesis and Treatment of Inflammation", (Ed. K.D.Rainsford) Kirkhauser, Basel, 489 (1981).

61. K.L.N.Blocka, D.E.Furst, E.M.Landaw, S.Droomgoole, A.L.Blomberg

and H.E.Paulus, J. Rheum., 9, (Suppl. 8), 110 (1982).

62. J.R.Ward, H.J.Williams, M.J.Egger, J.C.Reading, E.Boyce, M.Altz-Smith, C.O.Samuelson, R.F.Willkens, M.A.Solsky, S.P.Hayes, K.L.Blocka, A.Weinstein, R.F.Meenan, M.Guttadauria, S.B.Kaplan and J.Klippel, Arth. Rheum., 26, 1303 (1983).

63. J.R.Ward, H.J.Williams, E.Boyce, M.J.Egger, J.C.Reading and E.O.Samuelson, Am. J. Med.,   ,133 (1983).

64. N.L.Gottlieb and W.J.Wilbur, Am. J. Med.,   , 1 (1983).

65. G.J.Schroebilgen, personal communication.

66. E.Jellum, E.Munthe, G.Guldal and J.Aeseth, Ann. Rheum. Dis., 39, 155 (1980).

67. D.T.Walz, M.J.DiMartino and D.E.Griswold, J.Rheumatol., 9, (Suppl. 8), 54 (1982).

68. K.L.N.Blocka, H.E.Paulus and D.E.Furst, Clin. Pharm., 11, 133 (1986).

69. P.G.Jones, Gold Bull., 14, 102 (1981).

70. Von H.-N.Adams, W.Hiller and J.Strähle, Z. Anorg. Allgem. Chem., 485, 81 (1982).

71. A.A.Isab and P.J.Sadler, J. Chem. Soc. Chem. Commun., 1051 (1976).

72. A.A.Isab and P.J.Sadler, J. Chem. Soc. Dalton, 135 (1982).

73. E.Beutler, "Red Cell Metabolism: A Manual of Biochemical Methods", Grune and Stratton, New York, 113 (1975).

74. M.T.Coffer, C.F.Shaw, M.K.Eidsness, J.W.Watkins and R.C.Elder, Inorg. Chem., 25, 333 (1986).

75. M.T.Coffer, C.F.Shaw, A.L.Hormann, C.K.Mirabelli and S.T.Crooke, J.Inorg. Biochem, 30, 177 (1987).

76. E.M.Kinsch and D.W.Stephan, Inorg. Chim. Acta, 91, 263 (1984).

77. R.B.Simpson and H.A.Saroff, J. Am. Chem. Soc., 80, 2129 (1958).

78. B.Rosenberg, E.Renshaw, L.VanCamp, J.Hardwick and J.Drobnick, J. Bacteriology, 93, 716 (1967).

79. B.Rosenberg, L.VanCamp, E.Grimlay and A.J.Thompson, J. Biol. Chem., 242, 1347 (1967).

80. B.Rosenberg, Platinum Metals Rev., 15, 42 (1971).

81. D.T.Hill, G.R.Girard, B.M.Sutton, C.K.Mirabelli, L.F.Faucette and R.K.Johnson, Proc. 20th Great Lakes Regional Meeting, ACS Abstr. 204, Milwaukee (1986).

82. T.M.Simon, D.H.Kunishima, G.J.Vibert and A.Lorber, Cancer, 44, 1965 (1979).

83. T.M.Simon and A.Lorber, In Vitro, 14, 372 (1978).

84. T.M.Simon, D.H.Kunishima, G.J.Vibert and A.Lorber, J. Rheumatol., 6, 91 (1979).

85. T.M.Simon, D.H.Kunishima, G.J.Vibert and A.Lorber, Cancer Res., 41, 94 (1981).

86. C.K.Mirabelli, R.K.Johnson, C.-M.Sung, L.Faucette, K.Muirhead and S.T.Crooke, Cancer Res., 45, 32 (1985).

87. C.F.Shaw, A.Beery and G.S.Stocco, Inorg. Chim. Acta, 123, 213 (1986).

88. C.K.Mirabelli, R.K.Johnson, L.Faucette. C.-M.Sung, J.Bartus and S.T.Crooke, Proc. Am. Assoc. Cancer Research, Abstr. 1455 (1984).

89. C.K.Mirabelli, R.K.Johnson, R.M.Snyder, D.T.Hill, M.R.Mattern and S.T.Crooke, Proc. 20th Great Lakes Regional Meeting, ACS Abstr. 243 (1986).

90. C.Dragalescu, J.Heller, A.Maurer, S.Policec, V.Topcui, M.Csalci, S.Kirschner, S.Kravitz and R.Moraski, Int. Coord. Chem. Conf. XVI, 1, 99 (1974).

91. R.G.Pearson,"Hard and Soft Acids and Bases", Dowden, Hutchnson and Ross, 1973.

92. C.K.S.Pillai and U.S.Nandi, Biopolymers, 12, 1431 (1973).

93. D.W.Gibson, M.Beer and R.J.Barnett, Biochem., 10, 3669 (1971).

94. K.A.Hartman, Biochim. Biophys. Acta, 138, 192 (1967).

95. F.Bonati, A.Burini and B.R.Pietroni, Z. Naturforsch., 40B, 1749 (1985).

96. G.H.M.Calis, N.Hadjiliadis, Inorg. Chim. Acta, 91, 203 (1984).

97. M.Bressan, R.Ettore and P.Rigo, J. Magn. Reson., 26, 43 (1977).

98. M.S.Holowczak, M.D.Stancl and G.B.Wong, J. Am. Chem. Soc., 107, 5789 (1985).

99. C.K.Mirabelli, C.-M.Sung, J.P.Zimmerman, D.T.Hill, S.Mong and S.T.Crooke, Biochem. Pharm. 35, 1427 (1986).

100. C.K.Mirabelli, J.P.Zimmerman, H.R.Bartus, C.-M.Sung and S.T.Crooke,ibid., 1435.

101. C.E.Blank, J.C.Dabrowiak, J. Inorg. Biochem., 21, 21 (1984).

102. N.Beck, U.Nagel and Y.Rosopulos, Chem. Ber., 118, 931 (1985).

103. B.Ward, J.C.Dabrowiak, J. Am. Chem. Soc., 109, 3810 (1987).

104. G.B.Kauffman and L.A.Teter, Inorganic Syntheses, 7, 232 (1963).

105. M.J.Buerger, "X-ray Crystallography", John Wiley and Sons Inc.: New York (1942).

106. G.H.Stout and L.H.Jensen, "X-ray Structure Determination", The MacMillan Company: Toronto (1968).

107. P.Luger, "Modern X-ray Analysis on Single Crystals", Walter de Gruyter: Berlin (1980).

108. J.P.Glusker and K.N.Trueblood, "Crystal Structure Analysis; A Primer", 2nd edit., Oxford University Press: New York (1985).

109. R.P.Hughes, N.Krishnamachari, C.J.L.Lock, J.Powell and G.Turner, Inorg. Chem., 16, 314 (1977).

110. B.Lippert, C.J.L.Lock, B.Rosenberg and M.Zvagulis, Inorg. Chem., 16, 1525 (1977).

111. S.French and K.Wilson, Acta Cryst., 34A, 517 (1978).

112. W.L.Bond in "International Tables for X-ray Crystallography", Vol. II, Table 5.3.5B, Kynoch Press: Birmingham, 295 (1967).

113. J.C.Calabrese and R.M.Burnett, TAPER, Nicolet XRD Corp., locally modified by Z.Tun and called PSISCAN (1980).

114. D.T.Cromer and J.T.Waber in "International Tables for X-ray Crystallography", Vol. IV, Table 2.2.A, Kynoch Press: Birmingham, 72 (1967).

115. D.T.Cromer and J.A.Ibers in "International Tables for X-ray Crystallography", Vol. IV, Table 2.3.1, Kynoch Press: Birmingham, 149 (1967).

116. G.M.Sheldrick, SHELX, Program for Crystal Structure Determination, Univ. of Cambridge, England (1976).

117. J.M.Stewart, The XRAY76 System, Tech. Rept. TR-446, Computer Science Center, University of Maryland, College Park, Maryland (1976).

118. J.M.Stewart and S.R.Hall, The XTAL system of crystallographic programs, Tech. Rept. TR-1364, University of Maryland, College

Park, Maryland (1976).

119. J.Stephens, MOLGEOM, adapted from CUDLS, McMaster University,

   Canada (1973).

120. F.A.Ahmed and M.E.Pippy, NRC-22; Mean Plane and Torsional Angles,

   National Research Council of Canada, Ottawa, Canada (1976).

121. K.Davies, CHEMX, Chemical Design Ltd., Oxford, England (1986).

122. C.K.Johnson, ORTEP II, Report ORNL-5138, Oak Ridge National

   Laboratory, Tennessee, U.S.A. (1976).

123. K.Davies, SNOOPI, CHEMGRAF suite, Chemical Design Ltd., Oxford,

   England (1983).

124. K.Ruebenbauer and T.Birchall, Hyperfine Interactions, 7, 125

   (1979).

125. D.M.Maron and B.N.Ames, Mutation Research, 113 (1983) and

   references therein.

126. C.J.L.Lock in "Inorganic Chemistry in Biology and Medicine",

   A.E.Martell (editor), ACS Symposium Series, 140, American

   Chemical Society, Washington, D.C., 209 (1980).

127. D.T.Hill (Smithkline Corp.), U.S.Patent 4,098,887, Feb. 25 (1977).

128. J.A.McCleverty and M.M.M.da Mota, J. Chem. Soc. Dalt., 2571

   (1973).

129. D.S.Eggleston, D.F.Chodosh, R.L.Webb and L.L.Davis, Acta Cryst.,

   42C, 36 (1986).

130. W.P.Weber, G.W.Gokel and I.K.Ugi, Angew. Chem. Int. Ed. Eng., 11,

   530 (1972).

131. F.Bonati and G.Minghetti, J. Organomet. Chem., 59, 403 (1973).

132. B.M.Sutton, E.McGusty, D.T.Walz and M.J.DiMartino, J. Med. Chem.,

<u>15</u>, 1905 (1972).

133. S.Esperas, Acta Chem. Scand., <u>30A</u>, 527 (1976).

134. A.Bondi, J. Phys. Chem., <u>68</u>, 441 (1964).

135. N.C.Baenziger, W.E.Bennett and D.M.Soboroff, Acta Cryst., <u>32B</u>, 962 (1976).

136. F.A.Cotton and F.Zingales, J. Am. Chem. Soc., <u>83</u>, 351 (1961).

137. K.Nakamoto, "Infrared and Raman Spectra of Inorganic and Coordination Compounds", 3rd edition, John Wiley and Sons; Toronto, 1978 and references therein.

138. P.G.Jones, A.G.Maddock, M.J.Mays, M.M.Muir and A.F.Williams, J. Chem. Soc. Dalt., 1434 (1977).

139. S.Mansy, B.Rosenberg and A.J.Thomson, J. Am. Chem. Soc., <u>95</u>, 1633 (1973).

140. A.E.Finkelstein, O.R.Burrone, D.T.Walz and A.Misher, J. Rheumatol., <u>4</u>, 245 (1977).

141. H.S.Allaudeen, R.M.Snyder, M.H.Whitman and S.T.Crooke, Biochem. Pharm., <u>34</u>, 3243 (1985).

142. C.K.Mirabelli, R.K.Johnson, D.T.Hill, L.F.Faucette, G.R.Girard, G.Y.Kuo, C.M.Sung and S.T.Crooke, J. Med. Chem., <u>29</u>, 218 (1986).

143. K.C.Agrawal, K.B.Bears, D.Marcus and H.B.Jonassen, Proc. Am. Soc. Canc. Res., <u>19</u>, 23 (1978).

144. G.Banditelli, A.L.Bandini, G.Minghetti and F.Bonati, Can. J. Chem., <u>59</u>, 1241 (1981).

145. J.R.Lechat, R.H. de Almeida Santos, G.Banditelli and F.Bonati, Cryst. Struct. Commun., <u>11</u>, 471 (1982).

146. B.Bovio, F.Bonati, A.Burini and B.R.Pietroni, Z. Naturforsch.,

39B, 1747 (1984).

147. F.Bonati, A.Burini, B.R.Pietroni and M.Felici, J. Organomet. Chem., 273, 275 (1984).

148. J.J.Guy, P.G.Jones, M.J.Mays and G.M.Sheldrick, J. Chem. Soc. Dalt., 8 (1977).

149. K.Hoogsteen, Acta Cryst., 16, 28 (1963).

150. C.J.L.Lock, R.A.Speranzini and J.Powell, Can. J. Chem., 54, 53 (1976).

151. T.R.Krugh, J. Am. Chem. Soc., 95, 4761 (1973).

152. J.H.Goldstein and A.R.Tarpley Jr., J. Am. Chem. Soc., 93, 3573 (1971).

153. H.Susi and J.S.Ard, Spectrochim. Acta, 30A, 1843 (1974).

154. F.Guay, A.L.Beauchamp, C.Gilbert and R.Savoie, Can. J. Spect., 28, 13 (1983).

155. D.H.Whiffen, J. Chem. Soc., 1350 (1956).

156. K.Shobatake, C.Postmus, J.R.Ferraro and K.Nakamoto, Appl. Spect., 23, 12 (1969).

157. K.M.MacKay, D.B.Sowerby and W.C.Young, Spectrochim. Acta, 24A, 611 (1968).

158. M.Tsuboi, S.Takahashi and I.Harada in "Physico-Chemical Properties of Nucleic Acids", Vol. 2, Ed. J.Dushesne, Academic Press; New York, 91 (1973).

159. K.L.Wierzchowski, E.Litonska and D.Shugar, J. Am. Chem. Soc., 87, 4621 (1965).

160. F.Guay and A.L.Beauchamp, J. Am. Chem. Soc., 101, 6260 (1979).

161. K.Shobatake and K.Nakamoto, J. Am. Chem. Soc., 92, 3332 (1970).

162. H.E.Howard-Lock, personal communication.

163. S.Ahrland, J.Chatt and N.R.Davies, Quart. Rev. Chem. Soc., $\underline{12}$, 265 (1958).

164. G.Raudaschl-Sieber, B.Lippert, Inorg. Chem., $\underline{24}$, 736 (1985).

165. R.Faggiani, B.Lippert, C.J.L.Lock and R.A.Speranzini, Inorg. Chem., $\underline{21}$, 3216 (1982).

166. D.W.Gibson, M.Beer and R.J.Barnett, Biochemistry, $\underline{10}$, 3669 (1971).

167. M.Howe-Grant, K.C.Wu, W.R.Bauer and S.J.Lippard, Biochemistry, $\underline{15}$, 4339 (1976).

168. J.K.Barton, J.J.Dannenberg and A.L.Raphael, J. Am. Chem. Soc., $\underline{104}$, 4967 (1980).

169. L.Cattalini and M.L.Taube, Inorg. Chem., $\underline{5}$, 1145 (1966).

170. G.Annibale, G.Natile, B.Pitteri and L.Cattaline, J. Chem. Soc. Dalt., 728 (1978).

171. C.M.Harris and T.N.Lockyer, J. Chem. Soc., 3083 (1959).

172. C.M.Harris, J. Chem. Soc., 682 (1959).

173. N.F.Borkett, M.I.Bruce and J.D.Walsh, Aust. J. Chem., $\underline{33}$, 949 (1980).

174. G.L.Cohen, W.R.Bauer, J.K.Barton and S.J.Lippard, Science, $\underline{203}$, 1014 (1979).

175. S.Mong, C.H.Huang, A.W.Prestayko and S.T.Crooke, Cancer Res., $\underline{40}$, 3313 (1980).

176. S.Mong, C.J.Huang, A.W.Prestayko and S.T.Crooke, Cancer Res., $\underline{40}$, 3318 (1980).

177. P.J.Stone, A.D.Kelman, F.M.Sinex, M.M.Bhargavo and H.O.Halverson, J. Mol. Biol., $\underline{104}$, 793 (1976).

233

178. J.P.Macquet and J.Butour, Biochimie, <u>60</u>, 901 (1978).

179. "International Tables for X-ray Crystallography," Vol.

    A, Reidel Publ. Co.; Dordrecht, (1983) and references therein.

180. P.T.Beurskens, H.J.A.Blaauw, J.A.Cras and J.J.Steggerda, Inorg.

    Chem., <u>7</u>, 805 (1968).

181. P.T.Beurskens, J.A.Cras, and J.J.Steggerda, Inorg. Chem., <u>7</u>, 810

    (1968).

182. H.P.Klug, Acta Cryst., <u>21</u>, 536 (1966).

183. N.W.Alcock, K.P.Ang, K.F.Mok, and S.F.Tan, Acta Cryst., <u>34B</u>, 3364

    (1978).

184. M.A.Mazid, M.T.Razi and P.J.Sadler, Inorg. Chem., <u>20</u>, 2872 (1981).

185. R.K.Boggess and M.Zatko, J. Coord. Chem., <u>4</u>, 217 (1975).

186. J.J.Daly, J.Chem. Soc., 3799 (1964).

187. D.P.Santry, personal communication.

188. C.J.L.Lock and M.A.Turner, Acta Cryst., <u>43C</u>, 2096 (1987).

189. M.T.Razi, P.J.Sadler, D.T.Hill and B.M.Sutton, J. Chem. Soc.

    Dalt., 1331 (1983).

190. G.Ellman, Arch. Biochem. Biophys. <u>82</u>, 70 (1959).

191. R.S.Brown, J.Huguet and J.J.Curtis in "Metal Ions in Biological

    Systems," Vol. 15, H.Sigel editor, Marcel Dekker; New York, 55

    (1983).

192. R.S.Brown and J.Huguet, Can. J. Chem., <u>58</u>, 889 (1980).

193. S.J.Lippard, Angew. Chem. Int. Ed. Eng., <u>27</u>, 344 (1988).

194. K.K.Kannan, M.Petef, H. C-d-Dresdner and S.Lövgren, FEBS Lett.,

    <u>73</u>, 115 (1977).

195. K.K.Kannan, B.Notstrand, K.Fridborg, S.Lövgren, A.Ohlsson and

M.Petef, Proc. Natl. Acad. Sci. U.S.A., 72, 51 (1975).

196. R.S.Brown, N.J.Curtis, J.Huguet, J. Am. Chem. Soc., 103, 6953 (1981).

197. R.J.Read and M.N.G.James, J. Am. Chem. Soc., 103, 6947 (1981).

198. B.J.Hathaway and B.Walsh, J. Chem. Soc. Dalt., 681 (1980).

199. E.B.Fleischer, A.E.Gebala, D.R.Swift and P.A.Tasker, Inorg. Chem., 11, 2775 (1972).

200. M.Mikami-Kido and Y.Saito, Acta Cryst., 38B, 452 (1982).

201. P.Wooley, Nature, 258, 677 (1975).

202. B.J.Hathaway, J. Chem. Soc. Dalt., 1196 (1972) and references therein.

203. H.C.Allen, G.F.Kokozka and R.G.Inskeep, J. Am. Chem. Soc., 86, 1023 (1964).

204. R.V.Biagetti, W.G.Bottjer and H.M.Haendler, Inorg. Chem., 5, 379 (1966).

205. A.F.Cameron, D.W.Taylor and R.H.Nuttall, J. Chem. Soc. Dalt., 1603 (1972).

206. P.Pfeiffer and V.Pimmer, Z. Anorg. Chem., 48, 98 (1906).

207. N.G.Mitra and P.Sinha, J. Ind. Chem. Soc., 27, 29 (1950).

208. K.D.Karlin, P.L.Dahlstrom, J.C.Hayes, R.A.Simon and J.Zubieta, Cryst. Struct. Commun., 11, 907 (1982).

209. H.M.J.Hendriks, P.J.M.W.L.Birker, J.van Rijn, G.C.Verschoor and J. Reedijk, J. Am. Chem. Soc., 104, 3607 (1982).

210. C.J.O'Connor, R.J.Romananch, D.M.Robertson, E.E.Eduok and F.R.Fronczek, Inorg. Chem., 22, 449 (1983).

211. J.Gazo, Pure. Appl. Chem., 38, 279 (1974).

212. A.Murphy, B.J.Hathaway and T.J.King, J. Chem. Soc. Dalt., 1646 (1979).

213. J.Gazo, I.B.Bersuker, J.Garaj, M.Kabesova, J.Kohout, H.Langfelderova, M.Melnik, M.Seraton and F.Valach, Coord. Chem. Rev., 19, 253 (1976).

214. R.S.Drago, "Physical Methods in Chemistry," W.B.Saunders Co.; Toronto, 92 (1977).

215. C.K.Jørgensen, "Absorption Spectra and Chemical Bonding in Complexes," Pergamon Press, Addison Wesley Publ. Co. distrib; Reading, Mass. (1962) and references therein.

216. B.Nieuwenhuisje and J.Reedijk, Chem. Phys. Lett., 22, 201 (1973).

217. G.L.McPherson and C.P.Anderson, Inorg. Chem., 13, 677 (1974).

218. R.J.Dudley, B.J.Hathaway, P.G.Hodgson, P.C.Power and D.J.Loose, J. Chem. Soc. Dalt., 1005 (1974).

219. F.A.Walker, H.Sigel and D.B.McCormick, Inorg. Chem., 11, 2756 (1972).

220. D.R.Eaton, personal communication.

221. R.E.Stenkamp, L.C.Sieker and L.H.Jensen, J. Am. Chem. Soc., 106, 618 (1984).

222. W.H.Armstrong and S.J.Lippard, J. Am. Chem. Soc., 105, 4837 (1983).

223. W.H.Armstrong, A.Spool, G.C.Papaefthymiou, R.B.Frankel and S.J.Lippard, J. Am. Chem. Soc., 106, 3653 (1984).

224. K.Weighardt, K.Pohl and W.Gerbert, Angew. Chem. Int. Ed. Eng., 22, 727 (1983).

225. E.Konig and K.J.Watson, Chem. Phys. Lett., 6, 457 (1970).

226. J.D.Oliver, D.F.Mullica, B.B.Hutchinson and W.O.Milligan, Inorg. Chem., _19_, 165 (1980).

227. G.Vos, R.A.leFebre, R.A.G.deGraaff, J.G.Haasnoot and J.Reedijk, J. Am. Chem. Soc., _105_, 1682 (1983).

228. R.J.Doedens and L.F.Dahl, J. Am. Chem. Soc., _88_, 4847 (1966).

229. S.Z.Haider, K.M.A.Malik, K.J.Ahmed, H.Hess, H.Riffel and M.B.Hursthouse, Inorg. Chim. Acta, _72_, 21 (1983).

230. D.V.Naik and G.J.Palinik, Chem. Phys. Lett., _24_, 260 (1974).

231. N.N.Greenwood and T.C.Gibb, "Moessbauer Spectroscopy and Transition Metal Chemistry", Springer-Verlag; Berlin, 100 (1978).

232. B.Hutchinson, L.Daniels and G.Long, Chem. Commun., 1003 (1979).

233. J.P.Collman and E.T.Kittleman, Inorganic Syntheses, _8_, 149 (1966).

234. M.J.Abrams, R.Faggiani and C.J.L.Lock, Inorg. Chim. Acta, _106_, 69 (1985).

235. J.A.Broomhead, J.Evans, W.D.Grumley and M.Sterns, J. Chem. Soc. Dalt., 173 (1977).

236. A.D.Fowlie, D.A.House, W.T.Robinson and S.Rumbell, J. Chem. Soc. A, 803 (1970).

237. J.C.Taft and M.M.Jones, Inorganic Syntheses, _7_, 132 (1963).

238. C.A.Tolman, J. Am. Chem. Soc., _92_, 2956 (1970).

239. E.B.Wilson, Phys. Rev., _45_, 706 (1934).

240. A.R.Katritzky and A.R.Hands, J. Chem. Soc., 2202 (1958).

241. G.L.Cook and F.M.Church, J. Phys. Chem., _61_, 458 (1957).

242. A.R.Katritzky and A.P.Ambler in "Physical Methods in Heterocyclic Chemistry", Vol. 2, A.R.Katritzky (editor), Academic Press Inc.; New York, 274 (1963).

243. J.K.Wilmshurst and H.J.Bernstein, Can. J. Chem., <u>35</u>, 1183 (1957).

244. N.S.Gill, R.H.Nuttall, D.E.Scaife and D.W.A.Sharp, J. Inorg. Nucl. Chem., <u>18</u>, 79 (1961).

245. R.J.H.Clark and C.S.Williams, Spectrochim. Acta, <u>23A</u>, 1055 (1967).

246. N.F.Curtis and Y.M.Curtis, Inorg. Chem., <u>4</u>, 804 (1965).

247. A.B.P.Lever, E.Mantovani and B.S.Ramaswamy, Can. J. Chem., <u>49</u>, 1957 (1971).

248. M.Choca, J.R.Ferraro and K.Nakamoto, J. Chem. Soc. Dalt., 2297 (1972).

249. B.Hutchinson, M.Hoffbauer and J.Takemoto, Spectrochim. Acta, <u>32A</u>, 1785 (1976).

250. Y.Saito, J.Takemoto, B.Hutchinson and K.Nakamoto, Inorg. Chem., <u>11</u>, 2003 (1972).

APPENDIX

Table 3.2.A Anisotropic temperature factors ($\times 10^3$) for chloro(t-butylisocyanide)gold(I).

Atom	U_{11}	U_{22}	U_{33}	U_{23}	U_{13}	U_{12}
Au	49.7(4)	68.7(5)	57.1(4)	0	0	0
Cl	54(2)	112(4)	81(3)	0	0	0
C(1)	76(12)	50(9)	58(9)	0	0	0
N	56(8)	66(8)	58(8)	0	0	0
C(2)	38(8)	82(12)	55(9)	0	0	0
C(3)	71(9)	108(11)	111(11)	-7(10)	-15(7)	20(9)
C(4)	112(17)	103(16)	59(11)	0	0	0

Table 3.2.B. Vibrational data for isocyanide and related complexes

t-BuNC IR	t-BuNCAuCl IR	t-BuNCAuCl Raman	(t-BuNC)$_2$AuPF$_6$ IR	PhNC IR	PhNCAuCl IR	(PhNH)$_2$CAuCl IR	assgmt
						3260s	υNH
						3200m	"
				3100w		3135w	υCH
				3070w	3070w	3070w	"
				3030w			"
3000s		2998w	3000m				"
		2992w					
	2989m	2987m					
		2979w					
2955m	2960m	2958w	2955m				
	2938m	2027m	2920m				
2900m	2878w	2882w	2888m				
2120s	2248s	2262m	2251s	2119s	2233s		υCN
2060w		2259s					
				1960m			over-
				1890m			tones
				1805w			"
				1750w			"
				1590s	1590m	1597s	υring
						1554s,br	
				1497m	1482s	1490s	"
				1482s			
1480s	1476m		1480m				
1467m	1464w	1468w	1461m				
		1458w					
				1451m	1456m	1448s	
1439m	1450m	1447w					
1400m	1399m		1400m				
				1385w	1386m	1380m	
1374s	1374m		1373s				
	1369m						
						1328m	
				1282m	1290m	1295w	βCH
						1269m	
1239s	1236s	1239w	1239s				
		1237w					
1225s	1210sh		1184s				
	1190s						
				1181m	1200w	1219m	βCH
				1160m	1160w	1166w	

Table 3.2.B continued

t-BuNC IR	t-BuNCAuCl IR	t-BuNCAuCl Raman	(t-BuNC)$_2$AuPF$_6$ IR	PhNC IR	PhNCAuCl IR	(PhNH)$_2$CAuCl IR	assgmt
		1136w					
		1122w					
		1118w					
				1090w	1090w		
				1062m	1067m	1075m	
1040w	1045w	1042w	1046w				
				1020m	1019m	1013m	ring breathing
				1010m	999w		
					908m	911w	YCH
929w	933w	933w	938w				
863s	853m	859w	865m				
		839m					
		827m					
			830vs				υPF
744w	738w	744m	765w				
				745s	748s	747s	YCH
						730s	
701w			710w				
679m							
				673s	673s	682s	
						635w	
			551s				
					560m		
514m	523m	522w					
				510m	510m		
455m	466m	464w					
		378w					
	353m	354w			355m	328m,br	υAuCl
	345m	345w			436m		"
	217m	221w	223w				
					204w		
	116w	116w					
					109w		
		76w					
		72w					

abbreviations: s=strong, m=medium, w=weak, v=very, br=broad

Table 3.2.C Vibrational data for nicotinamide and its gold(I) complex

| free ligand | complex | | |
IR	IR	Raman	assgmt
3380s,br	3320s,br		νNH
3160s,br	3160s		"
		3090s	νCH
		3075m	
2790w	2780w		
1690s,br	1720s		νCO
1625s,br	1640s		"
1600m	1620s	1621w	νring
1581s	1577m	1588w	"
		1572m	
1490s	1483m	1483w	"
1430s	1435s	1428m	"
1402s,br	1395s	1412m	
1347m	1340w		
1258w	1249w	1245w	γCH
1231w			
1207s	1200m	1399w	
1154m	1153m	1162m	γCH
1126m	1120m	1126w	
1090m	1060w	1102m	
		1070w	
1031s	1022w	1030s	
992w			ring breathing
970m			
936m	920m		
829m	821m	823m	
	808w	809s	
775s	770m		γCH
700s	680s	679w	v-vib
641m	649m	651w	s-vib
600s			
515s	520m		y-vib
	448m	432w	t-vib
412s	390m	404s	w-vib
398m		390w	
	345w		
	302s		
	260s		
	176m		
		200s	u-vib
		193s	"
		150m	
	129m	129s	
	108m	110m	

Table 3.3.A Anisotropic temperature factors ($Å^2 \times 10^3$) for
(1-methylthyminato-N3-)triphenylphosphinegold(I)

Atom	U_{11}	U_{22}	U_{33}	U_{12}	U_{13}	U_{23}
Au	48.5(3)	41.8(3)	51.9(4)	3.2(4)	-5.9(4)	-9.8(4)
N(1)	74(11)	40(10)	108(14)	7(10)	-7(12)	12(9)
C(1)	132(23)	41(10)	224(35)	-7(14)	-22(23)	51(17)
C(2)	47(11)	59(11)	50(13)	14(10)	1(10)	17(9)
O(2)	123(14)	92(11)	62(10)	-14(11)	24(12)	-2(8)
N(3)	38(8)	38(7)	46(8)	-6(6)	-3(6)	5(7)
C(4)	35(9)	58(11)	69(12)	7(11)	10(10)	-8(10)
O(4)	78(11)	58(8)	95(12)	-10(8)	10(8)	-14(8)
C(5)	65(12)	65(12)	43(11)	3(13)	-9(12)	-15(9)
C(5')	87(18)	90(17)	76(16)	-11(12)	-3(12)	-22(12)
C(6)	45(12)	50(12)	96(17)	-2(8)	2(10)	0(11)
P	34(2)	49(2)	42(2)	8(2)	1(2)	-5(3)
C(7)	52(10)	45(9)	36(10)	-9(8)	5(10)	11(10)
C(8)	84(17)	100(20)	78(19)	-41(15)	7(13)	9(14)
C(9)	92(24)	175(42)	213(48)	4(26)	-40(26)	-22(39)
C(10)	127(32)	96(24)	151(36)	-6(23)	-50(25)	55(24)
C(11)	31(11)	219(34)	88(19)	12(18)	3(12)	66(23)
C(12)	50(13)	124(21)	71(16)	-26(13)	-9(12)	11(14)
C(13)	68(14)	30(9)	50(12)	-5(9)	-11(10)	12(8)
C(14)	47(11)	51(11)	90(18)	2(9)	4(11)	29(10)
C(15)	59(13)	52(12)	101(18)	22(10)	-8(12)	0(12)
C(16)	107(19)	79(17)	60(15)	58(15)	-6(14)	27(13)
C(17)	134(23)	58(14)	85(18)	57(15)	76(17)	38(12)
C(18)	105(19)	52(12)	63(14)	29(12)	10(12)	5(10)
C(19)	67(12)	32(10)	51(11)	12(9)	-5(9)	-18(9)
C(20)	126(24)	106(18)	43(12)	53(17)	11(14)	28(12)
C(21)	82(20)	135(28)	170(39)	21(20)	-20(22)	28(24)
C(22)	268(48)	87(22)	52(16)	110(28)	15(25)	-4(14)
C(23)	124(22)	83(18)	140(25)	57(18)	-78(20)	-7(20)
C(24)	78)14)	53(13)	60(13)	17(11)	-21(11)	-4(10)

Table 3.4.A Ames tests results for compounds 1 - 13 (see Table 3.4.1)

conc x 10^{-6}M	Average number of revertants per plate												
	Complexes												
	1	2	3	4	5	6	7	8	9	10	11	12	13
10						0	0	0	0	0	0	0	0
3						0	0	0	0	0	0	0	0
1						0	0	0	0	14	0	0	0
0.3		45	0			0	0	0	0	73	0	4	0
0.1	75	240	0	37	18	9	3	58	5	85	0	0	0
0.03						143	68	49	138	97	103	110	129
0.01						200	215	206	160	240	84	75	174
0.003			10	64	117	224	191	271	142	189	206	234	190
0.001						242	239	258	213	193	177	4	79
0.0003						331	313	240	301	262	270	244	240
0.0001						327	306	225	295	319	354	310	335
0.00003						352	309	331	311	199	294	316	343
0.00001						343	372	340	330	269	290	325	306
0.000003						370	365	387	311	254	152	354	297
0.000001						388	375	357	353	265	337	334	242
0.0000003						388	381	346	306	374	333	266	205
0.0000001						316	357	348	361	317	319	265	238
0.00000003						246	372	246	361	344	325	243	317
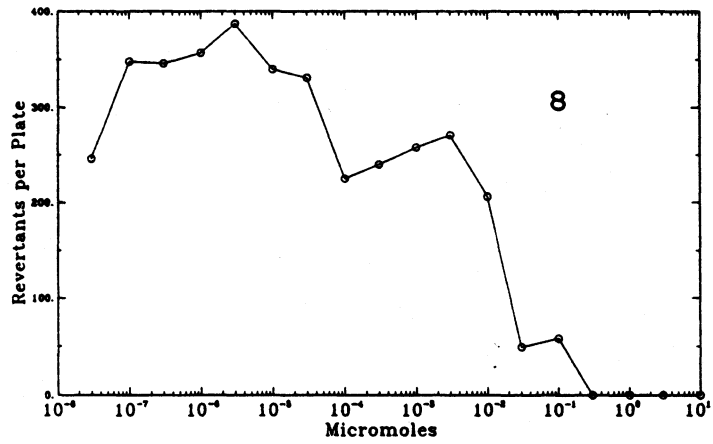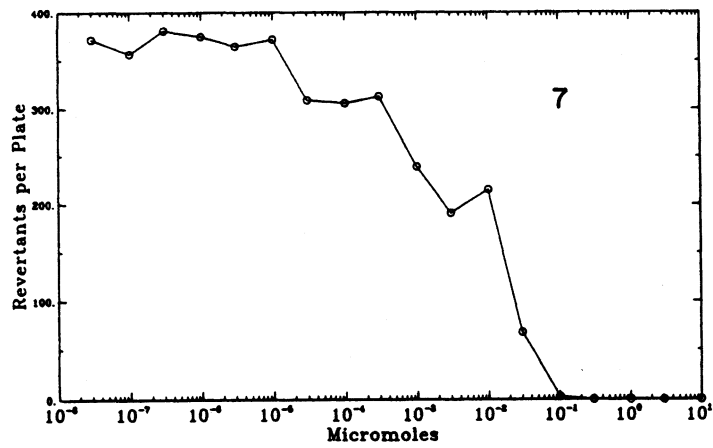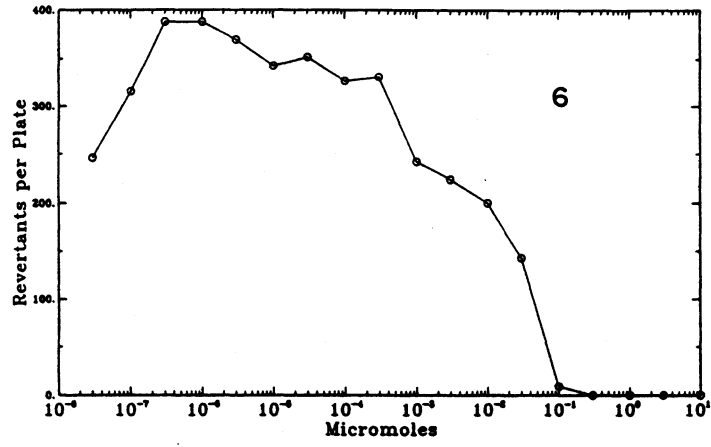
Figure 3.4.B Plots of Ames assay results
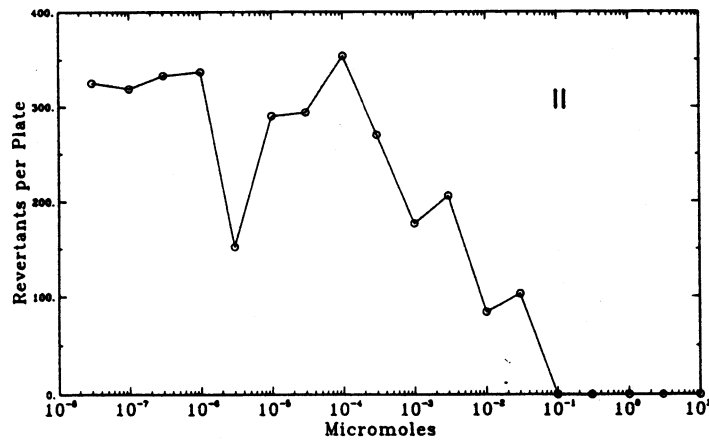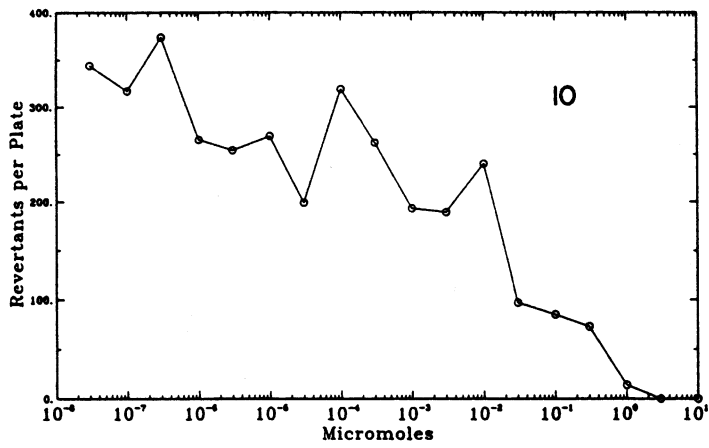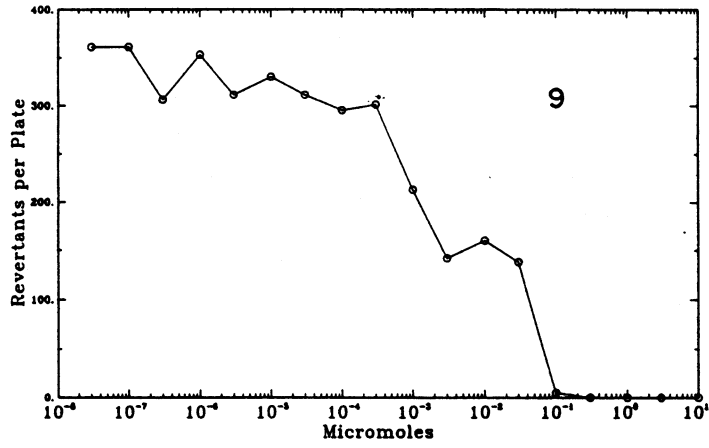
Figure 3.4.B continued
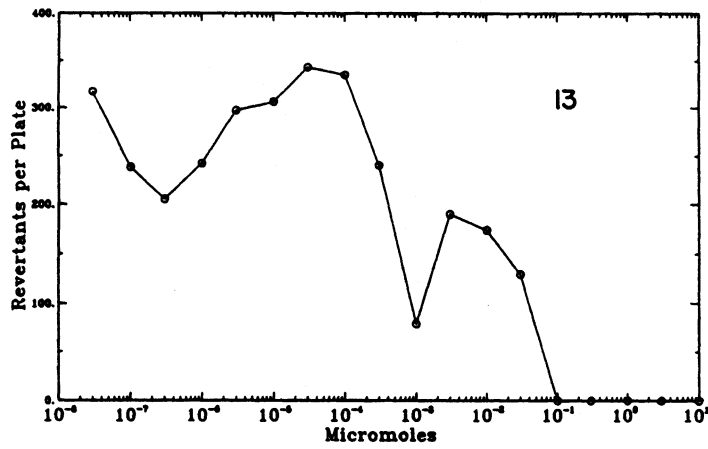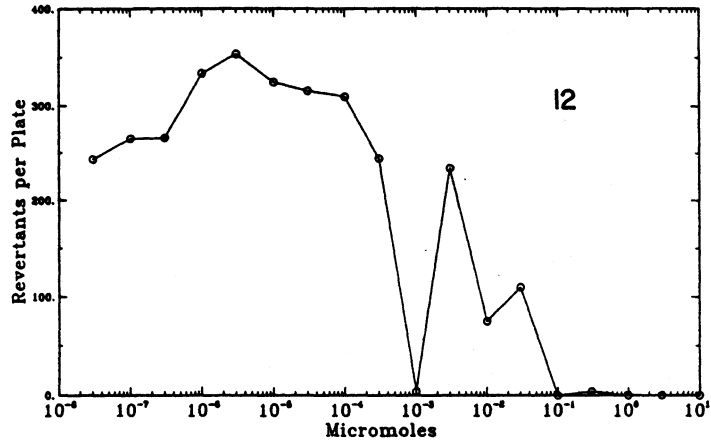
Figure 3.4.B continued

Table 3.4.A Anisotropic temperature factors ($Å^2 \times 10^3$) for dichloro-[N,N-bis-(2-hydroxyethyl)dithiocarbamate S,S']gold(III).

Atom	U_{11}	U_{22}	U_{33}	U_{23}	U_{13}	U_{12}
Au	37.2(2)	33.6(2)	32.8(2)	2.3(2)	1.9(2)	0.9(2)
Cl1	65(2)	30(2)	58(2)	-2(1)	4(2)	2(2)
Cl2	64(2)	65(3)	37(2)	4(2)	-1(2)	-1(2)
S1	52(2)	32(1)	33(1)	-6(1)	0(2)	0(2)
S2	65(2)	37(2)	32(1)	-5(1)	5(2)	-1(2)
C1	40(7)	28(6)	41(6)	0(5)	1(5)	4(6)
N	39(6)	30(5)	48(6)	-1(4)	1(4)	-4(4)
C2	40(7)	44(7)	41(7)	-13(6)	14(6)	-10(6)
C3	69(9)	43(9)	63(8)	-16(7)	3(9)	-18(9)
O1	97(9)	60(8)	82(7)	0(6)	28(7)	-29(7)
C4	53(9)	66(10)	37(7)	-3(7)	-7(6)	-5(8)
C5	77(11)	54(10)	41(7)	12(7)	15(8)	7(10)
O2	85(8)	63(7)	60(6)	-2(6)	16(7)	-21(7)

Table 4.2.A Vibrational data for auranofin and TPPAuTATG

auranofin	TPPAuTATG
	3100w
	2950w
2968s	
2930m	
2898m	
2859m	
1750vs,br	1750vs,br
	1570s
1455m	
	1449m
1420m	1420s
	1380m
1370s	1370s
1235vs,br	1235vs,br
1088m	1090w
1051m	1050sh
1029s	1029s
970m	980m
948m	
902m	909w
859w	
813m	810w
760m	760s
744m	745m
729m	
690m	
671w	
655w	
620m	
594m	
559m	
550m	549s
521m	510m
505m	500m
478m	
452m	455w
438m	
400w	
372m	

Table 4.3.A Anisotropic temperature factors ($Å^2 \times 10^3$) for tris-2-
pyridylphosphine.

Atom	U_{11}	U_{22}	U_{33}	U_{23}	U_{13}	U_{12}
P	39.6(4)	45.2(4)	40.3(3)	-0.8(3)	8.3(3)	-1.3(3)
C11	39(1)	38(1)	31(1)	-6(1)	3.4(9)	-1.3(2)
C21	43(2)	46(2)	39(1)	-1(1)	4(1)	5(1)
C31	65(2)	39(2)	41(1)	5(1)	7(1)	2(1)
C41	61(2)	47(2)	51(2)	2(1)	23(1)	-6(1)
C51	42(2)	52(2)	58(2)	3(1)	15(1)	5(1)
N1	42(1)	43(1)	46(1)	6.0(9)	10.6(9)	5(1)
C12	46(1)	38(1)	41(1)	2(1)	12(1)	1(1)
C22	57(2)	60(2)	56(2)	-7(2)	24(1)	-9(2)
C32	83(2)	68(2)	55(2)	-1(2)	38(2)	4(2)
C42	87(2)	55(2)	39(1)	-6(1)	14(2)	7(2)
C52	70(2)	61(2)	51(2)	-14(2)	11(2)	-11(2)
N2	57(2)	60(2)	44(1)	-8(1)	15(1)	-9(1)
C13	37(1)	43(1)	39(1)	-1(1)	1(1)	-9(1)
C23	62(2)	50(2)	44(2)	-1(1)	4(1)	-4(1)
C33	68(2)	63(2)	61(2)	22(2)	6(2)	5(2)
C43	66(2)	40(2)	84(2)	9(2)	33(2)	3(2)
C53	57(2)	46(2)	63(2)	-7(1)	25(1)	-8(1)
N3	45(1)	49(1)	47(1)	-6(1)	14(1)	-8(1)

Table 4.4.A. Anisotropic temperature factors ($Å^2 \times 10^3$) for chloro(tris-2-pyridylphosphine)gold(I), cell **A**.

Atom	U_{11}	U_{22}	U_{33}	U_{23}	U_{13}	U_{12}
Au	40.8(3)	36.3(3)	34.8(3)	18.7(2)	14.6(2)	22.4(2)
Cl	73(3)	69(3)	57(2)	45(2)	33(2)	43(2)
P	35(2)	31(2)	30(2)	14(1)	10(1)	16(2)
C11	45(8)	47(9)	30(7)	19(7)	20(6)	29(7)
C21	48(9)	34(8)	52(9)	16(7)	16(7)	17(7)
C31	39(9)	41(9)	66(11)	19(8)	19(8)	13(7)
C41	41(9)	53(11)	60(10)	33(9)	15(7)	12(8)
C51	64(11)	69(12)	56(11)	37(9)	18(9)	28(10)
N1	41(7)	70(8)	33(7)	30(6)	6(5)	26(6)
C12	43(8)	20(7)	36(7)	14(6)	12(6)	17(6)
C22	42(9)	54(10)	65(10)	29(8)	13(8)	26(8)
C32	68(12)	82(13)	91(14)	52(11)	47(11)	46(11)
C42	37(9)	64(11)	92(14)	47(11)	14(9)	17(8)
C52	36(9)	81(12)	77(12)	55(10)	19(8)	23(9)
N2	58(8)	58(9)	45(8)	18(7)	0(6)	28(7)
C13	24(7)	30(7)	46(8)	25(6)	6(6)	11(6)
C23	65(10)	35(8)	57(9)	22(7)	20(8)	30(8)
C33	50(9)	33(8)	52(8)	28(7)	19(7)	24(7)
C43	48(9)	45(9)	65(10)	27(8)	20(8)	28(8)
C53	68(11)	49(10)	80(11)	38(9)	37(9)	46(9)
N3	43(7)	55(8)	62(8)	32(7)	12(6)	23(6)
Au'	50.2(3)	46.4(3)	40.2(3)	26.7(2)	24.8(2)	31.3(3)
Cl'	82(3)	76(3)	55(2)	43(2)	46(2)	58(2)
P'	32(2)	41(2)	36(2)	23(2)	17(1)	20(2)
C11'	38(8)	49(9)	49(8)	6(7)	18(6)	30(7)
C21'	58(10)	54(10)	57(9)	31(8)	19(8)	39(8)
C31'	47(10)	67(12)	81(12)	44(10)	7(8)	26(9)
C41'	61(11)	87(14)	61(10)	49(10)	19(8)	40(10)
C51'	49(10)	71(12)	56(10)	33(9)	21(8)	19(9)
N1'	52(8)	52(8)	55(8)	16(6)	11(6)	33(7)
C12'	29(7)	28(7)	41(8)	14(6)	10(6)	11(6)
C22'	87(12)	92(13)	62(10)	59(10)	44(9)	76(11)
C32'	88(13)	107(16)	88(13)	72(13)	47(11)	70(13)
C42'	69(11)	59(11)	56(10)	39(9)	0(9)	27(9)
C52'	62(10)	58(10)	42(8)	36(8)	19(7)	36(8)
N2'	56(8)	59(8)	55(7)	34(6)	35(6)	41(7)
C13'	35(8)	59(10)	30(7)	29(7)	11(6)	14(8)
C23'	85(13)	50(11)	69(11)	30(9)	40(10)	32(10)
C33'	111(16)	30(10)	82(14)	27(10)	32(12)	-4(11)
C43'	130(18)	53(11)	46(9)	23(8)	34(11)	66(13)
C53'	69(12)	67(13)	87(13)	31(11)	11(10)	45(11)
N3'	67(9)	18(7)	80(9)	5(6)	10(7)	30(6)

Table 4.4.B   Anisotropic temperature factors ($Å^2$ x10^3) for
$C_{15}H_{12}N_3PAuCl$, cell **B**.

Atom	U_{11}	U_{22}	U_{33}	U_{23}	U_{13}	U_{12}
Au	55.2(1)	43.0(1)	39.4(1)	11.06(9)	24.5(1)	3.65(9)
Cl	88(1)	65.3(9)	67(1)	33.0(8)	50.5(9)	15.5(8)
P	47.3(8)	43.3(6)	36.7(6)	9.7(5)	20.0(6)	-0.2(5)
C11	46(3)	42(3)	42(3)	10(2)	17(2)	2(2)
C21	76(5)	70(4)	39(3)	-1(3)	12(3)	20(4)
C31	88(6)	69(5)	74(5)	-16(4)	28(4)	16(4)
C41	66(5)	55(4)	102(6)	9(4)	29(4)	13(3)
C51	80(5)	72(5)	67(5)	9(4)	12(4)	22(4)
N1	83(4)	55(3)	66(4)	9(3)	16(3)	19(3)
C12	46(3)	48(3)	44(3)	5(2)	20(3)	3(2)
C22	55(4)	57(4)	77(5)	15(3)	19(3)	17(3)
C32	64(5)	85(5)	82(6)	14(4)	25(4)	25(4)
C42	45(4)	102(6)	86(6)	-12(5)	22(4)	8(4)
C52	63(5)	110(7)	99(7)	32(6)	35(5)	-15(5)
N2	56(4)	83(4)	76(4)	38(3)	22(3)	-5(3)
C13	52(3)	45(3)	40(3)	8(2)	22(3)	3(2)
C23	102(6)	91(6)	61(5)	-16(4)	47(5)	-43(5)
C33	115(8)	119(8)	63(5)	-21(5)	55(6)	-40(7)
C43	84(5)	69(4)	52(4)	-9(3)	29(4)	-2(4)
C53	68(4)	66(4)	60(4)	-4(3)	25(4)	-13(3)
N3	59(3)	64(3)	46(3)	0(2)	26(2)	-13(2)

Table 5.2.A. Anisotropic temperature factors ($Å^2 \times 10^3$) for triaquo(tris-2-pyridylphosphine-N,N',N"-)zinc(II) dinitrate hydrate.

Atom	U_{11}	U_{22}	U_{33}	U_{23}	U_{13}	U_{12}
Zn	34.8(3)	29.4(2)	32.5(2)	2.9(2)	-0.3(2)	-1.4(2)
P	60.0(8)	28.9(6)	45.9(6)	1.3(5)	-2.4(6)	1.0(5)
N4	41(2)	48(2)	45(2)	-18(2)	4(2)	-7(2)
N5	46(3)	62(3)	67(3)	27(2)	7(2)	9(2)
O1	71(2)	56(2)	50(2)	-18(2)	21(2)	0(2)
O2	77(2)	54(2)	58(2)	0(2)	1(2)	18(2)
O3	69(2)	63(2)	38(2)	-5(2)	3(2)	-6(2)
O4	98(3)	60(2)	71(2)	8(2)	21(2)	16(2)
O5	53(2)	95(3)	85(3)	18(2)	-5(2)	20(2)
O6	45(2)	224(6)	65(2)	44(3)	-1(2)	42(3)
O7	39(2)	39(2)	44(2)	9(1)	-6(2)	-4(1)
O8	54(2)	44(2)	42(2)	-4(2)	7(2)	-4(2)
O9	35(2)	61(2)	42(2)	17(2)	0(1)	-4(2)
O10	46(2)	129(4)	56(2)	24(2)	-1(2)	-1(2)
C11	37(2)	40(2)	41(2)	5(2)	1(2)	2(2)
C21	55(3)	43(3)	48(3)	12(2)	-7(2)	3(2)
C31	53(3)	64(3)	44(3)	14(2)	-13(2)	6(3)
C41	45(3)	60(3)	35(2)	3(2)	-5(2)	-4(3)
C51	47(3)	40(2)	39(2)	1(2)	-1(2)	-5(2)
N1	43(2)	31(2)	34(2)	3(1)	-5(2)	-3(2)
C12	45(2)	37(2)	36(2)	-5(2)	-9(2)	0(2)
C22	53(3)	41(3)	49(3)	-15(2)	-8(2)	6(2)
C32	54(3)	62(3)	49(3)	-25(2)	3(2)	6(3)
C42	51(3)	69(3)	39(2)	-11(2)	8(2)	-2(3)
C52	50(3)	48(3)	34(2)	5(2)	2(2)	0(3)
N2	41(2)	39(2)	36(2)	1(2)	1(2)	5(2)
C13	46(3)	35(2)	31(2)	0(2)	-2(2)	-9(2)
C23	69(3)	41(3)	40(2)	1(2)	-5(3)	-20(2)
C33	70(4)	68(4)	48(3)	9(2)	-6(3)	-38(3)
C43	46(3)	78(4)	44(3)	4(2)	0(2)	-18(3)
C53	43(3)	51(3)	39(2)	3(2)	1(2)	-11(2)
N3	39(2)	37(2)	33(2)	3(1)	-1(2)	-7(2)

Table 5.3.A Anisotropic temperature factors ($Å^2 \times 10^3$) for
dinitrato(tris-2-pyridylphosphine-N,N′,N″-)copper(II)

Atom	U_{11}	U_{22}	U_{33}	U_{23}	U_{13}	U_{12}
Cu	44.7(3)	44.0(3)	37.4(3)	24.1(3)	32.4(3)	33.5(3)
P	52.3(7)	50.8(6)	39.2(6)	26.1(6)	35.2(6)	39.5(6)
C11	41(2)	52(3)	37(2)	30(2)	31(2)	33(2)
C21	51(3)	80(4)	56(3)	48(3)	43(3)	50(3)
C31	46(3)	74(4)	70(3)	50(3)	44(3)	37(3)
C41	45(3)	54(3)	56(3)	37(3)	32(3)	27(3)
C51	43(3)	44(3)	43(2)	28(2)	29(2)	27(2)
N1	36(2)	41(2)	37(2)	23(2)	28(2)	27(2)
C12	43(2)	37(2)	29(2)	20(2)	24(2)	27(2)
C22	62(3)	49(3)	35(2)	22(2)	30(2)	38(3)
C32	57(3)	43(3)	33(2)	16(2)	19(2)	24(3)
C42	47(3)	47(3)	41(3)	28(2)	23(2)	27(2)
C52	42(3)	48(3)	44(3)	29(2)	27(2)	29(2)
N2	41(2)	42(2)	34(2)	22(2)	26(2)	29(2)
C13	33(2)	35(2)	32(2)	17(2)	21(2)	21(2)
C23	49(3)	49(3)	44(2)	27(2)	31(2)	38(2)
C33	50(3)	49(3)	44(3)	31(2)	28(2)	34(2)
C43	38(2)	47(3)	33(2)	24(2)	23(2)	25(2)
C53	37(2)	40(2)	33(2)	21(2)	23(2)	24(2)
N3	38(2)	39(2)	34(2)	21(2)	27(2)	26(2)
N4	84(3)	83(3)	99(3)	59(3)	66(3)	61(3)
N5	136(5)	126(5)	82(4)	84(4)	98(4)	119(5)
O1	133(4)	117(4)	88(3)	77(3)	91(3)	101(3)
O2	116(3)	104(3)	82(3)	75(3)	85(3)	96(3)
O3	158(5)	134(4)	133(4)	106(4)	108(4)	131(4)
O4	73(3)	68(2)	71(3)	40(2)	46(2)	51(2)
O5	79(3)	116(4)	108(4)	66(4)	52(3)	62(3)
O6	274(8)	261(8)	195(6)	190(7)	219(7)	240(8)

Table 5.3.B Anisotropic temperature factors ($\AA^2$ x10^3) for
bis[chloro(tris-2-pyridylphosphine-P-)gold(I)-N,N',N''-]
copper(II) dinitrate dihydrate

Atom	U_{11}	U_{22}	U_{33}	U_{23}	U_{13}	U_{12}
Au1	59.7(6)	28.2(2)	43.8(2)	8.5(1)	30.6(3)	11.2(2)
Cu1	27(2)	25.3(8)	25.4(8)			
Cl1	75(4)	27(1)	57(2)	7(1)	37(2)	9(2)
P1	51(4)	30(2)	39(2)	8(1)	29(2)	13(2)
C11	49(13)	35(6)	24(5)	10(4)	20(6)	6(6)
C31	49(15)	61(9)	63(9)	16(7)	24(9)	13(8)
C41	79(18)	61(9)	69(10)	16(8)	45(11)	33(10)
C51	38(14)	59(8)	36(7)	11(6)	25(8)	11(8)
N1	45(11)	30(5)	47(6)	12(4)	39(6)	12(5)
C12	35(12)	36(6)	36(6)	9(5)	33(7)	19(6)
C22	46(13)	63(8)	34(7)	14(6)	31(8)	35(8)
C32	30(13)	83(11)	30(7)	8(6)	10(7)	31(9)
C42	66(15)	63(9)	50(8)	14(7)	37(9)	33(9)
C52	36(14)	56(8)	46(8)	-4(6)	29(8)	5(8)
N2	45(11)	38(5)	43(6)	6(4)	32(7)	13(6)
C13	35(12)	33(6)	34(6)	5(5)	27(7)	10(6)
C23	39(12)	36(6)	33(6)	-2(5)	6(6)	14(6)
C33	59(15)	59(9)	44(7)	-4(6)	31(8)	21(8)
C43	35(12)	49(8)	47(7)	13(6)	13(7)	15(7)
C53	49(13)	51(7)	34(6)	11(5)	33(7)	15(7)
N3	34(9)	35(5)	36(5)	9(4)	23(5)	9(5)
Au2	54.8(5)	29.1(2)	49.4(2)	14.6(2)	29.5(3)	16.0(2)
Cu2	31(2)	24.7(8)	22.2(8)			
Cl2	92(4)	40(2)	81(2)	29(2)	46(3)	34(2)
P2	50(3)	25(1)	38(2)	9(1)	24(2)	15(2)
C14	46(12)	29(6)	37(6)	10(5)	22(7)	11(6)
C24	58(14)	42(7)	46(7)	13(5)	34(8)	18(7)
C34	57(14)	50(7)	41(7)	8(6)	30(8)	15(8)
C44	50(13)	42(7)	45(7)	7(5)	28(8)	26(7)
C54	24(11)	29(6)	36(6)	-11(5)	10(6)	-2(6)
N4	38(10)	37(5)	35(5)	11(4)	24(5)	9(5)
C15	23(12)	34(6)	39(6)	6(5)	24(7)	6(6)
C25	61(16)	50(8)	60(9)	1(6)	47(10)	19(9)
C35	113(21)	42(8)	92(12)	3(8)	66(14)	5(10)
C45	73(17)	67(11)	54(9)	-1(7)	21(10)	-4(11)
C55	55(16)	46(8)	50(8)	0(6)	28(9)	6(8)
N5	55(11)	36(5)	43(6)	17(4)	33(6)	16(6)
C16	76(15)	38(7)	47(7)	7(5)	41(8)	19(8)
C26	51(15)	37(7)	72(10)	10(6)	48(10)	7(8)
C36	18(14)	63(9)	65(9)	3(7)	23(9)	13(8)
C46	61(15)	71(10)	48(8)	9(7)	33(9)	27(10)
C56	69(16)	61(9)	85(11)	33(8)	66(11)	37(10)

Table 5.3.B continued

N7	57(15)	85(11)	76(10)	-22(9)	37(10)	-20(10)
O1	85(13)	68(8)	151(13)	3(8)	22(10)	-11(8)
O2	127(15)	81(8)	109(11)	11(8)	83(11)	-5(9)
O3	238(23)	112(11)	121(12)	72(10)	115(14)	97(13)
N8	36(15)	142(18)	91(13)	15(13)	18(11)	6(12)
O4	127(18)	185(18)	172(17)	116(15)	46(15)	28(13)
O5	112(16)	129(12)	166(15)	99(12)	62(12)	53(11)
O6	209(28)	372(37)	131(17)	-65(20)	-40(17)	209(27)
O11	159(16)	73(8)	104(9)	36(7)	67(10)	23(9)
O22	138(17)	161(16)	140(14)	-25(12)	30(12)	-61(13)

Table 5.4.A Anisotropic temperature factors ($Å^2 \times 10^3$) for
diaquo(tris-2-pyridylphosphine-N,N'N")sulphatoiron(II)
trihydrate.

Atom	U_{11}	U_{22}	U_{33}	U_{23}	U_{13}	U_{12}
Fe	24.3(3)	30.2(3)	43.7(3)	5.2(2)	1.x(2)	4.6(2)
P	33.9(6)	33.8(5)	56.0(7)	-3.8(5)	1.3(5)	6.5(4)
C11	31(2)	59(3)	35(2)	-6(2)	-2(2)	17(2)
C21	56(3)	82(4)	50(3)	-17(3)	1(3)	27(3)
C31	73(4)	153(8)	34(3)	-12(4)	15(3)	46(5)
C41	61(4)	125(6)	39(3)	16(4)	14(3)	22(4)
C51	49(3)	77(4)	43(3)	18(3)	10(2)	13(3)
N1	32(2)	53(2)	35(2)	3(2)	3(2)	9(2)
C12	27(2)	36(2)	34(2)	2(2)	3(2)	1(2)
C22	34(2)	46(3)	39(2)	8(2)	0(2)	-5(2)
C32	21(2)	69(3)	47(3)	14(2)	3(2)	1(2)
C42	27(2)	68(3)	44(3)	7(2)	4(2)	17(2)
C52	36(2)	45(2)	42(2)	2(2)	2(2)	12(2)
N2	25(2)	38(2)	38(2)	0(1)	0(1)	6(1)
C13	27(2)	33(2)	46(2)	10(2)	9(2)	10(2)
C23	59(3)	40(3)	67(3)	18(2)	9(3)	17(2)
C33	69(4)	76(4)	59(3)	35(3)	5(3)	29(3)
C43	52(3)	78(4)	39(3)	13(3)	-3(2)	22(3)
C53	43(3)	48(3)	41(2)	6(2)	3(2)	11(2)
N3	31(2)	37(2)	36(2)	6(1)	5(1)	11(1)
O1	47(2)	65(2)	116(3)	48(2)	-24(2)	1(2)
O2	37(2)	64(2)	73(2)	-32(2)	-7(2)	19(2)
S1	30.7(5)	34.6(5)	50.2(6)	10.5(4)	3.0(4)	1.0(4)
O3	30(2)	36(2)	70(2)	19(1)	-1(1)	1(1)
O4	53(2)	54(2)	78(2)	33(2)	-11(2)	-2(2)
O5	35(2)	76(3)	104(3)	32(2)	17(2)	6(2)
O6	108(4)	58(2)	67(2)	-11(2)	1(2)	13(2)
O7	40(2)	92(3)	65(2)	-15(2)	-8(2)	32(2)

Table 5.5.A Anisotropic temperature factors ($Å^2 \times 10^4$) for
trichloro(chlorotris(2-pyridylphosphine-P-gold(I))-
N,N',N")chromium(III)

Atom	U_{11}	U_{22}	U_{33}	U_{23}	U_{13}	U_{12}
Au	288(2)	265(2)	163(2)	-54(2)	100(2)	-16(2)
Cl1	400(19)	462(21)	258(16)	-188(17)	183(15)	-137(18)
P	243(18)	227(18)	158(16)	-30(14)	98(15)	-5(15)
Cr	169(10)	166(10)	145(10)	-8(8)	56(8)	4(8)
Cl2	240(17)	314(18)	281(17)	-12(14)	139(14)	32(14)
Cl3	248(18)	288(18)	219(16)	42(13)	53(14)	30(14)
Cl4	311(18)	177(16)	255(17)	-12(13)	113(15)	-16(14)